UNIVERSITÀ DEGLI STUDI DI MESSINA

Dipartimento di Ingegneria

DOTTORATO IN INGEGNERIA E CHIMICA DEI MATERIALI E DELLE COSTRUZIONI XXXIII CICLO (2017-2020)

Random variables transformation for the response evaluation of structures

---

PhD Student:
Rossella Laudani

Supervisor:
Prof. Ing. Giovanni Falsone

UNIVERSITÀ DEGLI STUDI DI MESSINA

Abstract

Dipartimento di Ingegneria

Dottorato in Ingegneria e Chimica dei Materiali e delle Costruzioni XXXIII ciclo
(2017-2020)

Random variables transformation for the response evaluation of structures

by Rossella Laudani

The present PhD thesis deals with the use of the Probability Transformation Method (PTM) and of some of its extensions for solving mechanical and structural systems for which the response is modeled as random fields or variables that cannot be well-approximated as Gaussian. In particular, besides the study of stochastic systems, whose geometric and material properties are random, structural systems in which uncertainties in the model designed could arise, have been investigated. In the contexts of stochastic systems, the exact probabilistic solution of redundant stochastic beams, when the flexural deformability is random has been formulated. Moreover, a study was conducted for the stochastic analysis of cracked Euler Bernoulli beams when the cracks are modeled as a rotational internal spring with random amplitude and positions. Then, the concept of the local and nonlocal randomness in stochastic mechanics have been investigated through three research works in which a link between the statistical properties of random field and the local and non-local randomness in stochastic mechanics have been found. Finally, the dynamic stochastic analyses of linear structural systems excited by non-Gaussian excitations have been considered. In any case, this PhD thesis collects several research works with the main goal of gathering all the typologies of stochastic structural analyses in which the PTM can be advantageously applied, both in terms of accuracy and efficiency.

Contents

List of Figures

List of Tables

Chapter 1

Introduction

Over the last two decades, it has been recognized that uncertainty and absence of determinism reflects in engineering sciences. The uncertainties are intrinsic in any engineering problem. Mechanical properties, geometric parameters, boundary conditions, modeling errors as well as actions such as the impact of earthquakes, wind loads, imperfect road profiles, or turbulence flows are highly affected by variations and scatters values. Due to these uncertainties, any engineering systems can not be adequately represented by deterministic models.

Since one of the meanings of uncertainty is randomness, a natural way to handle uncertainties is to apply the theory of probability and random processes, by describing uncertainties as random variables or random fields. Roughly speaking, a random variable is a random element taking "uncertain variable" values. Random variables and/or random fields lead to handle with uncertain parameter systems.

Aim of the stochastic mechanics is dealing with the inherent uncertainties of the structural systems and analyzing the effects of them in the response. Essentially, the uncertainty present in many engineering analysis/design problems is modeled using three basic techniques: (a) probabilistic or stochastic modeling; (b) fuzzy sets based analysis, and (c) anti-optimization of structures. In stochastic mechanics, by applying the probability theory, several methods to model the uncertainties can be counted. Likewise, in the context of industrial fuzzy sets and logic for devising reliable machines and components have been developed, and a recent field has emerged, referred to as anti-optimization that identifies uncertainty with boundedness. Mainly, in interval analysis, the uncertain parameters are modeled as a simple range with assigned lower bound and upper bound.

Within the framework of probabilistic approaches, this thesis deals with several problems of stochastic mechanics through the probability transformation method (PTM). The PTM is based on the probabilistic approach of the space transformation laws of random vectors as well as on the principle of probability conservation and allows to work directly in terms of input and output probability density functions (PDFs). Without a doubt, the most intuitive and easiest way to investigate stochastic problems is to determine the response PDF of any response quantity. Moreover, in most cases, an assessment of the response in terms of PDF is highly advised, above all for the reliability analysis. Without neglecting the fact that working directly in terms of PDF avoids passing through the evaluation of the response statistical moments or cumulants, reducing drastically the stochastic analysis computational effort. The thesis aims to disseminate how the PTM represents an efficient choice for the probabilistic characterization of the structural and mechanical response. Overall, various applications of the PTM, both for static and dynamic analysis of systems characterized by uncertainties, will be introduced.

The present PhD thesis is organized as follows. After this Introduction, in Chapter 2 the PTM is described along with some basic concepts that may be useful to

understand the probabilistic method. Some simple numerical applications aimed to show how this probabilistic tool can be useful in the context of structural analysis are also presented. Chapter 3 deals with uncertain static structural systems when the uncertainties are modeled as random variables with assigned PDF. In the first two sections, an approach will be proposed in order to perform the stochastic response analysis of finite element (FE) modeled structural systems affected by uncertainties. In particular, the proposed approach will be matching the virtues of the Approximated Principal Deformation Modes method (APDM) with the PTM. Then, a closed-form solution of redundantly constrained bending beams in terms of the PDF when flexural deformability is a random parameter will be introduced. Finally, still in the context of uncertain structural systems, the stochastic response of beams characterized by the random amplitude of cracks and by the random cracks positions, besides their amplitude, will be achieved. In Chapter 4, two typical examples in structural engineering in which in this case the uncertainties are inherent in the model designed due to possible simplifying assumptions in analytical models and/or simplified methods will be analyzed. At first, the determination of the static structural response of beams and frames with partially restrained (semi-rigid) connections will be addressed. Then, the second example deals with the stochastic analysis of masonry infilled reinforced concrete (RC) frames. Assuming the macromodeling technique the equivalent diagonal pin-jointed strut width will be considered as a random variable, whose stochastic characterization stems from a wide set of empirical expressions proposed in the literature. In both examples, the response structural PDF will be evaluated through the application of the PTM. Chapter 5 will investigate the incidence of local and nonlocal randomness effects in stochastic mechanics. Motivated by the recent growing literature in the study of new random field models and in particular by the analysis of their fractal dimension and long memory, as those elements controlling local and nonlocal dependencies, the contents of this chapter will deal with three different stochastic topics. At first, the classical problem of peeling a beam off a substrate will be studied through a re-examination of Griffith's fracture criterion in the presence of local and nonlocal random properties. Then, the sensitivity of the stochastic response quantities to the local and non-local randomness dependence of the flexural deformability will be studied both for statically determinate and indeterminate stochastic beams, under different conditions of load and constrain. Finally, the statistical RF theory with fractal dimension and long memory characteristics will be applied in the turbulence flows. In particular, close inspection of these two randomness effects using field data from a sonic anemometer located within the atmospheric surface layer will be done. In Chapter 6, the random dynamic analysis of structures is addressed. Basically, PTM will be extended to the case of dynamical systems. A probabilistic approach which gives the direct relation between the single-time varying PDFs of input and output of a linear structural system subjected to assigned non-Gaussian stochastic process will be presented. The chapter continues with an extension of the above approach for the multiple times varying joint PDF (JPDFs). Finally, some notes that are the basic concepts for a new formulation of an evolutive PTM for dynamic linear uncertain systems, which is still under study face, will be reported. Moreover, it is worth emphasizing that for each chapter, numerical applications will be provided with the aim of demonstrating both the feasibility and accuracy of the different content of application of the PTM. Finally, a conclusive chapter summarizes the main results and highlights the main novelties introduced in the literature.

Chapter 2

The Probability Transformation Method

2.1 Introduction

The main aim of this Chapter is to give the basic preliminary concepts that may be useful in understanding the Probability Transformation Method (PTM), a probabilistic method that has been developed to achieve the probability information of stochastic responses of generic random systems.
Apart from computing the mean and the variance, reasonable only for the simplest case of linear systems with Gaussian random parameters and/or loads, in the stochastic mechanic's field, one of the major goals is to be able to calculate the response probability density function (PDF) of any response quantity of a generic stochastic system. In the literature, there are several papers related to the application of probabilistic methods and, in the last 50 years, many significant results have been obtained in this field. The Monte Carlo Simulation (MCS) is maybe the most universal method for the analysis of stochastic systems, but its usage is greatly limited by the prohibitive computational cost, especially when the response PDF is required (Papadrakakis and Papadopoulos, 1996; Hurtado and Barbat, 1998). Other methods for the evaluation of the response PDF of systems subjected to uncertainties are based on the so-called "closure techniques", consisting of truncating the cumulant series expansion of the response characteristic function (CF) at k-th term. These methods provide good results if the response is characterized by a relatively low non-Gaussianity but, unfortunately, when the response is strongly non-Gaussian, the number of k terms of the series may be particularly high and the convergence, which is not generally guaranteed, is particularly slow, in any case (Roberts and Spanos, 2003; Lin, 1967a; Wu and Lin, 1984).
Recently, an approach, based on a new version of the PTM (Falsone and Settineri, 2013a; Falsone and Settineri, 2013b), has been proposed for the study of some stochastic problems. The PTM is based on a well-known direct relationship between the PDFs of two vectors of random variables connected by an invertible law. The fundamental aspects of the PTM must be looked for in the theory of the space transformation of random vector as well as in the principle of probability conservation.
The chapter is organized as follows: the concept of a function of a random variable will be firstly introduced. Then, the principle of probability conservation over the problem of the evaluation of the PDF will be discussed, both for the function of one random variable and for the function of a random vector. Finally, the last section deals with the PTM. Moreover, in order to highlight the main goal of this chapter some numerical examples are reported.

2.2 The random variable $g(X)$

Suppose that X is an random variable (RV) and $g(X)$ is a function of the real variable X, i.e. a map G exists from X to Y. Then expression $Y = g(X)$ is a new RV. The cumulative ditribution function (CDF) $F_Y(y)$ of the RV so formed is the probability of the event $\{Y \leq y\}$. Thus

$$F_Y(y) = Pr\{Y \leq y\} = P\{g(X) \leq y\} \tag{2.1}$$

where $Pr\{\cdot\}$ is the probability measure. For a specific y, the values of x such that $g(x) \leq y$ form a set on the x axis denoted by R_y. Hence

$$F_Y(y) = Pr\{X \in R_y\} \tag{2.2}$$

The above leads to the conclusion that for $g(X)$ to be an rv, the function $g(X)$ must have the following properties (Papoulis and Pillai, 2002):

1. Its domain must include the range of the RV X.
2. It must be a *Baire* function, that is, for every y, the set R_y such that $g(X) \leq y$ must consist of the union and intersection of a countable number of intervals. Only then $\{Y \leq y\}$ is an event.
3. The events $\{g(X) = \pm\infty\}$ must have zero probability.

2.3 The Principle of Probability Conservation

As the conservation laws in nature, in the stochastic field, it is possible to statement the *principle of probability conservation*: the probability carried by a random event is conserved without introducing other stochastic factors. In other words, if the random factors involved in a stochastic system are preserved, i.e no new random factors arise nor existing factors vanish in a physical process, then the probability will be preserved in the evolution process of the system (Li and Chen, 2009). The conservation of probability is a basic principle of statistical mechanics. The best expression of this principle is enclosed in the Liouville equation (Tarasov, 2007), which will be returned to in chapter 6. In the next subsection, it will be shown how this principle is crucial in order to evaluate the output probability density function (PDF) for a generic stochastic system, and in particular, it will be possible to see how the principle of probability conservation is strictly linked to the theory of the transformation of a random function.

2.3.1 PDF of function of one random variable

In this subsection, the problem of the evaluation of the PDF of $Y = g(X)$ as a function of the PDF of X will be reported. In general it is possible to distinguish the following two cases:

1. If $g(X)$ is a monotonic function, then $g^{-1}(X)$ exists as the unique inverse function of $g(X)$. Consider a specific y on the y-axis, and a positive increment dy, the CDF of Y is differentiable; we then have

$$p_Y(y)dy = Pr\{y < Y(\xi) \leq y + dy\} \tag{2.3}$$

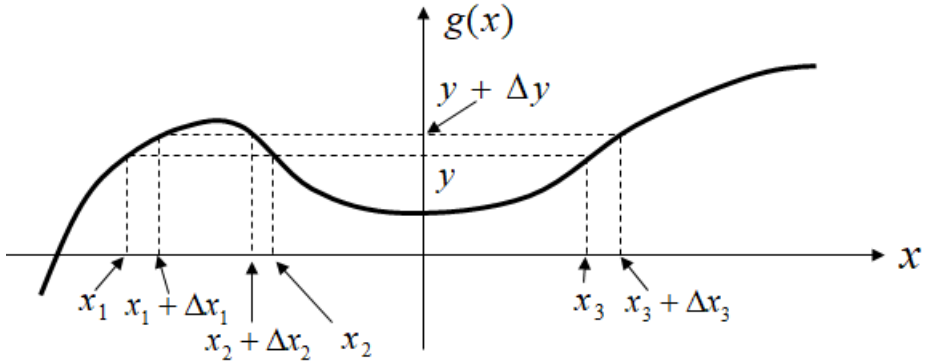

FIGURE 2.1: Transformations of random variables

or equivalently

$$p_Y(y) = \frac{d}{dy} Pr\{y < Y(\xi) \leq y + dy\} \tag{2.4}$$

where ξ represents a basic random event. Because

$$Pr\{y < Y(\xi) \leq y + dy\} = dPr\{\xi\}. \tag{2.5}$$

From Eq. 2.5 and taking into account that the event $\{y < Y(\xi) \leq y + dy\}$ can be expressed in terms of $X(\xi)$ as well:

$$Pr\{x < X(\xi) \leq x + dx\} = dPr\{\xi\} = p_X(x)dx \tag{2.6}$$

it follows that

$$Pr\{y < Y(\xi) \leq y + dy\} = Pr\{x < X(\xi) \leq x + dx\} = dPr\{\xi\} \tag{2.7}$$

This means that, in a mathematical transform, the probability measure will be preserved since the random events keep unchanged. Namely

$$p_Y(y)dy = p_X(x)dx \tag{2.8}$$

For the same set of ξ, the relationship between $X(\xi)$ and $Y(\xi)$ is given by $y = g(x)$. Consequently

$$p_Y(y) = \frac{dx}{dy} p_X(g^{-1}(y)) = \left[\frac{1}{dg(x)/dx}\right]_{x=g^{-1}(y)} p_X(g^{-1}(y)) \tag{2.9}$$

2. Suppose $g(X)$ is not monotonic but a single-valued function, i.e. it has only a finite number of maximum and minimum, and it eventually becomes monotonic as $|x| \to \infty$. Referring to Fig. 2.1, the equation $Y = g(X)$ has three solutions x_1, x_2, x_3 (for the specific y chosen there). As a result when $\{y < Y(\xi) \leq y + dy\}$, the RV X could be in any one of the three mutually exclusive intervals

$$\begin{aligned} &\{x_1 < X(\xi) \leq x_1 + dx_1\}, \quad \{x_2 < X(\xi) \leq x_2 + dx_2\} \quad or \\ &\{x_3 < X(\xi) \leq x_3 + dx_3\} \end{aligned} \tag{2.10}$$

Hence the probability of the event in Eq. 2.10 is the sum of the probability of the above three events, i.e.,

$$P\{y < Y(\xi) \leq y + dy\} = P\{x_1 < X(\xi) \leq x_1 + dx_1\} + P\{x_2 < X(\xi) \leq x_2 + dx_2\} + P\{x_3 < X(\xi) \leq x_3 + dx_3\} \tag{2.11}$$

For small dy and dx_i it can get

$$p_Y(y)dy = p_X(x_1)dx_1 + p_X(x_2)dx_2 + p_X(x_3)dx_3 \tag{2.12}$$

As above, from this last equation it is possible to say again that the probability measure will be preserved since the random events keep unchanged. In particular, in this case, $dx_1 > 0$, $dx_2 < 0$ and $dx_3 > 0$, so that Eq. 2.12 can be rewritten as

$$p_Y(y) = \sum_i p_X(x_i)\frac{|dx_i|}{dy} = \sum_i \frac{1}{|dy/dx_i|}p_X(x_i) \tag{2.13}$$

and as $dy \to 0$ Eq. 2.13 can be expressed as

$$p_Y(y) = \sum_i \frac{1}{|dy/dx|_{x_i}}p_X(x_i) = \sum_i \frac{1}{|g'(x_i)|}p_X(x_i) \tag{2.14}$$

The summation index i in Eq. 2.14 depends on Y, and for every Y the equation $y = g(x_i)$ must be solved to obtain the total number of solutions at every y, and the actual solutions $x_1, x_2, ...$ all in terms of y.

2.3.1.1 Numerical examples

Some examples of the problem of the determination of the PDF of $Y = g(X)$ as a function of the PDF of X are shown below.
For the probabilistic characterization of the random variable Y, the law of the function transformation $g(X)$ has a key role. In the simplest case of a linear transformation, if X is a Gaussian variable, the random variable Y is also Gaussian, so the probabilistic characterization is reduced to the evaluation of the first and second-order moments. But if the $g(X)$ defines a non linear transformation the first and second-order statistics are not sufficient to fully describe Y probabilistically and the use of Eqs. 2.9 and 2.14 represents a direct and quick way for evaluating the PDF of Y.

Let assume X is a Gaussian variable with zero mean and standard deviation equal to 1, the following examples of transformations are taking under examination:

A) $Y = aX + b$.

The above equation has a single solution

$$X = (Y - b)/a \tag{2.15}$$

for every Y. Hence

$$p_Y(Y) = \frac{1}{|a|} p_X\left(\frac{y-b}{a}\right) \tag{2.16}$$

where $g'(X) = a$.

B) $Y = aX^2 + b$.

The above is quadratic equation and has the following two solutions if $Y > 0$:

$$X_1 = -\frac{\sqrt{Y-b}}{\sqrt{a}} \quad X_2 = \frac{\sqrt{Y-b}}{\sqrt{a}} \tag{2.17}$$

and Eq. 2.14 yields:

$$p_Y(Y) = \frac{1}{\left|2\sqrt{a}\sqrt{y-b}\right|}\left[p_X\left(-\frac{\sqrt{y-b}}{\sqrt{a}}\right) + p_X\left(\frac{\sqrt{y-b}}{\sqrt{a}}\right)\right] \quad y > 0 \tag{2.18}$$

where $g'(X) = 2aX$.

C) $Y = \frac{1}{aX+b}$.

The above has the following inverse solution:

$$X = \frac{1-bY}{aY}, \quad Y \neq 0. \tag{2.19}$$

Then

$$p_Y(Y) = \frac{1}{|ay^2|} p_X\left(\frac{1-by}{ay}\right) \tag{2.20}$$

where $g'(X) = \frac{-a}{(aX+b)^2}$.

D) $Y = a\sqrt{X} + b$.

The above has the following inverse solution:

$$X = \frac{(b-Y)^2}{a^2} \tag{2.21}$$

Then

$$p_Y(Y) = \left|\frac{2}{a}\sqrt{\frac{(b-Y)^2}{a^2}}\right| p_X\left(\frac{(b-y)^2}{a^2}\right) \tag{2.22}$$

where $g'(X) = \frac{a}{2\sqrt{X}}$.

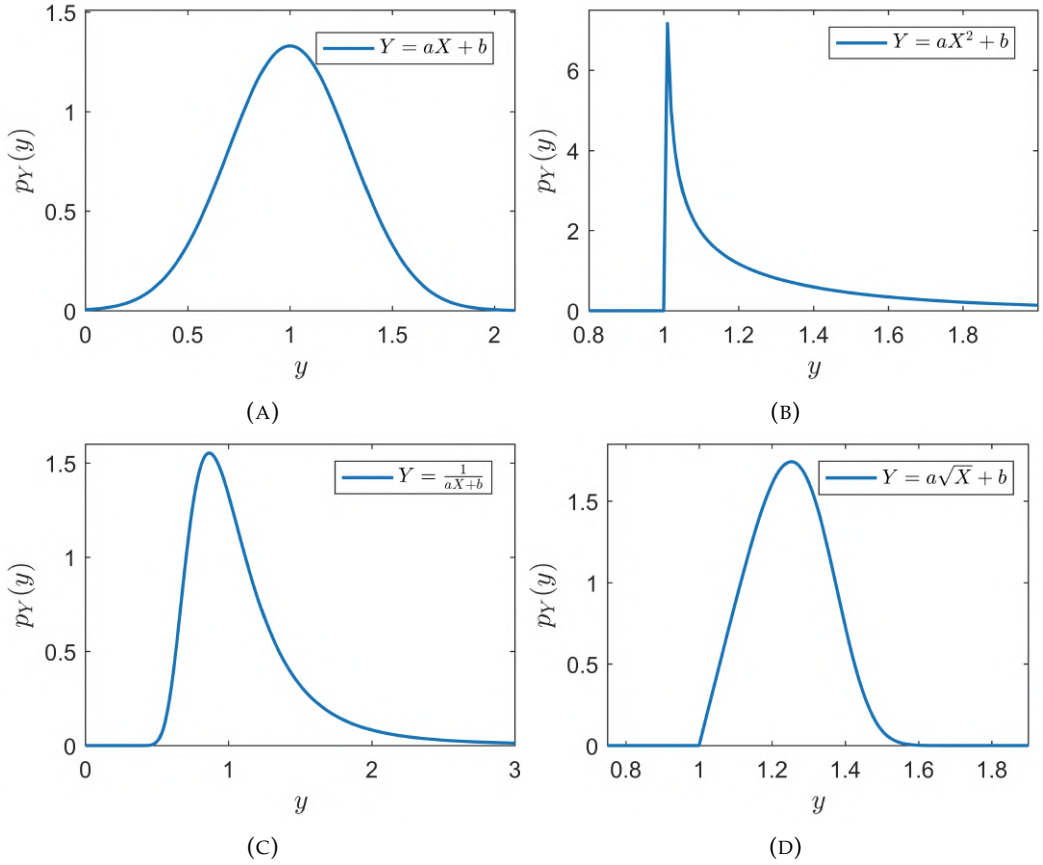

FIGURE 2.2: PDF of Y for four different transformations; with $a = 0.3$ and $b = 1$.

Fig. 2.2 summarises the four different PDF of RV Y and it is possible to appreciate the strong non-Gaussianity of the output if the $g(X)$ is a non-linear transformation as shown in the examples B), C) and D).

2.3.2 PDF of function of random vector

The results of the previous section 2.3.1 can be easily extended for the case of random vectors. If $\mathbf{X}(X_1, X_2, \cdots, X_n)^T$ is a n-dimensional random vector with JPDF $p_{\mathbf{X}}(\mathbf{x})$, namely:

$$Pr\{\mathbf{x} < \mathbf{X}(\xi) \leq \mathbf{x} + d\mathbf{x}\} = dPr\{\xi\} = p_{\mathbf{X}}(\mathbf{x})d\mathbf{x} \tag{2.23}$$

Suppose there is a map $G : \mathbf{X} \to \mathbf{Z}$ determining a vector $\mathbf{Z} = (Z_1, Z_2, \cdots, Z_m)^T$ by $\mathbf{X}$, i.e $\mathbf{X}(\cdot)$ is a n-dimensional invertible application, such that $\mathbf{h}^{-1}(\cdot) = \mathbf{f}(\cdot)$, that means

$$\mathbf{Z} = \mathbf{h}(\mathbf{X}); \quad \mathbf{X} = \mathbf{f}(\mathbf{Z}) \tag{2.24}$$

Here, n and m are respectively the dimension of $\mathbf{X}$ and $\mathbf{Z}$. Denoting the joint density of $\mathbf{Z}$ by $p_{\mathbf{Z}}(\mathbf{z})$, it is possible to write:

$$Pr\{\mathbf{z} < \mathbf{Z}(\xi) \leq \mathbf{z} + d\mathbf{z}\} = dPr\{\xi\} = p_{\mathbf{Z}}(\mathbf{z})d\mathbf{z} \tag{2.25}$$

Considering Eq. 2.25 in conjunction with Eq. 2.23 yields

$$p_{\mathbf{Z}}(\mathbf{z})d\mathbf{z} = p_{\mathbf{X}}(\mathbf{x})d\mathbf{x} \tag{2.26}$$

where, from Eq. 2.24:

$$\mathbf{z} = \mathbf{h}(\mathbf{x}) \tag{2.27}$$

Eqs 2.26 and 2.27 mean that when there exists a map from the space of $\mathbf{X}$ to the space of $\mathbf{Z}$, then if we can find $\mathbf{X}$ in an element domain $d\mathbf{x}$ in the space of $\mathbf{X}$ with a prescribed probability, then we must be able to find $\mathbf{Z}$ in a corresponding element domain $d\mathbf{z}$ in the space of $\mathbf{Y}$, which is determined by the map from $\mathbf{X}$ to $\mathbf{Z}$, with the same probability. The principle can be called the *principle of probability conservation* (Li and Chen, 2009). From Eqs. 2.26 and 2.27, for a one-to-one map and $n = m$, we have

$$p_{\mathbf{z}}(\mathbf{z}) = \frac{1}{|\det[\mathbf{J}_{\mathbf{h}}(\mathbf{z})]|} p_{\mathbf{x}}(\mathbf{f}(\mathbf{z})) = |\det[\mathbf{J}_{\mathbf{f}}(\mathbf{z})]|\, p_{\mathbf{x}}(\mathbf{f}(\mathbf{z})) \tag{2.28}$$

here $\mathbf{J}_{\mathbf{h}}(\mathbf{z})$ is the Jacobian matrix related to the transformations given in Eq. 2.28, that is

$$\mathbf{J}_{\mathbf{h}}(\mathbf{z}) = (\nabla_{\mathbf{x}}^T \otimes \mathbf{h}(\mathbf{x}))|_{\mathbf{x}=\mathbf{f}(\mathbf{z})} \tag{2.29}$$

where $\nabla_{\mathbf{x}}^T$ is the n-th oder row-vector differential operator collecting all the partial derivatives with respect to the component x_i of $\mathbf{x}$ and the symbol $\otimes$ indicates the Kronecker product (Graham, 2018).
From this section, the essential concept is the following: in a generic stochastic system "if no other stochastic factors are involved then the probability carried by a random event is conserved".

2.4 The Probability Transformation Method (PTM)

In the previous section, it possible to appreciate that the expression of Eq. 2.28 gives a direct deterministic relationship between the joint PDF (JPDF) of the random vector $\mathbf{z}$ and that of the random vector $\mathbf{x}$. In other words, the PDF of the output variables $p_{\mathbf{z}}(\mathbf{z})$ can be computed once that the PDF of the input variables $p_{\mathbf{x}}(\mathbf{x})$ are known and the transformation law is defined. It represents the fundamental reference relationship of the PTM.
It is noted that, due to Eq. 2.28, the vectors $\mathbf{x}$ and $\mathbf{z}$ should have the same number of components but it may happen that the numbers of components of the random vectors involved are different. However, this is not a restriction because some expedients must be performed, as shown below. For example, if n and m are the numbers of elements of $\mathbf{x}$ and $\mathbf{z}$, respectively, let suppose that $n > m$. In this case, an efficient expedient may be the augment of the number of output elements through $(n - m)$ generic variables, in such a way that the augmented vector $\bar{\mathbf{z}}^T = (\mathbf{z}^T \quad \hat{\mathbf{z}}^T)$, $\hat{\mathbf{z}}$ being the $(n - m)$-vector of the added variables, has the same number of elements of the input $\mathbf{x}$. Hence, the law expressed into Eq. 2.28 can be applied in the form

$$p_{\bar{\mathbf{z}}}(\bar{\mathbf{z}}) = \frac{1}{|\det[\mathbf{J}_{\bar{\mathbf{h}}}(\bar{\mathbf{z}})]|} p_{\mathbf{x}}(\bar{\mathbf{f}}(\bar{\mathbf{z}})) = |\det[\mathbf{J}_{\bar{\mathbf{f}}}(\bar{\mathbf{z}})]|\, p_{\mathbf{x}}(\bar{\mathbf{f}}(\bar{\mathbf{z}})) \tag{2.30}$$

where

$$\bar{\mathbf{h}}(\cdot) = \begin{pmatrix} \mathbf{h}(\cdot) \\ \hat{\mathbf{h}}(\cdot) \end{pmatrix}; \quad \bar{\mathbf{f}}(\cdot) = \bar{\mathbf{h}}^{-1}(\cdot) \tag{2.31}$$

Here it is important to underline that the vector $\hat{\mathbf{z}}$ is consisting of generic variables linked to the vector $\mathbf{x}$ through the generic subvector function $\hat{\mathbf{h}}(\cdot)$. So, through the definition of $\hat{\mathbf{h}}(\cdot)$ and $\bar{\mathbf{f}}(\cdot)$ it is possible to get a one to one vectorial map. Once that the JPDF $p_{\bar{\mathbf{z}}}(\bar{\mathbf{z}})$ has been evaluated by Eq. 2.31, the required JPDF $p_{\mathbf{z}}(\mathbf{z})$ is obtained

by the saturation of the $(n-m)$ added generic variables, that is,

$$p_{\mathbf{z}}(\mathbf{z}) = \int_{-\infty}^{\infty} \cdots \int_{-\infty}^{\infty} p_{\bar{\mathbf{z}}}(\bar{\mathbf{z}}) d\bar{z}_{n+1} \cdots d\bar{z}_m. \tag{2.32}$$

Cleary when $n < m$, the goal is the same of above: to extend the dimension of the vector $\mathbf{x}$ as the dimension of the output vector $\mathbf{z}$. An effective expedient may be to augment the input vector $\mathbf{x}$ with a deterministic zero $(m-n)$-vector $\mathbf{0}$. In this way, Eq. 2.24 can be rewritten as

$$\mathbf{z} = \mathbf{h}(\bar{\mathbf{x}}) = \begin{pmatrix} \tilde{\mathbf{h}}(\mathbf{x}) \\ \hat{\mathbf{h}}(\mathbf{x}) + \hat{\mathbf{x}} \end{pmatrix}; \quad \bar{\mathbf{x}} = \begin{pmatrix} \mathbf{x} \\ \hat{\mathbf{x}} \end{pmatrix}, \tag{2.33a-b}$$

In this case, the augmented m-dimensional vector $\mathbf{h}(\cdot)$ is constituted through the composition of the following two subvectors: (i) $\tilde{\mathbf{h}}(\cdot)$, the first subvector of Eq. 2.33(a), is the initial vector function of the n-dimensional application between the n-dimentional input and output vector, $\mathbf{z}$ and $\mathbf{x}$, respectively; (ii) the second subverctor is the sum of $\hat{\mathbf{h}}(\cdot)$ with $\hat{\mathbf{x}}$, where is the $(m-n)$-vector function that can be any additional applications between the $(m-n)$ components of $\mathbf{z}$ with the n components of $\mathbf{x}$, while $\hat{\mathbf{x}}$ is the $(m-n)$-vector deterministically zero. Hence, the JPDF of the enlarged vector $\mathbf{x}$ is given by

$$p_{\bar{\mathbf{x}}}(\bar{\mathbf{x}}) = p_{\mathbf{x}}(\mathbf{x}) \delta(\hat{\mathbf{x}}) \tag{2.34}$$

$\delta(\hat{\mathbf{x}})$ being the $(m-n)$-dimensional Dirac delta function placed at $\hat{\mathbf{x}} = \mathbf{0}$, representing the JPDF of $\hat{\mathbf{x}}$. Hence, the inverse relationships given into Eq. 2.24 can be rewritten in the form

$$\bar{\mathbf{x}} = \begin{pmatrix} \mathbf{x} \\ \hat{\mathbf{x}} \end{pmatrix} = \begin{pmatrix} \tilde{\mathbf{f}}(\tilde{\mathbf{z}}) \\ \hat{\mathbf{f}}(\mathbf{z}) \end{pmatrix}; \quad \tilde{\mathbf{f}}(\cdot) = \tilde{\mathbf{h}}^{-1}(\cdot); \quad \hat{\mathbf{f}}(\mathbf{z}) = \hat{\mathbf{z}} - \hat{\mathbf{h}}(\tilde{\mathbf{f}}(\tilde{\mathbf{z}})), \tag{2.35}$$

where the expression of the direct transformation given into Eq. 2.33 has been considered and where it has been assumed that the inverse expressions given into Eq. 2.35 exist. At this point, following the same procedure as that used for finding the classical PTM expression, it is not difficult to find the following relationship between the JPDF of $\mathbf{z}$ and the JPDF of $\mathbf{x}$ (Falsone and Laudani, 2019a):

$$p_{\mathbf{z}}(\mathbf{z}) = |\det[\mathbf{J}_{\tilde{\mathbf{f}}}(\tilde{\mathbf{z}})]| \, p_{\mathbf{x}}(\tilde{\mathbf{f}}(\tilde{\mathbf{z}})) \delta(\hat{\mathbf{z}} - \hat{\mathbf{h}}(\tilde{\mathbf{f}}(\tilde{\mathbf{z}}))), \tag{2.36}$$

with $\delta(\cdot)$ being the multidimensional Dirac delta function.

Another problem in the application of the PTM could be the evaluation of a marginal PDF of the response. This implies that starting from the knowledge of the full joint one $p_{\mathbf{z}}(\mathbf{z})$, a certain number of integrations must be performed in order to saturate this function respect to the non-required components. In (Falsone and Settineri, 2013a; Falsone and Settineri, 2013b) it was introduced a more effective alternative way to evaluate the marginal PDF of $\mathbf{z}$, $p_{z_j}(z_j)$, avoiding to saturate. By using the properties of the Dirac delta function $\delta(\cdot)$, Eq. 2.28 is rewritten in the following form

$$p_{\mathbf{z}}(\mathbf{z}) = \int_{-\infty}^{\infty} \cdots \int_{-\infty}^{\infty} \frac{1}{|\det[\mathbf{J}_{\mathbf{h}}(\mathbf{y})]|} p_{\mathbf{x}}(\mathbf{y}) \delta(\mathbf{y} - \mathbf{f}(\mathbf{z})) dy_1 \cdots dy_n. \tag{2.37}$$

wherein the multi-dimensional Dirac delta function centered in the point $\mathbf{y} = \mathbf{f}(\mathbf{z})$ is introduced

$$\delta(\mathbf{y} - \mathbf{f}(\mathbf{z})) = \delta(y_1 - f_1(\mathbf{z}))\delta(y_2 - f_2(\mathbf{z})) \cdots \delta(y_n - f_n(\mathbf{z})) \tag{2.38}$$

The multi-dimensional Dirac Delta introduced above has non-zero value only if $\mathbf{y} = \mathbf{f}(\mathbf{z})$; then, it is equivalent to a multi-dimensional Dirac Delta centered in $\mathbf{z} = \mathbf{f}^{-1}(\mathbf{y})\mathbf{h}(\mathbf{y})$, provided the determinant of the Jacobian matrix related to the application $\mathbf{h}(\mathbf{y})$ is introduced

$$\delta(\mathbf{y} - \mathbf{f}(\mathbf{z})) = |\det[\mathbf{J}_\mathbf{h}(\mathbf{y})]|\, \delta(\mathbf{z} - \mathbf{h}(\mathbf{y})) \tag{2.39}$$

The determinant of the Jacobian matrix $\mathbf{J}_\mathbf{h}$ guarantees that the functions appearing in both sides of Eq. 2.39 have unitary area. Substituting Eq. 2.39 into Eq. 2.37 yields

$$p_\mathbf{z}(\mathbf{z}) = \int_{-\infty}^{\infty} \cdots \int_{-\infty}^{\infty} p_\mathbf{x}(\mathbf{y})\delta(\mathbf{z} - \mathbf{h}(\mathbf{y}))dy_1 \cdots dy_n. \tag{2.40}$$

We now consider the single component z_j of the output random vector $\mathbf{z}$ defined by the scalar transformation $z_j = h_j(\mathbf{x})$. The PDF of z_j is readily computed by integrating both sides of Eq. 2.40 with respect to all the variables z_i, with $i = 1, 2, \cdots, n$ and $i \neq j$, thus obtaining

$$p_{z_j}(z_j) = \int_{-\infty}^{\infty} \cdots \int_{-\infty}^{\infty} p_\mathbf{x}(\mathbf{y})\delta(z_j - h_j(\mathbf{y}))dy_1 \cdots dy_n. \tag{2.41}$$

Eq. 2.41 is very suitable for defining the single response PDF. In an analogous way, the JPDF of two components $z_j = h_j(\mathbf{x})$ and $z_k = h_k(\mathbf{x})$ of the output random vector $\mathbf{z}$ is required, the following relationship can be used:

$$p_{z_j,z_k}(z_j, z_k) = \int_{-\infty}^{\infty} \cdots \int_{-\infty}^{\infty} p_\mathbf{x}(\mathbf{y})\delta(z_j - h_j(\mathbf{y}))\delta(z_k - h_k(\mathbf{y}))dy_1 \cdots dy_n. \tag{2.42}$$

It is important to note that Eqs. 2.40-2.42 show the useful property of not requiring the knowledge of the inverse transformation $\mathbf{f}(\cdot) = \mathbf{h}^{-1}(\cdot)$ that, in some cases, can represent a very hard task. Moreover, they do not depend on the number of elements of $\mathbf{z}$. On the contrary, they have the drawback of requiring n integrations respect to the component of $\mathbf{x}$. This last drawback is overcome when $h_j(\mathbf{x})$ is a linear combination of the components of $\mathbf{x}$, that is, when it is possible to write $h_j(\mathbf{x}) = \mathbf{h}_j^T\mathbf{x}$, $= \mathbf{h}_j$ being the n-vector collecting the coefficients of the combination. In fact, the computational effort related to the evaluation of the multiple integrals appearing in the previous equations can be sensibly reduced if the calculus is conducted in terms of the CF. The CF of z_j can be expressed as

$$\begin{aligned} M_{z_j}(\omega_j) &= \frac{1}{2\pi}\int_{-\infty}^{\infty} p_{z_j}(z_j)\exp(-i\omega_j z_j)dz_j \\ &= \frac{1}{2\pi}\int_{-\infty}^{\infty}\left[\int_{-\infty}^{\infty}\cdots\int_{-\infty}^{\infty} p_\mathbf{x}(\mathbf{y})\delta(z_j - \mathbf{h}_j^T\mathbf{y})dy_1\cdots dy_n\right]\exp(-i\omega_j z_j)dz_j. \end{aligned} \tag{2.43}$$

that, taking into account the properties of the Dirac Delta function, becomes

$$M_{z_j}(\omega_j) = \frac{1}{2\pi}\int_{-\infty}^{\infty}\cdots\int_{-\infty}^{\infty} p_\mathbf{x}(\mathbf{y})\exp(-i\omega_j\mathbf{h}_j^T\mathbf{y})dy_1\cdots dy_n. \tag{2.44}$$

Remembering that the multidimensional CF $M_{\mathbf{x}}(\boldsymbol{\theta})$ of the random vector $\mathbf{x}$ is related to the corresponding JPDF by the following relationship:

$$M_{\mathbf{x}}(\boldsymbol{\theta}) = \frac{1}{(2\pi)^n} \int_{-\infty}^{\infty} \cdots \int_{-\infty}^{\infty} p_{\mathbf{x}}(\mathbf{y}) \exp(-i\boldsymbol{\theta}^T \mathbf{y}) dy_1 \cdots dy_n. \tag{2.45}$$

then it is not difficult to verify that the following relationship holds:

$$M_{z_j}(\omega_j) = (2\pi)^{n-1} M_{\mathbf{x}}(\boldsymbol{\theta})|_{\boldsymbol{\theta}=\omega_j \mathbf{h}_j} \tag{2.46}$$

that evidences the fundamental result that the response CF $M_{z_j}(\omega_j)$ is always obtainable in closed form, once that the multidimensional CF of the input is known, without the necessity of any of integration. If the joint CF (JCF) of the two response variables z_j and z_k is required, it is easy to show that the following relationship holds:

$$M_{z_j z_k}(\omega_j, \omega_k) = (2\pi)^{n-2} M_{\mathbf{x}}(\boldsymbol{\theta})|_{\boldsymbol{\theta}=\omega_j \mathbf{h}_j + \omega_k \mathbf{h}_k} \tag{2.47}$$

The result given into Eq. 2.47 can be easily extended to the case of the cross-CF (C-CF) $M_{z_1,\cdots,z_n}(\omega_1, \cdots, \omega_n)$ of $m \leq n$ response variables. As a matter of the fact, it is easy to verify that the following relationship holds:

$$M_{z_1,\cdots,z_n}(\omega_1, \cdots, \omega_n) = (2\pi)^{n-m} M_{\mathbf{x}}(\boldsymbol{\theta})|_{\boldsymbol{\theta}=\sum_{i=1}^{m} \omega_i \mathbf{h}_i} \tag{2.48}$$

that, specified for $m = n$, gives the response complete CF. Once that the characteristic functions are evaluated the corresponding PDF can be obtained by Fourier anti-transform operations.

2.4.1 Numerical examples

The numerical examples reported in this subsection aim to highlight the use of the PTM to evaluate the response PDF of linear systems subjected to random static loads with generic PDF.

2.4.1.1 Example 1

As first example, the cantilever beam represented in Fig. 2.3 is taken into account. The Young modulus value and the inertia moment are: $E = 2.1 \times 10^9 N/m^2$ and $I = 1.35 \times 10^{-3} m^4$, respectively; while $L = 10m$. The PTM will be applied in order to determine the PDF of the vertical displacement and rotation of the free end. Assuming as system origin coinciding with the clamp constraint, the vertical displacement and rotation at the free end are described by the following expressions:

$$u_y(x = L) = \frac{F_1 L^3}{3EI} + \frac{F_2 L^3}{48EI} \tag{2.49}$$

$$\phi(x = L) = \frac{F_1 L^2}{2EI} + \frac{F_2 L^2}{8EI} \tag{2.50}$$

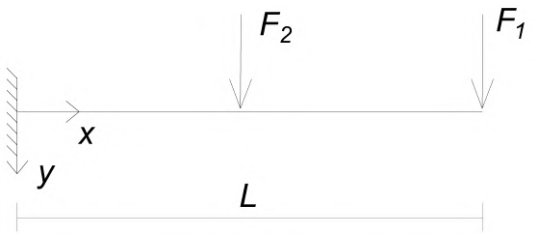

FIGURE 2.3: Example 1: The beam structure

The beam is forced by two random forces applied at the free end and at the center with $p_{\mathbf{F}}(\mathbf{F})$ known. The following three different distributions of the random vector $\mathbf{F}$ have been considered:

- Case 1) $\mathbf{F}$ is assumed is a Gaussian JPDF defined by the mean vector $\boldsymbol{\mu}_{\mathbf{F}}$ and the covariance matrix $\boldsymbol{\Sigma}_{\mathbf{F}}$ as follows:

$$\boldsymbol{\mu}_{\mathbf{F}} = \{1.2 \quad 0.1\} \times 10^5 N; \quad \boldsymbol{\Sigma}_{\mathbf{F}} = \begin{pmatrix} 1 & 0.6 \\ 0.6 & 1 \end{pmatrix} \times 10^9 N^2 \tag{2.51}$$

- Case 2) $\mathbf{F}$ is assumed uniformly distributed random variables, characterized by the following JPDF:

$$p_{\mathbf{F}}(\mathbf{F}) = \prod_{i=1}^{2} U\left(\alpha_{min_i}, \alpha_{max_i}\right) \tag{2.52}$$

  where α_{min_i} and α_{max_i} represent the minimum and maximum fluctuations around the mean vector of the Eq. 2.52, here it was assumed a fluctuation of the 30 percent.

- Case 3) $\mathbf{F}$ is assumed by the mixture PDF as follows:

$$p_{\mathbf{F}}(\mathbf{F}) = \sum_{i=1}^{2} w_i \times p_{\mathbf{F}_i}(\mathbf{F}_i) \tag{2.53}$$

  where w_i is the weight of the distribution, here assumed $w_1 = 0.2$ and $w_2 = 0.8$. While $p_{\mathbf{F}_i}(\mathbf{F}_i)$ is assumed as the Gaussian JPDF of the case 1);

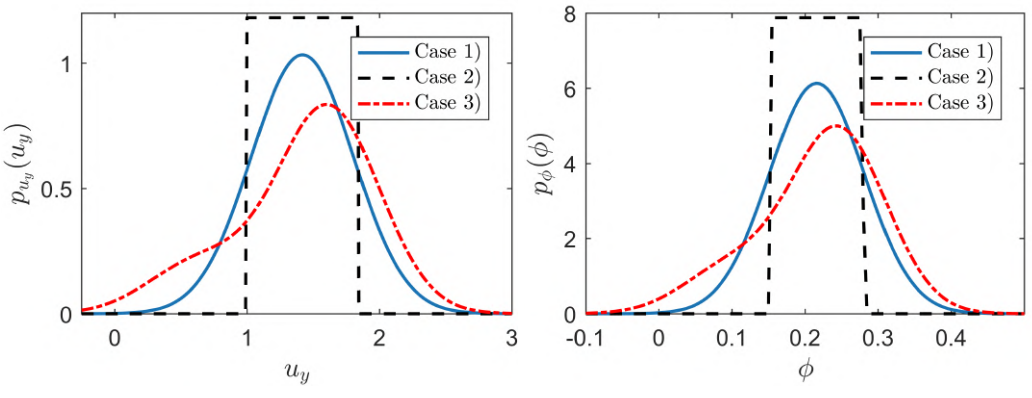

(A) (B)

FIGURE 2.4: Example 1: PDF of the vertical displacement at the free end (A); PDF of the rotation at the free end (B).

Fig. 2.4 shows the PDFs of the vertical displacement and rotation at the free end for the above three case of $p_{\mathbf{F}}(\mathbf{F})$. Clearly, due to the linearity of the system, both the response PDFs, $p_{u_y}(u_y)$ and $p_{\phi_y}(\phi)$, follow the same probabilistic distribution type of the random load.

2.4.1.2 Example 2

The frame structure shown in Fig. 2.5 is now taking under examination. All the columns have the same inertia moment $I_{column} = 3.125 \times 10^{-3} m^4$, while all the horizontal elements are characterized by inertia $I_{beam} = 1.143 \times 10^{-2} m^4$. The Young modulus value is $E = 2.1 \times 10^9 N/m^2$. The system is forced by three static random forces applied at each plane. In this example the evaluation of the PDF $p_{u_x^C}(u_x^C)$ of the third floor displacement is the goal of the analysis.

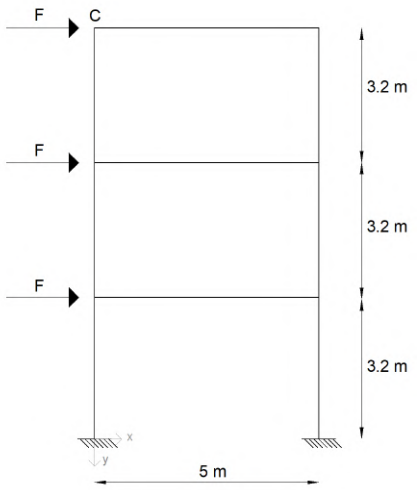

FIGURE 2.5: Example 2: The frame structure.

The three different distributions of the random vector $\mathbf{F}$ of the above example are assumed also for this example. In particular:

$$\boldsymbol{\mu}_{\mathbf{F}} = \begin{Bmatrix} 1.2 & 1.2 & 1.2 \end{Bmatrix} \times 10^5 N; \quad \boldsymbol{\Sigma}_{\mathbf{F}} = \begin{pmatrix} 1 & 0.6 & 0.3 \\ 0.6 & 1 & 0.6 \\ 0.3 & 0.6 & 1 \end{pmatrix} \times 10^9 N^2 \tag{2.54}$$

The PDFs of the horizontal displacement of node C are given in Fig. 2.6, for the all three cases of $p_{\mathbf{F}}(\mathbf{F})$. The frame structure system is characterized by a linear input-out relationship, thus about the behavior of the distribution PDF response, the same considerations of the previous example can be made.

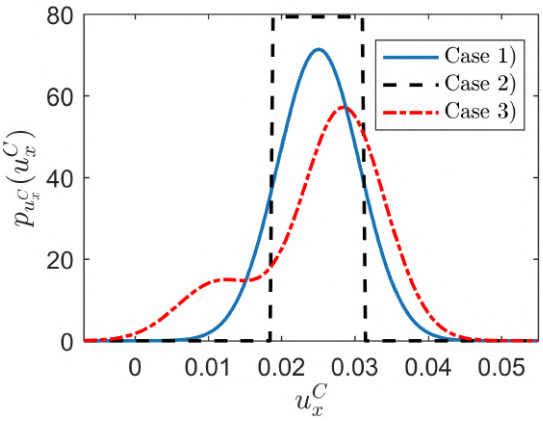

FIGURE 2.6: Example 2: PDF of the horizontal displacement of node C.

From the above examples, it is possible to appreciate how the PTM represents an efficient choice for the probabilistic characterization of the structural response, it is useful especially for some type of problems for which, in spite of their simplicity, it is very difficult to find explicit solutions. In fact, although for the linear systems examined the structural response PDFs follow the same probabilistic distribution type of the random load, in the case of non-Gaussian loads, the PTM allows to find the exact explicit PDFs of the output.

Chapter 3

Uncertain materials systems

3.1 Introduction

The analysis of structural systems is always affected by the uncertainties due to the characterization of materials and geometric quantities (random system parameters), in addition to the external actions (random loading). In many cases, the level of these uncertainties is so crucial that the use of deterministic methods for the structural response analyses may lead to unacceptable approximations. It has been recognized that in these cases the uncertainties, and consequently, the structural response, must be adequately represented as random quantities. The evaluation of the stochastic response is the central goal of stochastic mechanics.

In particular, in this chapter, the mechanical properties of several structural systems as random variables will be assuming. Then the evaluation of the response in terms of PDF will be explored. In general, an assessment of the response in terms of PDF is highly recommended, above all if reliability analysis is a required field, as well as the use of advanced specific analysis approaches, as the probabilistic methods.

It is known that there is no universal method suitable to solve any problem involving uncertainties in the system characteristics. Presently there exist thousand papers on approximated methods able to analyse the stochastic structures. Among these, the statistic approaches, based on the Monte Carlo simulations (Kahn, 1955; Metropolis and Ulam, 1949), are maybe the only universal and simplest from a theoretical point of view. In fact, they need the realization of a sufficiently great number of samples of the uncertain parameters and the solution of the corresponding deterministic problems. However, increasing the structural degrees of freedom and the number of uncertain parameters, the computational effort related to the statistic methods becomes extremely great. For this reason, some alternative non-statistic methods have been proposed in the literature. One of the oldest methods for the evaluation of the PDF of systems subjected to uncertainties is based on truncating the cumulant series expansion of the response CF (Lutes and Sarkani, 2004). This method provides good results if the response is characterized by a relatively low non-Gaussianity. When the response is strongly non-Gaussian, the number of terms of the series may be particularly high and the convergence, which is not generally guaranteed, is particularly slow, in any case. In addition, the direct evaluation of the terms of the series may not be simple. For this reason this method is often associated with the MCS method (Schuëller et al., 1989; Papadrakakis and Papadopoulos, 1996; Hurtado and Barbat, 1998).

In the literature, a relevant role is played by the methods based on the perturbation approaches that are based on a Taylor series expansion in terms of a set of zero mean random variables. The perturbation approaches provide accurate results for relatively low levels of uncertainty, for which only few terms of the series are

used (usually the first or the first and second order are considered). On the contrary, when the level of uncertainty of the structural parameters increases, the approach loses strongly its precision and, moreover, the computational effort strongly increases, due to the high number of terms of the series to be taken into account. In any case, the convergence of the approach is not guaranteed by the augmented order of the retained series terms. Major details on this method can be found in other works (Schuëller and Pradlwarter, 2009; Kleiber and Hien, 1992; Elishakoff, Ren, and Shinozuka, 1995a; Kamiński, 2007; Kaminski, 2013). On the other hand, extremely few closed-form solutions are available for meaningful comparison. As a consequence, the stochastic finite element (SFE) approach is usually identified with the classical finite element coupled with the perturbation approaches for taking into account the structural parameter uncertainties.

Another important class of methods for solving uncertain structural systems is based on the approaches, based on the projection of the solution on a complete stochastic basis. Two of the most used projection approaches are those based on the Karhunen-Loève expansion (Ghanem and Spanos, 2003) and on the polynomial chaos expansion. This last one is a Galerkin projection scheme based onWiener integral representation (Schuëller and Pradlwarter, 2009; Ghanem and Spanos, 2003). It requires the numerical evaluation of the series expansion terms (Ghanem and Kruger, 1996; Pellissetti and Ghanem, 2000) and can be particularly onerous if the terms of the series are not limited to a relatively small number. For this reason, recently, several efforts have been made to improve the approach (Field Jr and Grigoriu, 2004; Doostan, Ghanem, and Red-Horse, 2007). A comparison of different projection schemes for stochastic finite element analysis is given in the work of Sachdeva et al (Sachdeva, Nair, and Keane, 2006).

One more relevant category of methods dealing with uncertain system is that related to the use of the random matrix expansion of the structural stiffness matrix in order to perform explicitly its inversion (Neumann expansion) (Adhikari and Manohar, 1999; Yamazaki, Shinozuka, and Dasgupta, 1988). Then, once that the explicit inverse stiffnessmatrix is known, it is possible to obtain the statistics of the response or to perform a MCS to obtain the response PDF.

In 2002, Falsone and Impollonia (Falsone and Impollonia, 2002; Falsone and Impollonia, 2004) proposed the Approximated Principal Deformation Modes method (APDM) method, belonging to the class of MCS-based methods. It consists in breaking up the structural response in the base of the principal deformation modes of the structure: this allows of obtaining an approximation of the response, without the cost to invert the stiffness matrix of the system and enabling to reduce consistently the computational effort. Indeed, the statistics of the response are obtained by MCS applied directly on explicit expressions of the response. In a certain sense, the method enables the evaluation of an approximated inverse stiffness matrix (as the matrix expansion methods). Nevertheless, the APDM can be considered also as a projection method, because it consists essentially in the expansion of the structural response on a particular base through a finite number of functions, depending on the uncertain parameters, strictly related to the principal deformation modes of the structural system. In any case, the coefficient of the series can be evaluated explicitly in terms of the uncertain parameters.

Moreover, in the search field on uncertain structural systems, the study of beams in presence cracks have been seen intense research. In the recent literature, many authors have studied the Euler-Bernoulli beam in presence of an arbitrary number of cracks, providing closed-form solutions (Caddemi and Calio, 2008; Caddemi and Calio, 2009; Caddemi and Caliò, 2013). The idea to solve the multi-cracked beams,

which are treated as equivalent linear springs at the cracks' position, through the resolution of linear discontinuous differential equations using the so-called generalized functions has been studied in some deterministic aspects by Palmeri and Cicirello (Palmeri and Cicirello, 2011; Cicirello and Palmeri, 2014). From a probabilistic point of view, the stochastic response of a beam with certain and uncertain no-propagating crack has been treating in Cacciola and Muscolino. The evaluation of the structural response of single-cracked beam-like structures assuming the crack depth as an uncertain parameter is also addressed in some recent papers (Santoro and Muscolino, 2019; Santoro, Failla, and Muscolino, 2020), in which the method of interval analysis is adopted.

The goal of this chapter is the full probability characterization of any response random variable of some static uncertain structural systems. This characterization will be obtained in terms of the corresponding PDF through different applications of the PTM.

The content of this chapter is mainly based on some papers already published (Falsone and Laudani, 2019a; Falsone and Laudani, 2019b; Falsone and Laudani, 2020b) and is organized as follows. In section 3.2 it will be proposed a probabilistic method to evaluate the PDF response of linear uncertain structural systems. In particular, the proposed approach consists of combining the above-cited APDM with the PTM. Then, in section 3.3 will be shown how the proposed approach presented in section 3.2 gives exact results when the structures are statically determined. Section 3.4 is devoted to the determination of the exact closed-form solutions of redundantly constrained stochastic bending beams. Also for this problem, it will be possible to see an application of the PTM; in particular, the response PDF have been achieved thanks to the matching of the force method, for solving the redundancy, with the PTM. Finally, in section 3.5, an unpublished study about the static stochastic analysis of cracked Euler–Bernoulli beams will be presented. By applying the PTM, the stochastic response of beams characterized by the random amplitude of cracks and by the random cracks positions, besides of their amplitude, will be achieved. At last, in section 3.6, some concluding thoughts about the efficiency and the fundamental properties of the proposed approaches are given.

3.2 Matching the principal deformation mode method with the probability transformation method

This section deals with the probabilistic description of the random response of linear uncertain structural system when the uncertainties are modeled as random variables with assigned PDF. In particular, a novel approach is presented that allows the direct evaluation of the response PDF starting from the JPDF characterizing the structural uncertainties. It consists in matching adequately two methods, which are the Approximated Principal Deformation Modes method (APDM) and the PTM, in order to give an approach able to characterize the response of uncertain structural systems directly in terms of PDF and without using any expansive MCS.

3.2.1 A brief view on the APDM

The response of a discretized structural system having uncertain properties is governed by an equilibrium equation that can be expressed in the following form (Yamazaki, Shinozuka, and Dasgupta, 1988):

$$\mathbf{K}(\boldsymbol{\alpha})\mathbf{u}(\boldsymbol{\alpha}) = \mathbf{F} \tag{3.1}$$

where $\boldsymbol{\alpha} = [\alpha_1, \alpha_2, \cdots, \alpha_m]^T$ is the m-vector collecting the random uncertain parameters of the structural system, which is supposed to be defined through the knowledge of the JPDF, $p_{\boldsymbol{\alpha}}(\boldsymbol{\alpha})$; $\mathbf{K}(\boldsymbol{\alpha})$ is the structural stiffness $n \times n$ matrix depending on the uncertain parameters; $\mathbf{F}$ is the n-vector of the external actions, here considered deterministic, and $\mathbf{u}(\boldsymbol{\alpha})$ is the n-vector of the response displacements, depending on the structural parameters, and hence on $\boldsymbol{\alpha}$ besides of on the external actions. By following the work of Yamazaki et al, (Yamazaki, Shinozuka, and Dasgupta, 1988) the stiffness matrix can be expressed as follows:

$$\mathbf{K}(\boldsymbol{\alpha}) = \mathbf{K}_0 + \sum_{i=1}^{m} \mathbf{K}_i \alpha_i; \quad \mathbf{K}_0 = \mathbf{K}(\mathbf{0}) \tag{3.2}$$

where $\mathbf{K}_0$ is the deterministic stiffness matrix obtained setting $\alpha_i = 0$, with $i = 1, \cdots, m$, and $\mathbf{K}_i$ are deterministic matrices extracted from $\mathbf{K}(\boldsymbol{\alpha})$. The APDM owes its name to some properties of the principal deformation modes of the FE type used for the structural discretization. The basic idea of method lies on the following approximation of the response $\mathbf{u}(\boldsymbol{\alpha})$ of the system governed by Eq. 3.1:

$$\mathbf{u}(\boldsymbol{\alpha}) \approx \mathbf{u}_0 + \Delta\mathbf{u}(\alpha); \quad \Delta\mathbf{u}(\alpha) = \sum_{i=1}^{m} \mathbf{u}_i(\alpha_i) \tag{3.3}$$

where $\mathbf{u}_0$ is the deterministic response obtained setting $\alpha_i = 0$ with $i = 1, \cdots, m$, while $\mathbf{u}_i(\alpha_i)$ is the vector response obtained supposing that only the random variable α_i characterizes the structure uncertainties. It is important to note Eq. 3.3 is the generalization of the expression used in the first-order perturbation method, in which $\mathbf{u}_i(\alpha_i)$ is linear respect to α_i. Hence, they, $\mathbf{u}_0$ and $\mathbf{u}_i(\alpha_i)$, are the solutions of the following equations:

$$\mathbf{K}_0\mathbf{u}_0 = \mathbf{F}; \quad (\mathbf{K}_0 + \alpha_i\mathbf{K}_i)\mathbf{u}_i(\alpha_i) = -\alpha_i\mathbf{K}_i\mathbf{u}_0 \tag{3.4}$$

The authors have given the explicit closed-form expressions of the partial response vectors $\mathbf{u}_i(\alpha_i)$ that is,

$$\mathbf{u}_i(\alpha_i) = -\alpha_i\boldsymbol{\Phi}_i \left[\mathbf{I}_n + \alpha_i\boldsymbol{\Lambda}_i\right]^{-1} \boldsymbol{\Lambda}_i\boldsymbol{\Phi}_i^T\mathbf{F}, \tag{3.5}$$

where Λ_i and Φ_i are the eigenvalue and eigenvector matrices, respectively, of the matrix $\mathbf{K}_0^{-1}\mathbf{K}_i$, while $\mathbf{I}_n$ is the identity matrix of order n. This implies that the matrix into square brackets in Eq. 3.5 is diagonal, making very simple its inversion. Moreover, the number of the nonzero eigenvalues of the matrix $\mathbf{K}_0^{-1}\mathbf{K}_i$ is equal to the number of the structural principal modes directly affected by α_i, and this number, n_i is very small with respect to the number of degrees of freedom (DOF) n of the system, making simpler the evaluation of $\mathbf{u}_i(\alpha_i)$. In particular, if each random variable α_i influences only one FE, then the number of significant eigenvalues cannot be greater than the number of natural modes of the element that, in turn, depends on the type of FE chosen for discretizing the structure. For example, a bar-type FE is

characterized only by one natural deformation mode ($n_i = 1$); a beam-type FE (in a plane analysis) by two natural deformation modes ($n_i = 2$); a frame-type FE (in a plane analysis) by three natural deformation modes ($n_i = 3$). Hence, when ($n_i = 1$), the straightforward particularization of Eq. 3.5 gives

$$u_{i_j}(\alpha_i) = \Phi_{i_{jk}} \frac{\alpha_i \Lambda_{i_k} q_{0,i_k}}{1 + \alpha_i \Lambda_{i_k}} = \frac{a_{i_j} \alpha_i}{1 + b_{i_j} \alpha_i}, \tag{3.6}$$

where u_{i_j} is the jth of $\mathbf{u}_i$, Λ_{i_k} is the only nonzero eigenvalue of $\mathbf{K}_0^{-1}\mathbf{K}_i$ (the kth), and $\Phi_{i_{jk}}$ the corresponding element of the kth eigenvector. At last q_{0,i_k} is the kth element of the modal response vector $\mathbf{q}_{0,i} = \mathbf{\Phi}_i^{-1}\mathbf{u}_0$. The quantities a_{i_j} and b_{i_j} appearing in the last term of Eq. 3.6 can be obtained once that the eigenvalue problem of $\mathbf{K}_0^{-1}\mathbf{K}_i$ is solved. Alternatively, a more direct evaluation of these quantities can be obtained by solving twice Eq. 3.4 where two different deterministic sample values of α_i have been assigned.

When $n_i = 2$, as, for example, happens in the beam FE-discretized structures, the nonzero eigenvalues of the matrix $\mathbf{K}_0^{-1}\mathbf{K}_i$ are not more than two. In addition, in this case, the generic element of $\mathbf{u}_i$ can be obtained avoiding the solution of the eigenproblem, but using the following relationship:

$$u_{i_j}(\alpha_i) = \frac{a_{i_j} \alpha_i + b_{i_j} \alpha_i^2}{1 + c_{i_j} \alpha_i + d_{i_j} \alpha_i^2}, \tag{3.7}$$

where the four coefficients appearing can be obtained by solving four times Eq. 3.4, assigning four different deterministic sample values to the variable α_i.

At last, the generalization to the case $n_i = p$, p being the generic number of the structural principal deformation modes influenced by the uncertain parameter α_i is quite simple. In fact, Eqs. 3.6 and 3.7 can be generalized in

$$u_{i_j}(\alpha_i) = \frac{\sum_{k=1}^{p} b_{ik_j} \alpha_i^k}{1 + \sum_{k=1}^{p} d_{ik_j} \alpha_i^k}, \tag{3.8}$$

while $2p$ is the number of coefficients to be evaluated by means of $2p$ deterministic analyses.

It is important to note that, if the same random variable α_i affects more than one FE, as may happen, for example, when the random field of the uncertainties is discretized by a projection approach, (Sachdeva, Nair, and Keane, 2006) the APDM can be always used, but only by solving the eigenvalue problem for applying the expression given into Eq. 3.5.

In the work of Metropolis and Ulam, (Metropolis and Ulam, 1949) it has been evidenced that the application of the APDM is affected by an error $\mathbf{e}(\boldsymbol{\alpha})$ having the following expression:

$$\mathbf{e}(\boldsymbol{\alpha}) = -\sum_{i=1}^{m} \sum_{i \neq j=1}^{m} \alpha_i \mathbf{K}_i \mathbf{u}_j(\boldsymbol{\alpha}) \tag{3.9}$$

that evidences that it is strictly related to the presence of the cross-terms $\mathbf{K}_i\mathbf{u}_j$, neglected in the application of the present approach.Nevertheless, in the same work, the authors have shown that the accuracy level of this approach is good in many structural cases, even for relatively high levels of uncertainties, stressing a usually scarce influence of the cross terms on the response. For example, it has been shown

that, in the case of statically determined trusses, they are rigorously zero and the APDM method gives exact results.

3.2.2 Matching the APDM with the PTM

In this subsection, the APDM previously showed is applied combining it with the PTM. The approach that will be proposed allows finding an accurate probabilistic characterization of the response of a linear static structural system with uncertain parameters.

In Subsection 3.2.1, it has been shown that the application of the APDM method to the structural system governed by Eq. 3.1 implies the approximation of the response in the form

$$\mathbf{u}(\boldsymbol{\alpha}) \approx \mathbf{u}_0 + \sum_{i=1}^{m} \mathbf{u}_i(\alpha_i) = \mathbf{u}_0 + \Delta\mathbf{u}(\alpha). \tag{3.10}$$

The objective of this section is the evaluation of the JPDF $p_{\mathbf{u}_\Delta}(\mathbf{u}_\Delta)$ once that the JPDF $p_{\boldsymbol{\alpha}}(\boldsymbol{\alpha})$ is assigned. As seen in Subsection 3.2.1, it is possible to express the jth element of $\mathbf{u}_i(\alpha_i)$ as $u_{i_j} = h_{i_j}(\alpha_i)$ where the form of the function $h_{i_j}(\cdot)$ essentially depends on the number of principal deformation modes related to the FE type used for the structural discretization. In any case, the required inverse function $f_{i_j}(\cdot) \equiv h_{i_j}^{-1}(\cdot)$ can be always obtained in closed form. For example, for $n_p = 1$ and $n_p = 2$, the inverse relationships are given by

$$\begin{aligned} \alpha_i &= \frac{u_{i_j}}{a_{i_j} - b_{i_j} u_{i_j}}; \quad \alpha_i = \frac{a_{i_j} - c_{i_j} u_{i_j} \pm \sqrt{\Delta_{i_j}}}{2\left(b_{i_j} - d_{i_j} u_{i_j}\right)}; \\ \Delta_{i_j} &= \left(c_{i_j}^2 - 4d_{i_j}\right) u_{i_j}^2 + \left(4b_{i_j}^2 - 2a_{i_j} c_{i_j}\right) u_{i_j} + a_{i_j}^2 \end{aligned} \tag{3.11}$$

Eq. 3.11 shows that the inverse function has two values. In all the cases in which the inverse shows solutions, the PTM can be even applied, but the sum of the PDFs corresponding to the various solutions must be considered, that is,

$$p_{u_{i_j}}\left(u_{i_j}\right) = \sum_{k=1}^{n_p} \left| J_{f_{i_j}^{(k)}}\left(u_{i_j}\right) \right| p_{\alpha_i}\left(f_{i_j}^{(k)}\left(u_{i_j}\right)\right). \tag{3.12}$$

If the probabilistic characterization of the structural response component u_j is required, the application of the APDM method implies that

$$u_j = u_{0_j} + \sum_{i=1}^{m} u_{i_j}(\alpha_i) = u_{0_j} + \mathbf{1}^T \mathbf{u}_j(\boldsymbol{\alpha}) = u_{0_j} + u_{\Delta_j}(\boldsymbol{\alpha}) \tag{3.13}$$

where $\mathbf{1}$ is the m-vector whose components are all equal to one and $\mathbf{u}_j(\boldsymbol{\alpha})$ is the m-vector whose ith element is $u_{i_j}(\alpha_i)$. The JPDF of $\mathbf{u}_j(\boldsymbol{\alpha})$ is obtained by the application of the PTM and it has the following form:

$$p_{\mathbf{u}_j}\left(\mathbf{u}_j\right) = \left| \det\left[\mathbf{J}_{\mathbf{f}_j}\left(\mathbf{u}_j\right)\right] \right| p_{\boldsymbol{\alpha}}\left(\mathbf{f}_j\left(\mathbf{u}_j\right)\right). \tag{3.14}$$

It is easy to verify that the Jacobian $\mathbf{J}_{\mathbf{f}_j}$ is diagonal because the inverse functions $f_{i_j}(\cdot)$ depends only on the response component u_{i_j}. Hence, the following expression

is true:

$$\left|\det\left[\mathbf{J}_{\mathbf{f}}\left(\mathbf{u}_j\right)\right]\right| = \prod_{i=1}^{m}\left|\frac{df_{i_j}\left(u_{i_j}\right)}{du_{i_j}}\right|. \tag{3.15}$$

Eqs. 3.14 and 3.15 give the JPDF of the elements of the vector $\mathbf{u}_j(\boldsymbol{\alpha})$. In order to determine the JPDF of $u_{\Delta_j}(\boldsymbol{\alpha})$, Eq. 3.14 must be taken into account. It establishes a relation between the m-vector $\mathbf{u}_j(\boldsymbol{\alpha})$whose JPDF is given into Eq. 3.14, and the response component $u_{\Delta_j}(\boldsymbol{\alpha})$, whose pdf must be evaluated. At this purpose, the most efficient approach is that represented by the version of the PTM based on the use of the CF. In particular, the application of Eqs. 2.44 and 3.14 gives the following result:

$$M_{u_{\Delta_j}}(\omega) = (2\pi)^{m-1} M_{\mathbf{u}_j}(\boldsymbol{\theta})_{\boldsymbol{\theta}=\omega\mathbf{1}} \tag{3.16}$$

with $M_{\mathbf{u}_j}(\boldsymbol{\theta})$ being the JCF of the vector $\mathbf{u}_j$ that can be obtained by the Fourier transform of $p_{\mathbf{u}_j}\left(\mathbf{u}_j\right)$. In this way, the probabilistic characterization of the response quantity $u_{\Delta_j}(\boldsymbol{\alpha})$and, hence, of u_j is completed. If the joint probabilistic characterization of the two response components u_j and u_k is required, the application of the approach above described requires the evaluation of the joint CF $M_{u_{\Delta_j},u_{\Delta_k}}(\omega_1,\omega_2)$ at it is easy to express as follows:

$$M_{u_{\Delta_j},u_{\Delta_k}}(\omega_1,\omega_2) = (2\pi)^{m-2} M_{\mathbf{u}_j,\mathbf{u}_k}(\boldsymbol{\theta}_1,\boldsymbol{\theta}_2)_{\boldsymbol{\theta}_1=\omega_1\mathbf{1},\boldsymbol{\theta}_2=\omega_2\mathbf{1}}. \tag{3.17}$$

The JCF $M_{\mathbf{u}_j,\mathbf{u}_k}(\boldsymbol{\theta}_1,\boldsymbol{\theta}_2)$ is the double Fourier transform of the JPDF $p_{\mathbf{u}_j,\mathbf{u}_k}(\mathbf{u}_j,\mathbf{u}_k)$ that can be obtained by applying the PTM to a transformation law in which the m-vector $\boldsymbol{\alpha}$ is the input and the two m-vectors $\mathbf{u}_j$ and $\mathbf{u}_k$ represent the output. Hence, in this case, the number of input elements is smaller than the number of output elements and the version of PTM expressed into Eqs. 2.33-2.36 be used. This implies that the expression of $p_{\mathbf{u}_j,\mathbf{u}_k}(\mathbf{u}_j,\mathbf{u}_k)$, particularizing Eq. 2.36 to this case, is given by

$$\begin{aligned} p_{\mathbf{u}_j,\mathbf{u}_k}\left(\mathbf{u}_j,\mathbf{u}_k\right) &= \left|\det\left[\mathbf{J}_{\mathbf{f}_j}\left(\mathbf{u}_j\right)\right]\right| p_{\boldsymbol{\alpha}}\left(\mathbf{f}_j\left(\mathbf{u}_j\right)\right)\delta\left(\mathbf{u}_k-\mathbf{h}_k\left(\mathbf{f}_j\left(\mathbf{u}_j\right)\right)\right) \\ &= \prod_{i=1}^{m}\left|\frac{df_{i_j}\left(u_{i_j}\right)}{du_{i_j}}\right| p_{\boldsymbol{\alpha}}\left(\mathbf{f}_j\left(\mathbf{u}_j\right)\right)\delta\left(\mathbf{u}_k-\mathbf{h}_k\left(\mathbf{f}_j\left(\mathbf{u}_j\right)\right)\right). \end{aligned} \tag{3.18}$$

This approach can be generalized to higher-order probabilistic characterizations of the response.

3.2.3 Numerical example

The effectiveness of the proposed method is tested through some numerical examples in which the structural uncertainty is always due to the characteristics of the Young modulus of each FE in which the structural system has been discretized. In particular, it is assumed that the Young modulus related to the generic FE can be expressed as

$$E_i = E_0\left(1+\alpha_i\right); \quad i = 1,2,\cdots,m \tag{3.19}$$

with m being the number of the FEs used in the discretization, while E_0 is the mean value of the Young modulus. In all the examples, the responses of interest are the structural displacements and/or the internal forces in some fixed sections. They are certainly random and must be characterized through the definition of their PDFs.

The examples reported have been chosen in such a way that the corresponding FE type are characterized by a different number of principal deformation modes, n_p.

3.2.3.1 *Bar-type FE*

As first example, the truss structure represented in Fig. 3.1 is taken into account. All the bars have the same cross-section $(1 \times 10^{-4} m^2)$ and a random Young modulus defined as in Eq. 3.19, where $i = 1, \cdots, 15$ and $E_0 = 2.10 \times 10^8 kN/m^2$. The random variables α_i are assumed to be uniformly distributed in the range $[-a, a]$. It is important to note that, in spite of the apparent simplicity of this kind of distribution, it has strongly non-Gaussian features, and hence, it is an interesting choice to test the efficiency of the proposed approach. Three static horizontal deterministic forces are applied: a force $F = 10kN$ applied to node C, a force $2F$ applied to node B and a force $3F$ applied to the node A.

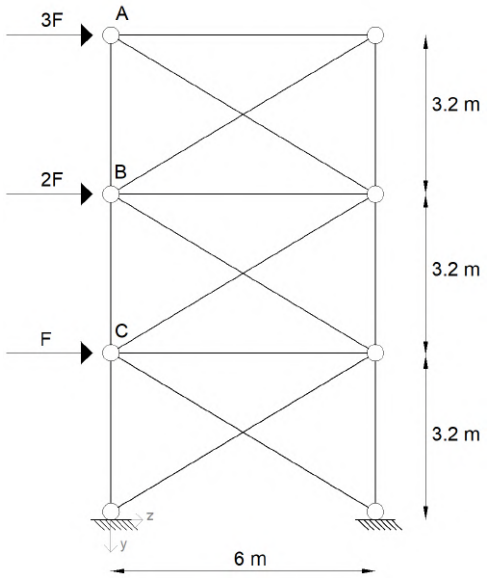

FIGURE 3.1: The truss-structure.

With the aim of probabilistically characterizing the horizontal displacement of node A through its PDF $p_{u_A}(u_A)$, the approach proposed in this work, particularized to the case in which $n_p = 1$, is applied. The JPDF $p_{\mathbf{u}_A}(\mathbf{u}_A)$ of the vector $\mathbf{u}_A(\boldsymbol{\alpha})$ has been obtained by using Eqs. 3.14 and 3.14, where, from Eq. 3.11,

$$\alpha_i = \frac{u_{i_A}}{a_{i_A} - b_{i_A} u_{i_A}} \rightarrow u_{i_A} = \frac{a_{i_A} \alpha_i}{1 + b_{i_A} \alpha_i} = f_{i_A} \alpha_i. \tag{3.20}$$

After having obtained the JCF $M_{\mathbf{u}_A}(\boldsymbol{\theta})$, it has been possible to evaluate the CF $M_{u_A}(\omega)$by the use of Eq. 3.16. Lastly, the corresponding PDF has been obtained by its inverse Fourier transform.

In Fig. 3.2, the PDF $p_{u_A}(u_A)$ is reported in the two cases of $a = 0.15$, corresponding to a standard deviation $\sigma_{\alpha_i} = 0.09$, and of $a = 0.35$ with $\sigma_{\alpha_i} = 0.20$, respectively. It is to be stressed that the level of uncertainty related to these values of standard deviations is relatively high, above all for the second distribution. The results obtained by the proposed approach (APDM+PTM) are compared with those provided by the classic MCS (5×10^5samples) and with those obtained by applying the MCS to the results of the APDM, that is to Eq. 3.6 (APDM+MCS). The graphics of Fig. 3.2

show the good level of accuracy of the proposed procedure. Moreover, the use of the (APDM+PTM) approach has allowed a computing time saving of 98.5% respect to the MCS and of 96% respect to the (APDM+MCS).

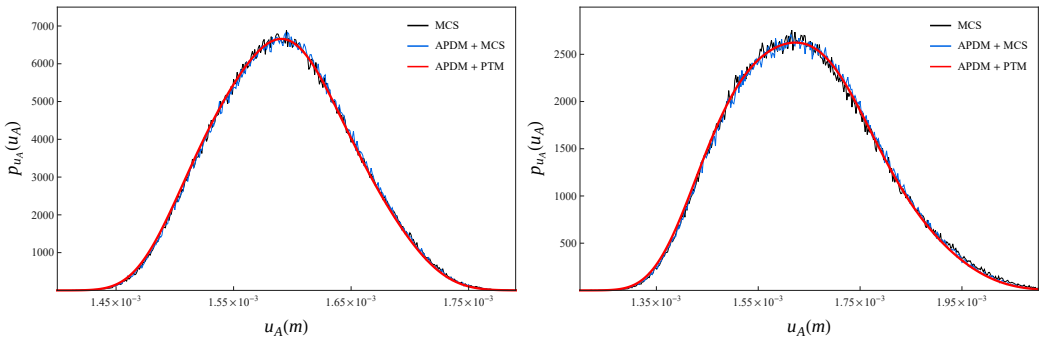

FIGURE 3.2: Probability density function of the horizontal displacement u_A for $\alpha_i \in [-0.15, 0.15]$ and for (B) $\alpha_i \in [-0.35, 0.35]$.

The evaluation of the JPDF of two response components, the horizontal displacements of nodes A and B, has required the knowledge of the JPDF $p_{\mathbf{u}_A\mathbf{u}_B}(\mathbf{u}_A, \mathbf{u}_B)$, that has been obtained by the application of Eq. 3.18. The Fourier transform of this function has given the corresponding JCF, from which it is has been possible to find $M_{u_A u_B}(\omega_1, \omega_1)$ by using Eq. 3.18. At last, the Fourier transform of this function has produced the JPDF of interest $p_{u_A u_B}(u_A, u_B)$.

In Figs. 3.3 and 3.4, the JPDF of the displacements of nodes A and B, $p_{u_A u_B}(u_A, u_B)$, and of nodes A and C, $p_{u_A u_C}(u_A, u_C)$, are shown.

From the study of these figures, the greater level of correlation between the random variables u_A and u_B than that between u_A and u_C can be appreciated, due to the fact that nodes A and B are directly connected by a bar, on the contrary of nodes A and C.

3.2.3.2 *Beam-type FE*

The second example considered in this work is the clamped-clamped beam shown in Fig. 3.5. Its length is $L = 8\ m$, while its cross-section is rectangular with area equal to $1.5 \times 10^{-3}\ m^2$. The external action is a uniformly distributed deterministic load with intensity $q = 100\ kN/m$. The discretization is made through four beam-type FEs of equal length. The random Young modulus is defined as in Eq. 3.19, with $i = 1, \cdots, 4$ and $E0 = 3 \times 10^7\ kN/m^2$. As each FE is characterized by two natural deformation modes $(n_p = 2)$, two different inverse functions $f_{i_j}^{(1)}(\dots)$ and $f_{i_j}^{(2)}(\dots)$ have been obtained for it (Eq. 3.11) and the JPDF $p_{\mathbf{u}_j}(\mathbf{u}_j)$ has been obtained by the following relation:

$$p_{\mathbf{u}_j}(\mathbf{u}_j) = \sum_{k=1}^{n_p} \left| \mathbf{J}_{\mathbf{f}_j^{(k)}}(\mathbf{u}_j) \right| p_{\boldsymbol{\alpha}}\left(\mathbf{f}_j^{(k)}(\mathbf{u}_j)\right). \tag{3.21}$$

At this point, the application has followed the same steps considered for the truss in the previous subsection. For this example, some different distributions of the random variables have been considered. Firstly, the random variables α_i has marginal PDF uniformly distributed in the range $[-0.3, 0.3]$ $(\sigma_{\alpha_i} = 0.173)$ and exponential correlation function $\rho(\Delta x) = \exp(-|\Delta x|/\lambda)$, Δx being the distance between two

cross-sections of the beam and λ the correlation length of the random field characterizing the uncertainties. Two several values of the correlation length have been considered: $\lambda = 0.3L$ and $\lambda = 2L$. Figs. 3.6 and 3.7 show the corresponding PDF, $p_{u_C}(u_C)$, of the central node deflection and the PDFs of the bending moment, $p_M(M)$, and of the shear force, $p_T(T)$, at the left extreme node. As second kind of distribution of uncertainties, the random variables α_i have been considered to be zero-mean Gaussian variables, with standard deviation $\sigma_{\alpha_i} = 0.15$. In Fig. 3.8, the PDF $p_{u_C}(u_C)$ is reported, making the comparison between the case of independent α_i and the case in which they are correlated with the previous exponential correlation function $\rho(\Delta x)$, with $\lambda = 2L$. Even for this example, the good level of accuracy can be easily verified in both the cases of independent and correlated uncertainty variables. With reference to the computational effort, the use of the (APDM+PTM).

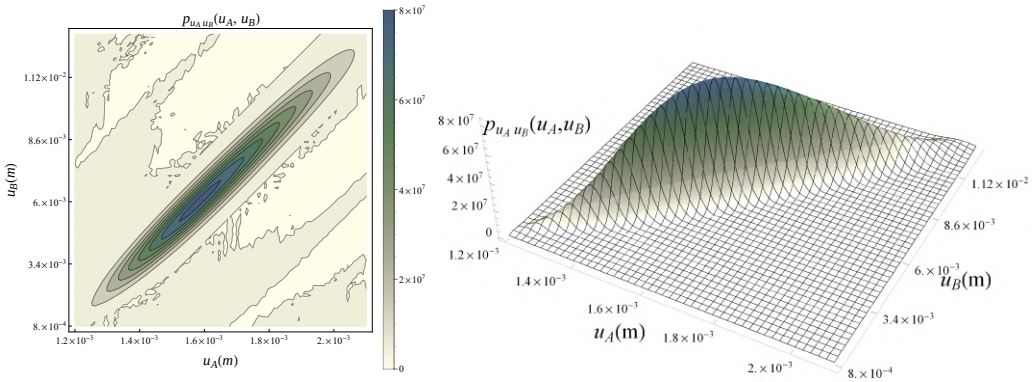

(A)

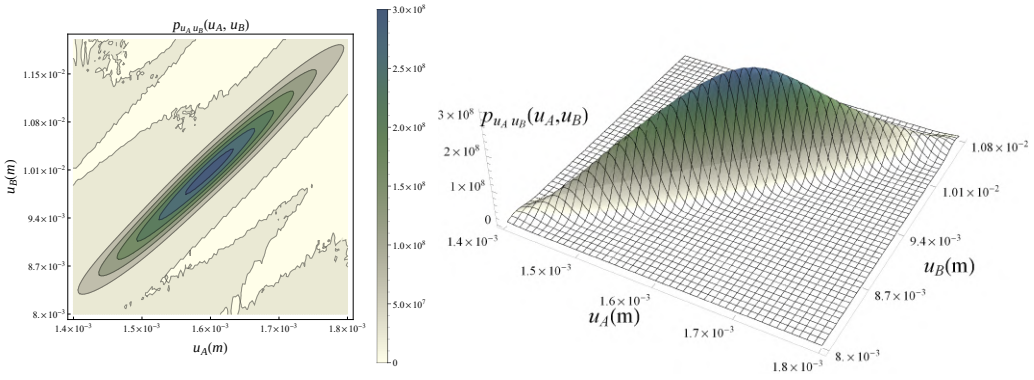

(B)

FIGURE 3.3: Joint probability density function of horizontal displacements of nodes A and B for uniformly distributed uncertainties: (A) $\alpha_i \in [-0.15, 0.15]$ (B) $\alpha_i \in [-0.35, 0.35]$.

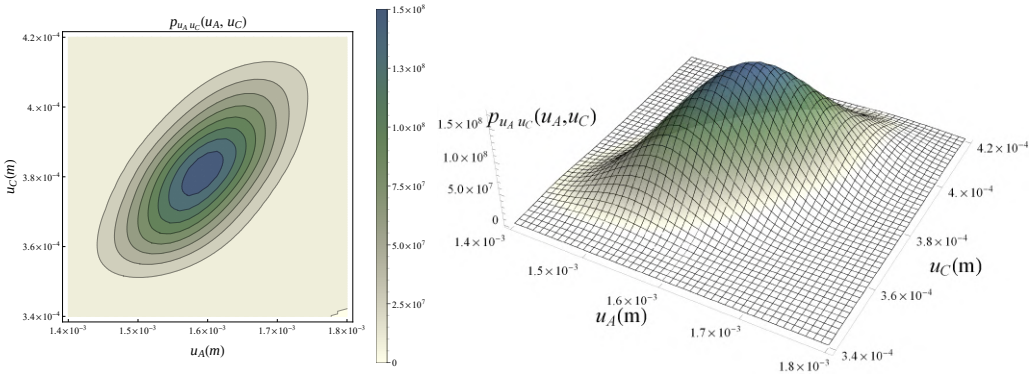

(A)

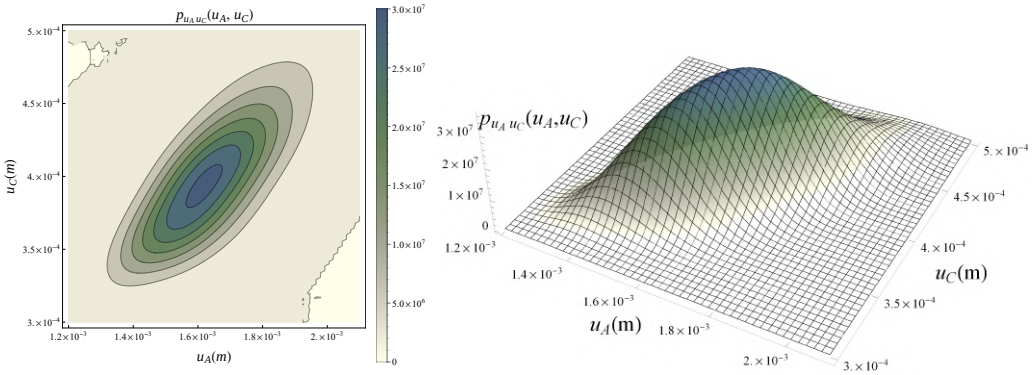

(B)

FIGURE 3.4: Joint probability density function of horizontal displacements of nodes A and C for uniformly distributed uncertainties: (A) $\alpha_i \in [-0.15, 0.15]$ (B) $\alpha_i \in [-0.35, 0.35]$.

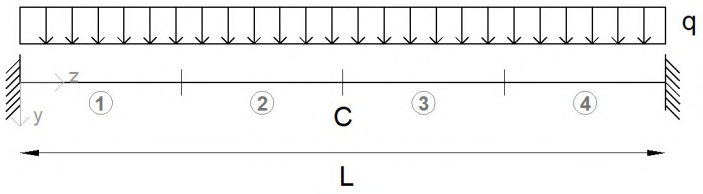

FIGURE 3.5: The Clamped-clamped beam.

Finally, the behavior of the response PDFs near the tail region has been analyzed. From the analysis of the results shown in Fig. 3.9, one can appreciate how the good level of accuracy of the proposed approach is maintained even in the tail region. This is confirmed by the failure probability values obtained by either the (APDM+MCS) approach and the (APDM+PTM) one, in the case of correlated Gaussian uncertainties, that are $P_f = 5 \times 10^{-7}$ and $P_f = 6 \times 10^{-7}$, respectively, having fixed a failure value of $u_{C_f} = 1.8 \times 10^{-2} m$.

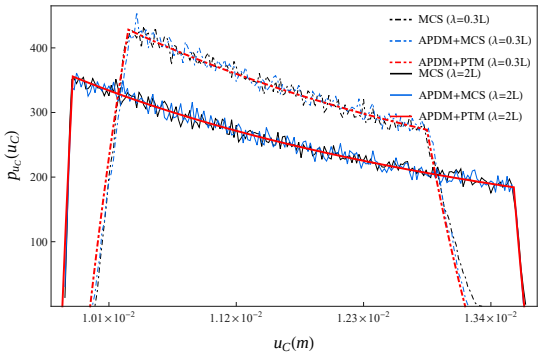

FIGURE 3.6: Probability density function of the central node displacement u_C for uniformly distributed uncertainties for $\lambda = 0.3L$ and $\lambda = 2L$.

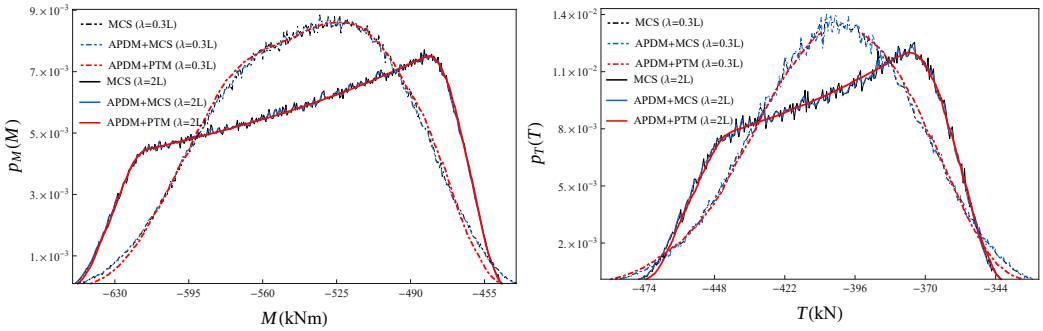

FIGURE 3.7: Probability density functions of the (A) bending moment and the (B) shear force at the left constrained extreme of the beam for uniformly distributed uncertainties for $\lambda = 0.3L$ and $\lambda = 2L$.

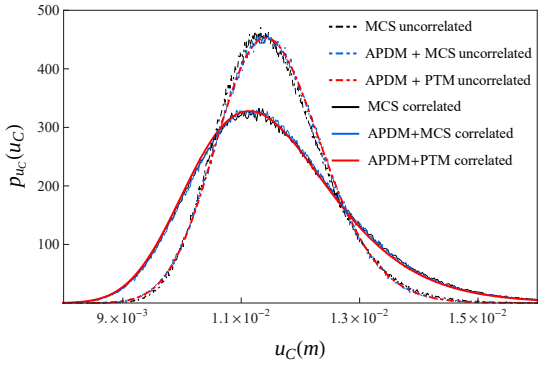

FIGURE 3.8: Probability density function of the central node displacement u_C for Gaussian distribution in the two hypothesis of uncorrelated and correlated uncertainties.

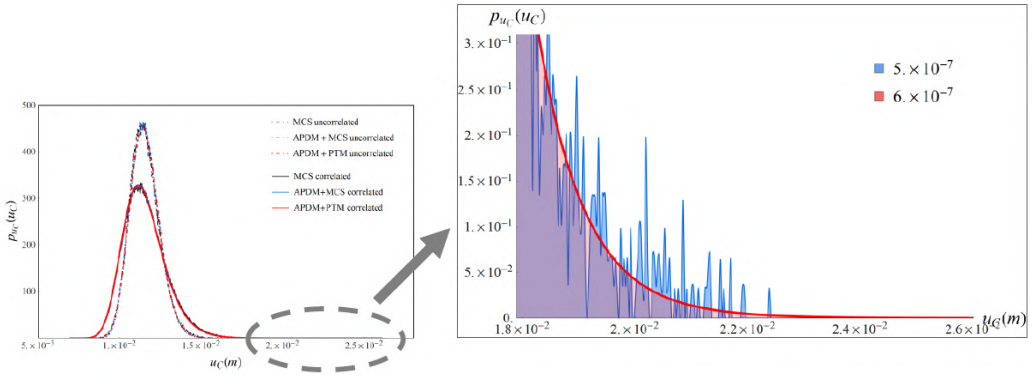

FIGURE 3.9: Behavior of probability density function of the central node displacement u_C near the tail region for Gaussian correlated uncertainties.

3.2.3.3 *Frame-type FE*

The frame structure shown in Fig. 3.10 has been considered. All the columns have the same cross-section, with area $A_{column} = 1.5 \times 10^{-1} m^2$ and inertia moment $I_{column} = 3.125 \times 10^{-3} m^4$, while all the horizontal elements are characterized by a cross-section with area $A_{beam} = 2.8 \times 10^{-1} m^2$ and inertia moment $I_{beam} = 1.143 \times 10^{-2} m^4$. The system is forced by three static deterministic forces, of the same intensity, $F = 1000$ kN, applied at each plane. A random Young modulus is defined as in Eq. 3.19, with $i = 1, \cdots, 9$ and $E_0 = 3 \times 10^7$ kN/m^2. The application of the (APDM+PTM) approach follows the same steps considered in the previous two subsections, paying attention to the fact that the frame-type FE is characterized by $n_p = 3$. In this case, the random variables α_i have been chosen to be zero-mean Gaussian and characterized by a standard deviation $\sigma_{\alpha_i} = 0.15$. Moreover, in order to take into account the correlation that may exist between the mechanical properties of close FEs, a correlation coefficient equal to 0.5 has been assumed for elements that have one node in common, living uncorrelated all the other ones. The PDFs of the horizontal displacement and of the moment of node C are given in Fig. 3.11, for independent correlated uncertainties, respectively. Even in this case, the good level of accuracy of the proposed approach, respect to the MCS and the (APDM+MCS), ones is clear. At the same time, the computational effort has been reduced of 64% respect to the application of the MCS and of 50% respect to the application of the (APDM+MCS).

3.2.3.4 *Two-dimensional FE-discretized structure*

The last example here considered is the plane-stress problem represented in Figure 3.12. The two-dimensional FEs used for the discretization are the triangular element with three vertex nodes and six DOFs.

The following data are assumed as known (deterministic) input parameters: the panel length is $L = 4.5$ m, the height is $H = 9$ m, the Poisson coefficient is equal to 0.2, and the linear distributed load has a maximum intensity $q = 5000$ kN/m. The Young modulus is uncertain and modeled by a two-dimensional stochastic field with constant mean value $E_0 = 3 \times 10^7$ kN/m^2 and expressed as

$$E_i = E_0 \left(1 + \alpha(x, y)\right). \tag{3.22}$$

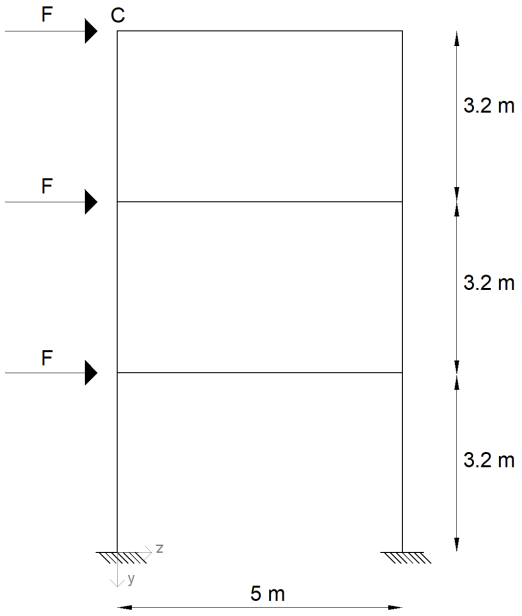

FIGURE 3.10: The frame structure.

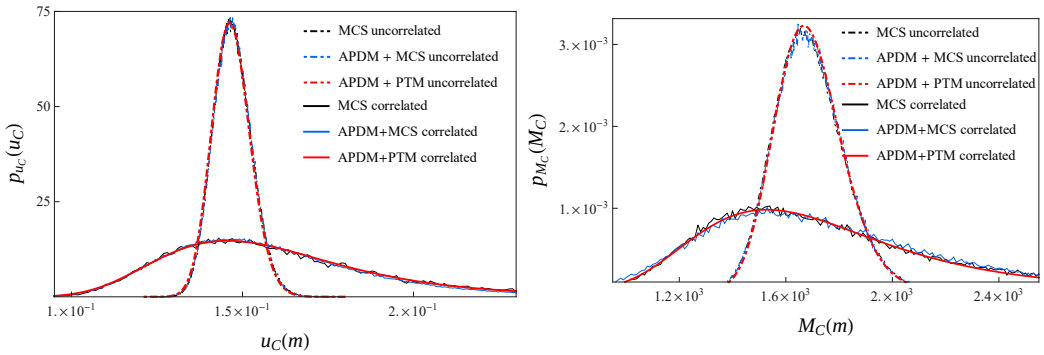

(A) (B)

FIGURE 3.11: Probability density function of the (A) horizontal displacements and (B) moment of nodes C for Gaussian distribution in the two hypothesis of uncorrelated and correlated uncertainties.

The zero mean two-dimensional stochastic field $\alpha(x, y)$ is assumed to be as a Gaussian one with squared exponential covariance function

$$\Sigma_\alpha\left(|\mathbf{\Delta x}|\right) = \sigma_\alpha^2 \rho\left(|\mathbf{\Delta x}|\right) = \sigma_\alpha^2 \exp\left(\frac{|\mathbf{\Delta x}|}{\lambda}\right)^2, \tag{3.23}$$

where $|\mathbf{\Delta x}|$ is the distance between two points of the field, $\sigma_\alpha = 0.15$ and $\lambda = 0.25L$. The random field has been discretized by using the midpoint method, (Liu, Mani, and Belytschko, 1987) obtaining that the uncertain Young modulus is defined by eighteen correlated random variables α_i. These FEs are characterized by three principal deformation modes $(n_p = 3)$. The PDFs of the vertical and horizontal displacements of node 13, are depicted in Fig. 3.13. In this case, the use of the (APDM+PTM) approach has allowed a computing time saving of 70% respect to the MCS and of 60% respect to the (APDM+MCS).

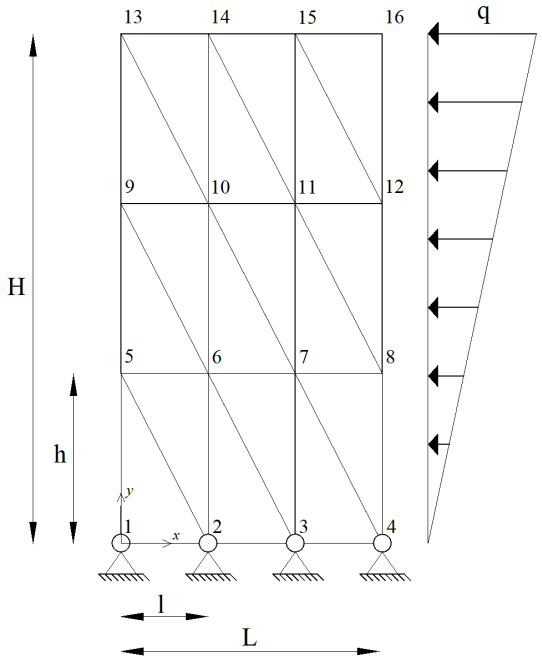

FIGURE 3.12: The plate structure.

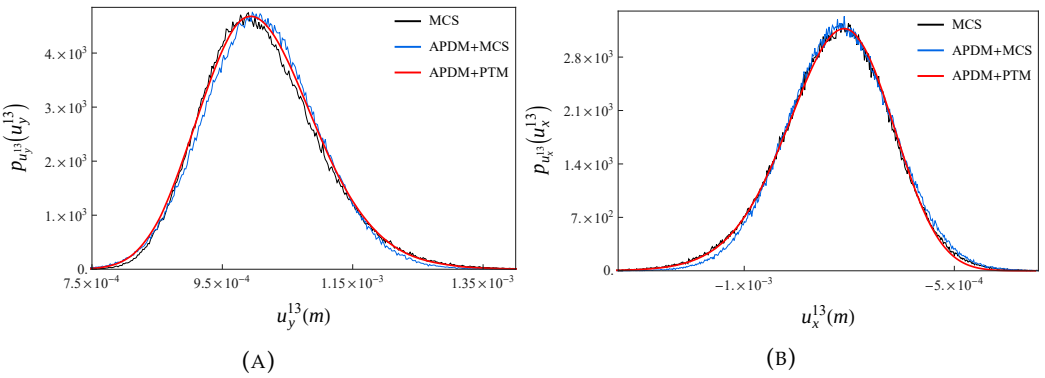

FIGURE 3.13: Probability density function of the (A) vertical and (B) horizontal displacement of node 13.

3.2.4 Some remarks

The APDM and the PTM have been adequately matched in order to implement a procedure able to characterize the response of linear uncertain structures directly in terms of PDF. This has been possible due to the properties of the APDM, in finding explicit relationships between the stochastic structural response and the random variables representing the uncertainties, and of the PTM, in finding the explicit relationships in terms of PDFs between input and output variables of a given transformation law. This approach can be applied to discretized structural systems, paying attention to the FE type used; in fact, in function of the approach used for discretizing the random field related to the uncertainties, the number n_p of principal deformation modes of the FEs influences the form of the expressions to be used.

The application of the (APDM+PTM) approach to some simple examples, in which various FE types have been used, depending on the structure-type considered, has always shown its good properties, in terms of both accuracy and computational effort. In particular, these properties have been revealed even for medium-high level of uncertainties, respect to those usually considered in many approaches in the literature.

3.3 Exact response probability density functions of some uncertain structural systems

The aim of this section is defining an approach able to give exact results in terms of the response PDF for particular class uncertain structures. The uncertain structures have been identified in the discretized statically determined ones and the probability approach of the section 3.2 has been applied.

In the previous section has been shown a probabilistic approach identified in the coupling of the approximated principal deformation modes method (APDM) and of the PTM. The first one gives the explicit relationships between the response variables and the uncertainty ones, in particular, it is will be shown that the relationships are exact when the structures are statically determined. Then, the PTM allows determining the explicit relationship between the PDFs of the response and of the uncertainty variables. It will be shown the results of some applications have confirmed the goodness of these choices and that the proposed approach gives always exact results for both correlated and uncorrelated uncertainty random variables.

3.3.1 Proposed approach

In subsection 3.2.1 the APDM has been presented. This method is remarkable for the purpose of this section because in the case of statically determinate structures it gives the exact explicit relationships between the response components and the random variables defining the structural uncertainties (Falsone and Impollonia, 2004). For these structures the APDM becomes the Exact Principal Deformation Mode approach (EPDM) (approximated $\rightarrow$ exact). In this way a class of structures for which it is possible to find exact close relationships between response quantities and uncertainty quantities has been identified.

In the subsection 3.2.1 it has been evidenced that the APDM is affected by an error $\mathbf{e}(\boldsymbol{\alpha})$ having the following expression:

$$\mathbf{e}(\boldsymbol{\alpha}) = -\sum_{i=1}^{m}\sum_{i\neq j=1}^{m} \alpha_i \mathbf{K}_i \mathbf{u}_j(\boldsymbol{\alpha}) \tag{3.24}$$

that shows of being strictly related to the presence of the cross-terms $\mathbf{K}_i\mathbf{u}_j$, neglected in the APDM. These cross-terms may assume an important physical significance remembering that $\mathbf{u}_j$ is the structural displacement when only the random variable α_j affects the structure. Consequently, they represent the nodal forces arising in a structure characterized by the stiffness matrix $\mathbf{K}_i$ and subjected to the nodal displacements $\mathbf{u}_j$. Then, if the discretized structure is statically determinate, these terms are rigorously zero, for $i \neq j$, and no error is related to the use of Eq. 3.3. Hence, for statically determinate discretized structures, the APDM becomes the EPDM approach, giving the exact relationships between the structural response and the random variables describing the uncertainties.

Then, the next step is the evaluation of the exact response PDF through the matching of the EPDM with the PTM as it was shown in subsection 3.2.2.

3.3.2 Numerical example

The numerical examples reported in this section aim to verify and highlight the fundamental statement of the present work showing that, for statically determinate discretized uncertain structures, the joint use of the EPDM and of the PTM allows to obtain the exact response PDFs. It is assumed that, in all the considered examples, the structural uncertain parameter is represented by the Young modulus of each FE in which the structural system has been discretized. In particular, the Young modulus of the generic FE is modelled as in Eq. 3.19. The examples reported have been chosen in such a way that the corresponding FE typology are characterized by a different number of principal deformation modes, n_p.

3.3.2.1 *Bar type FE*

For this FE typology, two examples of statically determinate structural systems are taken into account. The truss-structure represented in Fig. 3.14 is first considered. It is characterized by the following geometrical and mechanical deterministic parameters: $L = 5\ m$, $H = 4\ m$; all the bars have the same cross-sections area $(4 \times 10^{-2} m^2)$ and a random Young modulus defined as in Eq. 3.19, where $i = 1, \cdots, 9$ and $E_0 = 2.10 \times 10^8\ kN/m^2$. The random variables α_i are assumed to be uniformly distributed in the range $[-0.30, 0.30]$. The truss-structure is forced by static deterministic forces: a force $F = 10\ kN$ applied to the nodes B and D, and a force $2F$ applied to the node C.

The results presented here confirm that the proposed approach leads to the exact expression of $\mathbf{u}(\boldsymbol{\alpha})$, and, hence, by applying Eq. 3.16, to the exact PDF of any responses of interest. The PDFs of some nodal displacements have been obtained, comparing the results obtained by the proposed approach and those by Monte Carlo simulations (for these last ones 5×10^5 samples have been considered). In Fig. 3.15, the PDF of the vertical displacement of node C, $p_{u_y^C}\left(u_y^C\right)$, and the PDF of the horizontal displacement of node E, $p_{u_x^E}\left(u_x^E\right)$, are, respectively, reported.

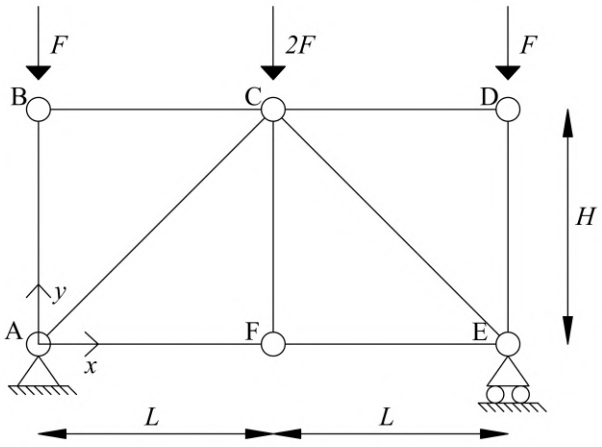

FIGURE 3.14: The truss-structure.

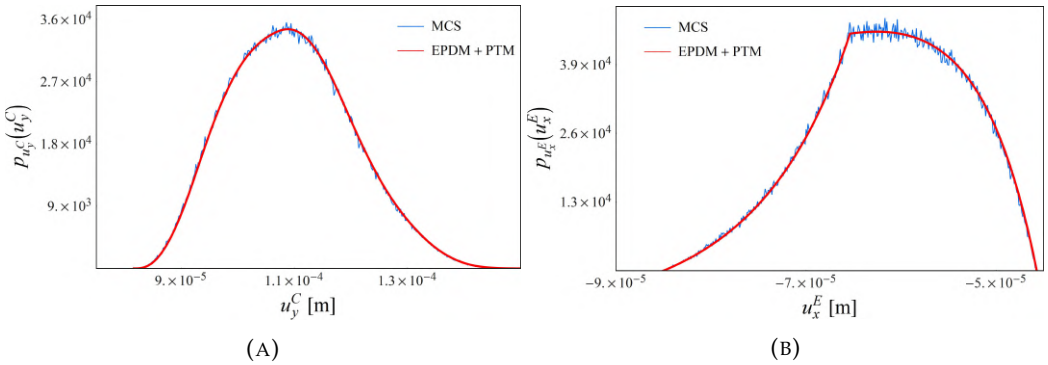

(A) (B)

FIGURE 3.15: PDF of the vertical displacement of node C (A) and of the horizontal displacement of node E (B).

Successively, the statically determined beam represented in Fig. 3.16 is taken into account. Its length is $L = 8\ m$, while its cross section is rectangular with area equal to $1.5 \times 10^{-3} m^2$. The external actions are a uniformly distributed axial load with intensity $q = 150\ kN/m$ and a static deterministic axial force applied to the free end with intensity $F = qL$. Due to the load characteristics, the discretization can be made by means of bar-type FEs. In particular, four FE of equal length have been used. The random Young modulus is defined as in Eq. 3.19, with $i = 1, \cdots, 4$ and $E_0 = 3 \times 10^7 kN/m^2$.

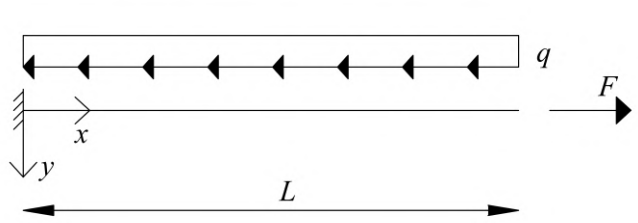

FIGURE 3.16: Cantilever beam (bar type FE).

In Fig. 3.17 the PDF of the horizontal displacement of the free end is reported for the case that the random variables α_i are assumed to be uniformly distributed in the range $[-0.4, 0.4]$. By inspection of Fig. 3.17 the goodness of the comparison is clear, even if a high level of uncertainty is present in the beam Young modulus.

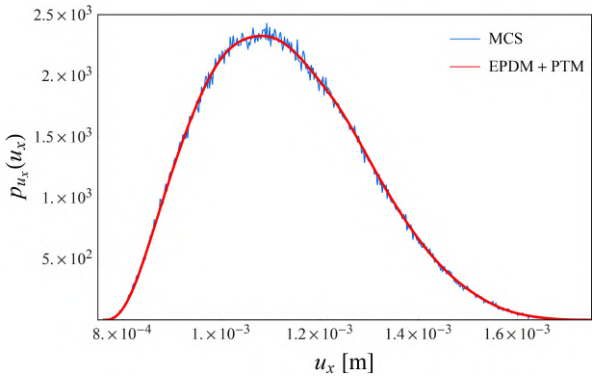

FIGURE 3.17: PDF of the horizontal displacement of the free end.

3.3.2.2 Beam-type FE

The statically determinated cantilever beam under the deterministic transversal load $q = 50\ kN/m$ is now considered. The beam (Fig. 3.18) differs from the previous one only for the condition of load and it is characterized by an inertia moment equal to $I = 3.125 \times 10^{-3} m^4$. Two different distributions of random variables α_i are examined: firstly, they have been assumed to be zero-mean, Gaussian, independent and defined by a variance $\sigma^2 = (0.20)^2$; in the second case, the same random variables are considered as correlated following the given correlation law:

$$\rho = \exp\left(-\frac{\Delta x}{\lambda}\right) \tag{3.25}$$

where Δx is the distance between two points along the beam axes and $\lambda$is the correlation length, assumed in this example equal to $\lambda = 0.8L$.

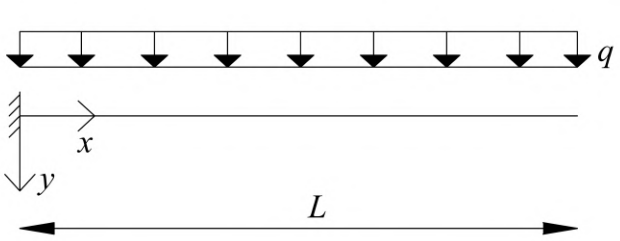

FIGURE 3.18: Cantilever beam (beam-type FE).

The discretization is made by means of four beam-type FEs of equal length. The midpoint method is adopted to discretise the random field by four random variables α_i, so that a random variable is representative of the fluctuation of the Young modulus in each element.

By the application of the EPDM + PTM approach and paying attention to the fact that the beam-type FE is characterized by $n_p = 2$, it is possible obtain the exact PDF of any transversal displacement. The PDFs of the vertical displacement and of the rotation of the free end section are given in Figs. 3.19 and 3.20 for both the cases of uncorrelated and correlated random variables α_i. Once again the EPDM + PTM approach is compared with the MCS applied in Eq. 3.1, performed by 5×10^5 samples. Even in this example, the results are practically overlapped.

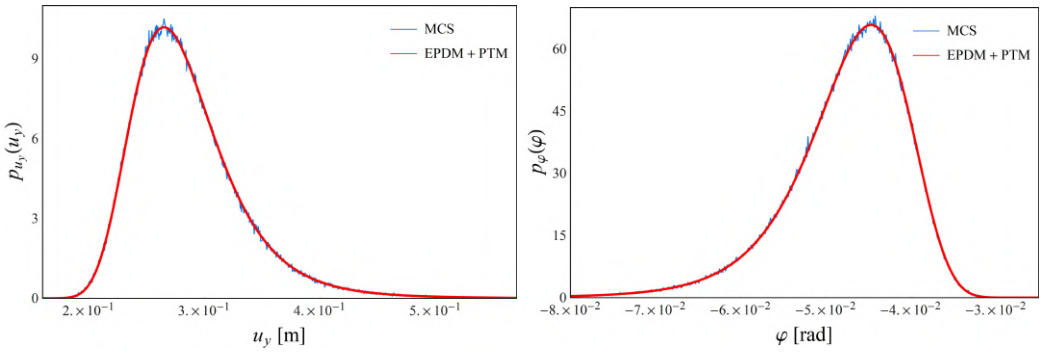

FIGURE 3.19: PDF of the vertical displacement (A) and rotation (B) of the cantilever free end; uncorrelated random variables α_i.

It is important to note that the proposed gives the exact results even when the uncertainties are strongly correlated, as it must be, due to the fact that the correlation properties of the uncertainties have no influence on the fundamental steps of the EPDM + PTM approach, but only on the definition of the input JPDF.

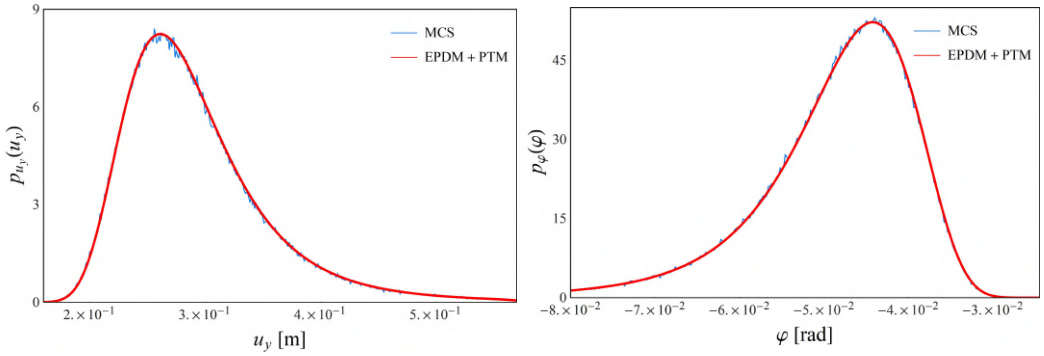

(A) (B)

FIGURE 3.20: PDF of the vertical displacement (A) and rotation (B) of the cantilever free end; correlated random variables α_i.

3.3.2.3 *Two-dimensional FE*

As the last example, the two-dimensional panel under plane stress of Fig. 3.21 has been analysed utilising the two-dimensional FE. The two-dimensional element considered herein is the simple triangular element with 6 DOF (each node has two degrees of freedom, the displacements u_x and u_y). The following data assumed as known (deterministic) input parameters: the length is $L = 6\ m$, the height is $H = 3\ m$, the Poisson coefficient is equal to 0.2 and the external actions are two uniformly distributed loads with intensity $p = q = 1000\ kN/m$. The Young modulus is uncertain and modelled by a two-dimensional stochastic field with constant mean value $E_0 = 3 \times 10^7\ kN/m^2$ and expressed as:

$$E = E_0 \left(1 + \alpha\left(x, y\right)\right). \tag{3.26}$$

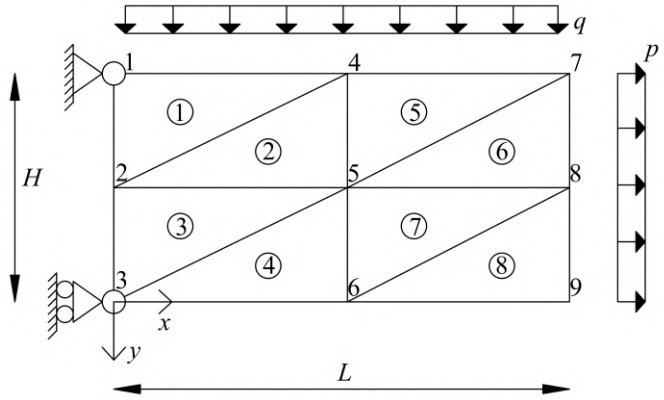

FIGURE 3.21: Two-dimensional panel.

The zero mean two-dimensional stochastic field $\alpha(x,y)$ is assumed as Gaussian with the squared exponential covariance function:

$$\Sigma_\alpha(|\Delta x|) = \sigma^2\rho(|\Delta x|) = \sigma^2 \exp\left(-\frac{|\Delta x|}{\lambda}\right)^2 \tag{3.27}$$

where $|\Delta x|$ is the distance between two points of the field, σ^2 is the variance and $\lambda = 0.2H$ is the correlation coefficient. The midpoint method is adopted to discretise the random field by eight random variables α_i, so that a random variable is representative of the fluctuation of the Young modulus in each element. Three natural deformations are present in the generic element, hence, for this example $n_p = 3$.

The PDFs of the horizontal and vertical displacement of the node 8, respectively, are depicted in Figs. 3.22, according to the proposed method and for $\sigma^2 = (0.1)^2$. The comparison has been made with respect to the classical Monte Carlo simulation, performed by 2×10^5 samples.

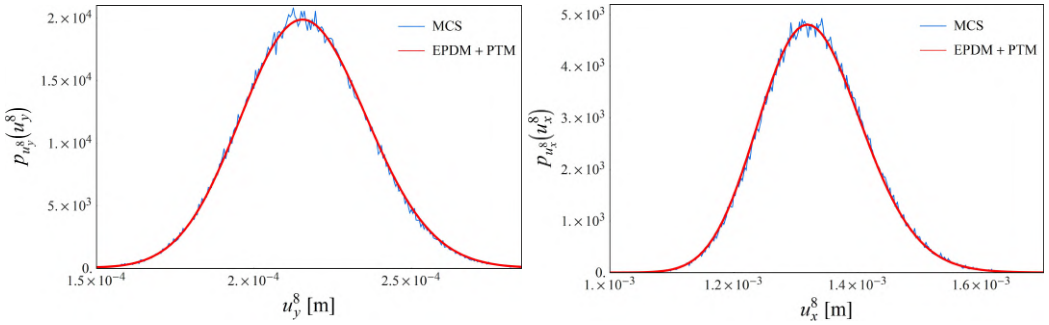

(A) (B)

FIGURE 3.22: PDF of the vertical (A) and horizontal (B) displacement of node 8. Correlated random variables α_i.

In order to confirm that the correlation assumptions have no influence on the capability of the proposed approach to give the exact response PDF for statically determined uncertain structures, the same panel before studied is considered under the assumption of uncorrelated random variables α_i. The confirming results are represented in Figs. 3.23.

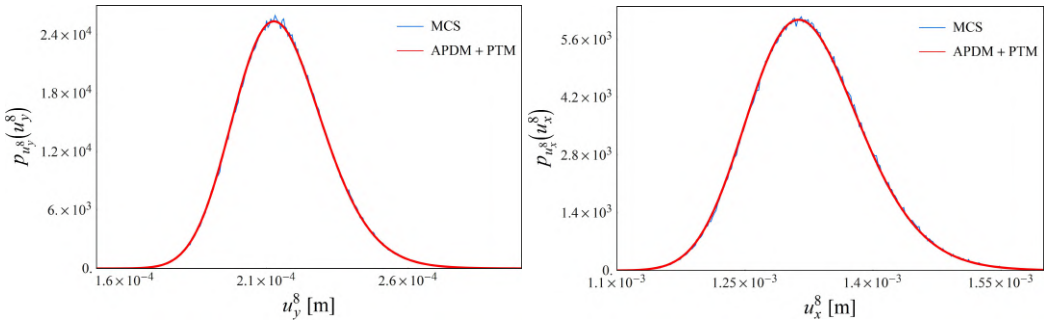

(A) (B)

FIGURE 3.23: PDF of the vertical (A) and horizontal (B) displacement of node 8. Uncorrelated random variables α_i.

3.3.3 Some remarks

The goal of identifying a strategy for the evaluation of the exact response PDF of discretized statically determinate uncertain structures has been reached. This thanks to the application of the EPDM, which gives exact results if applied to the statically determinate structures, coupled with the application of the PTM able to give explicitly the response PDF once that the relationships between the response random variables and the uncertainty random variables are explicitly given. When the uncertain structure is discretized by a FE approach, attention must be paid to the FE type used because it determines the number n_p of principal deformation modes influenced by each uncertainty random variable and this number influences the form of the expressions to be used in the analysis. It is important to note that this is a peculiar property of the APDM approach that cannot be stressed if other projection methods are used for discretizing the uncertainty random fields.

At last, the applications have confirmed the prevised results, regardless of the level of correlation of the uncertainty random variables.

3.4 Closed-form solutions of redundantly constrained stochastic bending beams

This section addresses the determination of the closed-form solutions of redundantly constrained stochastic bending beams in terms of the PDF.

For example, for the bending problem of stochastic beams, that are characterized by spatially random deformability (or its inverse, the stiffness), the closed-form solution is available only for the statically determinate beams (Elishakoff, Ren, and Shinozuka, 1995b). Meanwhile, for redundantly constrained beams, only approximated solutions can be found. Even if the exact solution is obtained for particularly simple cases, its fundamental importance is essentially due to the fact that it can serve as benchmark solution for assessing the performance of various approximate analytical or numerical techniques. Moreover, the exact solution is not limited by the level of randomness of beams that can be very high. Consequently, it can be utilized to verify the accuracy of existing approximate solutions.

In this section, some simple redundantly constrained stochastic beams are studied. In particular, for simplicity care, the degree of redundancy is limited to one, even if the proposed approach could be applied for higher orders. The randomness of the beams are assigned. In particular, the bending deformability is assumed to be modelled as a mono-axial Gaussian random field, but any kind of assigned random field could be used. The goal of the work is the full characterization of any response random variable of the beam, both static (internal force) and kinematic (displacements). This characterization is obtained in terms of the corresponding PDF. These results have been achieved thank to the application of the force method for solving the redundancy and the application of the PTM.

3.4.1 Statically determinate stochastic beams

The beam under consideration has a linear axis, is constrained in such a way that it is statically determinate and it is characterized by a flexural deformability (that is the inverse of the flexural stiffness) that is supposed to be a Gaussian homogeneous

random field given by:

$$D(z) = \frac{1}{EI(z)} = D_0(1 + \alpha(z)) \tag{3.28}$$

where D_0 is the mean value, while the correlation is represented as:

$$\sigma_D^2(z_1, z_2) = \sigma_D^2(|z_1 - z_2|) = D_0^2 \sigma_\alpha^2(|z_1 - z_2|) \tag{3.29}$$

For any external load condition, from the equilibrium conditions, it is always possible to find the bending moment function $M(z)$, that is deterministic, if the load and the constraints are deterministic.
The value of the transversal displacement $u(\bar{z})$ at any abscissa $z = \bar{z}$ can be obtained by the application of the PLV in the form:

$$u(\bar{z}) = \int_0^l D(z) M(z) M^{(1)}(z, \bar{z}) dz \tag{3.30}$$

where $M^{(1)}(z, \bar{z})$ is the bending moment law in the beam due to a unitary transversal load acting at $z = \bar{z}$. As well as $M(z)$, the function $M^{(1)}(z, \bar{z})$ is deterministic, too. Consequently, taking into account Eqs. 3.28 and 3.29, 3.30 shows that the transversal displacement $u(\bar{z})$ is a Gaussian random variable characterized by the following mean value and variance:

$$\mu_u(\bar{z}) = D_0 \int_0^l D(z) M(z) M^{(1)}(z, \bar{z}) dz, \tag{3.31a}$$

$$\sigma_u^2(\bar{z}) = D_0^2 \int_0^l \int_0^l M(z_1) M(z_2) M^{(1)}(z_1, \bar{z}) M^{(1)}(z_2, \bar{z}) \sigma_\alpha^2(|z_1 - z_2|) dz \tag{3.31b}$$

Depending on the type of laws of $\sigma_\alpha^2(|z_1 - z_2|)$, $M(z)$ and $M^{(1)}(z, \bar{z})$, the previous integrals can be easily solved and, often, a closed form solution can be obtained. Hence, for statically determinate stochastic beams, the probabilistic characterization of displacements does not show any particular difficulty. This result was evidenced in some works since 1995 (Elishakoff, Ren, and Shinozuka, 1995b).

3.4.2 Statically redundant stochastic beams

In this subsection, the stochastic beams treated in the previous section are considered when they are statically redundant, showing as the problem of the response probabilistic characterization becomes more complicated. Nevertheless, it will be shown that it is possible to obtain a closed form solution, for some statically redundant stochastic beams, too.

For explaining the approach used, the simple stochastic beam represented in Fig. 3.24 (A) is taken into consideration. It is characterized by only one redundant force and, with the aim of applying the force method for solving the redundancy, the scheme represented in Fig. 3.24 (B) is considered. The redundant force X is obtained by imposing the cinematic constrain condition $u_A = 0$. In particular, it is possible to write:

$$u_A = u_A^{(q)} + u_A^{(X)} = 0 \tag{3.32}$$

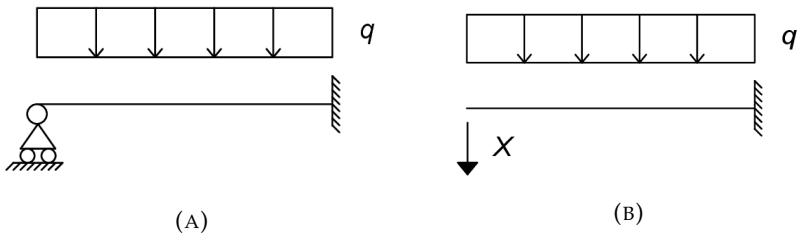

FIGURE 3.24: Statically redundant stochastic beam, example 1.

$u_A^{(q)}$ and $u_A^{(X)}$ being the contribution to the displacement due to the external load and to the redundant force, respectively, i.e.:

$$u_A^{(q)} = \frac{q}{2}\int_0^l z^3 D(z)dz = \frac{q}{2}A, \tag{3.33a}$$

$$u_A^{(X)} = X\int_0^l z^2 D(z)dz = XB \tag{3.33b}$$

where A and B are two Gaussian random variables defined by the mean values:

$$\mu_A = D_0\int_0^l z^3 dz = \frac{D_0 l^4}{4}, \tag{3.34a}$$

$$\mu_B = D_0\int_0^l z^2 dz = \frac{D_0 l^3}{3} \tag{3.34b}$$

and by the variances

$$\sigma_A^2 = D_0^2\int_0^l\int_0^l z_1^3 z_2^2 \sigma_\alpha^2(|z_1 - z_2|)dz_1 dz_2, \tag{3.35a}$$

$$\sigma_B^2 = D_0^2\int_0^l\int_0^l z_1^2 z_2^2 \sigma_\alpha^2(|z_1 - z_2|)dz_1 dz_2 \tag{3.35b}$$

The relationships given in Eq. 3.32 and Eqs. 3.33 allow to characterize the redundant force as:

$$X = -\frac{q}{2}\frac{A}{B} \tag{3.36}$$

showing that it is a non-Gaussian random variable given by the ratio between two known Gaussian variables.

The PDF of X can be obtained in a closed form by applying the PTM to Eq. 3.36. At this purpose, it is necessary to know the Gaussian JPDF $p_{AB}(a,b)$ that needs the evaluation of the cross-variance σ_{AB}, besides of the already evaluated mean values μ_A and μ_B and variances σ_A^2 and σ_B^2. This cross-variance can be easily obtained starting by the expressions of A and B given in Eqs. 3.33, that is:

$$\sigma_{AB} = D_0^2\int_0^l\int_0^l z_1^3 z_2^2 \sigma_\alpha^2(|z_1 - z_2|)dz_1 dz_2 \tag{3.37}$$

In this way the expression of the Gaussian JPDF $p_{AB}(a,b)$ can be easily obtained. Once that the expression of $\sigma_\alpha^2(|z_1 - z_2|)$ is defined, the variances and cross-variances

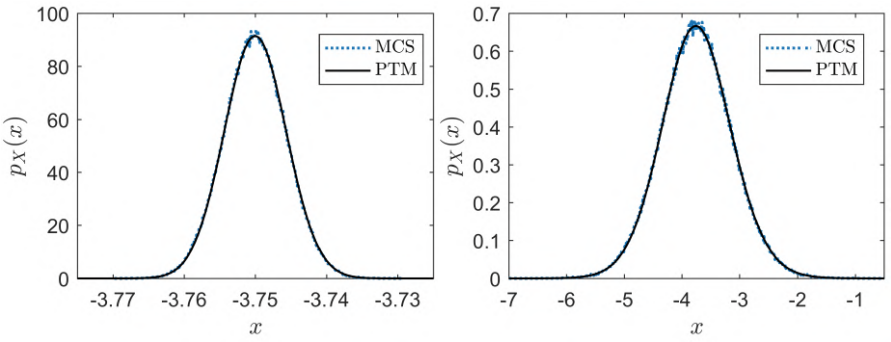

(A) (B)

FIGURE 3.25: PDF of the redundant force X: (A) Gaussian delta-correlated field; (B) Gaussian field with exponential correlation function. Example 1.

given into Eqs. 3.35 and 3.37 can be defined. At last, the application of the PTM allows the evaluation of the JPDF $p_{XY}(x,y)$, Y being an auxiliary random variables that, for example, can be opportunely chosen equal to the Gaussian variable A, obtaining:

$$p_{XY}(x,y) = p_{XA}(x,a) = q\frac{a}{x^2}p_{AB}\left(a, -\frac{q}{2}\frac{a}{x}\right) \tag{3.38}$$

At last, the PDF $p_X(x)$ is obtained by the saturation of $p_{XY}(x,y)$ respect to the variable $Y \equiv A$, that is:

$$p_X(x) = \int_{-\infty}^{+\infty} p_{XA}(x,a)da \tag{3.39}$$

This last evaluation is strongly simplified by the knowledge of the mean and variance of the Gaussian variable A. Assuming the flexural deformability $D(z)$ as in Eq. 3.28, in Fig. 3.25 is reported the PDF of the redundant force X, $p_X(x)$, for two different scenarios of Gaussian field defined by a variance $\sigma_\alpha^2 = (1/4)^2$. In particular, Fig. 3.25 (A) shows the case when is a Gaussian delta-correlated field while in Fig. 3.25 (B) $D(z)$ is modelled as Gaussian field with the following exponential correlation function $\rho(\Delta x) = \exp(|-\Delta x| / \lambda)$, $|-\Delta x|$ being the distance between two cross-sections of the beam and λ the correlation length of the random field characterizing the uncertainties, assumed in this example equal to $\lambda = 0.5L$. The exact probability density functions obtained by the proposed approach are compared with those provided by the classic MCS performed with 5×10^5 samples. The graphics of Fig. 3.25 show the high level of accuracy of the proposed procedure.

Once that the redundant force has been characterized from a probabilistic point of view, then any internal force $S(\bar{z})$ (bending moment or shear force at any abscissa $z = \bar{z}$) can be characterized, too. Indeed, it can be written:

$$S(\bar{z}) = S^{(q)}(\bar{z}) + S^{(X)}(\bar{z}) \tag{3.40}$$

$S^{(q)}(\bar{z})$ and $S^{(X)}(\bar{z})$ being the values of the internal forces when the statically determinate structure of the Fig. 3.24 (B) is loaded only by the external force and only by the redundant force, respectively. The first addend is obviously deterministic, while

the second one can be rewritten as:

$$S^{(X)}(\bar{z}) = XS^{(1)}(\bar{z}) \tag{3.41}$$

where $S^{(1)}(\bar{z})$ is the internal force when the redundant force is deterministically unitary. The Eqs. 3.40 and 3.41 imply that $S(\bar{z})$ is linearly dependent on the random variable X. Consequently, its complete probabilistic characterization can be easily defined, once that the PDF $p_X(x)$ is known.
The evaluation of the transversal displacements $u(\bar{z})$ is less immediate than the evaluation of $S(\bar{z})$. Indeed, if the relationship analogous to Eq. 3.40 is considered for the displacement, then

$$u(\bar{z}) = u^{(q)}(\bar{z}) + u^{(X)}(\bar{z}) \tag{3.42}$$

where, in this case, both the variables $u^{(q)}(\bar{z})$ and $u^{(X)}(\bar{z})$ are random. In particular, their expressions are:

$$u^{(q)}(\bar{z}) = \frac{q}{2}\int_{\bar{z}}^{l} z^2(z-\bar{z})D(z)dy = \frac{q}{2}C(\bar{z}), \tag{3.43a}$$

$$u^{(X)}(\bar{z}) = X\int_{\bar{z}}^{l} z(z-\bar{z})D(z)dz = XG(\bar{z}) \tag{3.43b}$$

where $C(\bar{z})$ and $G(\bar{z})$ are two Gaussian random variables having the following mean values and variances:

$$\mu_C(\bar{z}) = D_0\int_{\bar{z}}^{l} z^2(z-\bar{z})dz = \frac{D_0}{12}\left(3l^4 - 4l^3\bar{z} - \bar{z}^4\right), \tag{3.44a}$$

$$\mu_G(\bar{z}) = D_0\int_{\bar{z}}^{l} z(z-\bar{z})dz = \frac{D_0}{6}\left(2l^3 - 3l^2\bar{z} + \bar{z}^3\right), \tag{3.44b}$$

$$\sigma_C^2(\bar{z}) = D_0^2\int_{\bar{z}}^{l}\int_{\bar{z}}^{l} z_1^2 z_2^2(z_1-\bar{z})(z_2-\bar{z})\sigma_\alpha^2(|z_1-z_2|)dz_1dz_2, \tag{3.44c}$$

$$\sigma_G^2(\bar{z}) = D_0^2\int_{\bar{z}}^{l}\int_{\bar{z}}^{l} z_1 z_2(z_1-\bar{z})(z_2-\bar{z})\sigma_\alpha^2(|z_1-z_2|)dz_1dz_2 \tag{3.44d}$$

Rewriting Eq. 3.42 in terms of the random variables introduced above, the following expression is obtained:

$$u(\bar{z}) = \frac{q}{2}C(\bar{z}) + XG(\bar{z}) = \frac{q}{2}\left(C(\bar{z}) - \frac{A}{B}G(\bar{z})\right) \tag{3.45}$$

The random variables appearing in the second member of Eq. 3.45 are jointly Gaussian and are characterized by a Gaussian JPDF whose expression is known if, besides of the means and the variances of the four quantities, even their cross-variances are obtained. One of them has been already given in Eq. 3.37. The expressions of the

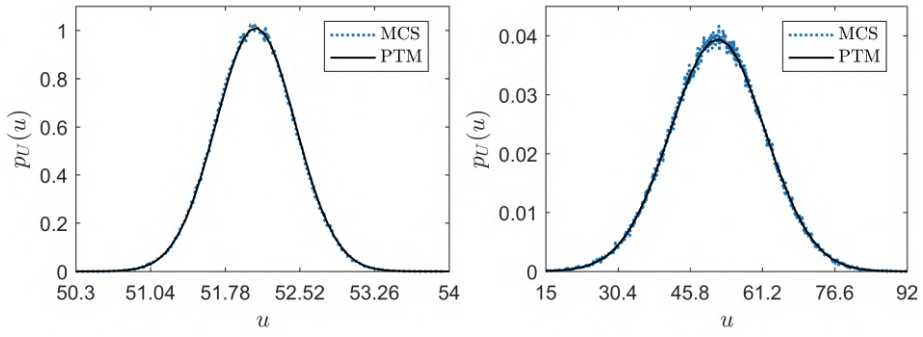

(A) (B)

FIGURE 3.26: PDF of the transversal displacement $u(\bar{z} = L/2)$: (A) Gaussian delta-correlated field; (B) Gaussian field with exponential correlation function. Example 1.

other ones are:

$$\sigma_{AC}(\bar{z}) = D_0^2 \int_0^l \int_{\bar{z}}^l z_1^3 z_2^2 (z_2 - \bar{z}) \sigma_\alpha^2(|z_1 - z_2|) dz_1 dz_2, \tag{3.46a}$$

$$\sigma_{AG}(\bar{z}) = D_0^2 \int_0^l \int_{\bar{z}}^l z_1^3 z_2 (z_2 - \bar{z}) \sigma_\alpha^2(|z_1 - z_2|) dz_1 dz_2, \tag{3.46b}$$

$$\sigma_{BC}(\bar{z}) = D_0^2 \int_0^l \int_{\bar{z}}^l z_1^2 z_2^2 (z_2 - \bar{z}) \sigma_\alpha^2(|z_1 - z_2|) dz_1 dz_2, \tag{3.46c}$$

$$\sigma_{BG}(\bar{z}) = D_0^2 \int_0^l \int_{\bar{z}}^l z_1^2 z_2 (z_2 - \bar{z}) \sigma_\alpha^2(|z_1 - z_2|) dz_1 dz_2, \tag{3.46d}$$

$$\sigma_{CG}(\bar{z}) = D_0^2 \int_{\bar{z}}^l \int_{\bar{z}}^l z_1^2 z_2 (z_1 - \bar{z})(z_2 - \bar{z}) \sigma_\alpha^2(|z_1 - z_2|) dz_1 dz_2 \tag{3.46e}$$

Once that the Gaussian JPDF $p_{ABCG}(a, b, c(\bar{z}), g(\bar{z}))$ is built, then the PTM can be applied for the evaluation of the PDF $p_U(u)$, taking into account Eq. 3.45 and by considering three auxiliary variables that can be, for example, the same variables A, B and $C(\bar{z}$. Then the following expression is obtained:

$$p_{ABCu}(a, b, c(\bar{z}), u(\bar{z})) = \frac{q}{2} \frac{a}{b} p_{ABCG}\left(a, b, c(\bar{z}), \frac{b}{a}\left(c(\bar{z}) - \frac{2}{q} u(\bar{z})\right)\right) \tag{3.47}$$

At last, the PDF $p_U(u)$ is obtained by saturing the previous expression respect to the variables A, B and $C(\bar{z})$. Again, this saturation is simplified by the fact that these are Gaussian known variables. Fig. 3.26 shows the PDF of the transversal displacement $u(\bar{z})$, with $\bar{z} = L/2$, for the above two assumptions of Gaussian field $D(z)$. Even for transversal displacements, the good level of accuracy of the proposed approach, respect to the MCS ones is clear.

Another redundant stochastic beam considered here is that represented in Fig. 3.26 (A). Even in this case, only one redundant force is present and the statically determinate scheme represented in Fig. 3.26 (B) is chosen for the application of the force method. Hence, the corresponding redundant force is the bending moment in A and the cinematic constrain condition to be imposed regards the rotation in A, that is $\varphi_A = \varphi_A^{(0)} + \varphi_A^{(X)} = 0$. At this point, the probabilistic characterization of X, of any

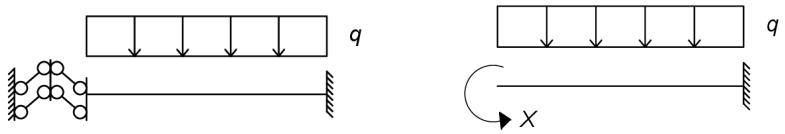

(A) (B)

FIGURE 3.27: Statically redundant stochastic beam, example 2.

internal force and of any displacement of the stochastic beam can be achieved by following the same steps considered for the previous beam. Fig. 3.28 and 3.29 show the PDF of the redundant force X, $p_X(x)$, and the transversal displacement $u(\bar{z} = L/2)$ for the previous two assumptions of Gaussian field , respectively. The comparison with respect to MCS, performed by 5×10^5 samples, allows you to emphasize again the effectiveness of the procedure proposed.

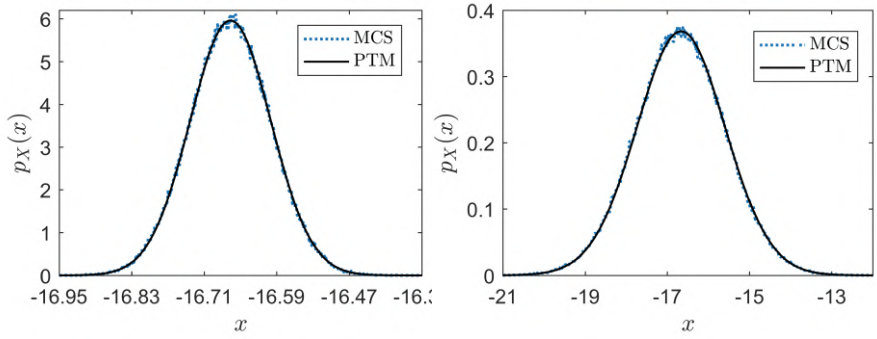

(A) (B)

FIGURE 3.28: PDF of the redundant force X: (A) Gaussian delta-correlated field; (B) Gaussian field with exponential correlation function. Example 2.

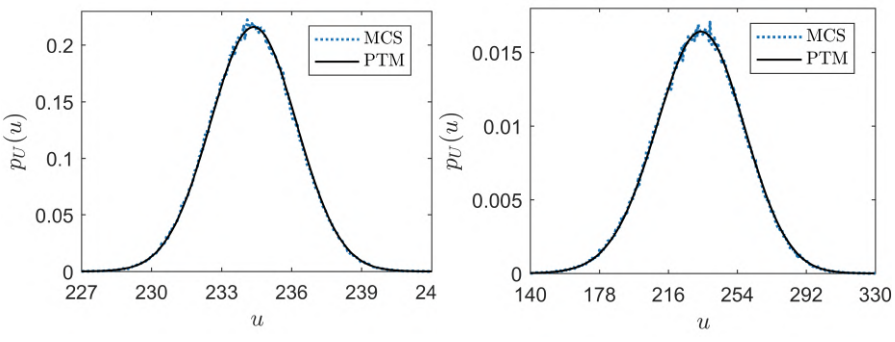

(A) (B)

FIGURE 3.29: PDF of the transversal displacement $u(\bar{z} = L/2)$: (A) Gaussian delta-correlated field; (B) Gaussian field with exponential correlation function. Example 2

3.4.3 Some remarks

In this section, the closed-form solutions in terms of PDF for redundantly constrained stochastic bending beams are determinated. This through the application of the

force method, which is helpful for solving the redundancy, coupled with the PTM able to give explicitly the response PDF once that the relationships between the response random variables and the spatially random variables are explicitly given. The closed-form of the PDF of the response random variable of the beam, both static (internal force) and kinematic (displacements), for some simple redundantly constrained stochastic beams are obtained.

Even if the exact solution is obtained for simple examples in which the degree of redundancy is limited to one, the proposed approach could be applied for higher orders and is not limited by the level of randomness of beams. Indeed, the aim of the work is to provide a new stochastic procedure that can serve as a benchmark solution for assessing the performance of various approximate analytical or numerical techniques.

At last, for completeness, the exact PDF of the static and kinematic responses are compared with those provided by MCS techniques. The high level of accuracy of the results allows to confirm the effectiveness of the procedure proposed.

3.5 Stochastic cracked beams

During the last few decades, intense research on the problem concerning the analysis of beam-like structures in the presence of cracks has been done. The presence of singularities like the concentrated cracks, which interrupt the continuity of the physical and geometrical properties of the beams, modify the static and dynamic behavior of them. This section deals with the static stochastic analysis of cracked Euler–Bernoulli beams. The crack is modeled as rotational spring, which can be represented as a discontinuity in the well-noted beam-bending differential equations. By using the properties of the generalized functions (Falsone, 2002), the proposed approach leads to the evaluation of the stochastic response, which depends on four integration constants (to be computed by enforcing the boundary conditions), thanks to the application of the PTM. In particular, in this work, the effect of the following two assumptions are studied: (i) the random amplitude of cracks; (ii) the random cracks positions, besides of their amplitude. The first assumption implies that the rotational spring stiffness is modeled as a random variable. The second one will be carried out considering that the cracks are distributed along the z-axis following the Poisson law.

3.5.1 Beams with random amplitude of cracks

Let consider a bending Euler-Bernoulli beam, constrained at the extremes with any kind of constrain and characterized by a bending stiffness EI, constant along the axis z. The beam shows the presence of a certain number n of fixed cracks, placed at assigned abscissas z_i, with $i = 1, \cdots, n$, that are modelled as a rotational internal spring of random stiffness k_i. By using the properties of the generalized functions and of their formal derivatives, it can be easily shown that the four-th order governing the beam equilibrium can be written as:

$$u''''(z) = \frac{q(z)}{EI} - \sum_{i=1}^{n} \Delta\varphi_i \delta''(z - z_i) \tag{3.48}$$

$q(z)$ being the external load, δ'' is the second order formal derivative of the Dirac's delta function $\delta(z - z_i)$ and $\Delta\varphi_i$ is the relative rotation in correspondence of the i-th

rotational spring. $\Delta\varphi_i$ can be related to the bending moment $M(z_i)$ acting in the sections adjacent to the spring through the constitutive relation of the spring:

$$\Delta\varphi_i = \frac{M(z_i)}{k_i} = -\frac{EI}{k_i}u''(z_i) \tag{3.49}$$

where k_i and $\Delta\varphi_i$ are random variables, the relationship between moment and curvature for an Euler-Bernoulli beam has been taken into account. Then, Eq. 3.48 can be rewritten as:

$$u''''(z) = \frac{q(z)}{EI} + \sum_{i=1}^{n}\frac{EI}{k_i}u''(z_i)\,\Delta\varphi_i\delta''(z-z_i) \tag{3.50}$$

The integrations respect to z of this equation up to the evaluation of the displacement $u(z)$ lead to:

$$u'''(z) = \frac{q^{(1)}(z)}{EI} + \sum_{i=1}^{n}\frac{EI}{k_i}u''(z_i)\,\delta'(z-z_i) + C_1 \tag{3.51a}$$

$$u''(z) = \frac{q^{(2)}(z)}{EI} + \sum_{i=1}^{n}\frac{EI}{k_i}u''(z_i)\,\delta(z-z_i) + C_1 z + C_2 \tag{3.51b}$$

$$u'(z) = \frac{q^{(3)}(z)}{EI} + \sum_{i=1}^{n}\frac{EI}{k_i}u''(z_i)\,U(z-z_i) + C_1\frac{z^2}{2} + C_2 z + C_3 \tag{3.51c}$$

$$u(z) = \frac{q^{(4)}(z)}{EI} + \sum_{i=1}^{n}\frac{EI}{k_i}u''(z_i)\,R(z-z_i) + C_1\frac{z^3}{6} + C_2\frac{z^2}{2} + C_3 z + C_4 \tag{3.51d}$$

where C_j, with $j = 1,\cdots,4$ are the usual integration constants depending on the conditions at the beam extremes, $q^{(j)}(z)$ represents the indefinite integral of order j of the function $q(z)$ and, at last $U(z-z_i)$ and $R(z-z_i)$ are the so-called "unit step function" and "ramp function", that are generalized functions that can be described by:

$$U(z-z_i) = 0 \quad if \quad z < z_i; \quad 1 \quad z > z_i \tag{3.52a}$$

$$R(z-z_i) = 0 \quad if \quad z < z_i; \quad (z-z_i) \quad z > z_i \tag{3.52b}$$

Once that the law $u(z)$ has been defined, the other cinematic and static response characteristic, such the rotation $\varphi(z)$, the internal bending moment $M(z)$and internal shear force $T(z)$, can be evaluated:

$$\varphi(z) = -u'(z) = -\left[\frac{q^{(3)}(z)}{EI} + \sum_{i=1}^{n}\frac{EI}{k_i}u''(z_i)\,U(z-z_i) + C_1\frac{z^2}{2} + C_2 z + C_3\right] \tag{3.53a}$$

$$M(z) = -EIu''(z) = -q^{(2)} - EI\left[\sum_{i=1}^{n}\frac{EI}{k_i}u''(z_i)\,\delta(z-z_i) + C_1 z + C_2\right] \tag{3.53b}$$

$$T(z) = -EIu'''(z) = -q^{(1)} - EI\left[\sum_{i=1}^{n}\frac{EI}{k_i}u''(z_i)\,\delta'(z-z_i) + C_1\right] \tag{3.53c}$$

The presence of the Dirac's delta and its derivative placed at $z = z_i$ could induce some worries due to the fact that the laws $M(z)$ and $T(z)$ cannot have any singularity at $z = z_i$. These worries are removed if one realizes that these functions have infinite value when and zero value at all the other abscissas, even in the immediate proximity to $z = z_i$, that is, at $z = z_i^+$ and $z = z_i^-$, where the evaluations of $M(z_i)$

and $T(z_i)$ has significance. Moreover, in the first of Eqs. 3.10 the presence of the unit step function $U(z-z_i)$ has to be noted. It implies a skip in the law $\varphi(z)$ passing from z_i^- to z_i^+. This skip is justified by the presence of the internal rotational spring. At the same time the presence of the ramp functions is justified in the displacement law $u(z)$ determining a finite variation of angles of the axis line.
At last, it is important to note that when the spring stiffness assumes the limit value $k_i = 0$ the internal constrain has to be considered as an usual hinge and the section is completely fractured. While, when it assumes the other limit value $k_i \to \infty$, no internal constrain is present, corresponding to the case of intact section.
In the following, the assumption of random amplitude of cracks is made. This implies that the rotational spring stiffness is modelled as a random variable. Moreover, it is reasonable to consider that k_i, with $i = 1, \cdots, n$ are assumed to be independent random variables characterized by the same PDF. As will be seen later, it is more convenient to introduce the variable $d_i = 1/k_i$ that can be considered as the deformability of the rotational spring. If the randomness is defined in terms of the PDF of k_i, then it is necessary to express it in terms of PDF of d_i. This last one can be easily obtained from the knowledge of the first on by a simple use of the PTM.
The fundamental equations governing the problem are exactly those already seen in the deterministic case. In particular, the cinematic and static beam quantities have the following expression where d_i has been used instead of k_i:

$$u(z) = \frac{q^{(4)}(z)}{EI} + \sum_{i=1}^{n} EId_i u''(z_i) R(z-z_i) + C_1\frac{z^3}{6} + C_2\frac{z^2}{2} + C_3 z + C_4 \tag{3.54a}$$

$$\varphi(z) = -\left[\frac{q^{(3)}(z)}{EI} + \sum_{i=1}^{n} EId_i u''(z_i) U(z-z_i) + C_1\frac{z^2}{2} + C_2 z + C_3\right] \tag{3.54b}$$

$$M(z) = -q^{(2)} - EI\left[\sum_{i=1}^{n} EId_i u''(z_i)\,\delta(z-z_i) + C_1 z + C_2\right] \tag{3.54c}$$

$$T(z) = -q^{(1)} - EI\left[\sum_{i=1}^{n} \frac{EI}{k_i} u''(z_i)\,\delta'(z-z_i) + C_1\right] \tag{3.54d}$$

As will be seen in the numerical applications section, when the cracked beam is constrained in such a way that it is statically determined, then the internal forces $M(z)$ and $T(z)$ are deterministic functions because of the deterministic character of the constants C_1 and C_2 and because of the no-influence of the generalized functions $delta(z-z_i)$ and $\delta'(z-z_i)$ on them. On the contrary, the cinematic response quantities, $u(z)$ and $\varphi(z)$, are one-dimensional random fields, due to both the fact that at least one of C_3 and C_4 is a random variable and the influence of the random variable d_i in their expressions. In particular, it will be shown that, in the case of the presence of two hinges at the beam extremes, $C_4 = 0$ w.p.1, while C_3 is a random variable depending on a linear combination of the random variables d_i with $i = 1, \cdots, n$. The application of the PTM allows the easy evaluation of the PDF of C_3 once that the PDFs of d_i are known. At this point, both $u(z)$ and $\varphi(z)$ can be considered as linear combinations of the random variables d_i and C_3. Consequently, it is possible to find their PDFs again thanks to the use of the PTM.
The case of statically redundant beams is a little more complicated. Indeed, also the internal static forces are random, due to the randomness of C_1 and/or C_2. In particular, they are expressed as the ratio of two polynomials of the variables d_i.
Even in this case, the PTM allows to evaluate the corresponding PDFs. Then, the probabilistic characterization of all cinematic and internal static response quantities

can be obtained by considering that each of them is a polynomial in the random variables d_i and C_j (with $j = 1, 2, \cdots, 4$).

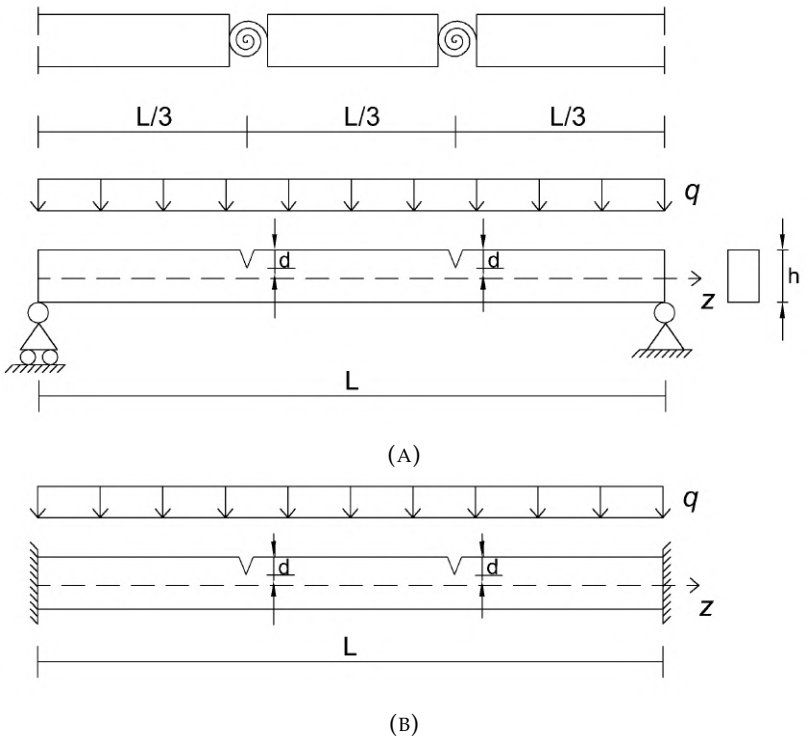

FIGURE 3.30: Statically determinate beam with cracks; (B) Redundant determinate beams

3.5.1.1 Numerical applications

The procedure presented has been applied to the stochastic analysis of the statically determinate beam (Fig. 3.30 (A)) and then for the redundant beam (Fig. 3.30 (B)). Both beams are assumed with the same mechanical and geometric characteristics, that are: Young's modulus $E = 25 \times 10^9\ N/m^2$, moments of inertia $I = 1.35 \times 10^{-3}$ $m^4$and length L=10 m. The external action is a uniformly distributed deterministic load with intensity $q = 5 \times 10^3\ KN/m$. The beams show the presence of a two fixed cracks, placed at the abscissas $z = L/3$ and $z = 2L/3$, that are modelled as a rotational internal spring of equivalent stiffness $k_1 = k_2 = k_{equ}$ (Caddemi and Calio, 2009), with

$$k_{equ} = \frac{EI}{h}\frac{1}{C(\beta)} \tag{3.55}$$

where $\beta = d/h$ is defined as the ratio between the crack depth d and the cross-section height h, and $C(\beta)$ is the dimensionless local compliance. In particular, the following model proposed by (Bilello, 2001) it was assumed:

$$C(\beta) = \frac{\beta(2-\beta)}{0.9(\beta-1)^2} \tag{3.56}$$

The two rotational spring stiffness are modeled as independent random variables characterized by the same PDF. It was introduced the variable $d_1 = 1/k_1 = d_2 = 1/k_2 = d_{equ} = 1/k_{equ}$ that can be considered as the deformability of the rotational spring. Then the PDF of d_{equ} it was defined assuming the crack depth d equal $h/2$.

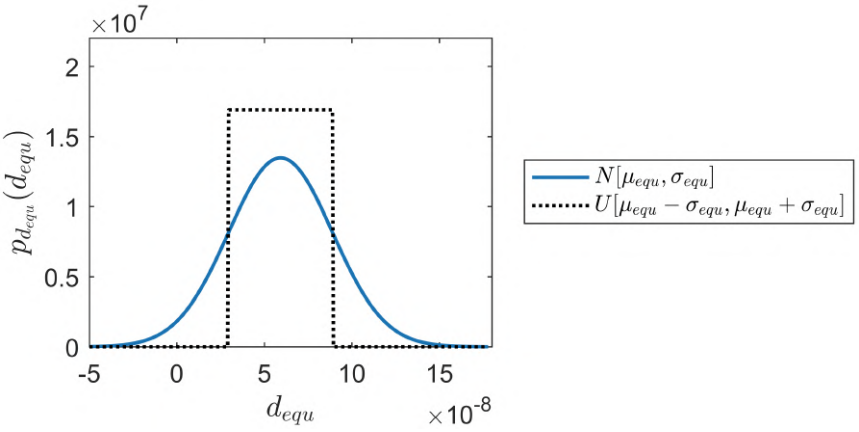

FIGURE 3.31: PDF of d_{equ}: Uniform distribution assumption (dotted line); Gaussian distribution assumption (continuous line).

Two types of probability distribution of d_{equ} have been taking into account: firstly, it has been assumed to be Gaussian defined by a mean value μ_{equ} given by Eq. 3.55 and variance around the mean value of $\sigma^2_{equ} = (0.5)^2$; in the second case, the probability distribution of d_{equ} has considered being uniformly distributed in the range $\left[\mu_{equ} - \sigma_{equ}, \mu_{equ} + \sigma_{equ}\right]$ (Fig. 3.31). For the statically determinate beam (Fig. 3.30(A)), the Figs. 3.32 and 3.33 show the PDF of $u(z)$ and $\varphi(z)$ when z=L/2. From Eqs. 3.54(A)-(B), it is possible to appreciate that in these expressions, the random variable involved d_i are iid (independent, identically distributed) and the sum is a linear operation that doesn't distort symmetry. In fact, for the case of the sum of two uniformly distributed d_i, the PDF of $u(z = L/2)$ and $\varphi(z = L/2)$ show the typical triangular distribution.

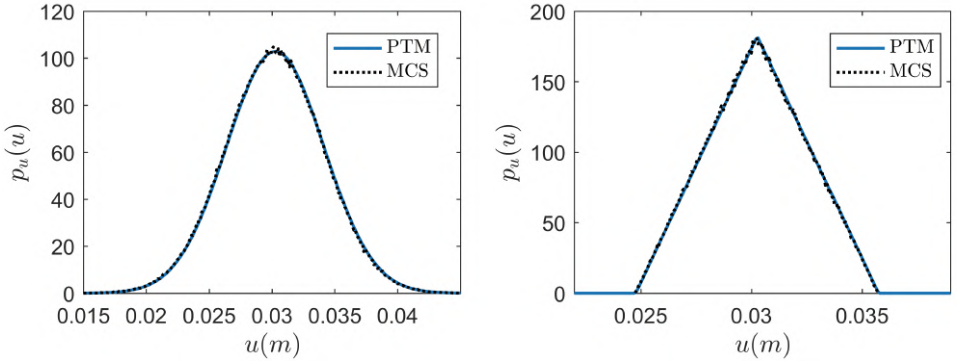

(A) (B)

FIGURE 3.32: Statically determinate beam: PDF of $u(z = L/2)$ (A) Gaussian distribution assumption of d_{equ}; (B) Uniform distribution assumption of d_{equ}

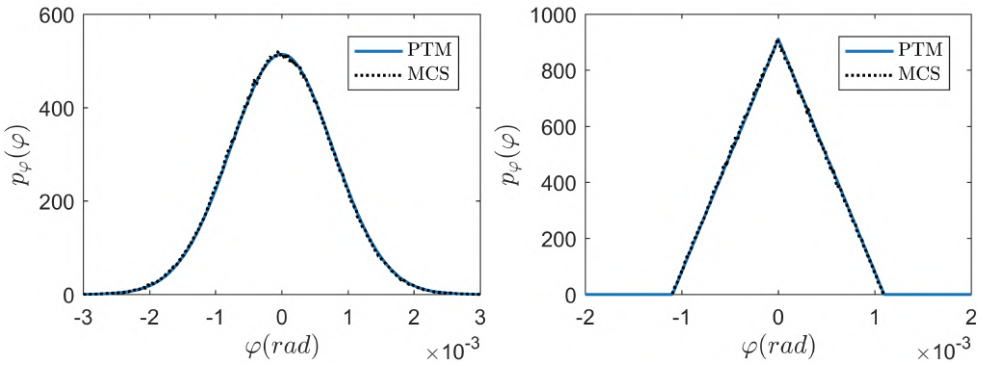

(A) (B)

FIGURE 3.33: Statically determinate beam: PDF of $\varphi(z = L/2)$ (A) Gaussian distribution assumption of d_{equ}; (B) Uniform distribution assumption of d_{equ}

Finally, the statically redundant beam in Fig. 3.30(B) is taking into account. The same two distribution assumption of d_{equ} are considered. Figs. 3.34 and 3.35 show the PDF of $u(z)$ and $\varphi(z)$ when $z = L/2$. In this case, due to the internal static forces are random, in the expressions of Eqs. 3.54 a nonlinear polynomial sum in the random variables d_i and C_j appear. In fact, this is very distinguishable for the case of uniformly distributed d_i, the nonlinear operation involved does not preserve the previous symmetry behavior. The same considerations can be drawn from the PDF of $M(z)$ and $T(z)$ at $z = 0$ (Figs. 3.36 and 3.37). The results obtained in Figs. 3.32-3.37 are compared with those provided by the classic MCS (10^6 samples), providing a good level of accuracy of the proposed procedure.

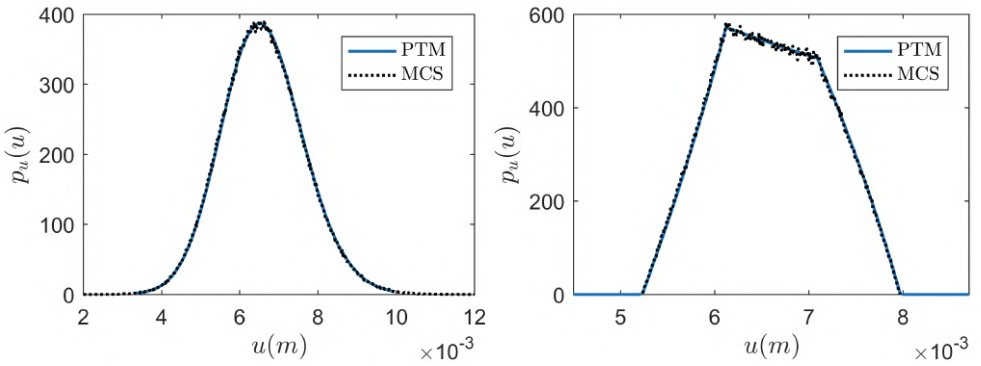

(A) (B)

FIGURE 3.34: Statically redundant beam: PDF of $u(z = L/2)$ (A) Gaussian distribution assumption of d_{equ};(B) Uniform distribution assumption of d_{equ}

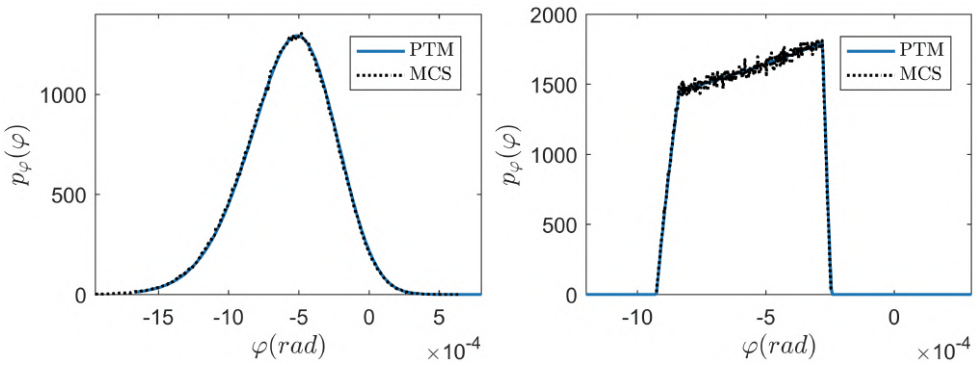

(A) (B)

FIGURE 3.35: Statically redundant beam: PDF of $\varphi(z = L/2)$ (A) Gaussian distribution assumption of d_{equ};(B) Uniform distribution assumption of d_{equ}

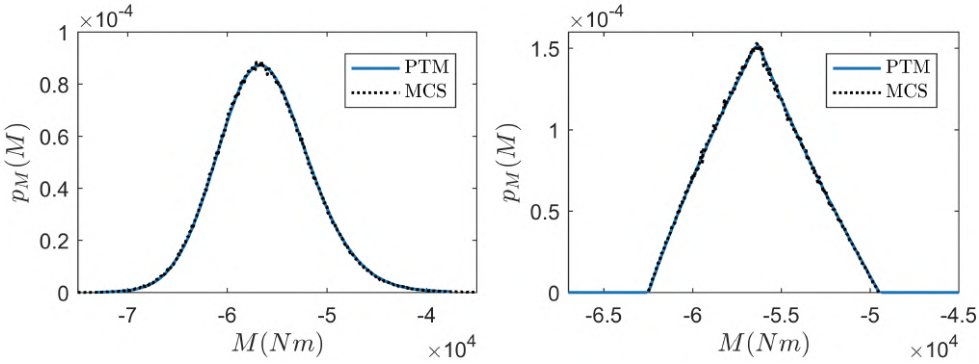

(A) (B)

FIGURE 3.36: Statically redundant beam: PDF of $M(z = 0)$ (A) Gaussian distribution assumption of d_{equ};(B) Uniform distribution assumption of d_{equ}

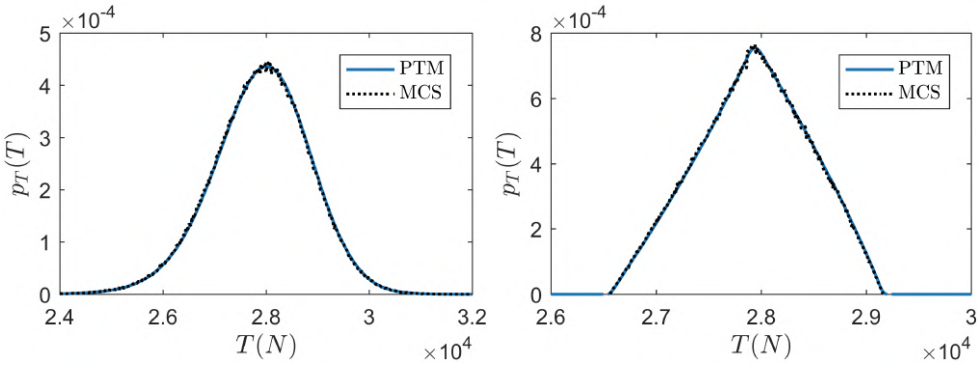

(A) (B)

FIGURE 3.37: Statically redundant beam: PDF of $T(z = 0)$ (A) Gaussian distribution assumption of d_{equ};(B) Uniform distribution assumption of d_{equ}

3.5.2 Beams with random position of the random cracks

The more realistic model of cracks in a beam is when their positions are random, besides of their amplitude. One way to model the random position behavior could be to assume that the cracks are distributed along the z-axis following the Poisson law. As consequence, for example, the bending moment law shows the presence of the term $\sum_{i=1}^{N(n)} EId_i u''(z_i)\,\delta(z-z_i)$, which is a stochastic field belonging to the class of the so-called filtered Poisson field. In particular it has the form:

$$D(z) = \sum_{i=1}^{N(z)} Y_i h(z, z_i), \tag{3.57}$$

in which $Y_i = EId_i$ and $h(z, z_i) \equiv u''(z_i)\,\delta(z-z_i)$ are considered. In Eq. 3.57, $N(z)$ is a Poisson process, characterized by the mean rate λ, while Y_i are independent random variables having the same PDF. At this point some basic notes on the Poisson stochastic fields (processes) will be reported, then the Eqs. 3.54 will be particularized for this last new assumption.

3.5.2.1 Some basic concepts related to the filtered Poisson processes

A stochastic process $X(z)$ belongs to the class of the filtered Poisson stochastic fields (processes) if it can be expressed as:

$$X(z) = \sum_{i=1}^{N(n)} w(z, z_i, Y_i), \tag{3.58}$$

where $w(\cdot,\cdot,\cdot)$ is some real function, $N(z)$ is a Poisson process, with rate λ and characterized by the abscissas of the events $0 \le z_1 \le \cdots \le z_i \le \cdots$, and, lastly, Y_i is a sequence of independent identically distributed random variables. This means that $X(z)$ is the sum of pulses occurring up to z, that are $w(z, z_i, Y_i)$, with $0 \le z_i \le z$. It is obvious that: $w(z, z_i, Y_i) = 0$ if $z_i > z$.
The probabilistic description of $X(z)$ can be obtained thanks to the Parzen theorem (1964) that establishes that, for any $z_2 > z_1 > 0$, the joint CF of $X(z_1)$ and $X(z_2)$ is given by:

$$\begin{aligned}\phi(\theta_1, \theta_2; z_1, z_2) =& \exp\left\{\lambda \int \int_0^{z_1} \mathrm{E}\left[\exp\left(i\theta_1 w(z_1, \tau, Y) + i\theta_2 w(z_2, \tau, Y)\right) - 1\right] d\tau\right\} + \\ & \lambda \int_{z_1}^{z_2} \mathrm{E}\left[\exp\left(i\theta_2 w(z_2, \tau, Y)\right) - 1\right] d\tau\end{aligned}$$

Directly from this result, other useful ones can be deduced. For example, setting $\theta_2 = 0$, the CF of $X(z)$ is obtained as:

$$\phi(\theta; z) = \exp\left\{\lambda \int_0^{z} \mathrm{E}\left[\exp\left(i\theta_1 w(z_1, \tau, Y)\right) - 1\right] d\tau\right\} \tag{3.59}$$

while, taking the derivatives of $\log\left[\phi\left(\theta_1,\theta_2;z_1,z_2\right)\right]$, one obtains:

$$\mathrm{E}\left[X(z)\right]=\lambda\int_0^z \mathrm{E}\left[w\left(z,\tau,Y\right)\right]d\tau \tag{3.60a}$$

$$\mathrm{var}\left[X(z)\right]=\lambda\int_0^z \mathrm{E}\left[w^2\left(z,\tau,Y\right)\right]d\tau \tag{3.60b}$$

$$\mathrm{cov}\left[X(z_1),X(z_2)\right]=\lambda\int_0^{z_1} \mathrm{E}\left[w\left(z_1,\tau,Y\right)w\left(z_2,\tau,Y\right)\right]d\tau \quad z_2>z_1 \tag{3.60c}$$

If a multivariate field $\mathbf{X}(z)=\{X_1(z),\cdots,X_k(z)\}$ is considered, let take a single Poisson process, $\{w(z)\}$, with rate λ and events at $\cdots\leq 0\leq z_1\leq\cdots\leq z_i\leq\cdots$. With each event z_i a vector $\mathbf{Y}_i$ is associated such that $\{\mathbf{Y}_i\}$ forms a sequence of independent identically distributed random vectors; moreover, $\{\mathbf{Y}_i\}$ must be independent of $\{w(z)\}$, too. Each vector $\mathbf{Y}_i=\{\mathbf{Y}_{1i},\cdots,\mathbf{Y}_{ki}\}$ may have dependent component; moreover $k\neq m$ can be possible. Then, a multivariate filtered Poisson field is defined as:

$$X_i(z)=\sum_{i=1}^{N(z)} w_i\left(z,z_i,Y_{pi}\right),\quad p=1,\cdots,k \tag{3.61}$$

Consequently, the JCF of and can be considered as a generalization of that given in Eq. 3.59, i.e.:

$$\begin{aligned}\phi\left(\boldsymbol{\theta}_1,\ \boldsymbol{\theta}_2;z_1,z_2\right)=&\exp\left\{\lambda\int\int_0^{z_1}\mathrm{E}\left[\exp\left(i\boldsymbol{\theta}_1^T\mathbf{w}\left(z_1,\tau,\mathbf{Y}\right)+i\boldsymbol{\theta}_2^T\mathbf{w}\left(z_2,\tau,\mathbf{Y}\right)\right)-1\right]d\tau\right\}+\\ &\lambda\int_{z_1}^{z_2}\mathrm{E}\left[\exp\left(i\boldsymbol{\theta}_2\mathbf{w}\left(z_2,\tau,\mathbf{Y}\right)\right)-1\right]d\tau\end{aligned} \tag{3.62a}$$

where $\boldsymbol{\theta}_1$ and $\boldsymbol{\theta}_2$ are two k-vectors of real variables. Using this result, the complete probabilistic characterization of the multivariate process $\mathbf{X}\left(z,z_i,\mathbf{Y}_i\right)$ can be obtained. For example:

$$\mathrm{cov}\left[X_i\left(z_1\right),X_j\left(z_2\right)\right]=\lambda\int_0^{z_1}\mathrm{E}\left[w_i\left(z_1,\tau,\mathbf{Y}\right)w_j\left(z_21,\tau,\mathbf{Y}\right)\right]d\tau,\quad z_2>z_1 \tag{3.63}$$

An important class of filtered Poisson fields is represented by the linear ones, that are represented as follows:

$$X(z)=\sum_{i=1}^{N(z)} Y_i w\left(z-z_i\right) \tag{3.64}$$

among them, an example is the so-called shot noise process, represented as:

$$X(z)=\sum_{i=1}^{N(z)} Y_i\exp\left[-b\left(z-z_i\right)\right] \tag{3.65}$$

where $b>0$ is the constant decay rate and the random variables Y_i are exponentially distributed, that means they have the following PDF:

$$p_Y(y)=\frac{1}{\mu}\exp\left[-\frac{y}{\mu}\right] \tag{3.66}$$

It is easy to verify that the CF of $X(z)$ has the following expression:

$$\phi(\theta; z) = \left(\frac{1 - i\mu\theta \exp(-bz)}{1 - i\mu\theta} \right)^{\frac{\lambda}{b}} \tag{3.67}$$

When $z \to \infty$ the process becomes stationary and its CF is given by:

$$\phi(\theta) = \left(\frac{1}{1 - i\mu\theta} \right)^{\frac{\lambda}{b}} \tag{3.68}$$

Another important example of linear filtered Poisson field is the so-called "compound Poisson process" in which the functions $w(z - z_i)$ are represented by the unit step functions $U(z - z_i)$. Thus, the compound Poisson process is characterized by samples having the following expression:

$$X(z) = \sum_{i=1}^{N(z)} Y_i U(z - z_i) \tag{3.69}$$

Particularizing the expressions of the CF given above, it is easy to evaluate the CF of the compound Poisson process in the form:

$$\phi_X(\theta) = \exp(\lambda z [\phi_Y(\theta) - 1]) \tag{3.70}$$

$\phi_Y(\theta)$ being the CF of the random variables Y_i.
The formal derivative of the compound Poisson process arises another useful process called "delta-correlated Poisson process", or also "Poisson white noise", whose samples are defined by the following expression:

$$X(z) = \sum_{i=1}^{N(z)} Y_i \delta(z - z_i) \tag{3.71}$$

where $\delta(z - z_i)$ is the Dirac delta function placed at the abscissa z_i. It can be shown that the corresponding CF assumes the form:

$$\phi_X(\theta) = \exp\{\lambda z (\mathrm{E}[iY\theta] - 1)\} \tag{3.72}$$

The corresponding log-CF leads to the following fundamental result relative to the k-order cumulant of $X(z)$:

$$\kappa_k[X(z_1), X(z_2), \cdots, X(z_k)] = \mathbf{E}\left[Y^k\right] \delta(z - z_1)(z - z_2) \cdots (z - z_k) \tag{3.73}$$

Another very used filtered Poisson process is the nonhomogeneous ones, that are characterized by a rate $\lambda(z)$, that is deterministic function, and by samples defined as:

$$X(z) = \sum_{i=1}^{N(z)} w(z, z_i, Y(z_i)) \tag{3.74}$$

where the events $Y_i = Y(z_i)$ are each other independent and whose each distribution depends on z_i. The corresponding CF, related to $X(z_1)$ and $X(z_2)$, is given by:

$$\begin{aligned}\phi(\theta_1,\theta_2;z_1,z_2) =& \exp\left\{\int_0^{z_1}\lambda(\tau)\mathrm{E}\left[\exp\left(i\theta_1 w(z_1,\tau,Y(\tau))+i\theta_2 w(z_2,\tau,Y(\tau))\right)-1\right]d\tau\right\}\\ &+\int_{z_1}^{z_2}\lambda(\tau)\mathrm{E}\left[\exp\left(i\theta_2 w(z_2,\tau,Y(\tau))\right)-1\right]d\tau\end{aligned} \tag{3.75}$$

Again, if it is assumed $\theta_2 = 0$, the CF of $X(z)$ assumes the expression:

$$\phi(\theta;z) = \exp\left\{\int_0^{z}\lambda(\tau)\mathrm{E}\left[\exp\left(i\theta w(z,\tau,Y(\tau))\right)-1\right]d\tau\right\}. \tag{3.76}$$

Now, taking into account the Eq. 3.57, the random field $D(z)$ is fully probabilistically characterized by the knowledge of its CF, having the following expression:

$$\phi_{D(z)}(\theta) = \exp\left\{\lambda\int_0^{z}\mathrm{E}\left[\exp\left(i\theta Y h(z,\tau)\right)-1\right]d\tau\right\}. \tag{3.77}$$

So, this new assumption on the deformability of the rotational springs modeling the presence of cracks leads to writing the Eqs. 3.54 as:

$$u(z) = \frac{q^{(4)}(z)}{EI} + \sum_{i=1}^{N(z)} Y_i u''(z_i) R(z-z_i) + C_1\frac{z^3}{6} + C_2\frac{z^2}{2} + C_3 z + C_4 \tag{3.78a}$$

$$\varphi(z) = -\left[\frac{q^{(3)}(z)}{EI} + \sum_{i=1}^{N(z)} Y_i u''(z_i) U(z-z_i) + C_1\frac{z^2}{2} + C_2 z + C_3\right] \tag{3.78b}$$

$$M(z) = -q^{(2)} - EI\left[\sum_{i=1}^{N(z)} Y_i u''(z_i)\,\delta(z-z_i) + C_1 z + C_2\right] \tag{3.78c}$$

$$T(z) = -q^{(1)} - EI\left[\sum_{i=1}^{N(z)} Y_i u''(z_i)\,\delta'(z-z_i) + C_1\right] \tag{3.78d}$$

Taking into account what before specified about the no influence of the functions $\delta(z-z_i)$ and $\delta'(z-z_i)$ on the internal forces $M(z)$ and $T(z)$, Eqs. 3.78(c-d) can be reduced as follows:

$$M(z) = -q^{(2)} - EI\left[C_1 z + C_2\right] \tag{3.79a}$$

$$T(z) = -q^{(1)} - EIC_1 \tag{3.79b}$$

Then the expressions of the response beam quantities can be rewritten as:

$$u(z) = \frac{q^{(4)}(z)}{EI} + \sum_{i=1}^{N(z)} Y_i h_u(z, z_i) + C_1 \frac{z^3}{6} + C_2 \frac{z^2}{2} + C_3 z + C_4 \tag{3.80a}$$

$$\varphi(z) = -\left[\frac{q^{(3)}(z)}{EI} + \sum_{i=1}^{N(z)} Y_i h_\varphi(z, z_i) + C_1 \frac{z^2}{2} + C_2 z + C_3 \right] \tag{3.80b}$$

$$M(z) = -q^{(2)} - EI\left[C_1 z + C_2\right] \tag{3.80c}$$

$$T(z) = -q^{(1)} - EIC_1 \tag{3.80d}$$

where:

$$h_u(z, z_i) = u''(z_i) R(z - z_i); \quad h_\varphi(z, z_i) = u''(z_i) U(z - z_i) \tag{3.81}$$

and

$$u''(z_i) = -\frac{1}{EI} q^{(2)}(z_i) - (C_1 z_i + C_2) \tag{3.82}$$

that is a random variable depending on the random variables C_1 and C_2. Even in this case, for statically determined beams, the internal forces $M(z)$ and $T(z)$ are deterministic functions because of the same reasons of the previous case. While, the cinematic response quantities, $u(z)$ and $\varphi(z)$, are one-dimensional random fields. In particular, the field in the expression of summation $\varphi(z)$ represents a compound Poisson process, with CF expression of Eq. 3.70 while that of $u(z)$ is a linear shot noise. The CF expression of a linear shot noise Poisson process can be obtained as follow. Supposing that the function $w(z - z_i)$ are represented by the ramp function $R(z - z_i)$, that can be generalized through the unit step function:

$$R(z - z_i) = (z - z_i) U(z - z_i) = \begin{cases} 0 & if \quad z < z_i \\ (z - z_i) & if \quad z > z_i \end{cases} \tag{3.83}$$

Indeed, particularizing the expression of the CF defined in 3.78, it is easy to get the CF of the linear shot noise Poisson process:

$$\begin{aligned} \Phi_x(\theta) &= exp\left\{ \lambda \int_0^z E\left[exp\left(i\theta Y(z-\tau) U(z-\tau)\right) - 1\right] d\tau \right\} \\ &= exp\left\{ -\lambda z + \lambda \left(\int_0^z U(z-\tau) \Phi_Y(\theta = (z-\tau)\theta) d\tau \right) \right\} \end{aligned} \tag{3.84}$$

where the fundamental result of the PTM in terms of the CF has been taking into account.

3.5.2.2 Numerical applications

The case of a beam constrained with two hinges at the extremes is taking into consideration. The mechanical and geometric characteristics of the previous beam examples are held. The constraints condition implies that $C_2 = C_4 = 0$, while C_3 is given by the sum of a deterministic quantity and of a random variable that can be considered as a filtered Poisson process evaluated at $z = L$. The Poisson process is here characterized by the mean rate $\lambda = 0.3$. As a consequence, the quantity given into Eq. 3.82 becomes deterministic. The sequence of the independent identically distributed random variables $Y_i = EId_i$ is assumed with the deformability of the rotational spring d_i equal to d_{equ}. The equivalent deformability d_{equ} is a Gaussian variable defined by a mean value μ_{equ} given by Eq. 3.55 and variance around

the mean value of $\sigma^2_{equ} = (0.5)^2$. Keeping in mind the CF expressions of the linear shot noise Poisson process and of the compound Poisson process provided in Eqs. 3.84 and 3.70, respectively, Fig. 3.38 shows the PDF of $u(z)$ and $\varphi(z)$ when $z = L/2$. Again, these results are considered together with those coming out from a MCS characterized by 5×10^5 samples.

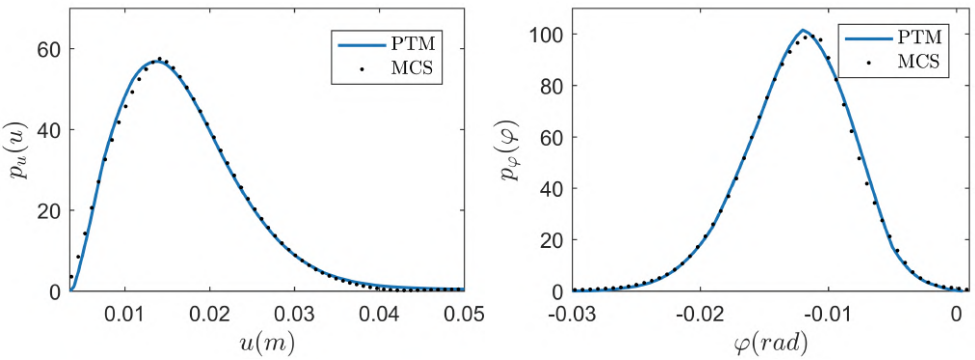

(A) (B)

FIGURE 3.38: Cracked determinate beam with random cracks position, besides of their amplitude: PDF of $u(z = L/2)$ (A) Gaussian distribution assumption of d_{equ}; (B) PDF of $\varphi(z = L/2)$

The case of statically redundant beams is a little more complicated. In this case, also the internal static forces are random, due to the randomness of one or both C_1 and C_2.

3.6 Some remarks

The aim of this section is to propose a stochastic procedure able to evaluate the cinematic and static beam random quantities when a certain number of cracks are present. In section 3.6.1, the cracks are modeled as a rotational internal spring of stiffness k_i and the amplitude of cracks is assumed random. The numerical application shows the PDF of $u(z = L/2)$ and $\varphi(z = L/2)$ for two examples of statistically determinate and redundant beams. Then, in section 3.6.2, beams with random position of the random cracks are treated. In this case, it was modeled the random position behavior assuming that the cracks are distributed along the z-axis following the Poisson law. In particular, it is possible to appreciate that the field in the expression of summation $\varphi(z)$ represents a compound Poisson process, while that of $u(z)$ is linear shot noise. For both assumptions, the PDF of cinematic and static beam stochastic quantities have been found through the application of the PTM.

3.7 Conclusion

In this chapter, the stochastic analysis of structural systems with uncertain properties has been addressed. The PTM has been adequately applied in order to implement a stochastic procedure able to characterize the response of linear uncertain structures directly in terms of PDF. In sections 3.2 and 3.3, a stochastic approach has been identified in the coupling of the APDM and of the PTM in order to evaluate the PDF response of discretized uncertain structures. In particular, as have been shown in section 3.3, in the case of statically determinate structures, the stochastic procedure

presented gives the exact results in terms of the response PDF. Then, in section 3.4, the problem to find an exact solution of redundantly constrained stochastic bending beams it was addressed. In particular, a closed-form solution in terms of the PDF for beam characterized by spatially random deformability has been identified through the application of the force method and the application of the PTM. Finally, the end section of this chapter deals with a study to analyze the stochastic response of multi-cracked beams considering the case where both the amplitude and the position of the cracks are uncertain. Once again, it is possible to appreciate that the PTM is a good stochastic tool when stochastic problems are treated. At last, it should be added that the applications of the approaches proposed have always shown their good properties, in terms of both accuracy and computational effort.

Chapter 4

Uncertain structural systems

4.1 Introduction

Structural analyses require the definition of some basic variables, such as geometry and dimensions, material properties and loads, in addition to boundary conditions, methods of modeling and analysis (Ayyub, 1997). During the design process, the task of the structural engineer is to make reasonable justifiable assumptions, in order to develop a workable and safe project. In general, the designer is often called upon to select a suitable solution among several alternatives for the modeling and analysis of structural systems. Doubtless, different methodologies may be applied, depending on the design phase, the knowledge and expertise of the involved designer. Consequently, imprecise data and imperfect knowledge may lead to uncertainties, so the final design solution is almost always an engineering approximation, thus intrinsically prone to uncertainties.

The application of the PTM on two typical examples in structural engineering in which the uncertainties in the model designed are due to simplifying assumptions in analytical models and/or simplified methods will be proposed. The content of this chapter is based on two papers already published (De Domenico, Falsone, and Laudani, 2018b; De Domenico, Falsone, and Laudani, 2018a). In section 4.1 it will be investigating a probabilistic method for the determination of the static structural response of beams and frames with partially restrained (semi-rigid) connections by modeling the spring stiffness terms (or equivalently, the fixity factors of the beam) as uniformly distributed random variables. In conventional analysis and design of framed structures, the behavior of beam to column connections is treated as either ideally pinned or perfectly rigid, which circumvents the need of properly accounting for the actual connection stiffness. On the other hand, experimental findings exhibit a broad spectrum of behaviors of the connections in between these two extreme cases, so that semi rigid, or partially restrained, connections are more appropriate idealizations, (Jones, Kirby, and Nethercort, 1983; Bjorhovde, Colson, and Brozzetti, 1990). In the literature, the commonly used approach is to incorporate moment rotation relationships to describe the behavior of the joint, which is generally featured by a nonlinear constitutive behavior whose main parameters are calibrated according to experimental data (Jones, Kirby, and Nethercort, 1983; Chen and Lui, 1987; Kishi and Chen, 1990). Experimental testing on the rotational stiffness often leads to a large scatter of measures, even when the same kind of connection is investigated: for instance in (Rauscher and Gerstle, 1992) the coefficient of variation of the initial stiffness of double web angle steel connections was as high as 23%. This indicates that results arising from a deterministic model of the connection may lead to wrong estimates of the actual behavior. Moreover, due to the large scatter of experimental data it is quite difficult for an engineer to decide which value of the rotational stiffness to use, and to assess which consequences such an assumption has in the

design process. On the contrary, these questions could be answered by incorporating the randomness of the beam constraints within a probability-based design approach. To deal with semi-rigid connections modelled as random variables, various approaches were proposed in the literature: typically, MCS techniques (Thai et al., 2016) in conjunction with stochastic finite elements (Hadianfard and Razani, 2003; Çavdar et al., 2009; Adhikari and Manohar, 1999) or the perturbation method (Sakurai, Ellingwood, and Kushiyama, 2001) were adopted; alternatively, interval analysis is performed in (Tangaramvong et al., 2016) to obtain the extreme stochastic response of a semi-rigid frame. However, the accuracy of the approximated results underlying the MCS is strictly related to the number of samples that are generated. Indeed, the PDF of the response is approximated with reasonable accuracy provided that thousands of simulations, not to say millions, are carried out, especially when strongly nonlinear input-output relationships are involved. Along this research line, the PTM will be employed to readily derive the exact PDFs of some response indicators.

In section 4.2, masonry infilled reinforced concrete (RC) frames will be analyzed through the PTM. The infill panels are, in the majority of cases, made by masonry, whose structural behavior is extremely complex, being affected by a number of uncertain parameters such as the mechanical characteristics of the raw materials (clay, concrete), the mortar thickness and quality, the brick geometry and arrangement, the relative stiffness of the frame and of the infill panel, as well as the actual workmanship expertise, to name just a few. The above sources of uncertainty and irregularity, and the heterogeneous nature of the masonry panels make the related modeling task a rather intricate process. Indeed, there is lack of repeatability of results, even when carrying out experiments under macroscopically identical geometrical and mechanical conditions. In this regard, experiments have been conducted on infill walls since the late 50s, see e.g., (Benjamin and Williams, 1957; Benjamin and Williams, 1958; Matthies et al., 1997a; Žarnić and Tomaževič, 1985) for some landmark contributions involving monotonic loading, and (Esteva, 1966; Chandrasekaran and Chandra, 1970; Klingner and Bertero, 1977; Valiasis and Stylianidis, 1989; Mehrabi et al., 1994; Dawe, Schriver, and Sofocleous, 1989; Dolce et al., 2005) for cycling loading, harmonic excitations and shake-table tests. The mentioned papers were mostly focused on the in-plane behavior of the masonry infills, whereas a wealth of literature also exists for the out-of-plane behavior, see e.g., (Angel et al., 1994; Felice and Giannini, 2001; Flanagan and Bennett, 1999; Pasca, Liberatore, and Masiani, 2017) for just a few examples. The failure mode of a masonry infill subject to horizontal (seismically-induced) loads may range from compression failure of diagonal strut (also referred to as "corner crushing"), which is quite frequent and typically occurs for low-compressive-strength infill materials, damage in the frame members (also referred to as frame failure mode), which originates from a damage mechanism of the column due to the forces transferred from the infill wall to the surrounding frame (it generally takes place for masonry infills having high compressive strength), diagonal cracking failure mode, sliding shear or out-of-plane failure whereby damage accumulates in the central zone of the infill panel due to the arching mechanism (Kheirollahi, 2013). The aforementioned references, although limited to just a few contributions, together with the variety of failure modes mentioned before give the general idea of the complexity in modeling the masonry infill behavior while properly accounting for its stiffening contribution and for the interaction with the surrounding frame in a RC framed building. Several researchers investigated this

subject with a variety of numerical techniques, with different underlying theoretical bases and applicable to different scales of observations. Typical modeling approaches include micro-models (Doven and Kafkas, 2017), macro-models or homogeneization models (Milani and Benasciutti, 2010). Some literature surveys can be found in a couple of papers by Asteris and co-workers (Asteris et al., 2011; Asteris et al., 2013; Asteris et al., 2015b; Asteris et al., 2017b), and a quite recent overview of linear and nonlinear, micro-modelling, meso-modelling and macro-modelling approaches has been presented in (Tarque et al., 2015) and references therein. Extensive and in-depth state-of-the-art reports can be found in the following works (Amanat and Hoque, 2006; Crowley and Pinho, 2004; Crowley and Pinho, 2006; Asteris et al., 2016b; Asteris, 2016). In line with this research field a macro-modeling technique, based on an equivalent diagonal pin-jointed strut, will be reported to for modeling the stiffening contribution of the masonry panels. Since it is quite difficult to decide which mechanical characteristics to assume for the diagonal struts in such simplified model, the strut width is here considered as a random variable, whose stochastic characterization stems from a wide set of empirical expressions proposed in the literature. At last, in section 4.3, some concluding observations will be reported.

4.2 Probability based structural response of steel beams and frames with uncertain semi rigid connections

In this section is attempt to characterize, from a probabilistic point of view, the static structural response of an individual beam (which is isolated from a more general framed structure) and of simple frames with partially restrained end nodes. More specifically, it was investigate to what extent the uncertainty in the semi-rigid constraints affects the stochastic structural response in terms of a few indicators that are of interest for design purposes, including the element-stiffness-matrix terms, the reactions at the beam ends, the mid-span deflection and the mid-span bending moment. The PTM, is employed to readily derive the exact PDFs of the above response indicators. Connection flexibility at the beam ends is incorporated based on a linear approximation, i.e., only the first branch of the actual nonlinear moment-rotation curve is addressed, which is characterized by a constant initial stiffness. The beam fixity factors or connection percentages are treated as uniformly distributed random variables. The analysis of the PDFs of the aforementioned response indicators sheds light on the vital importance of a probability-based approach: indeed, results inferred from deterministic average values, which could be adopted for a preliminary assessment, may lead to misleading estimates of the actual beam response because they are considerably different from the median of the corresponding PDF. More importantly, it is seen that such deterministic average values may in some cases represent non-conservative estimates from a design viewpoint.

Although most of the presented numerical applications refer to steel semi-rigid connections, the present research work is of analytical nature and the discussed approach and analysis method is, in principle, applicable also to other fields, for instance precast reinforced concrete structures, steel-braced reinforced concrete frames, steel-concrete composite frame systems, timber-concrete composite beams, as well as timber structures. Therefore, the aim of this section is directed towards a general class of engineering problems, not just confined to steel frames.

4.2.1 Deterministic response of beams with semi-rigid nodes

4.2.1.1 Beams with semi-rigid end nodes modeled via rotational springs

Typically, framed structures are analyzed and designed considering some idealizations (cf. Fig. 4.1). For instance, reinforced concrete framed structures are usually treated as frames with perfectly rigid beam-to-column connections, whereas steel framed structures are modelled with ideally pinned connections at the joints. In reality, the moment-rotation relationship of joints is more appropriately and more generally described by semi-rigid (or partially restrained) connections, in that the actual rotational behavior lies in between the two extreme cases of pinned (zero rotational stiffness) and rigid (zero rotation) connection. The partially restrained joints considerably affect the overall moment distributions and displacements of the structure, so that it is of interest to incorporate semi-rigid connections into the model. Accounting for the actual semi-rigid behavior of connections in the design of structures is both realistic and economical, because the redistribution of internal stress leads to more balanced results between the two extreme scenarios of pinned and rigid connections.

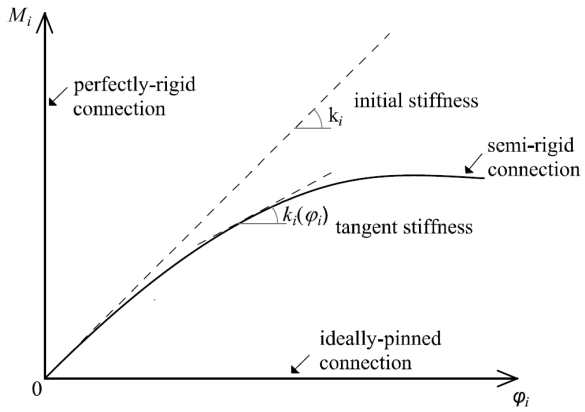

FIGURE 4.1: Typical moment-rotation behavior of rigid and pinned idealizations along with that of semi-rigid beam-to-column connection.

An effective and straightforward way to incorporate the characteristics of semi-rigid connections is by means of rotational springs at the beam end nodes. The moment-rotation behavior of the i-th joint of a structure is thus modelled either through a constant spring rotational stiffness k_i, thus relying on a linearized model, or via a more complicated nonlinear spring rotational stiffness function $k_i(\phi_i)$ wherein the tangent stiffness depends on the actual value of the rotation experienced by the joint ϕ_i. In this section, attention is limited to the former case, in that the partially restraint is featured by a constant spring stiffness k_i. This stiffness represents the so-called initial stiffness of the connection that is identified in the first branch of the actual nonlinear moment-rotation curve (i.e., corresponding to reasonably low rotation values, cf. again Fig. 4.1). These simplifying assumptions restrict the scope of the present work to structures subjected to static loading. Moreover, due to the linear rotational behavior, the following results and conclusions only apply to serviceability limit states, where the functioning of the structure or structural members under normal use is of interest. Extension to ultimate limit states would be desirable to investigate the probability based response beyond the elastic limit, for instance in terms of collapse moment or ultimate rotation. This would require extension of the

present study by incorporating a nonlinear rotational relation, which is the object of an ongoing research of the authors. With reference to the sketch depicted in Fig. 4.2, a constant cross-section beam of length L, having moment of inertia I and made of a material with Young's modulus E is partially restrained at its end nodes 1 and 2 by two rotational springs. The relation between rotations at the beam ends $\varphi_i^{(b)}$ $(i = 1,2)$ and rotations of the nodal restraints φ_i $(i = 1,2)$ is expressed as

$$\begin{aligned} \varphi_1 - \varphi_1^{(r)} &= \varphi_1^{(b)} = -\left.\frac{dw(x)}{dx}\right|_{x=0}; \\ \varphi_2 - \varphi_2^{(r)} &= \varphi_2^{(b)} = -\left.\frac{dw(x)}{dx}\right|_{x=L} \end{aligned} \tag{4.1}$$

where $\varphi_i^{(r)}$ $(i = 1,2)$ represents the additional, *relative* spring rotation due to the flexibility of the rotational springs and $w(x)$ is the transversal displacement of the beam axis. In the absence of rotational springs, that is in the case of perfectly rigid connections, $\varphi_i^{(r)} \to 0$ and $\varphi_i \equiv \varphi_i^{(b)}$ $(i = 1,2)$, and, consequently, the distinction between rotations at the beam ends and rotations at the nodal restraints is meaningless. On the contrary, due to the flexibility of the connection, a relative rotation $\varphi_i^{(r)}$ $(i = 1,2)$ is induced by the rotational springs. The bending moment at the beam ends depends on the relative rotations $\varphi_i^{(r)}$ and on the spring rotational stiffness k_i or, equivalently, the spring deformability $\lambda_i = 1/k_i$ as follows

$$M_i = -k_i \varphi_i^{(r)} = -\frac{\varphi_i^{(r)}}{\lambda_i} \quad (i = 1,2) \tag{4.2}$$

where the minus sign means that the moment reaction at the beam end is opposed to the relative spring rotation. Focusing on the flexural behavior of the beam, we consider the element displacement array $\mathbf{u}^T = [\varphi_1, w_1, \varphi_2, w_2]$.

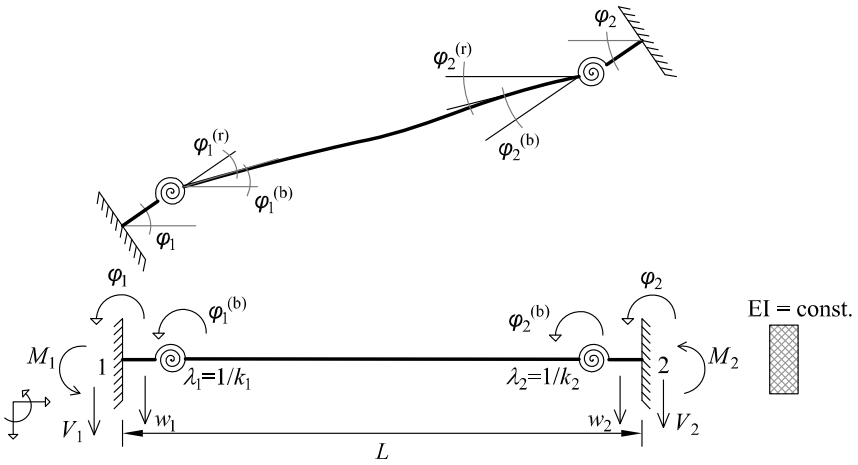

FIGURE 4.2: Sketch and conventions of a beam with partially restrained (semi-rigid) end nodes.

The stiffness matrix of a beam having rotational springs at its ends may easily be

constructed by analyzing four loading scenarios in which we impose one displacement at a time equal to one and the remaining three displacements equal to zero. Through the fourth-order beam-bending differential equation, for each loading scenario we compute moment and transversal-force reactions at either nodes, collected in the force array $\mathbf{F}^T = [M_1, V_1, M_2, V_2]$ (cf. again Fig. 4.2).

The values of the $\mathbf{F}$ terms form the four columns of the stiffness matrix of the partially restrained beam element $\mathbf{S}(\lambda_1, \lambda_2)$, which depends on the spring deformability $\lambda_i (i = 1, 2)$ and can be expressed in the following compact form

$$\mathbf{S}(\lambda_1, \lambda_2) = \mathbf{S}_r \mathbf{S}_c(\lambda_1, \lambda_2) \tag{4.3}$$

The matrix $\mathbf{S}_r$ entering Eq. 4.3 is the classical element stiffness matrix of the beam supposed rigid at its end 0, whereas $\mathbf{S}_c(\lambda_1, \lambda_2)$ is a corrective *dimensionless* matrix arising from the flexibility of the connection, which depends on the spring deformability terms λ_1 and λ_2 as follows

$$\mathbf{S}_c(\lambda_1, \lambda_2) = \frac{1}{\Delta(\lambda_1, \lambda_2)} \times \begin{pmatrix} 1 + \frac{3EI}{L}\lambda_2 & 1 + \frac{2EI}{L}\lambda_2 & 1 & 1 + \frac{2EI}{L}\lambda_2 \\ 1 + \frac{2EI}{L}\lambda_2 & 1 + \frac{EI}{L}(\lambda_1 + \lambda_2) & 1 + \frac{2EI}{L}\lambda_1 & \frac{EI}{L}(\lambda_1 + \lambda_2) \\ 1 & 1 + \frac{2EI}{L}\lambda_1 & 1 + \frac{2EI}{L}\lambda_1 & 1 + \frac{3EI}{L}\lambda_1 \\ 1 + \frac{2EI}{L}\lambda_2 & 1 + \frac{EI}{L}(\lambda_1 + \lambda_2) & 1 + \frac{2EI}{L}\lambda_1 & 1 + \frac{EI}{L}(\lambda_1 + \lambda_2) \end{pmatrix} \tag{4.4}$$

where the function $\Delta(\lambda_1, \lambda_2)$ is defined as

$$\Delta(\lambda_1, \lambda_2) = 1 + \frac{4EI}{L}(\lambda_1, \lambda_2) + \frac{12(EI)^2}{L^2}\lambda_1\lambda_2 \tag{4.5}$$

As an example, the first-column terms of the element stiffness matrix $\mathbf{S}(\lambda_1, \lambda_2)$ read

$$\begin{aligned} s_{11} &= \frac{4EI}{L\Delta(\lambda_1, \lambda_2)}\left(1 + \frac{3EI}{L}\lambda_2\right); \\ s_{12} &= \frac{-6EI}{L^2\Delta(\lambda_1, \lambda_2)}\left(1 + \frac{2EI}{L}\lambda_2\right) = -s_{14}; \\ s_{13} &= \frac{2EI}{L\Delta(\lambda_1, \lambda_2)} \end{aligned} \tag{4.6}$$

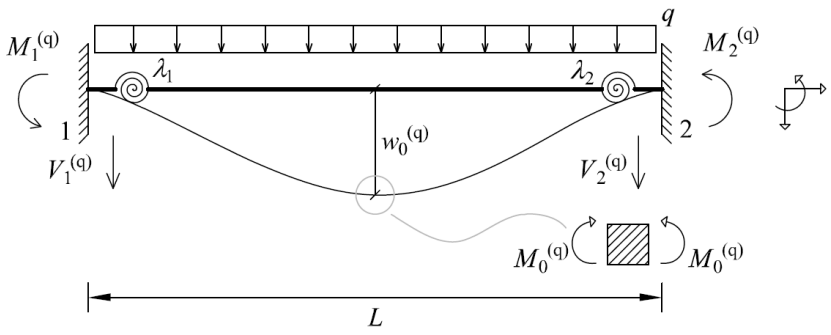

FIGURE 4.3: Beam with partially-restrained (semi-rigid) end nodes subject to a uniformly distributed load.

This format of the stiffness matrix, which is similar to other forms presented in

the relevant literature, (e.g., Sekulovic and Salatic, 2001; Kartal et al., 2010), makes it easy to retrieve the limit cases of a beam with perfectly rigid (clamped) and ideally hinged end nodes by assuming $\lambda_i \to 0$ and $\lambda_i \to \infty$ $(i = 1, 2)$, respectively. For example, the rotational stiffness at the node 1 is particularized in the following forms

$$\begin{aligned}
&\lim_{\substack{\lambda_1 \to 0 \\ \lambda_2 \to 0}} s_{11} = \frac{4EI}{L} \equiv s_{11rigid}; \\
&\lim_{\substack{\lambda_1 \to 0 \\ \lambda_2 \to \infty}} s_{11} = \frac{3EI}{L} \equiv s_{11rigid-hinged}; \\
&\lim_{\substack{\lambda_1 \to \infty \\ \lambda_2 \to \infty}} s_{11} = \frac{4EI}{L} \equiv s_{11hinged};
\end{aligned} \tag{4.7}$$

Furthermore, it is of interest to evaluate the nodal actions transmitted to the beam end nodes due to the loads applied along the beam axis, which could be useful for implementation of an automated finite element program. A uniformly distributed transversal load of magnitude q is considered, as sketched in Fig. 4.3. The fourth-order beam bending differential equation with the appropriate boundary conditions leads to

$$\begin{aligned}
M_1^{(q)} &= \frac{qL^2}{12} \frac{1}{\Delta(\lambda_1, \lambda_2)} \left(1 + \frac{6EI}{L} \lambda_2\right); \\
M_2^{(q)} &= -\frac{qL^2}{12} \frac{1}{\Delta(\lambda_1, \lambda_2)} \left(1 + \frac{6EI}{L} \lambda_1\right); \\
V_1^{(q)} &= -\frac{qL}{2} \frac{1}{\Delta(\lambda_1, \lambda_2)} \left(\eta(\lambda_1, \lambda_2) + \frac{2EI}{L} \lambda_2\right); \\
V_2^{(q)} &= -\frac{qL}{2} \frac{1}{\Delta(\lambda_1, \lambda_2)} \left(\eta(\lambda_1, \lambda_2) + \frac{2EI}{L} \lambda_1\right)
\end{aligned} \tag{4.8}$$

that are the moment reactions and transversal reactions at the end nodes, where the function $\eta(\lambda_1, \lambda_2)$ is defined as

$$\eta(\lambda_1, \lambda_2) = 1 + \frac{3EI}{L}(\lambda_1 + \lambda_2) + \frac{12(EI)^2}{L^2} \lambda_1 \lambda_2 \tag{4.9}$$

The deterministic limit cases of a rigid, rigid-hinged and hinged beam are retrieved as

$$\begin{aligned}
&\lim_{\substack{\lambda_1 \to 0 \\ \lambda_2 \to 0}} M_1^{(q)} = \frac{qL^2}{12} \equiv M_{1rigid}^{(q)}; \\
&\lim_{\substack{\lambda_1 \to 0 \\ \lambda_2 \to \infty}} M_1^{(q)} = \frac{qL^2}{8} \equiv M_{1rigid-hinged}^{(q)}; \\
&\lim_{\substack{\lambda_1 \to \infty \\ \lambda_2 \to \infty}} M_1^{(q)} = 0 \equiv M_{1hinged}^{(q)};
\end{aligned} \tag{4.10}$$

Finally, we also compute the mid-span moment $M_0^{(q)}$ due to sagging bending

$$M_0^{(q)} = \frac{qL^2}{24} \times \frac{1}{\Delta(\lambda_1, \lambda_2)} \left(1 + \frac{6EI}{L}(\lambda_1 + \lambda_2) + \frac{36(EI)^2}{L^2} \lambda_1 \lambda_2\right) \tag{4.11}$$

and the mid-span deflection $w_0^{(q)}$

$$w_0^{(q)} = \frac{qL^4}{384EI} \times \frac{1}{\Delta(\lambda_1,\lambda_2)} \left(1 + \frac{8EI}{L}(\lambda_1+\lambda_2) + \frac{60(EI)^2}{L^2}\lambda_1\lambda_2\right) \tag{4.12}$$

All these quantities are purposely written as the term related to the fixed beam multiplied by a dimensionless function whose shape is quite similar from variable to variable. Limit cases can easily be retrieved, e.g., concerning Eqs. 4.11 and 4.12.

$$\begin{aligned} &\lim_{\substack{\lambda_1\to 0\\ \lambda_2\to 0}} M_0^{(q)} = \frac{qL^2}{24} \equiv M_{0rigid}^{(q)}; \quad \lim_{\substack{\lambda_1\to \infty\\ \lambda_2\to \infty}} M_0^{(q)} = \frac{qL^2}{8} \equiv M_{0hinged}^{(q)}; \\ &\lim_{\substack{\lambda_1\to 0\\ \lambda_2\to 0}} w_0^{(q)} = \frac{qL^4}{384EI} \equiv w_{0rigid}^{(q)}; \quad \lim_{\substack{\lambda_1\to \infty\\ \lambda_2\to \infty}} w_0^{(q)} = \frac{5qL^4}{384EI} \equiv W_{0hinged}^{(q)}; \end{aligned} \tag{4.13}$$

4.2.1.2 Frames with semi-rigid end nodes modeled via rotational springs

The analysis is here extended to simple frames with semi-rigid nodes, Fig. 4.4: two situations are considered, a single-bay frame with semi-rigid beam-to-column connections (frame I) and a single-bay frame with semirigid column-to-foundation connections (frame II). Although it could be argued that these frames are too simple, the choice to adopt one-bay and one-floor frames is motivated by convenience reasons: indeed, for these very simple frames, it is easy to derive compact closed-form expressions of the displacements and reactions as explicit functions of the rotational spring deformability terms, which is related to the main focus of the present study. For simplicity, the quantities E, I and L of the beam and of the columns are assumed to be identical. The structural response is easily derived via the displacement method. Neglecting the axial deformations in structural elements, the unknown displacements are collected in the array $\mathbf{u}^T = [\varphi_B, \varphi_C, \delta]$ and the stiffness matrix is expressed as

$$\begin{aligned} \mathbf{K}^{(I)}(\lambda_1,\lambda_2) &= \begin{pmatrix} s_{11}(\lambda_1,\lambda_2) + \frac{4EI}{L} & s_{31}(\lambda_1,\lambda_2) & \frac{6EI}{L^2} \\ s_{13}(\lambda_1,\lambda_2) & s_{33}(\lambda_1,\lambda_2) + \frac{4EI}{L} & \frac{6EI}{L^2} \\ \frac{6EI}{L^2} & \frac{6EI}{L^2} & \frac{24EI}{L^2} \end{pmatrix} \\ \mathbf{K}^{(II)}(\lambda_1,\lambda_2=0) &= \begin{pmatrix} s_{33}(\lambda_1) + \frac{4EI}{L} & \frac{2EI}{L} & s_{43}(\lambda_1) \\ \frac{2EI}{L} & s_{33}(\lambda_1,\lambda_2) + \frac{4EI}{L} & s_{43}(\lambda_1) \\ s_{34}(\lambda_1) & s_{34}(\lambda_1) & 2s_{44}(\lambda_1) \end{pmatrix} \end{aligned} \tag{4.14}$$

wherein S_{ij} is the term of the stiffness matrix $\mathbf{S}(\lambda_1,\lambda_2)$ of the beam element with partially restrained nodes that has been defined in Eqs. 4.3 and 4.4. Once the stiffness matrix is constructed, the unknown displacements $\mathbf{u}$ are readily computed via

$$\mathbf{u}^{(i)} = \mathbf{K}^{(i)^{-1}}(\lambda_1,\lambda_2)\,\mathbf{F}^{(i)}(\lambda_1,\lambda_2) \quad \text{with} \quad (i = I, II). \tag{4.15}$$

where the force vectors $\mathbf{F}^{(i)}$ for the two frames are given by

$$\mathbf{F}^{(I)}(\lambda_1,\lambda_2) = \begin{bmatrix} 0 \\ 0 \\ P \end{bmatrix} - \begin{bmatrix} M_1^{(q)}(\lambda_1,\lambda_2) \\ M_2^{(q)}(\lambda_1,\lambda_2) \\ P \end{bmatrix}; \quad \mathbf{F}^{(II)} = \begin{bmatrix} 0 \\ 0 \\ P \end{bmatrix} - \begin{bmatrix} qL^2/12 \\ -qL^2/12 \\ P \end{bmatrix} \tag{4.16}$$

For example, the rotation in the node C and the lateral displacement in the frame I are

$$\varphi_C^{(I)} = \varphi_C^{(q,I)} + \varphi_C^{(P,I)} = \frac{1}{\Gamma(\lambda_1,\lambda_2)} \times \left[\frac{qL^3}{72EI}\left(1+\frac{3EI}{7L}(5\lambda_1-3\lambda_2)\right) + \frac{-PL^2}{28EI}\left(1+\frac{2EI}{3L}(4\lambda_1+7\lambda_2)+\frac{8(EI)^2}{L^2}\lambda_1\lambda_2\right)\right]$$
$$\delta_C^{(I)} = \delta_C^{(q,I)} + \delta_C^{(P,I)} = \frac{1}{\Gamma(\lambda_1,\lambda_2)} \times \left[\frac{qL^3}{84EI}(-\lambda_1+\lambda_2) + \frac{PL^3}{84EI}\left(1+\frac{28EI}{15L}(\lambda_1+\lambda_2)+\frac{48(EI)^2\lambda_1\lambda_2}{15L^2}\lambda_1\lambda_2\right)\right] \tag{4.17}$$

where the superposition principle is resorted to by adding the two separate effects arising from the loads q and P. In Eq. 4.17, the function $\Gamma(\lambda_1,\lambda_2)$ is defined as

$$\Gamma(\lambda_1,\lambda_2) = 1 + \frac{23EI}{21L}(\lambda_1+\lambda_2) + \frac{8(EI)^2}{7L^2}\lambda_1\lambda_2 \tag{4.18}$$

The resulting bending moments at the beam-to-column connection and at the column base are

$$M_B^{(I)} = M_B^{(q,I)} + M_B^{(P,I)} = \frac{1}{\Gamma(\lambda_1,\lambda_2)} \times \left[\frac{qL^2}{18}\left(1+\frac{6EI}{7L}\lambda_2\right) - \frac{3PL}{14}\left(1+\frac{4EI}{4L}\lambda_2\right)\right]$$
$$M_D^{(I)} = M_D^{(q,I)} + M_D^{(P,I)} = \frac{1}{\Gamma(\lambda_1,\lambda_2)} \times \left[\frac{qL^2}{36}\left(1+\frac{3EI}{7L}(-\lambda_1+3\lambda_2)\right) + \frac{2PL}{7}\left(1+\frac{EI}{6L}(10\lambda_1+7\lambda_2)+\frac{2(EI)^2\lambda_1\lambda_2}{L^2}\lambda_1\lambda_2\right)\right] \tag{4.19}$$

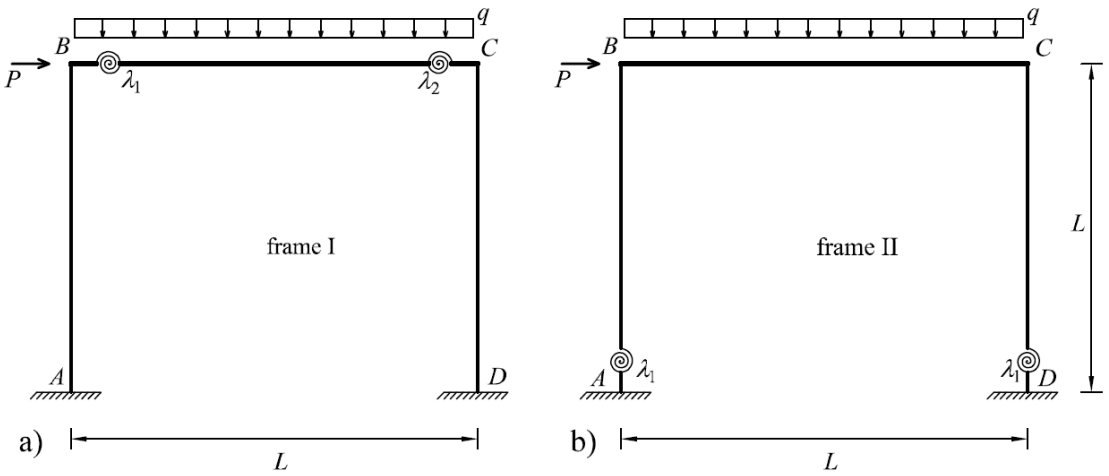

FIGURE 4.4: Single-bay frame analyzed with different connection types.

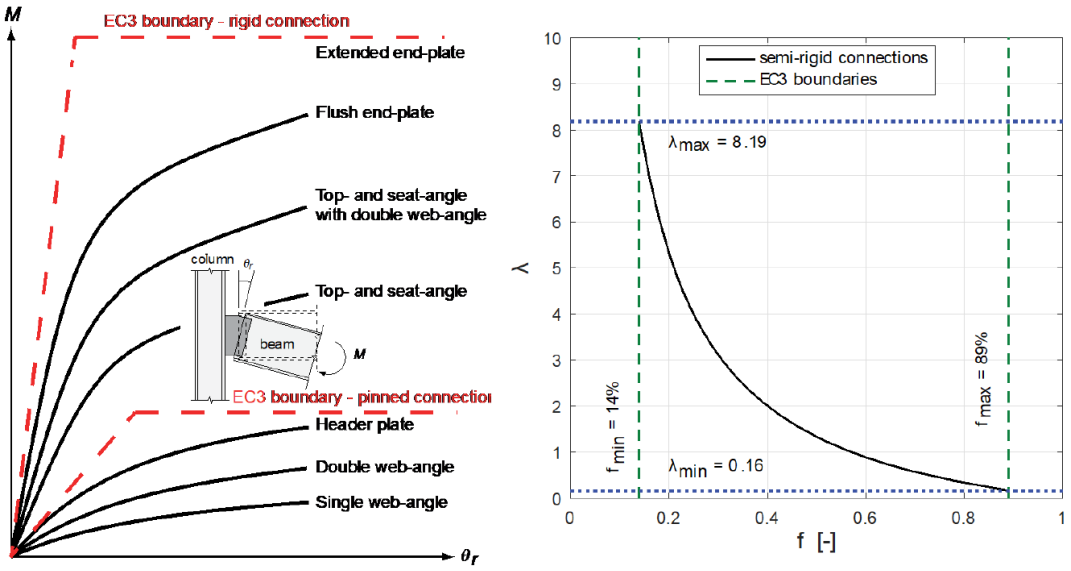

FIGURE 4.5: Moment-rotation curves for various beam-to-column connections along with Eurocode 3 boundaries (adapted from Chen, 2011 (left) and corresponding rotational spring deformability of the beam (right).

In a similar way, the lateral displacement and the bending moments in the frame II are

$$\delta^{(II)} = \delta^{(q,II)} + \delta^{(P,II)} \equiv \delta^{(P,II)} = \frac{1}{\Delta^{(P,II)}(\lambda_1)} \times \frac{5PL^3}{84EI}\left(1 + \frac{18EI}{5L}\lambda_1\right)$$
$$M_B^{(II)} = M_B^{(q,II)} + M_B^{(P,II)} = \frac{1}{\Delta^{(q,II)}(\lambda_1)} \times \frac{qL^2}{18}\left(1 + \frac{3EI}{L}\lambda_1\right) - \frac{1}{\Delta^{(P,II)}(\lambda_1)} \times$$
$$\frac{3PL}{14}\left(1 + \frac{2EI}{L}\lambda_1\right)$$
$$M_D^{(II)} = M_D^{(q,II)} + M_D^{(P,II)} = \frac{1}{\Delta^{(q,II)}(\lambda_1)} \times \frac{qL^2}{36}\left(1 + \frac{3EI}{L}\lambda_1\right) + \frac{1}{\Delta^{(P,II)}(\lambda_1)} \times \frac{2PL}{7}. \tag{4.20}$$

in which the functions $\Delta^{(q,II)}(\lambda_1)$ and $\Delta^{(p,II)}(\lambda_1)$are given by

$$\Delta^{(q,II)}(\lambda_1) = 1 + \frac{10EI}{3L}\lambda_1; \quad \Delta^{(P,II)}(\lambda_1) = 1 + \frac{6EI}{7L}\lambda_1 \tag{4.21}$$

By inspection of Eqs. 4.17-4.20, it is observed that any variable of the structural response can be expressed as a term related to the perfectly rigid case multiplied by a dimensionless corrective function that depends on the rotational spring deformability of the beams. Anyway, dealing with more complex, though certainly more realistic, frames with multiple bays and floors, would not add significant insight into the probability-based study here conducted.
The main difference would be related to the slightly more complicated expressions of the displacements and reactions that would arise in this case, which would require finite element discretizations and would make the analysts lose the direct relationship between response and uncertain stiffness factor expressed in a compact manner by the previous equations.

4.2.1.3 From the rotational spring deformability to the connection fixity factor

In order to investigate a range of behaviors that are actually representative of semi-rigid connections, attention is now focused on the concept of *fixity factors* (Chiorean, 2009; Sekulovic and Salatic, 2001; Simoes, 1996; Thai et al., 2016; Kartal et al., 2010). It is widely recognized that an estimate of the *initial* stiffness of a joint can be expressed in terms of the element stiffness (related to the Young's modulus E along with the moment of inertia I and the length L of the beam) and a dimensionless fixity factor f as follows

$$k_{joint} = \frac{4EI}{L}\frac{3f}{4(1-f)} \tag{4.22}$$

The fixity factor represents the semi-rigid behavior as connection percentage and it varies from 0% for a zero joint stiffness (ideally pinned connection) to 100% when the joint stiffness is infinity (perfectly rigid connection). In the sequel of the section, attention is focused on steel semi-rigid connections, although the methods presented are not material-specific or element-specific, as already stated in the Introduction. The choice to discuss more in-depth steel semi-rigid connections for the numerical applications is useful to link the present study to a practical problem encountered in the structural analysis of structures with semi-rigid connections. With regard to the steel framed structures, in the Eurocode 3 (CEN, 2005) a classification has been established of the fixity factors for pinned, rigid and semi-rigid joints. In particular, the limit values of the fixity factor for pinned and rigid joints are 14% and 89%, respectively (Thai et al., 2016). In other words, joints having $f < 0.14$ could be dealt with as pinned, whereas joints with $f > 0.89$ could be approximately described through the perfectly rigid idealization. Some qualitative moment rotation curves of typical beam-to-column connections in steel structures are shown in Fig. 4.5(a). Since the present investigation is concerned with semi-rigid connections in general, the analysis discussed below will be extended to the entire interval $f \in [0.14, 0.89]$. This is reflected by an interval in terms of rotational spring stiffness and, similarly, in terms of rotational spring deformability (normalized with respect to the perfectly rigid case) $\lambda \in [0.16, 8.19]$, the latter depicted in Fig. 4.5(b). From a probabilistic point of view, if no accurate experimental background is available on the actual beam-to-column connection, the spring deformability of the joint could reasonably be assumed as a uniformly distributed random variable with lower bound and upper bound values equal to 0.16 and 8.19, respectively. This is what is done in the sequel of the section, although these figures are far from being representative of all the beam-to-column connections.

Obviously, the analyst may decide to deal with a narrower, more realistic interval whenever experimental evidence leads to scattered data whose variability range is reduced as compared to the above one. Indeed, the design scenario is usually determined in terms of a single, or just few connection types involved in a steel frame. In these cases, dealing with a more restricted interval of λ values that is more appropriate for the specific type of connection used (e.g., extended end plate, top-and-seat angle, etc.) is reasonable. Implications of this choice will be briefly outlined in the following sections.

4.2.2 Probability-based response of beams with semirigid nodes

In this subsection, it will present some results concerning the probabilistic structural response, in terms of PDF and cumulative distribution function (CDF), of beams

with partially restrained nodes. First, it will be investigating the uncertainty propagation from the beam end constraints to the elements of the beam stiffness matrix $\mathbf{S}(\lambda_1, \lambda_2)$ reported in Eqs. 4.3 and 4.4. To this aim, based on the probabilistic characterization of the fixity factors as per the EC3 (CEN, 2005; Thai et al., 2016), discussed above, it will be computed the exact PDF of the various terms of the stiffness matrix through the PTM. The semi-rigid end nodes are modeled via rotational spring deformability that are uniformly distributed random variables within the interval $\lambda \in [0.16, 8.19]$. For the sake of generality, all the variables reported in this study are shown in a dimensionless form by normalizing them with respect to the perfectly rigid case, i.e., the beam with clamped ends ($\lambda = 0$). As an example, the normalized rotational spring stiffness at the node 1 is expressed as

$$\bar{s}_{11}(\lambda_1, \lambda_2) = \frac{s_{11}(\lambda_1, \lambda_2)}{s_{11r}} = \frac{1}{\Delta(\lambda_1, \lambda_2)}\left(1 + \frac{3EI}{L}\lambda_2\right) = \frac{\left(1 + \frac{3EI}{L}\lambda_2\right)}{1 + \frac{4EI}{L}(\lambda_1, \lambda_2) + \frac{12(EI)^2}{L^2}\lambda_1\lambda_2} \tag{4.23}$$

where $s_{11}(\lambda_1, \lambda_2)$ is the term reported in Eq. 4.6(1) and $s_{11r} = 4EI/L$ denotes the rotational stiffness of the corresponding clamped beam. Similar normalizations are employed for all the other terms. Therefore, such dimensionless variables are not affected by the magnitude of the EI/L ratio and the corresponding PDF and CDF results can be applied to any beam.

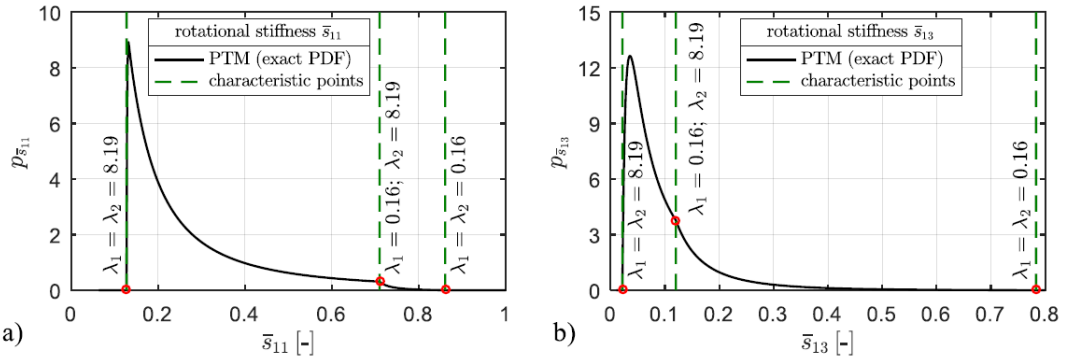

FIGURE 4.6: Qualitative examination of rotational stiffness PDF and characteristic points in partially restrained beams: (a) normalized $\bar{s}_{11}$ PDF; (b) normalized $\bar{s}_{13}$ PDF

In Fig. 4.6, the PDF of the normalized beam rotational stiffness $\bar{s}_{11}$ and $\bar{s}_{13}$ s is depicted. Dealing with semi-rigid connections leads to a narrower interval than $[0 - 1]$ in the corresponding rotational stiffness: indeed, the extreme value $\bar{s}_{11} \to 1$ (or also $\bar{s}_{13} \to 1$) would be attained for $\lambda_1 = \lambda_2 \to 0$ (beam with perfectly rigid connections), whereas $\bar{s}_{11} \to 0$ (or also $\bar{s}_{13} \to 0$) would be obtained for $\lambda_1 = \lambda_2 \to \infty$(beam having ideally pinned connections). In particular, it will be seen below that two *characteristic points* are found that represent a lower bound and an upper bound of the two rotational stiffness terms, namely $\bar{s}_{11} \in [0.12772 - 0.86071]$ and $\bar{s}_{13} \in [0.021596 - 0.78327]$.
The lower bound is associated with the couple $\lambda_1 = \lambda_2 = 8.19$ while the upper bound is related to couple $\lambda_1 = \lambda_2 = 0.16$. These figures are strictly related to the choice of the interval $\lambda \in [0.16, 8.19]$ made above. It is clearly seen in Fig. 4.6 that, assuming λ_1 and λ_2 as uniformly distributed random variables, the terms of the beam stiffness matrix are far from being uniformly distributed between their lower

bound and upper bound values. This is due to the nonlinear relationship between rotational spring deformability and rotational beam stiffness, cf. Eq. 4.23. In particular, both the $\bar{s}_{11}$ and $\bar{s}_{13}$ PDF are strongly asymmetrically distributed and are shifted towards the "lower bound case" that resembles an ideally pinned connection 1 2 ($\lambda_1 = \lambda_2 = 8.19$) . An additional , third characteristic point is identified in the PDF curve as a cusp (red circle in the plot of Fig. 4.6), which corresponds to the couple $\lambda_1 = 0.16$ and $\lambda_2 = 8.19$. This point may be meant as the semi-rigid counter part of a clamped-hinged beam idealization. This also explains the reason why such cusp occurs closer to the upper bound case for $\bar{s}_{11}$ (rotational stiffness at the node 1 that is "quasi-rigid") and is located closer to the lower bound case for $\bar{s}_{13}$ (rotational stiffness at the node 2 that is "quasi-hinged").

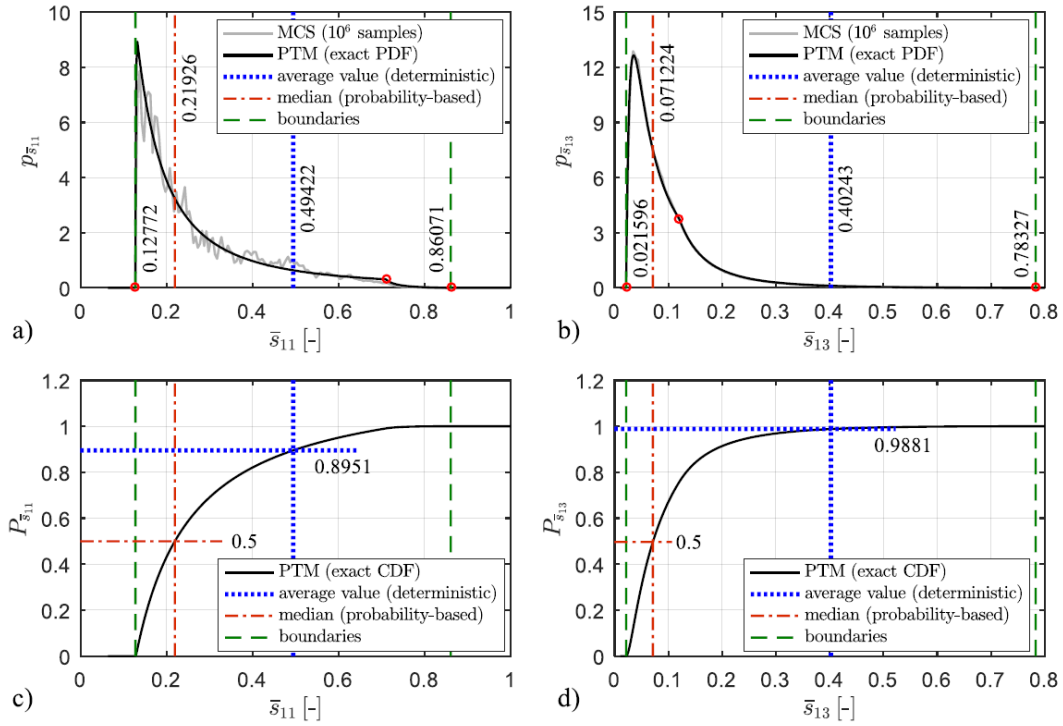

FIGURE 4.7: Probabilistic response, in terms of rotational stiffness, of partially restrained beams: (a) normalized $\bar{s}_{11}$ PDF; (b) normalized $\bar{s}_{13}$ PDF; (c) normalized $\bar{s}_{11}$ CDF; (d) normalized $\bar{s}_{13}$ CDF.

The implications of such probability-based outcomes in a design process are investigated. To this aim, in Fig. 4.7 we particularize the qualitative PDF shown in Fig. 4.6 by computing the median of the distribution. This median may be considered as a reference design value from a probabilistic point of view. Indeed, there is just a probability of 50% that, within the class of semi-rigid connections characterized by the assumed interval $\lambda \in [0.16, 8.19]$, the median is exceeded. It seems reasonable to compare the median with the average value that would be calculated according to a deterministic approach, i.e., the mid-point between the two extreme values (boundaries) corresponding to the two extreme cases of quasi-rigid ($\lambda_1 = \lambda_2 = 0.16$) and quasi-pinned connections ($\lambda_1 = \lambda_2 = 8.19$). By inspection of Fig. 4.7, it is observed that the median (probability-based design value) and the average value (deterministic quantity) are largely different from each other. In particular, the average value of s_{11} is 0.49422 and represents the 89.51^{th} percentile of the distribution (see the CDF

depicted in Fig. 4.7(c)), whereas the median is 0.12772. This means that if one is dealing with the wide class of semi-rigid connections featured by $\lambda \in [0.16, 8.19]$ the element stiffness, on average, would be overestimated of around 125% by assuming the value calculated from the deterministic approach. Similar conclusions can be drawn for the $\bar{s}_{13}$ stiffness term, in which the median (0.071224) and the average value (0.40243) differ for up to 465%. In this case, the average value represents the 98.81^{th} percentile of the distribution.

The peculiarity of a probability-based approach for semi-rigid connections is that a design value of the stiffness (and of any other quantity of interest for design purposes) that is related to a given non-exceeding probability (i.e., associated to a given limit state) can straightforwardly be identified. The probabilistic nature of the structural response can also be accounted for via the MCS. Nevertheless, only an approximation of the exact PDF may be obtained in this case: the number of samples needed to construct a reasonably accurate PDF exceeds millions, see again Fig. 4.7(a) and 4.7(b), which implies higher computational times. This concept is even more marked when the input-output relationship is nonlinear, as in the case of $\bar{s}_{11}$, cf. Eq. 4.23.

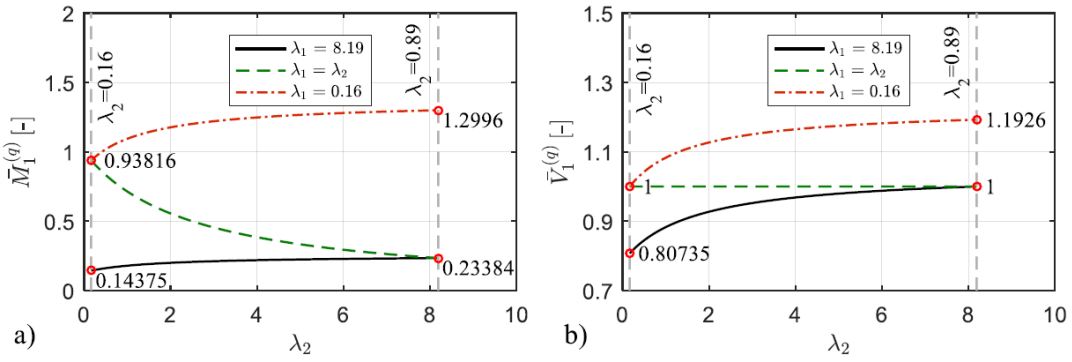

FIGURE 4.8: Variability of the nodal reactions with the spring deformability terms: (a) $\bar{M}_1^{(q)}$; (b) $\bar{V}_1^{(q)}$.

The PDF of the nodal reactions $\bar{M}_1^{(q)}$ and $\bar{V}_1^{(q)}$ of the partially restrained beam subject to a uniformly distributed load q is qualitatively different. Among the possible $\bar{M}_1^{(q)}$ values that may occur depending on the spring deformability λ_1 and λ_2, the minimum moment reaction (equal to 0.14375) occurs when $\lambda_1 = 8.19$ and $\lambda_2 = 0.16$, i.e., in the semi-rigid counterpart of a hinged-clamped beam idealization, whereas the maximum moment reaction (equal to 1.2996) takes place in the other way around for $\lambda_1 = 0.16$ and $\lambda_2 = 8.19$, i.e., in the semi-rigid approximation of a clamped-hinged beam, cf. Fig. 4.8. Other two characteristic points are detected in the $\bar{M}_1^{(q)}$ PDF, see Fig. 4.8(a): one is that for ($\bar{M}_1^{(q)} = 0.23384$, which corresponds to a cusp) and the other is for $\lambda_1 = \lambda_2 = 0.16$, $\bar{M}_1^{(q)} = 0.93816$.

In quite a similar way, the characteristic points of the transversal reaction $\bar{V}_1^{(q)}$ PDF are identified and associated to limit values of the λ_i values, cf. Fig. 4.8(b). As expected, deviations of $\bar{V}_1^{(q)}$ from the value $\bar{V}_1^{(q)} = 1$ only occur when the two spring deformability terms are different from each other, i.e., for asymmetric beam restraints. Partially restrained beams with identical spring deformability at the two beam ends behave like clamped-clamped or hingedhinged beams in terms of transversal nodal reactions. In the limit cases of quasi hinged-clamped ($\lambda_1 = 8.19, \quad \lambda_2 =$

0.16) and quasi clamped-hinged beams ($\lambda_1 = 0.16, \quad \lambda_2 = 8.19$) the extreme values of $\bar{V}_1^{(q)}$ are 0.80735 and 1.1926, respectively. The quantitative analysis of Fig. 4.9 reveals that the average value of the moment reaction (0.72169) represents the 85.39^{th} of the distribution and deviates from the corresponding median value (0.36202) of 99.35%; on the contrary, due to the symmetric format of the $\bar{V}_1^{(q)}$ PDF, average and median values are coincident.

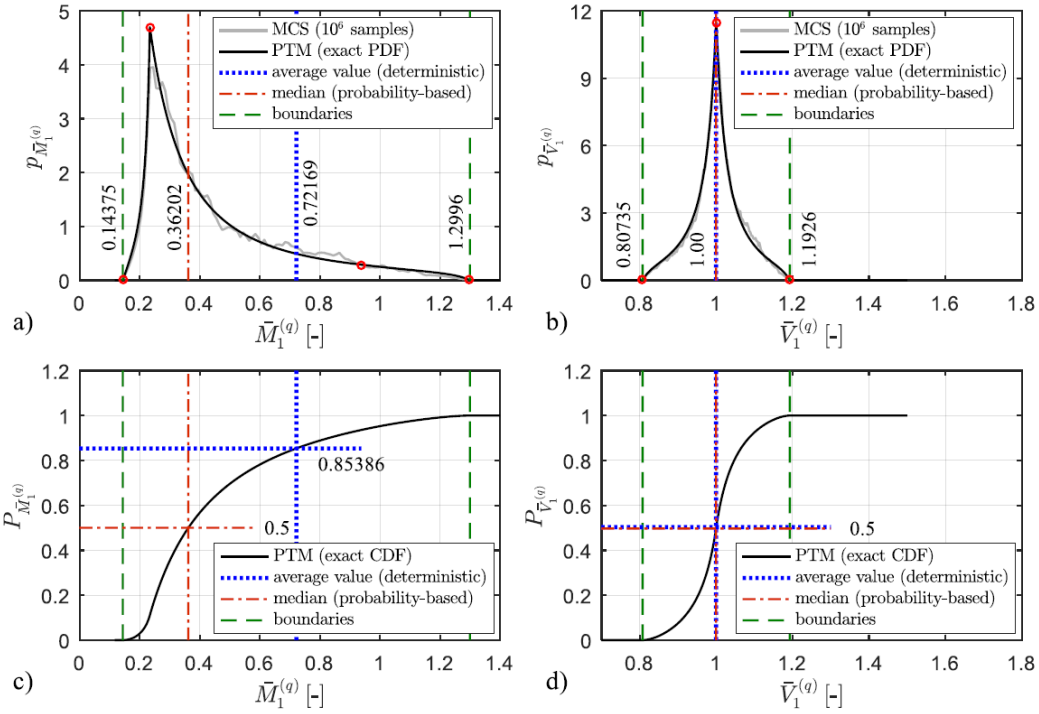

FIGURE 4.9: Probabilistic response of partially restrained beams subject to a uniformly distributed load: (a) $\bar{M}_1^{(q)}$ PDF; $\bar{V}_1^{(q)}$ PDF; (c) $\bar{M}_1^{(q)}$ CDF; (d) $\bar{V}_1^{(q)}$ CDF.

Finally, in Figs. 4.10 and 4.11, the mid-span bending moment $\bar{M}_0^{(q)}$ and the mid-span deflection $\bar{w}_0^{(q)}$ are characterized from a probabilistic point of view. These results are consistent with those of the stiffness terms, as the $\bar{M}_0^{(q)}$ and the $\bar{w}_0^{(q)}$ PDFs are both concentrated close to the quasi-pinned connection boundary (right side corresponding to $\lambda_1 = \lambda_2 = 8.19$). The mid-span response is related to the overall deformability of the beam, therefore it is not affected by the specific values of λ_1 and λ_2 at the two end nodes individually considered, but rather it only depends on the sum $\lambda_1 + \lambda_2$, which is physically reasonable. For instance, the same response in terms of bending moment and deflection would be obtained for $\lambda_1 = 8.19$, $\lambda_2 = 0.16$ and for $\lambda_1 = 0.16$, $\lambda_2 = 8.19$, cf. Fig. 4.10. Quantitative analysis of the $\bar{M}_0^{(q)}$ and the $\bar{w}_0^{(q)}$ PDFs, shown in Fig. 4.11, is of paramount importance from a design viewpoint: adopting the average (deterministic) value of mid-span moment and mid-span deflection means that the design is being carried out with the 19.42^{th} and with the 19.41^{th} percentile of the corresponding distribution, respectively. In other words, the deterministic approach would lead to assuming non-conservative (unsafe) estimates of mid-span moment and mid-span deflection that are lower than the median of the corresponding PDFs. In particular, the deterministic approach would underestimate

the median of $\bar{M}_0^{(q)}$ by 15.26% and the median of $\bar{w}_0^{(q)}$ by 19.89%, respectively.

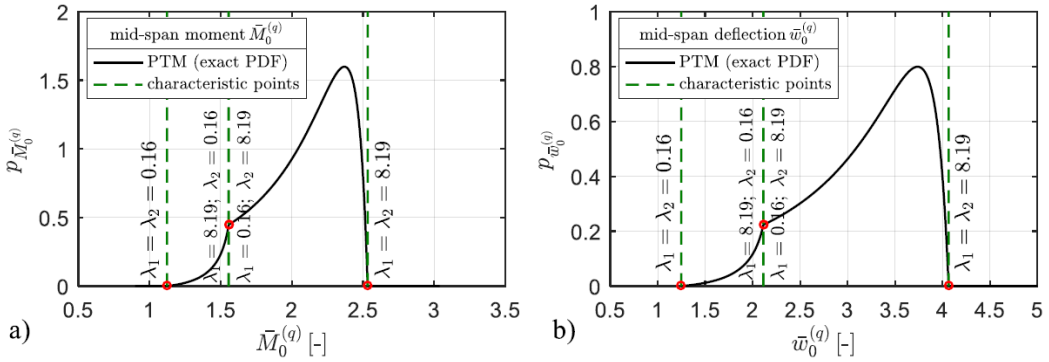

FIGURE 4.10: Qualitative examination of PDF of mid-span moment and mid-span deflection in partially restrained beams subject to a uniformly load q: (a) $\bar{M}_0^{(q)}$ PDF; (b) $\bar{w}_0^{(q)}$ PDF.

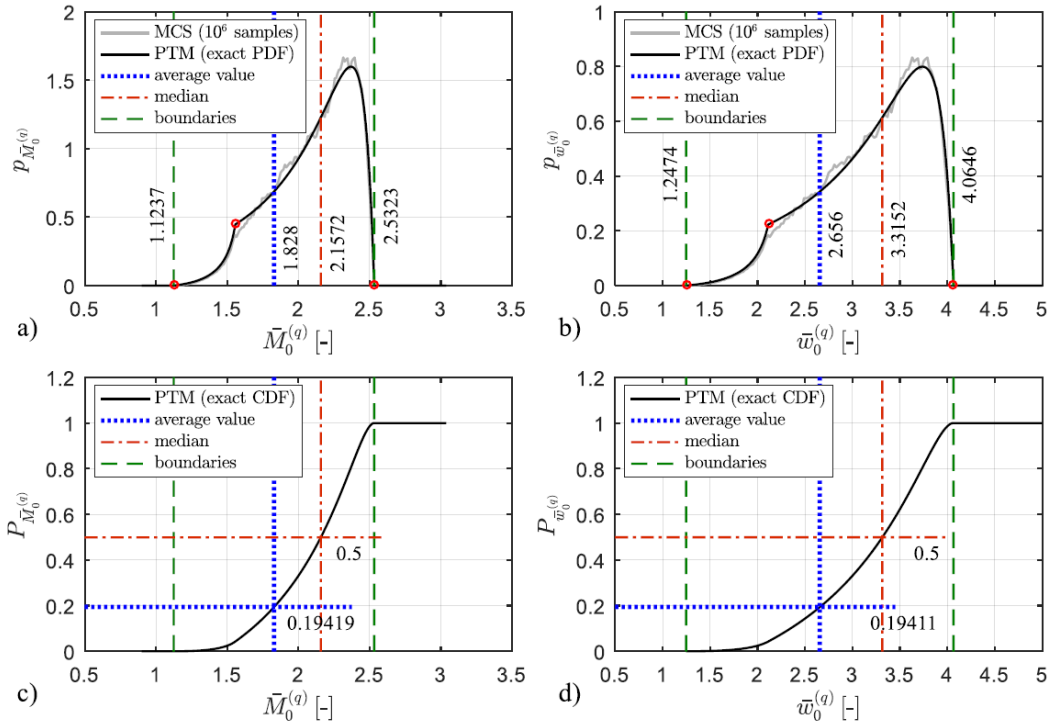

FIGURE 4.11: Probabilistic response of partially restrained beams subject to a uniformly distributed load: (a) $\bar{M}_1^{(q)}$ PDF; $\bar{V}_1^{(q)}$ PDF; (c) $\bar{M}_1^{(q)}$ CDF; (d) $\bar{V}_1^{(q)}$ CDF.

In Table 4.1, the main results of the present investigation are summarized. In particular, we report the two boundaries of the response indicators computed by assuming proper combinations of the two λ_1 and λ_2 deformability terms as discussed above.
The average value is the mean of these two bounds, which is compared to the median value. Considerable errors are found from this comparison, which alert the design engineer that misleading outcomes may result from a deterministic approach

response indicator	probability-based approach	deterministic approach				error (%)
	median (50th percentile)	lower bound	upper bound	average value	average percentile (%)	
$\bar{s}_{11}$	0.21926	2.62	2.53	3.34	2.67	2.46
$\bar{s}_{13}$	0.07122	0.021596	0.78327	0.40243	98.81	465.02
$\bar{M}_1^{(q)}$	0.36202	0.14375	1.2996	0.72169	85.39	99.35
$\bar{V}_1^{(q)}$	1.00	0.80735	1.1926	1.00	50.00	0.00
$\bar{M}_0^{(q)}$	2.1572	1.1237	2.5323	1.828	19.42	-15.26
$\bar{w}_0^{(q)}$	3.3152	1.2474	4.0646	2.656	19.41	-19.89

TABLE 4.1: Probability-based approach versus deterministic approach for the design of beams with semi-rigid connections.

applied to beams with partially restrained nodes if the fixity factors can be modelled as uniformly distributed random variables. These values, along with the PDFs illustrated above, could be employed to decide which value of rotational stiffness, mid-span deflection, bending moment (and so forth) to assume in a design process, and to assess which consequences such an assumption has from a probabilistic point of view.

It is worth noting that the above calculation considers a quite large spectrum of fixity factors, which encompasses the whole range of semi-rigid connections discussed in Section "From the rotational spring deformability to the connection fixity factor". However, when the type of connection is chosen for a steel framed structure, the range of variability of the fixity factor, and also of the spring deformability λ, is reduced as compared to the one assumed above, see e.g.,(Abdalla and Chen, 1995; Kim and Choi, 2001). Which implications this restricted interval has in a design process is here briefly outlined.
To this aim, just as an example we suppose that a topand- seat angle connection is adopted and a more realistic interval of λ is considered. Following the qualitative plot of Fig. 4.5(a), among the steel semi-rigid connections this quite flexible type of connection is close to the pinned EC3 connection boundary, therefore it has been characterized in terms of a $\lambda_{ref} = 7.0$ value, assumed as a reference value in a design process. In line with the scope of the section, in order to incorporate the largely scattered results that may arise from experiments, a $\pm 50\%$ deviation is assumed so that the λ variable is a uniformly distributed variable in the range $\left[0.5\lambda_{ref}, 1.5\lambda_{ref}\right]$. The probabilistic response of a beam complying with this more realistic assumption is illustrated in Fig. 4.12 in terms of mid-span bending moment $\bar{M}_0^{(q)}$ and deflection $\bar{w}_0^{(q)}$ PDF and CDF, respectively.

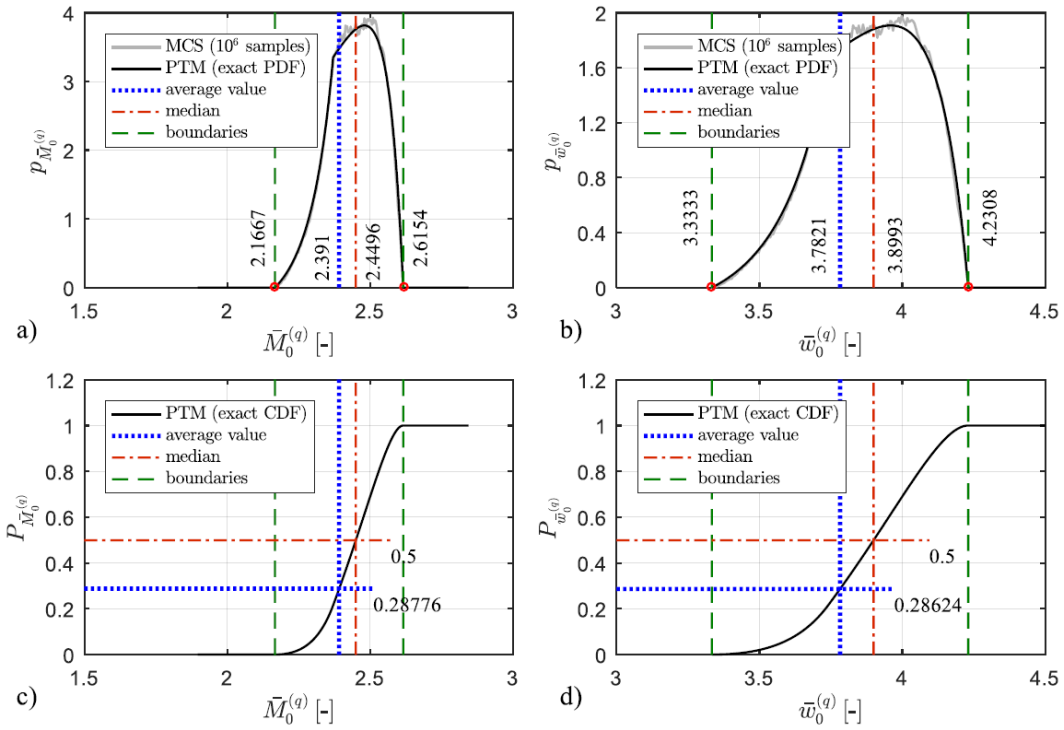

FIGURE 4.12: Probabilistic response of beams with top-and-seat angle connections ($\lambda_{ref} = 7.0$, $\pm 50\%$ variation) subject to a uniform load: (a) $\bar{M}_0^{(q)}$ PDF; (b) $\bar{w}_0^{(q)}$ PDF; (c) $\bar{M}_0^{(q)}$ CDF; (d) $\bar{w}_0^{(q)}$ CDF.

It is interesting to compare Fig. 4.11 with Fig. 4.12 that report the same results but arise from two different probabilistic characterizations of the beam-to-column connections. This comparison reveals that, as expected, the narrower interval of the λ values leads to a reduced variability of the response indicators. If the variation of λ were neglected and the calculation were performed assuming a deterministic $\lambda_{ref} = 7.0$ value, a normalized moment and deflection equal to 2.391 and 3.7821 would be obtained (the average value in this case corresponds to the deterministic assumption $\lambda = \lambda_{ref}$). These values represent the 28.77^{th} and 28.62^{th} percentile of the corresponding distribution, respectively. Therefore, similar design implications to the above calculation are deduced, as the deterministic approach leads to non-conservative estimates of mid-span moment and mid-span deflection that are lower than the median of the corresponding PDFs. This result has been already obtained with the larger λ interval examined above. The underestimation is however less pronounced than the previous case with larger λ interval, and the associated relative error is reduced accordingly.

Obviously, the higher is the dispersion, the more uncertain are the results. On the contrary, if λ were a deterministic variable, i.e., $\lambda = \lambda_{ref}$ without variation, all the response indicators would follow a Dirac Delta distribution centered at the average value and the probabilistic study here proposed would provide no added value as compared to a deterministic analysis. This underlines that the above conclusions are far from being of general validity, and the specific situation should be analyzed from case to case on the basis of available experimental data and input parameters (e.g., type of connections involved in a specific project).

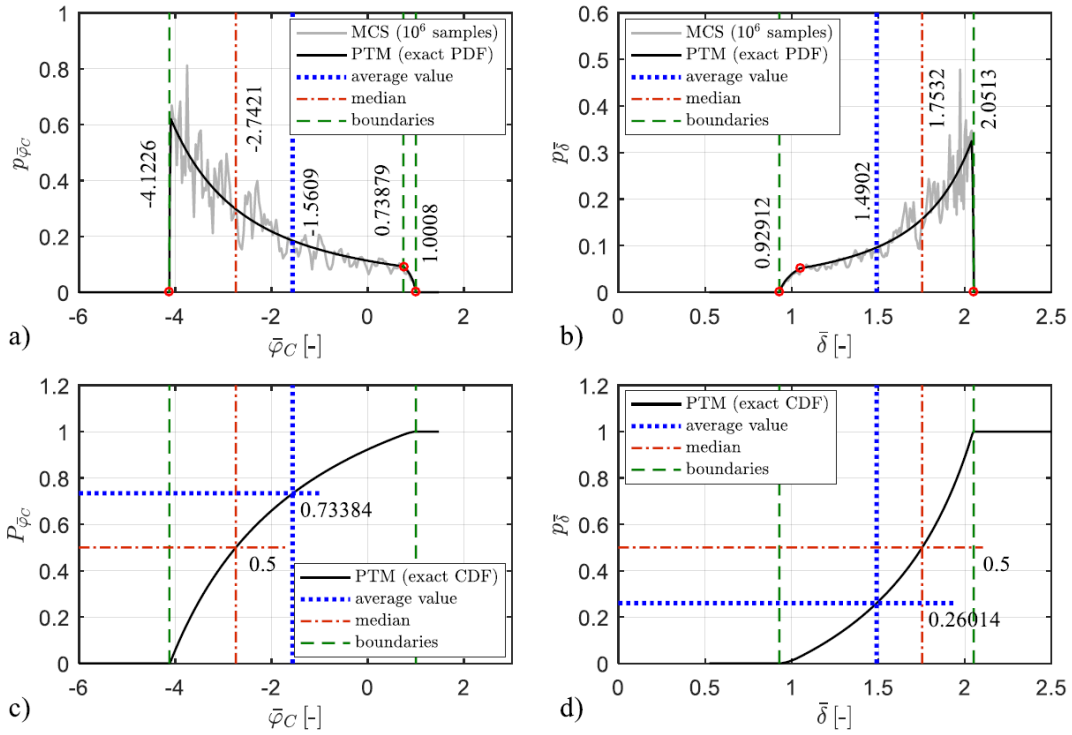

FIGURE 4.13: Probabilistic response of frame I with semi-rigid beam-to-column connections: (a) normalized $\bar{\varphi}_C$ PDF; (b) normalized $\bar{\delta}_C$ PDF

4.2.3 Probabilistic response of frames with semi-rigid nodes

In this Section we present results concerning the probabilistic structural response of frames with semi-rigid connections. A single-bay frame with semi-rigid beam-tocolumn connections (frame I) and a single-bay frame with semi-rigid column-to-foundation connections (frame II) are investigated, as sketched in Fig. 4.4.

4.2.3.1 Single-bay frame with semi-rigid beam-to-column connections

The probabilistic response of the frame I subject to both a uniformly distributed load q applied on the BC partially restrained beam and a point load $P = qL$ applied to the node B is investigated. In Fig. 4.13, the PDF of node C rotation $\bar{\varphi}_C$ and lateral displacement $\bar{\delta}$ are illustrated. It is observed that when dealing with frames, due to the strongly nonlinear character of the relationships between the fixity factors and the response indicators (much higher than the individual beam, cf. Eqs. 4.17), the number of samples needed to closely approximate the exact PDF by the MCS should be very high, largely exceeding one million. It is interesting to note that, due to the range of variability in the beam-to-column connection stiffness, a very large variability of the nodal rotations is expected, and the $\bar{\varphi}_C$ value may even change its sign as compared to the perfectly rigid case. However, this result is ascribed to the quite large assumed interval of fixity factors, as already noted above. Additionally, it is worth noting that in more realistic frames with a significant number of bays and floors, the influence of joint stiffness on the global response is certainly reduced as compared to this very simple frame structure with only one floor and one bay. In Fig. 4.14, the response in terms of moment reaction at the beam-to-column connection $\bar{M}_B$ and at the column base $\bar{M}_D$ is scrutinized from a probabilistic point of view.

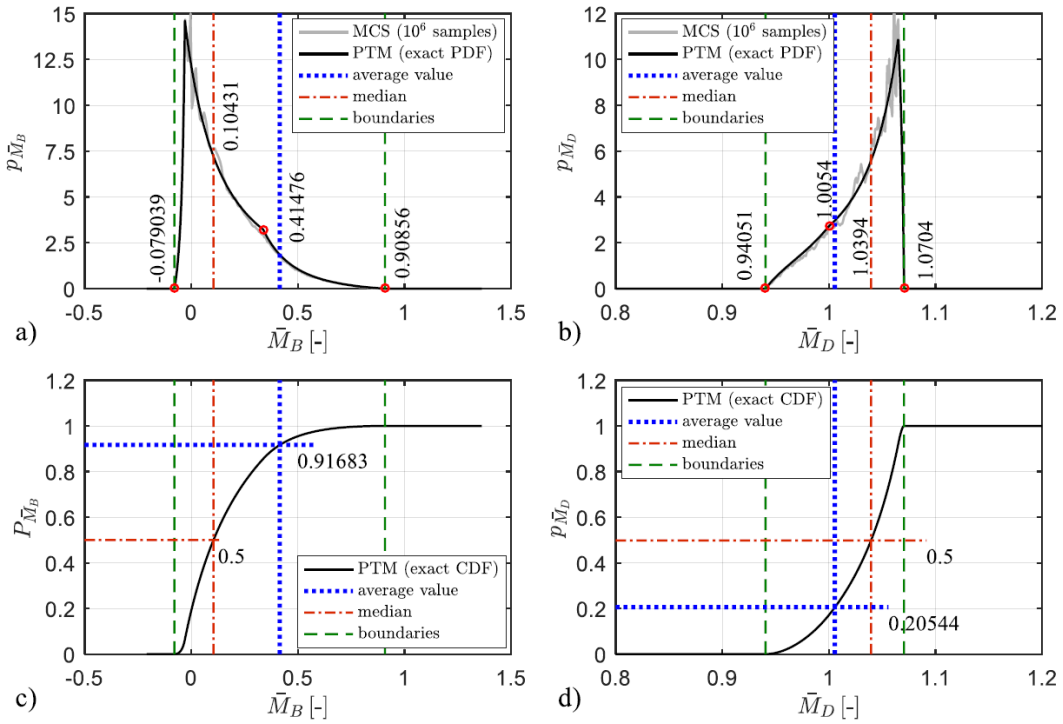

FIGURE 4.14: Probabilistic response of frame I with semi-rigid beam-to-column connections: (a) normalized $\bar{M}_B$ PDF; (b) normalized $\bar{M}_D$ PDF; (c) normalized $\bar{M}_B$ CDF; (d) normalized $\bar{M}_D$ CDF.

In line with the expectations, one million of samples in the MCS seems to be a satisfactory number for approximating the exact PDF of $\bar{M}_B$ but not that of $\bar{M}_D$ that involves a slightly more intricate relationship in terms of fixity factors, cf. Eqs. 4.19.

Average and median $\bar{M}_B$ values differ for almost 300%, which means that a design based on the average value would disproportionally overestimate the design moment at the node B. Indeed, the average value (0.41476) represents the 91.68^{th} percentile of the $\bar{M}_B$ distribution. Moreover, a small influence of the semi-rigid connections on the moment at the column base $\bar{M}_D$ is detected, which is physically consistent as the randomness is concentrated on the beam and not on the column. Indeed, the variability of D M is comprised to within nearly a $\pm$7%of the perfectly-rigid case, with extreme values equal to 0.94051 and 1.0704 corresponding to the couples ($\lambda_1 = 8.19, \lambda_2 = 0.16$) and ($\lambda_1 = \lambda_2 = 8.19$), respectively. Owing to the narrow interval in which the $\bar{M}_D$ PDF is concentrated and considering the $\bar{M}_B$ PDF, it can be concluded that deterministic approaches would lead to reasonable approximations of the moment reaction at the column base but not of the moment reaction at the beam-to-column connection.

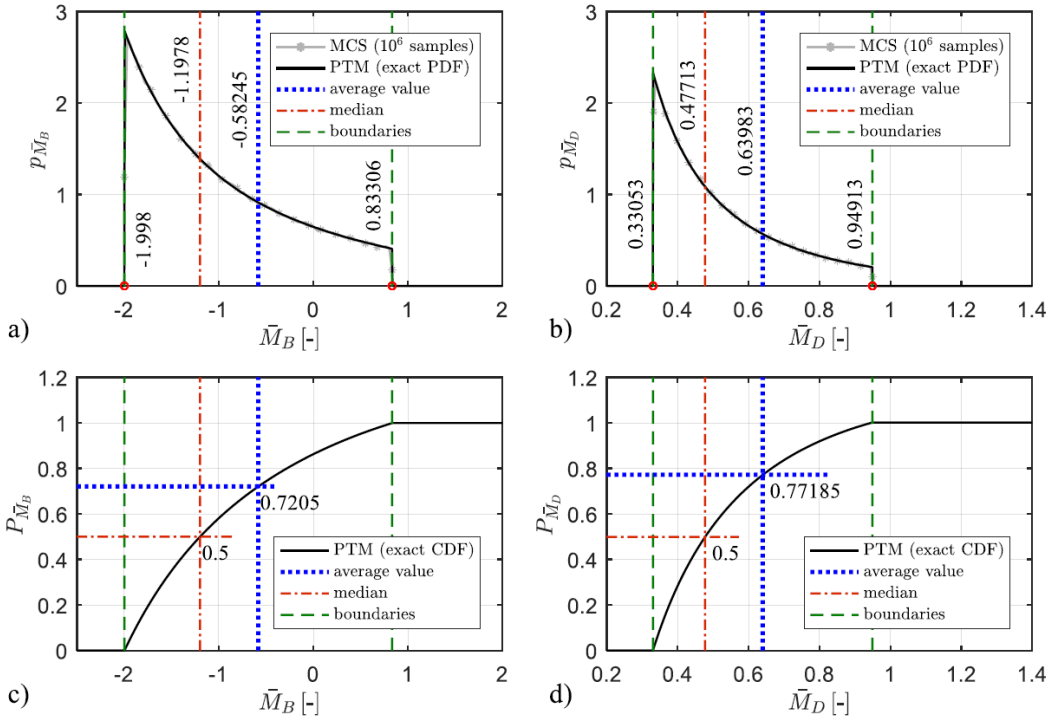

FIGURE 4.15: Probabilistic response of frame II with semi-rigid column-to-foundation connections:: (a) normalized $\bar{M}_B$ PDF; (b) normalized $\bar{M}_D$ PDF; (c) normalized $\bar{M}_B$ CDF; (d) normalized $\bar{M}_D$ CDF.

uniform distribution
for fixity factors)

response indicator	uniform distribution for fixity factors		lognormal distribution for fixity factors	
	median (50th percentile)	average value percentile (%)	median (50th percentile)	average value percentile (%)
$\bar{M}_B$	-1.1978	72.05	-1.2031	74.65
$\bar{M}_D$	0.47713	77.18	0.47806	80.94

TABLE 4.2: Probability-based approach versus deterministic approach for the design of beams with semi-rigid connections.

4.2.3.2 Single-bay frame with semi-rigid column-to-foundation connections

The probabilistic response of the single-bay frame with semi-rigid column-to- foundation connections is finally sought. By inspection of Fig. 4.15, it emerges that in this case the moment reaction $\bar{M}_D$ PDF at the column base is not confined to within a rather narrow interval, as in the previous frame, but is widely distributed and extends from 0.33053 to 0.94913. This is physically consistent, because in this case the randomness of the connection concerns just the base of the columns, therefore in contrast to the previous case the fixity factors lead to a significant variability of the $\bar{M}_D$ value. The deterministic average values of $\bar{M}_B$ and $\bar{M}_D$ represent the 72.05^{th} and the 77.18^{th} percentile of the distribution, respectively. Therefore, in this case resorting to a probabilistic design approach would lead to more economical solutions, based on lower moments at both the beam-to-column connection and at the column

base. The peculiar interval-like trend of the $\bar{M}_B$ and $\bar{M}_D$ PDFs shown in Fig. 4.15(a) and 4.15(b) is just a consequence of the uniform distribution assumption of the fixity factors. It seems interesting to scrutinize to what extent the probability-based structural response varies if a different assumption were made on the probabilistic distribution of the fixity factors.

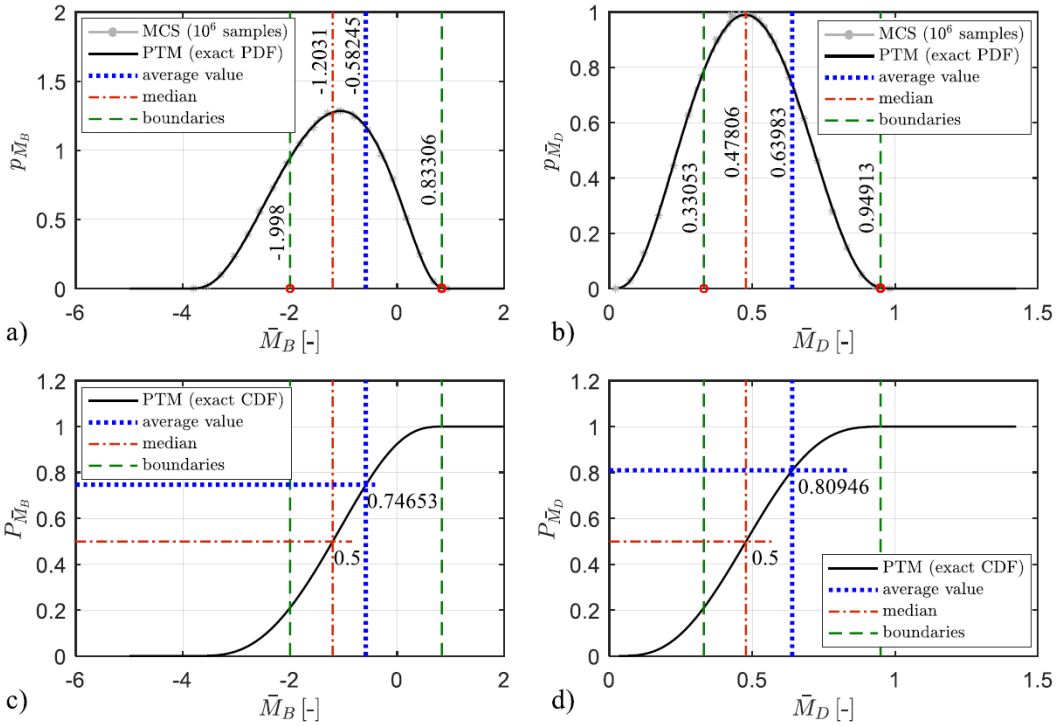

FIGURE 4.16: Same as Fig. 4.15 but with a lognormal distribution assumption for the fixity factors.

To this aim, in Fig. 4.16, we report the $\bar{M}_B$ and $\bar{M}_D$ PDFs by assuming that the fixity factors follow a lognormal distribution in place of a uniform distribution. The parameters of the lognormal distribution have been selected according to the following criterion

$$\mu = \frac{0.16 + 8.29}{2} = 0.525; \quad \mu_{log} = 1.4297; \quad \sigma = \frac{0.16 + 8.29}{10} = 0.525835527 \quad (4.24)$$

Although the PDFs of $\bar{M}_B$ and $\bar{M}_D$ resulting from the lognormal distribution are qualitatively different from those of Fig. 4.15, these distributions leads to really similar considerations from a design viewpoint: for instance, the median of $\bar{M}_B$ is -1.2031 against the value -1.1978 found for a uniform distribution. Other relevant comparisons are listed in Table 4.2. This comparison highlights that the results discussed in this section can be considered of quite general validity, since they are little affected by the choice of the fixity factors distribution. Obviously, the design engineer should carefully reflect upon this assumption and should adopt the most appropriate fixity factors distribution on the basis of available experimental data regarding the specific semi-rigid connections involved in the project.

4.2.4 Some remarks

A fully probabilistic approach has been presented to describe the structural response of steel beams and frames with uncertain semi-rigid connections. The non-perfect constraints and joints are endowed of an uncertain degree of rotational stiffness, through the definition of the deformability of the springs via random variables. Incidentally, closed-form expressions of a few structural response indicators of beams and simple frames with partially restrained nodes have been presented. The randomness of the structural response has been entirely ascribed to the uncertainty in the fixity factors at the beam end nodes, thus related to the rotational deformability of the springs. The adopted probabilistic approach, based on the application of the PTM to vector-valued random variables related by means of the nonlinear laws above cited, permits one to compute the exact PDF of the structural response based on the distribution of the fixity factors. Therefore, the design engineer can straightforwardly identify the value of certain indicators of the structural response associated to a given non-exceeding probability, which is very important in the framework of limit state design. The characterization of the rotational spring stiffness terms should be based upon experimental findings and laboratory calibration, which is beyond the scope of the proposed analytical study. In this section, reference has been made to the EC3 provisions, wherein limit values of the fixity factors for steel semi-rigid connections are indicated. We have reasonably assumed that the fixity factors are uniformly distributed within such EC3 interval, although the proposed analysis method is applicable to a more general class of elements and materials, not confined to steel framed structures. The PDFs of a few indicators of the structural response have been derived for both beams and simple frames.
Design considerations have emerged when comparing the probability-based approach with a deterministic approach based on the average values, the latter referring to the intermediate values of the fixity factors between the two extreme cases. Misleading (and in some cases non - conservative) conclusions from a design viewpoint might be drawn unless the probabilistic nature of the structural response is properly accounted for, i.e., when resorting to a deterministic approach. As an example, if the deterministic average values were assumed in the design process, one would underestimate the mid-span deflection of around 20% and, similarly, the mid-span bending moment of nearly 15% as compared to the median (probability-based) value. However, there is not a unified and common trend for all the response indicators, for instance some response quantities such as the moment reaction at the joint, are overestimated and not underestimated. From the obtained results, it is possible to state that the more reliable reactions and deflections than those derived from a deterministic approach are however obtained, which leads to more realistic and economical design decisions especially when experimental data on the connection stiffness are quite scattered.
Although the design engineer could decide to select more appropriate distributions than the uniform on the basis of available experimental data, it has been observed that the obtained results are little affected by the distribution itself. On the contrary, it is of relevant importance to identify appropriate upper bounds and lower bounds of the fixity factors for the given connections (that are element-specific and material-specific data) involved in a given structure, which falls beyond the scope of the present section. In this regard, literature review papers as well as experimental testing should assist the designer in such choice. With no doubt, the range of variability of the fixity factors alters the outcomes of the probability-based investigation. In many practical cases, this range is narrower than the interval adopted in

this section, especially because the type of connection is known in a framed structure. However, the general qualitative conclusions drawn for the quite large interval adopted in this section remain, as demonstrated by the analysis of a more reasonable case in which a specific connection type has been selected and a more realistic interval has been considered. Rather than providing precise probabilistic results for each specific connection type, the aim of this section is just limited to present a more accurate method of analysis and to alert the engineer that certain design implications arise when resorting to a nonprobabilistic (deterministic) design approach. Semi-rigid connections, by nature characterized by largely scattered results, should be more appropriately dealt with via a fully probabilistic approach.

4.3 In-plane response of masonry infilled RC framed structures: A probabilistic macromodeling approach

Typically, reinforced concrete (RC) framed structures are infilled with non-structural panels in order to separate the internal building space from the external environment. The structural behavior of infill panels made by masonry is extremely complex, characterized by uncertainties in the mechanical characteristics of the raw materials (clay, concrete), the mortar thickness and quality, the brick geometry and arrangement, the relative stiffness of the frame and of the infill panel, as well as the actual workmanship expertise. Although they are considered as non-structural components in the structural calculation, masonry infills do modify the stiffness, strength and ductility response scenarios of the overall RC frame. Therefore, neglecting their presence in structural analysis and design of masonry infilled RC frames may lead to inaccurate predictions and wrong design conclusions. Additionally, the actual behavior is further complicated by the presence of irregularities in the distribution of infills in plan and elevation of the building, and the resulting overall interaction between infill walls and surrounding frame (Asteris et al., 2015a; Khoshnoud and Marsono, 2016; Asteris et al., 2017a). This interaction may or may not be beneficial from a design viewpoint, for instance an irregular distribution of infills may produce torsional behaviors along with triggering undesired phenomena of soft stories, as demonstrated by observations after catastrophic earthquakes, see the emblematic examples illustrated in Fig. 4.17. Additionally, in common practice infill walls include openings (e.g., doors, windows) and this further complicates the determination of the mechanical response of masonry infilled frames (Asteris et al., 2011; Asteris et al., 2016a).

Considering the experimentally observed uncertain nature of the masonry behavior along with the dissemination of a large number of predictive expressions, the aim of this section is to propose a probabilistic approach for the analysis of masonry infilled RC frames. This probabilistic framework is particularly motivated by the scatter of experimental results on which most of the predictive (simplified) expressions are based, which may induce doubts about which mechanical characteristics to assume for the diagonal struts in a simplified model.

The presence of a variety of empirical expressions in the literature makes it difficult to decide which is the most suitable one for design purposes, even more complicated by the uncertain nature of the masonry behavior. In this section, we face the problem of determining the structural response of masonry infilled reinforced concrete (RC) frames from a probabilistic perspective, by assuming the diagonal strut (modeling the masonry panel) as a random variable. In this way, the suitability of the different expressions proposed in the literature may be assessed in terms of how

closely they predict the mean values (or some characteristic values) of the relevant probability density function.

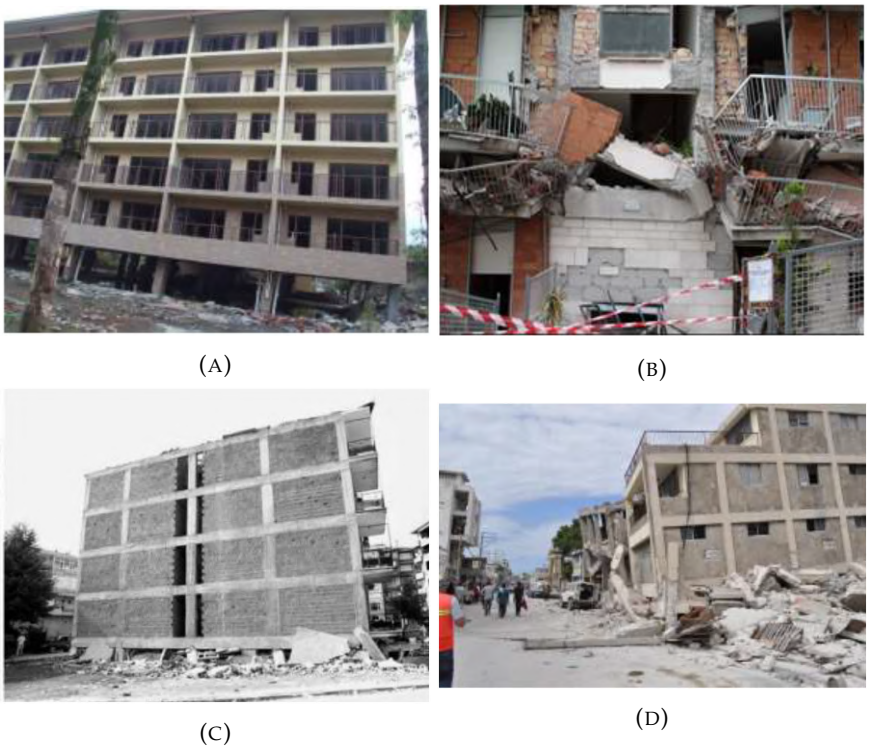

(A) (B) (C) (D)

FIGURE 4.17: Examples of poor seismic performance of RC frames with masonry infill walls: first-story damage in 2008 Wenchuan earthquake (China, Mw = 8.0) (A), intermediate story collapses due to infill failure in 1999 L'Aquila earthquake (Italy, Mw = 6.3) (B), first-two-story collapse in 1999 Kocaeli (Turkey, Mw = 7.4) (C) and in 2010 Haiti earthquake (Mw = 7.0) (D)

Additionally, the probabilistic framework allows the evaluation of the implications of the uncertain nature of the masonry infills in a set of response indicators. This is important to asses to what extent the randomness of the masonry infills propagates in the structural response. In literature, probabilistic approaches to this problem are very few (Erdolen and Doran, 2012) and usually rely on Monte-Carlo-based sampling techniques involving repetitive operations and computational effort, especially for structures with many degrees of freedom (DOFs). On the contrary, the focus of this section is on a more effective numerical procedure through which the probabilistic characterization of the response of a masonry infilled RC frame can be identified in a direct manner. The advantage of this procedure is that no sampling operation is required (unlike Monte Carlo method or other techniques from the literature). This implies great computational efficiency in comparison with other methods. Another strength of this procedure is its simplicity when handling uncertain parameters like the ones involved in the equivalent diagonal truss elements associated with the macro-modeling assumption of the masonry infills, as will be in-depth clarified in the following parts of the section.

4.3.1 Macro-modelling approach and overview of expressions

The modeling of the masonry infills and of their stiffening contribution to the surrounding RC frame has been a topic of great interest for decades. Since the Polyakov's work in 1960 (Polyakov, 1960), the most simplified way to account for the masonry panel has been to introduce an equivalent diagonal strut element that incorporates the stiffening contribution of the masonry infill. In this simplified manner, underlying a macro-modeling approach, the geometrical characteristics of the equivalent diagonal strut are chosen such that they reflect the geometrical and mechanical properties of the actual masonry panel. A schematic representation of this macro-modeling approach is reported in Fig. 4.18, wherein the main geometric characteristics of both the masonry panel and the equivalent diagonal strut are illustrated.

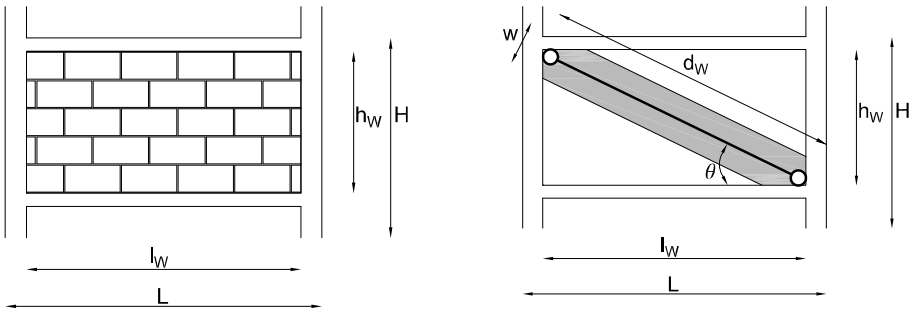

(A) Schematic representation of the masonry infill (B) Conventions used for the macro-modeling approach

FIGURE 4.18: Schematic representation of the masonry infill (A) and conventions used for the macro-modeling approach (B)

For monotonic loading only one strut is introduced in the compression direction, whereas for more general cyclic loading a couple of struts along the two main diagonals would be necessary. The former assumption is adopted in this section, as we will restrict our attention to monotonic loading conditions. There exist more complicated macro-modeling layouts that involve more than a single diagonal strut element to represent the masonry panel behavior and to properly account for the interaction between the strut and the shear response of the column (Crisafulli, 1997). Moreover, concentric and eccentric struts have also been investigated (Al-Chaar, 2002), and it has demonstrated that a series of off-diagonal strut elements are more appropriate to capture the local effects arising from the interaction between masonry panel and surrounding frame (Crisafulli, 1997). Furthermore, linear elastic and nonlinear hysteretic constitutive models can be adopted to represent the stress-strain relationship of the equivalent strut, for example incorporating nonlinear fiber elements (Crisafulli, Carr, and Park, 2000).
All these complex models strive for describing the actual behavior of the masonry panel with increasing accuracy. Considering all the uncertainties involved in the correct modeling and in the determination of the most appropriate parameters that reflect the actual, experimentally observed, masonry panel response, a variety of empirical expressions have been proposed in the literature so far. Due to the stochastic nature of the masonry behavior and the large scatter of the corresponding experimental results, it is quite difficult to decide which mechanical characteristics to assume for the diagonal struts in a simplified model. Even within the simplest

framework of modelling the masonry panel via a single linear-elastic diagonal strut element, there exist a variety of formulae proposed by different authors in the last few decades. The validity of these expressions is limited to the specific geometric and mechanical properties of the masonry panel on which these formulae were calibrated.

The aim of this section is to present a probabilistic approach for the determination of the in-plane response of masonry infilled RC framed structures. Attention is paid to the simplest modeling assumption of a single linear-elastic diagonal strut element, but the generality of the proposed probabilistic approach is not confined to such assumption and extension to multiple struts would be possible, although the generalization to nonlinear behavior seems to be not straightforward. The cross area of the strut is generally computed as the product of the panel thickness t_w and an equivalent width w. The latter parameter w is here assumed as a random variable to take into consideration the uncertain nature of the masonry panel. The development and dissemination of a large number of formulae for w makes it difficult to make a reliable choice of the diagonal strut properties. As an emblematic example, the stiffening contribution arising from a macro-modeling of the masonry panel is reported in Fig. 4.19 (in terms of the w/d_w ratio) for a variety of empirical expressions, thus highlighting the variability of different formulations proposed in the literature. Consequently, the probabilistic characterization of w, discussed in the next section, will be based upon an ensemble of empirical expressions. The expressions considered in this study are all listed in Table 4.3, where the following positions have been considered

$$\lambda_h = \sqrt[4]{\frac{E_w t_w \sin 2\theta}{4 E_c I_c h_w}} H \tag{4.25}$$

with E_w and E_c the Young's modulus of masonry and reinforced concrete, respectively, I_c the second moment of the cross-sectional area of the column,

$$\beta = \frac{E_c A_c}{G_w A_w} \tag{4.26}$$

where $A_c = b_c h_c$ is the column gross area and $A_w = t_w l_w$ is the area of the masonry panel in the horizontal plane, while G_w is the shear modulus of the masonry. The b value in Eq. 4.26 must satisfy the following constraints: $0.9 \leq \beta \leq 11$ and $0.75 \leq 2.5 l_w/h_w \leq 2.5$. Furthermore, the relative stiffness of beam and column λ_b and λ_c, respectively, and the related contact lengths z_b and z_c of the Hendry expression (Hendry, 1981) are defined as

$$\lambda_b = \sqrt[4]{\frac{E_w t_w \sin 2\theta}{4 E_c I_b h_w}}; \quad \lambda_c = \sqrt[4]{\frac{E_w t_w \sin 2\theta}{4 E_c I_c h_w}}; \quad z_{b,c} = \frac{\pi}{2\lambda_b}; \quad z_c = \frac{\pi}{2\lambda_c} \tag{4.27}$$

with I_b denoting the second moment of the cross-sectional area of the beam. Finally, in the expression by Cavaleri, Fossetti, and Papia, 2005 and Amato et al., 2008 the parameters are

$$\begin{aligned} &c = 0.249 - 0.0116\nu_d + 0.567\nu_d^2; \quad \delta = 0.146 - 0.0073\nu_d + 0.126\nu_d^2; \\ &k = \frac{1}{0.75 + 0.25\frac{L}{H}} \left(1 + \left(18\lambda^* + 200\right)\varepsilon_v\right); \quad \varepsilon_v = \frac{F_v}{2 A_c E_c}; \\ &\lambda^* = \frac{E_d}{E_c} \frac{t_w \left(H - h_b/2\right)}{A_c} \left(\frac{\left(H - h_b/2\right)^2}{L^2} + \frac{A_c}{4 A_b} \frac{1}{\left(H - h_b/2\right)} \right) \end{aligned} \tag{4.28}$$

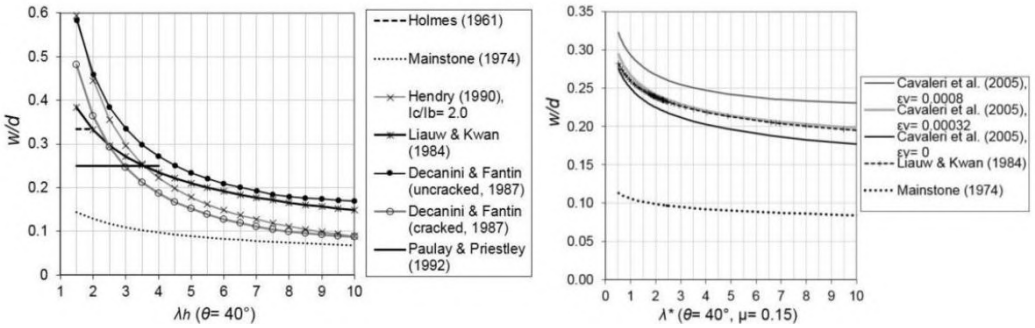

FIGURE 4.19: Variability of the stiffening contribution (w/d) with respect to the geometrical and mechanical parameters of the masonry infills (λ_h and λ^*) – after (Tarque et al., 2015)

The expression conditions listed in the right column of Table 4.3 represent some upper bound and lower bound values of the analytical expressions. In case of a given threshold being exceeded, the limit value is assumed as an admissible range.

4.3.2 Probability characterization of masonry infills

The analysis performed in this work is limited to static loading conditions and serviceability limit states, whereby the behavior of the masonry infills may be assumed as linear-elastic.
In other words, no significant damage is expected to occur in the masonry infills. The uncertain mechanical behavior of the masonry infills and the related effects on RC framed structures has given rise to the dissemination of a large number of studies. In the framework of macromodeling approaches, many empirical expressions have been proposed, as overviewed in the previous section. However, the validity of these empirical formulae is strictly related to the assumptions made for their development, and to the set of geometrical and mechanical properties considered for the validation of the corresponding models. As already said, it is quite difficult to decide which mechanical characteristics to assume for the diagonal struts in a simplified model. Therefore, in this research work we attempt to evaluate the effects of the masonry infills uncertainty on the structural response of RC frames. To this aim, the strut width is here considered as a random variable, whose stochastic properties stems from the above set of empirical expressions.
In particular, for given geometrical and mechanical properties of an assigned masonry infilled RC frame, all the parameters and coefficients entering the expressions reported in Table 4.3 are known. Therefore, a set of w_i values can be derived by applying the different formulae. At this stage, from this discrete set of values a probabilistic characterization of the strut width w can be extrapolated in the form of a PDF $p_w(w)$. The characteristics of such $p_w(w)$ are thus related to a set of empirical or macromodeling-based approaches proposed in the literature by different authors. The mean value of the probability distribution $p_w(w)$ is denoted as w_0. It is meant that such 0 w value is related to the whole set of expressions, and takes into account the possible circumstance that different formulae may give rise to similar w_i values. This circumstance indicates a higher probability of occurrence of a specific interval within the present stochastic framework. Moreover, the dispersion of all the w_i values may be associated with the variance of the corresponding distribution $p_w(w)$.

Authors (year)	w/d_w expression	Note
Holmes (1961)	$w/d_w = 1/3$	valid for $\lambda_h < 2$ (see Eq. 4.25) 4.27
Stafford Smith (1967)	$0.10 < w/d_w < 0.25$	the value graphically depends on λ_h
Mainstone (1971)	$w/d_w = 0.16\lambda_h^{-0.3}$	λ_h is computed throug Eq. 4.25 4.25
Mainstone (1974)	$w/d_w = 0.17\lambda_h^{-0.4}$	adopted by FEMA-274 and FEMA-306
Bazan and Meli (1980)	$w = (0.35 + 0.022\beta)h_w$	β is computed via Eq. 4.26
Hendry (1981)	$w = \frac{1}{2}\sqrt{z_b^2 + z_c^2}$	z_b and z_c computed ia Eqs. 4.27
Tassios (1984)	$w/d_w = 0.20\beta\sin\theta$	valid for $1 \leq \beta \leq 5$
Liauw and Kwan (1984)	$w/d_w = \frac{0.95\sin 2\theta}{2\sqrt{\lambda_h}}$	valid for $25° \leq \theta \leq 50°$
Decanini and Fantin (1987)	$w/d_w = 0.010 + \frac{0.707}{\lambda_h}$ $w/d_w = 0.040 + \frac{0.470}{\lambda_h}$	for $\lambda_h \leq 7.85$ for $\lambda_h > 7.85$
Paulay and Priestley (1992)	$w/d_w = 1/3$	valid for $\lambda_h < 4$
Durrani and Luo (1994)	$w/d_w = \gamma\sin 2\theta$	$\gamma = 0.32\sqrt{\sin 2\theta}\left(\frac{H^4 E_w t_w}{m E_c I_c h_w}^{-0.1}\right)$ $m = 6\left(1 + \frac{6}{\pi}\frac{E_b I_b H}{E_c I_c L}\right)$
Flanagan and Bennet (1999)	$w = \frac{\pi}{C\lambda_h \cos\theta}$	C is an empirical value dependent on the in-plane drift displacement
Cavaleri et al. (2005) and Amato et al. (2008)	$w/d_w = \frac{k}{z}\frac{c}{(\lambda^*)^\delta}$	c and δ are functions of the Poisson's ratio, k is a function of the vertical load and z is a geometric parameter

TABLE 4.3: Expressions for calculation of the w/d_w ratio considered in the proposed probabilistic study (after Tarque et al.)

In the spirit of perturbation approach of stochastic analysis, the strut width w can be modelled as a one dimensional random variable with constant (deterministic) mean value w_0 and fluctuation α according to the expression

$$w = w_0\,(1 + \alpha) \tag{4.29}$$

In so doing, instead of treating the strut width itself as a random variable, the basic random variables of this problem are represented by the zero-mean fluctuations α of the strut width with respect to its mean value w_0. In Fig. 4.20, two possible representations of the probabilistic characterization of the α variable are illustrated. From the discrete set of w_i values, arising from the group of expressions reported above, it is possible to extrapolate a best-fitting PDF representation (here presented in the form of either a normal PDF or a uniform PDF) from which the mean value w_0 and the dispersion characteristics can be identified. By application of relation 4.29 the probabilistic characterization of the zero-mean fluctuation α is straightforward, which is described in the bottom part of Fig. 4.20. From a probabilistic point of view, while the uniform distribution implies that all the w_i values have equal probability of occurrence between the minimum and maximum w_i values (denoted as w_{min} and

w_{max}, respectively), the normal distribution takes into account the concentration of the w_i values around the mean value w_0 (which is the most likely value, meaning that the majority of the above empirical expressions lead to values around such w_0).

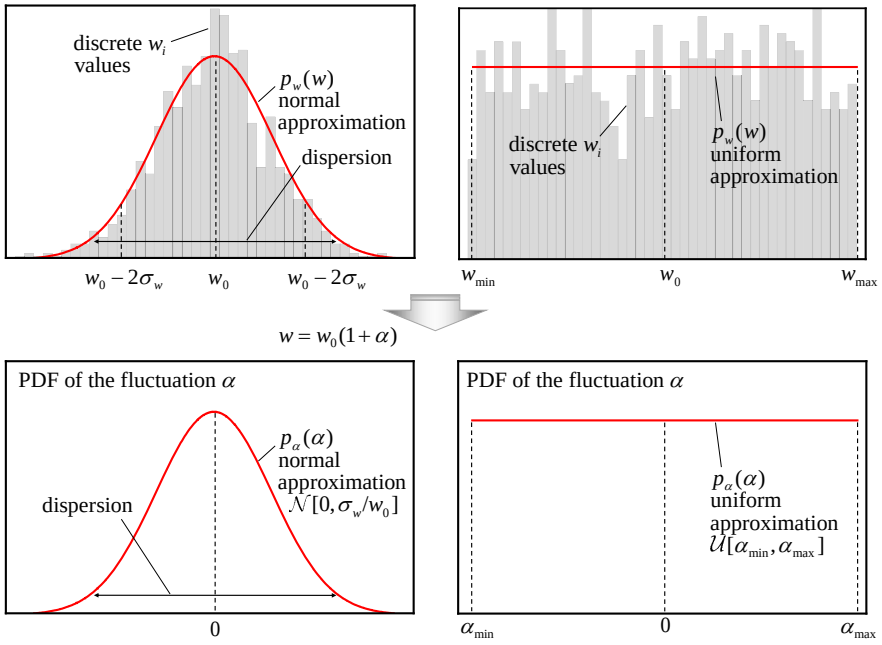

FIGURE 4.20: PDF of the w and of the α variable in the normal (left) and uniform (right) approximation

Additionally, in the case of the normal distribution the statistical values $w_0 \equiv \mu_w$ and w_i are directly estimated from the discrete set of the w_i values, whereas for the uniform distribution two steps arise: 1) estimation of the best-fitting uniform PDF $p_w(w)$ from the discrete set of the w_i values, 2) evaluation of the statistical moments, including mean and standard deviation $m_w \equiv w_0$ and s_w, respectively, and determination of the boundaries α_{min} and α_{max} of the zero-mean fluctuation PDF $p_\alpha(\alpha)$ as $\pm s_w/m_w$. This conversion between the $p_w(w)$ distribution and the $p_\alpha(\alpha)$ is necessary to obtain a zero-mean PDF for the fluctuations, which is consistent with Eq. 4.29. Furthermore, it is worth noting that in a real masonry infilled RC frame there are more than just one equivalent diagonal strut element due to the presence of several masonry infills. From a probabilistic point of view, it is therefore necessary to introduce a zero-mean multivariate normal distribution defined by a covariance matrix $\mathbf{\Sigma}_{\boldsymbol{\alpha}}$ involving cross-correlation terms between the various struts $\boldsymbol{\alpha} = [\alpha_1, \alpha_2, \cdots, \alpha_m]^T$. It is reasonably expected that two adjacent masonry infills are more correlated than two farther ones, which suggests to introduce a correlation function ρ dependent upon the distance between the centroid of each diagonal strut element d, i.e., $\rho = rho(d)$. For the simplest scenario of just two masonry infills, in Fig. 4.21 the two-dimensional PDF of the $\boldsymbol{\alpha} = [\alpha_1, \alpha_2]^T$ vector of fluctuations is sketched in the two cases of uncorrelated and correlated fluctuations, in the latter case assuming a correlation factor $\rho = 0.8$.

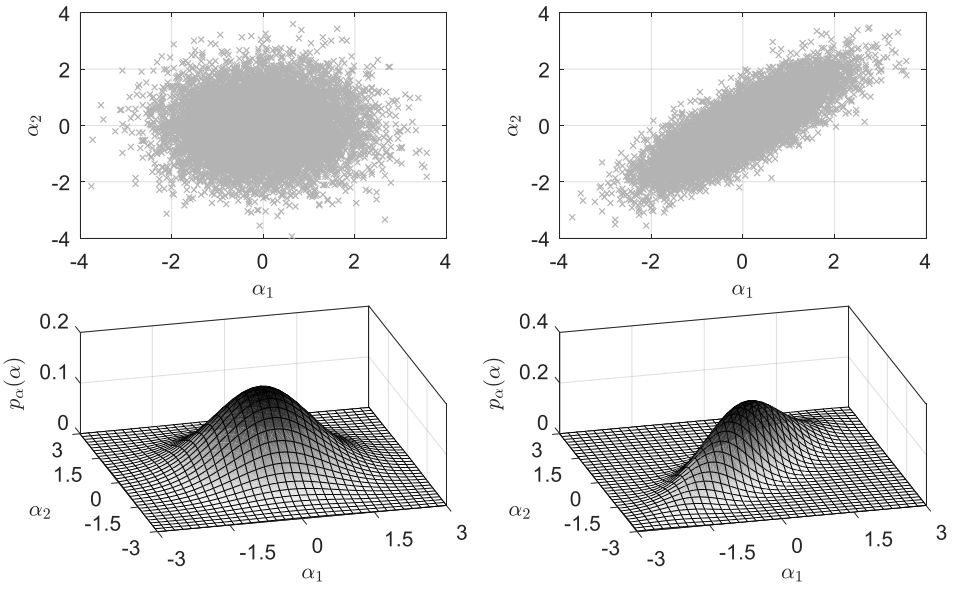

FIGURE 4.21: Comparison of $\boldsymbol{\alpha} = [\alpha_1, \alpha_2]^T$ vector of fluctuations for uncorrelated ((a), $\rho = 0$) and correlated assumptions ((b), $\rho = 0.8$)

4.3.3 Probability-based modelling techniques

As said above, the topic dealt with in this section is part of a broader and more general class of problems which are related to the structural analysis of systems with uncertain parameters. In particular, the uncertain variables can be of geometrical or mechanical nature. Here, the stochastic modeling of the masonry equivalent strut width implicitly incorporates both the uncertainty in the mechanical parameters of the masonry and the uncertainty of the geometric definition of the equivalent truss member.

The structural response of masonry infilled RC framed structures is investigated via the probability approach of the section 3.2, i.e. a handy probabilistic method of analysis that combines the APDM method with the PTM. This combined method, first time applied to masonry infilled RC frames, leads to the determination of the PDF response directly, i.e., without requiring any sampling technique. In order to summarize and clarify the main steps of the proposed algorithm, a schematic flow-chart has been constructed and reported in Fig. 4.22. In this flow-chart it is clearly shown how the two probabilistic methods (APDM and PTM) are linked together to derive the PDF of the system response directly, resorting to the use of the CF as explained above.

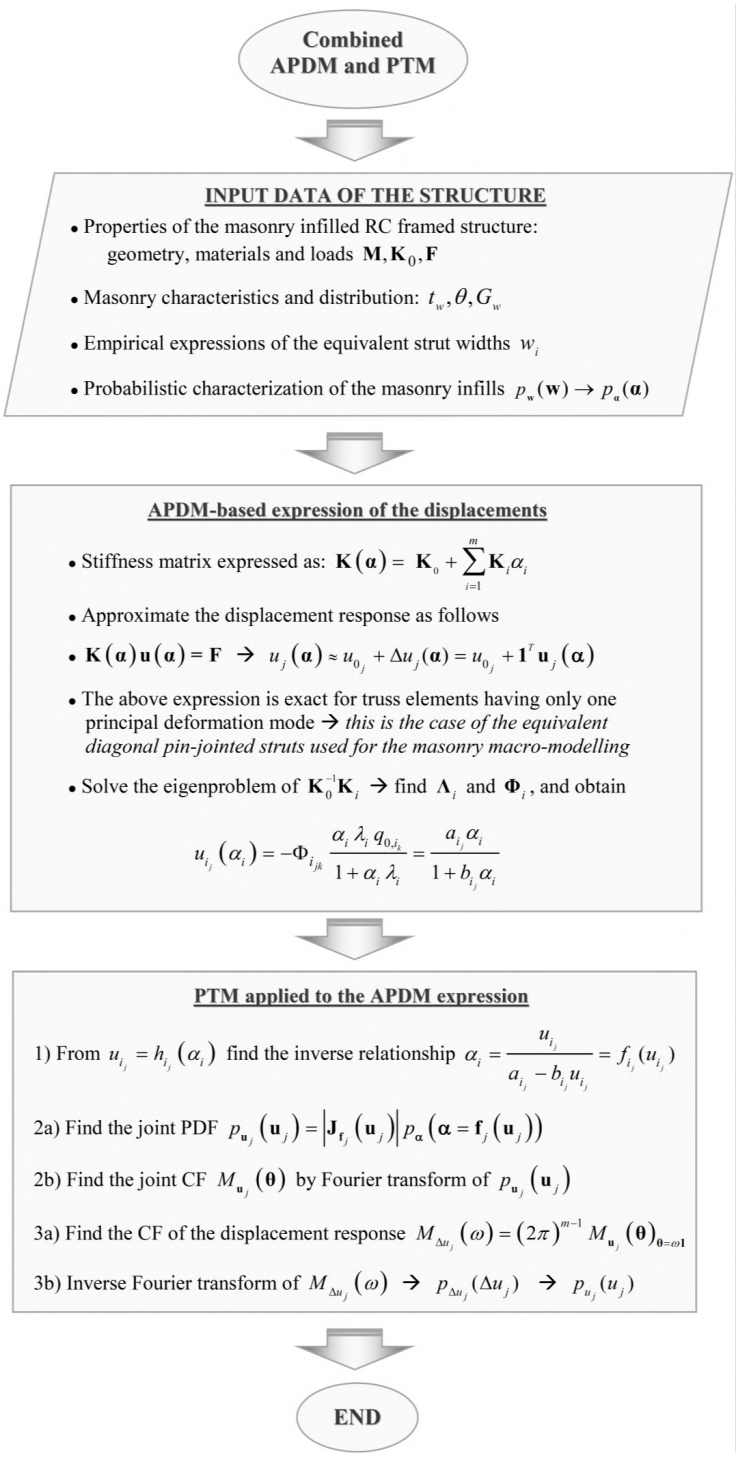

FIGURE 4.22: Flow chart of the proposed probabilistic procedure

4.3.4 Numerical examples

The proposed probabilistic procedure is here applied to compute the PDF of the response of masonry infilled RC frames in which the equivalent diagonal pin-jointed

struts are assumed uncertain. For the sake of simplicity, reference is made to a planar frame of a regular RC structure.

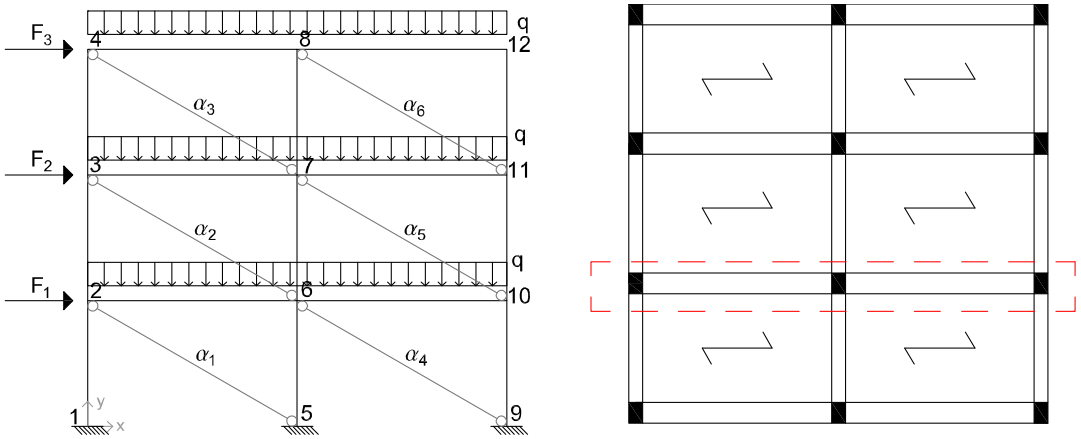

FIGURE 4.23: Sketch of the RC frame analyzed in the numerical example

level	G_1kN/m^2 + G_2kN/m^2	QkN/m^2	ψ_2 [1]
Floor	8.0	2.0	0.3

TABLE 4.4: Distributed load per unit area applied to the one-way floor slab for every level of the building

The elevation and plan views of the RC structure is shown in Fig. 4.23. The following data are assumed as known (deterministically) input parameters: bay width equal to 6.0 m , inter-story height 3.2 m , column sections 40 × 60 cm , beam sections 30 × 50 cm , concrete having Young's modulus $E_c = 30$ GPa , which is typical of ordinary concrete structural elements (Pisano, Fuschi, and De Domenico, 2013a; Pisano, Fuschi, and De Domenico, 2013b; Pisano, Fuschi, and De Domenico, 2014; Pisano, Fuschi, and De Domenico, 2015; De Domenico et al., 2014; De Domenico, Pisano, and Fuschi, 2014; De Domenico, 2015), masonry with mean Young's modulus $E_w = 5$ GPa, mean Poisson's ratio in the diagonal direction $\nu_d = 0.25$, and thickness $t_w = 40$ cm. The loads acting on the planar frame are calculated based on the loads per unit area reported in Table 4.4.
The seismic analysis is performed by means of an equivalent static lateral force procedure, with a distribution of horizontal forces detected by the response spectrum of the installation site, whose shape is reported in Fig. 4.24. The installation site is placed in Messina, Italy, and the peak ground acceleration (PGA) is $\ddot{u}_{g0} = 0.254g$ with g denoting the gravity acceleration. The first (fundamental) period of vibration is calculated according to the simplified formula for reinforced concrete building (Todaro, 2008)

$$T_1 = CH^{3/4} = 0.075(9.6)^{3/4} \times 0.41s \tag{4.30}$$

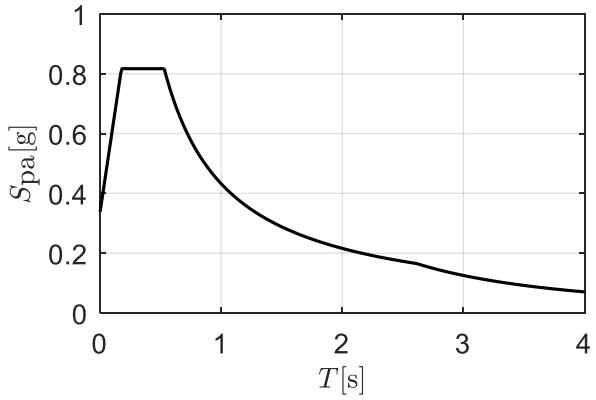

FIGURE 4.24: Elastic response spectrum of the installation site of the building

The lateral (equivalent) seismic forces acting along the building height are distributed according to the fundamental mode of vibration of the building (Todaro, 2008), and are scaled to the spectral acceleration of the elastic response spectrum at the first mode of vibration $S_{pa}(T_1)$

$$F_i = F_h \frac{z_i \cdot W_i}{\sum_j z_j \cdot W_j} \tag{4.31}$$

with $F_h = S_{pa}(T_1) \cdot \lambda \cdot W_{tot}/g$, $\lambda = 0.85$ (Todaro, 2008), and $W_{tot} = \sum_j W_j$ is the total weight of the building. Adopting the elastic- (rather than the design-) response spectrum for computing the seismic force distribution is consistent with the assumption of a linear-elastic behavior of the masonry infilled RC frame as a whole, i.e., only the elastic response is investigated in this work. Investigating the post-elastic behavior of the structure would imply a modification of the proposed procedure to incorporate a nonlinear constitutive behavior of the diagonal struts (Crisafulli, Carr, and Park, 2000) and, consequently, would justify the adoption of a behavior factor greater than one to describe the energy dissipation mechanisms occurring in the structure. The main aim of this work is the probabilistic characterization of the in-plane elastic response of the masonry infilled RC frame, while the analysis of this postelastic behavior is left for future research.
The results presented in this Section aim to highlight the influence of the uncertain characteristics of the masonry infills on a few response indicators of the RC frame. To this aim, the PDFs of several response indicators have been computed through the combined APDM and PTM methods of analysis. To validate the proposed probabilistic procedure, comparison against Monte Carlo simulation results (obtained with thousands of samples and, consequently, requiring much higher computational effort) is made for just a few selected quantities. Moreover, to demonstrate the consistency of the results of the combined APDM+PTM with the APDM method proposed by Falsone and Impollonia (Falsone and Impollonia, 2002) in addition to the Monte Carlo technique we also compare the results with the procedure presented in (Falsone and Impollonia, 2002). In this way, the improvements and computational savings achieved by the proposed probabilistic procedure can be assessed in comparison with two alternative probabilistic techniques.
Considering the geometric and mechanical properties of the analyzed masonry infilled RC frame, application of the empirical expressions reported in Table 1 along

with the assumptions outlined above provides the probabilistic characterization of the equivalent strut widths in terms of a physically-based (in the spirit of a macro-modelling approach) JPDF $p_{\boldsymbol{\alpha}}(\boldsymbol{\alpha})$ of the fluctuations $\boldsymbol{\alpha} = [\alpha_1, \cdots, \alpha_6]^T$ The adjective "physically-based" refers to the fact that the input PDF $p_{\boldsymbol{\alpha}}(\boldsymbol{\alpha})$ derives from some empirical (macro-modelling) expressions proposed in the literature. Therefore, the expressions reported in Table 1 form the basis of the probabilistic characterization of the fluctuations in this probabilistic study Subsequently, the procedures proposed are applied to obtain a probabilistic characterization of the system response in terms of a variety of response indicators. As an example, in Fig. 4.25 the PDF of the last-floor displacement (corresponding to node 4, i.e., u_{x4}) is shown. In this first case, we assumed that the $\boldsymbol{\alpha} = [\alpha_1, \cdots, \alpha_6]^T$ fluctuation variables are probabilistically described by a zero-mean multivariate normal distribution that best fits the empirical values. Moreover, the $\boldsymbol{\alpha} = [\alpha_1, \cdots, \alpha_6]^T$ fluctuations are also assumed as uncorrelated random variables in this first example. By inspection of Fig. 4.25 it is noted that the proposed probabilistic procedure is able to provide the PDF of the displacement response, which is only approximately described by the other two techniques (MCS and APDM) depending on the number of samples utilized. The first consideration is about the mean value of the top -story displacement, that is, $\mu_{x4} = 8.87 \times 10^{-3}$ m. The displacement response spectrum corresponding to the first natural period of the frame without diagonal pin-jointed struts ($T_1 = 0.41s$) is $\mu_{x4,spectrum} = 3.24 \times 10^{-2}$ m.

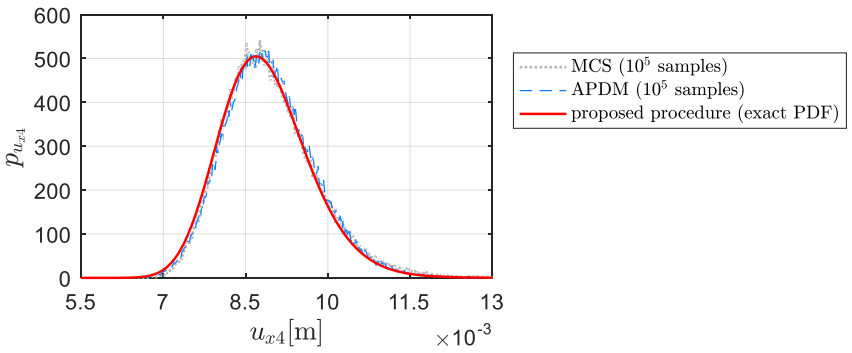

FIGURE 4.25: PDF of the last-floor displacement (node 4) for normal distribution assumption and uncorrelated fluctuations: Comparison between the three probabilistic methods

Obviously, the introduction of the struts leads to a significantly reduce, of almost four times, the displacement due to a stiffening contribution that reduces the first natural period accordingly. Furthermore, the deterministic value of the displacement computed adopting the largest stiffness of the diagonal struts among the empirical expressions reported in Table 4.3 is $u_{x,4min} = 6.80 \times 10^{-3}$ m, while that corresponding to the minimum strut width (related to the minimum stiffness) is $u_{x,4max} = 1.21 \times 10^{-2}$ m. Next, in order to take into account the correlation that may exist between the mechanical properties of masonry infills that are close to each other, a correlation function has been introduced. According to the previous sections, this correlation function depends upon the distance between the centroid of each diagonal strut element, i.e., $\rho = \rho(d)$, in particular the following exponential

decaying function has been assumed

$$\rho = \exp\left(-\frac{d}{\lambda}\right) \tag{4.32}$$

where $d = \left\|x_i - x_j\right\|$ is the Euclidean distance between the centroid of the strut i and j, while $\lambda = 15$ m is an arbitrary correlation length that is here chosen such that two adjacent masonry infills have a correlation equal to 0.8. In Fig. 4.26 the PDF of the top-story displacement (node 4) is illustrated for normal distribution assumption of the fluctuations, but assuming the correlation function given in Eq. 4.32. It is noted that the introducing cross-correlation terms within the covariance matrix of the fluctuation $\mathbf{\Sigma}_{\boldsymbol{\alpha}}$ requires a larger number of samples to approximate the PDF given by the proposed probabilistic procedure. Indeed, for the given number of samples adopted also for the previous case (10^5 samples), little deviations are observed by comparing the PDF with the APDM-based approximated one. The PDF and cumulative distribution function (CDF) of the last-floor displacement in the two cases of uncorrelated and correlated fluctuations $\boldsymbol{\alpha} = [\alpha_1, \cdots, \alpha_6]^T$ are depicted in Fig. 4.27.

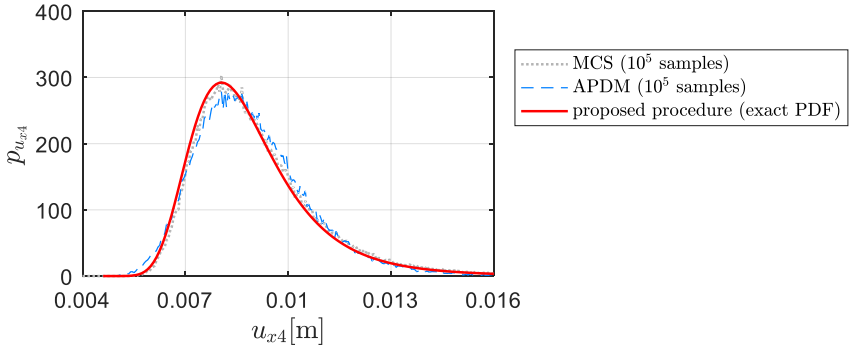

FIGURE 4.26: PDF of the last-floor displacement (node 4) for normal distribution assumption and correlated fluctuations between the struts: Comparison between the three probabilistic methods

It is noted that the two assumptions not only lead to a slightly different mean value μ_{ux4} (which is lower in the correlated case), but also produce remarkable differences in terms of characteristic values (95th percentile of the distribution). In particular, such characteristic value is about 20% higher in the correlated case due to the different shape of the distribution. Also, in the more realistic scenario of correlated fluctuations the dispersion of the displacement values is found to be higher than in the case of uncorrelated fluctuations. Furthermore, it is also noticed that the deterministic value of the last-floor displacement computed assuming that no fluctuations are present in the masonry panels (i.e., $w = w_0$ and $a = 0$ for all the equivalent diagonal struts) is in between the two mean values in the uncorrelated and correlated cases.

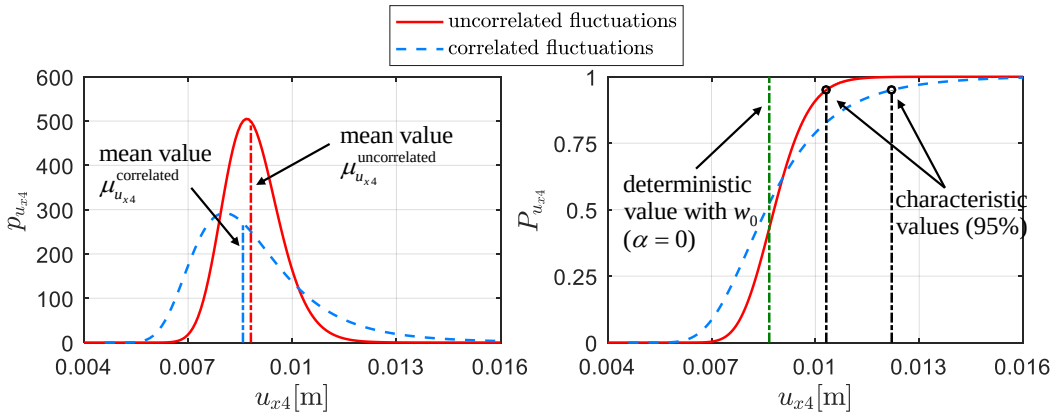

FIGURE 4.27: PDF (left) and CDF (right) of the last-floor displacement (node 4) for normal distribution in the two hypotheses of uncorrelated and correlated fluctuations $\boldsymbol{\alpha} = [\alpha_1, \cdots, \alpha_6]^T$

For completeness, the PDF of the last-floor displacement (node 4) has also been computed via the uniform distribution assumption for the fluctuations, which implies that all the empirical macro-modelling expressions have an equal probability of occurrence. By looking at Fig. 4.28, similar trends to those already observed in Fig. 4.25 for the normal distribution assumption are obtained, and similar conclusions can be drawn. In Fig. 4.29, the three distributions are compared with each other. It is noted that both the mean value and the characteristic value (95th percentile of the distribution) of the last-floor displacement are lower in the case of uniform distribution as compared to the two normal distributions. In the case of the uniform distribution the dispersion around the mean value is reduced, whereas in the case of normal distribution with correlated fluctuations the dispersion is amplified. Moreover, the deterministic value of u_{x4} in the absence of fluctuations is more or less comprised between the three mean values of the three above mentioned distributions.

Once the displacement vector $\mathbf{u}$ has been characterized probabilistically through the knowledge of the relevant PDF $p_{\mathbf{u}}(\mathbf{u})$, any other response indicator of interest can easily be computed as a linear combination of the components of the $\mathbf{u}$ vector, according to the finite element method. As an example, in Fig. 4.31 the PDF of the third inter-story drift $\Delta u_{x43} = u_{x4} - u_{x3}$ is displayed as computed by the three probabilistic procedures considering that the fluctuations are uniformly distributed between the α_{min} and α_{max} values.

In the same graph, we also report the deterministic interstory drift values calculated by assuming the minimum and maximum values of the i w discrete set. As expected, since α_{min} and α_{max} do not reflect the values of w_{min} and w_{max}, the deterministic max value does not represent the 100th percentile of the PDF $p_{\Delta u_{x43}}$, which is consistent with what explained in the sections above. The PDF has a slightly asymmetric shape and all the three probabilistic procedure are in good agreement with each other. In Fig. 4.31, the PDF and CDF of the third inter-story drift $\Delta u_{x43} = u_{x4} - u_{x3}$ is illustrated and compared for the case of normal distribution (uncorrelated and correlated) and uniform distribution of the fluctuations.

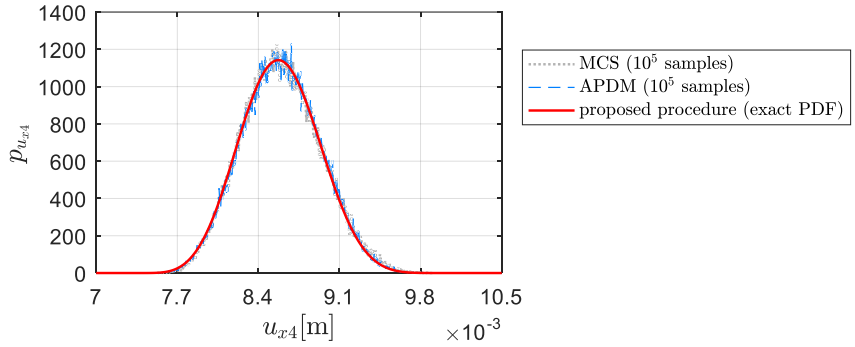

FIGURE 4.28: PDF of the last-floor displacement (node 4) for uniform distribution assumption of the fluctuations: Comparison between the three probabilistic methods

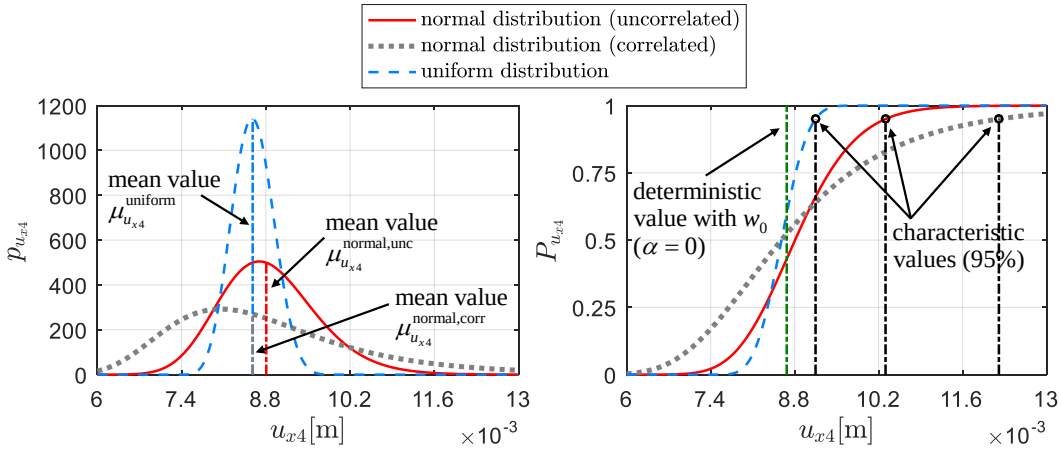

FIGURE 4.29: PDF of the last-floor displacement (node 4) for uniform distribution assumption of the fluctuations: Comparison between the three probabilistic methods

The results are more or less in line with the previous trends observed for the last-floor displacement u_{x4}: the characteristic value of the distribution is lower in the case of uniform distribution than the normal distributions. However, the mean value from the uniform distribution is in between that of the normal distribution for uncorrelated and correlated assumptions, which is different from the results discussed above for u_{x4}, although the three mean values are very close to each other. The dispersion of the $p_{\Delta u_{x43}}$ is reduced for uniform distribution as compared to normal distribution, whereas it is amplified in the case of normal distribution with correlated fluctuations. The deterministic value obtained with w_0 (in the absence of fluctuations, $\alpha = 0$) lies in between the two mean values calculated with the uniform and normal distributions assumptions of the fluctuations.

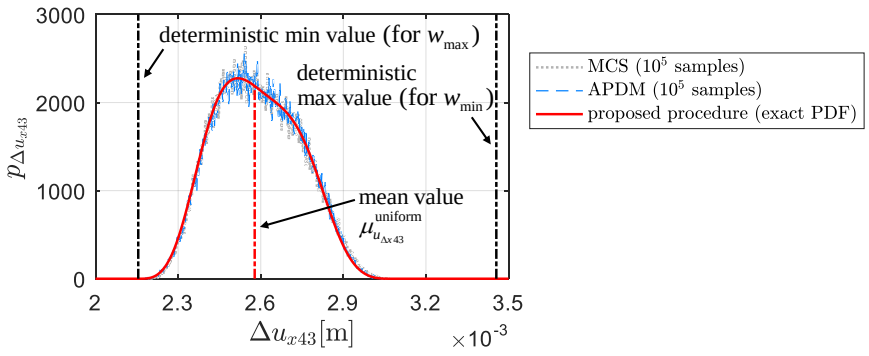

FIGURE 4.30: PDF of the third interstory drift for uniform distribution assumption of the fluctuations: Comparison between the three probabilistic methodss

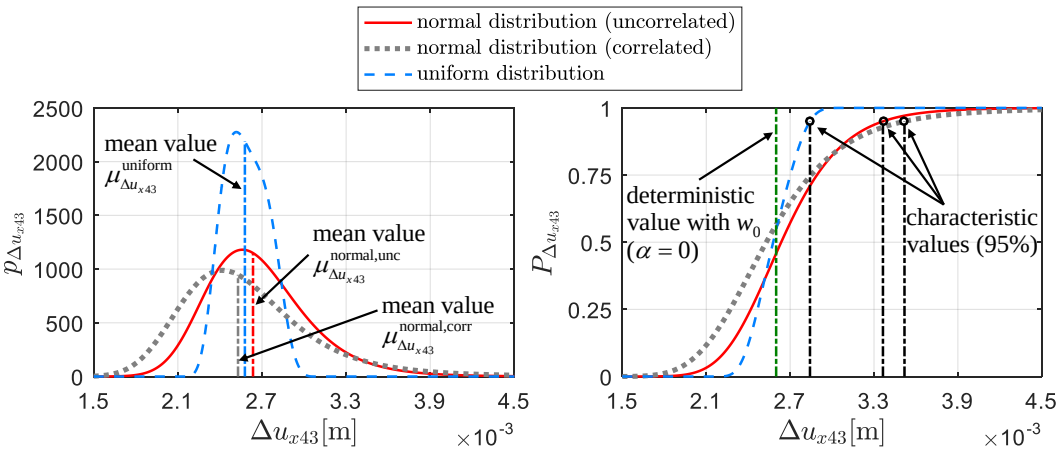

FIGURE 4.31: PDF (left) and CDF (right) of the third interstory drift ($\Delta u_{x43} = u_{x4} - u_{x3}$) for normal (uncorrelated and correlated) and uniform distribution assumption

It has been observed that the influence of the stiffening contributions offered by the equivalent pin-jointed diagonal struts is more significant for determining the stress and strain in the column elements rather than in the beam elements. This is reasonable, since the masonry infills increase the lateral stiffness of the frame as compared to the case in which they are ignored in the calculation.
To quantify this effect, in Fig. 4.32, the PDF and CDF of the moment at the top of the column 3-2 (M_{32}) are shown. It is noted that the introduction of the struts with uncertain mechanical properties even produce changes in the signs of the moments for a frame subject to an equivalent distribution of seismic lateral forces as those considered in this example through Eq. 4.31. In this case, it is also noted that the correlated fluctuations yield a PDF that has less dispersion than in the case of uncorrelated fluctuations. This is in opposite trend as compared to the previous plots. However, from a broader examination of other response quantities (not reported here for the sake of brevity) it was found that the dispersion of such indicators can be higher or lower by comparing the correlated and uncorrelated assumptions. Therefore, no apparent

relationship between the correlation of the fluctuations and the shape of the PDF can be inferred, since no clear tendency is observed.

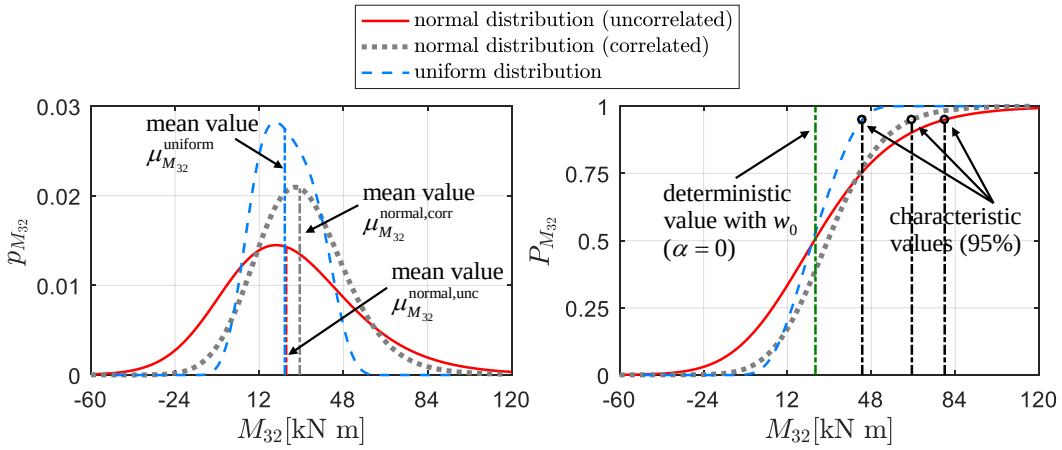

FIGURE 4.32: PDF (left) and CDF (right) of the moment at the top of the column 3-2 (M_{32}) for normal (uncorrelated and correlated) and uniform distribution assumption

response quantity	response designation	deterministic value for $w = w_0$ ($\alpha = 0$)	mean value μ	standard deviation σ	COV σ/μ
top-story displacement	u_{x4} [m]	0.0087	0.0086	0.00034	0.039
last interstory drift	$\Delta u_{x43}[m]$	0.0026	0.0026	0.00015	0.059
moment on the top of the column	M_{32} [kNm]	24.02	23.38	12.47	0.53
moment on the beam end	M_{37} [kNm]	33.10	33.61	3.97	0.12
moment reaction at the base of the central column	R_{M5} [kNm]	249.5	258.00	60.27	0.23
shear force on the top of the column	V_{32} [kN]	6.10	5.88	7.92	1.35
shear force on the beam end	V_{37} [kN]	81.43	81.64	1.28	0.016

TABLE 4.5: List of characteristic parameters of the probabilistic distribution of a set of response quantities (uniform distribution assumption of the fluctuations)

On the contrary, the influence of the fluctuations on the stress and strains in the beam elements is less pronounced. As an example, in Fig. 4.33, the PDF and CDF of the moment at the left side of the beam 3-7 (M_{37}) are illustrated. Unlike the probabilistic characterization of the moment on the column, in this case the values are almost entirely positive (i.e., they do not exhibit sign changes), and the influence of the uncertainty in the masonry panels is less pronounced. In this case, the correlated

fluctuations give more dispersed values, in line with other response quantities. Furthermore, the deterministic value of M_{37} identified by an analysis with $w = w_0$ and $\alpha = 0$ for all the struts is again bounded by the mean values of the PDFs for uniform and normal distribution assumptions. In order to highlight the remarkably different influence of the uncertain mechanical properties of the masonry infills on the column and beam elements, in Fig. 4.34, the PDFs of the moments on the beam and column elements are compared with each other. The two Figs refer to different distribution assumptions of the fluctuations (normal and uniform), but the general qualitative conclusions for the two cases are almost identical. These conclusions are confirmed also for other response quantities, for instance, moments evaluated at other nodes or shear forces.

response quantity	response designation	deterministic value for $w = w_0$ ($\alpha = 0$)	mean value μ	standard deviation σ	COV σ/μ
top-story displacement	u_{x4} [m]	0.0087	0.0089	0.0008	0.93
last interstory drift	$\Delta u_{x43}[m]$	0.0026	0.0027	0.00038	0.14
moment on the top of the column	M_{32} [kNm]	24.02	26.14	30.36	1.16
moment on the beam end	M_{37} [kNm]	33.10	30.55	9.79	0.32
moment reaction at the base of the central column	R_{M5} [kNm]	249.5	256.15	47.29	0.18
shear force on the top of the column	V_{32} [kN]	6.10	7.12	19.14	2.69
shear force on the beam end	V_{37} [kN]	81.43	80.69	3.18	0.039

TABLE 4.6: List of characteristic parameters of the probabilistic distribution of a set of response quantities (normal uncorrelated distribution of the fluctuations)

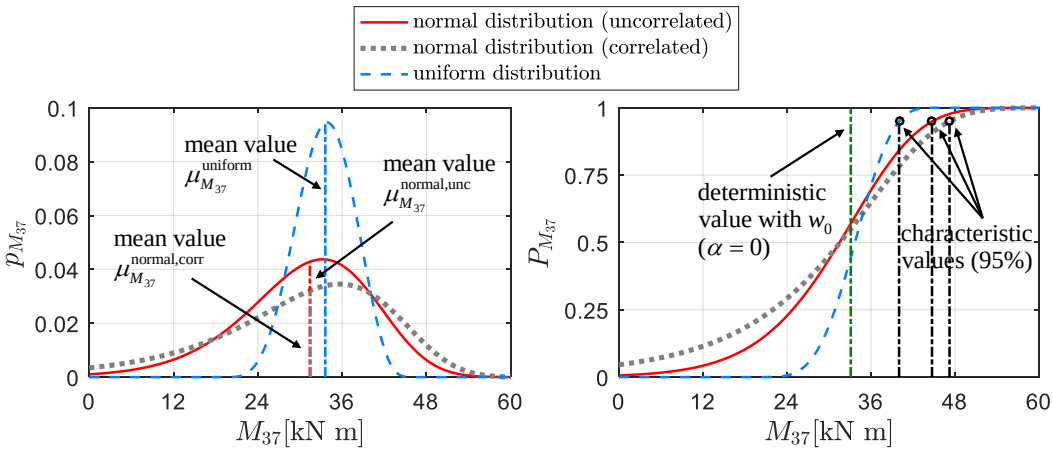

FIGURE 4.33: PDF (left) and CDF (right) of the moment at the top of the column 3-7 (M_{37}) for normal (uncorrelated and correlated) and uniform distribution assumption

response quantity	response designation	deterministic value for $w = w_0$ ($\alpha = 0$)	mean value μ	standard deviation σ	COV σ/μ
top-story displacement	u_{x4} [m]	0.0087	0.0089	0.0017	0.19
last interstory drift	$\Delta u_{x43}[m]$	0.0026	0.0027	0.0005	0.19
moment on the top of the column	M_{32} [kNm]	24.02	26.87	20.58	0.77
moment on the beam end	M_{37} [kNm]	33.10	30.27	14.65	0.48
moment reaction at the base of the central column	R_{M5} [kNm]	249.5	257.59	58.19	0.22
shear force on the top of the column	V_{32} [kN]	6.10	5.24	10.62	2.03
shear force on the beam end	V_{37} [kN]	81.43	80.65	5.2	0.064

TABLE 4.7: List of characteristic parameters of the probabilistic distribution of a set of response quantities (normal correlated distribution of the fluctuations))

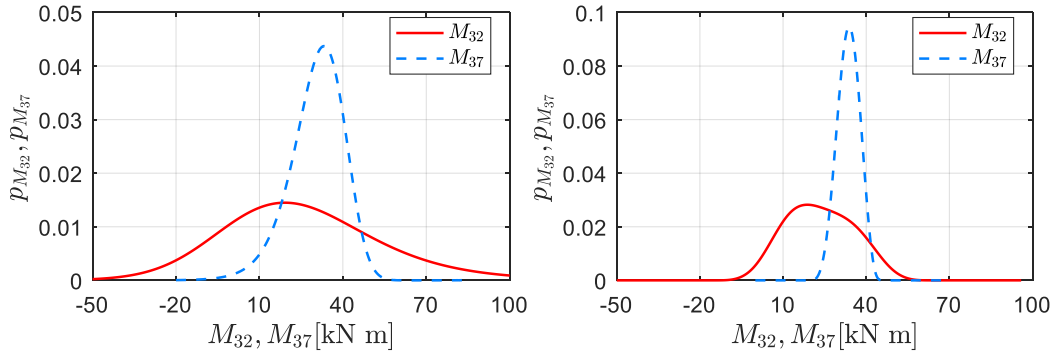

FIGURE 4.34: Comparison of PDF of the moment on the column (M_{32}) and beam (M_{37}) for normal uncorrelated (left) and uniform (right) distribution assumption of the fluctuations

Therefore, uncertain mechanical properties of the masonry infills have a great influence on the column stress and strain values, and a reduced influence on the beam response quantities. The proposed procedure also enables the determination of the JPDF between two or more response quantities. As an example, in Fig. 4.35, the JPDF of the moments on the beam M_{37} and that on the column M_{32} is displayed, namely $p_{M_{32}M_{37}}(M_{32}, M_{37})$. This JPDF can be interpreted for drawing some general conclusions from a design viewpoint. It is well-known that capacity design establishes a hierarchy of zones among the structural members (Avramidis et al., 2015), which is a concept incorporated in seismic provisions (Council, 1997; Todaro, 2008). The failure mode of the beam is usually deemed to be more ductile than that of the column.

Therefore, capacity design principles promote failure mechanisms occurring in the beam before those occurring in the column. In a simplified manner, it can be assumed that the design flexural resistance M_{Rd} is related to the design bending moment M_{Ed} calculated in the analysis. Therefore, it is interesting to scrutinize to what extent the typical ratio between moments in beam and column elements is affected by the uncertainty on the masonry panels. To this aim, in the contour plots on the bottom part of Fig. 4.35 a dashed line has been reported that corresponds to $M_{32} = M_{37}$. This means that points lying above this dashed line in the first quadrant and lying below this dashed line in the third quadrant represent situations in which $|M_{32}| > |M_{37}|$, thus jeopardizing the correct principle of the strength hierarchy underlying the "weak-beam-strongcolumns" principle. This, in turn, is likely to produce less ductile collapse mechanism in the masonry infilled RC frame, provided the design resistance is assumed in line with the design bending moments. It is noted that there exists such a probability of occurrence of this phenomenon in both the normal and uniform distribution assumption of the fluctuations. This outcome is affected by the distribution of the stress in the masonry infilled RC frame induced by the presence of the uncertain masonry panels. Although the present analysis is extremely simplified, it is possible to recognize than this link is important to provide physical meaning and usefulness of the proposed probabilistic approach of analysis in the case of RC frames with uncertain masonry infills. A summary of the results is reported in Table 4.5, Tables 4.6 and 4.7 for uniform, normal uncorrelated and normal correlated fluctuations, respectively. By inspection of these tables, the following conclusions can be drawn:

- from the PDF are very close to the deterministic values that can be computed by an analysis of the RC frame in which the diagonal pin-jointed struts are assigned the mean width value $w = w_0$, i.e., with a zero value of the fluctuations according to a mere deterministic analysis;
- the dispersion of the distribution expressed by the standard deviation σ is different from case to case: in general, the sensitivity of the response indicators to the uncertainty of the masonry infills is more pronounced for column-related quantities (e.g., the moment on the top of the column M_{32} or the shear force V_{32}) than for beam-related variables;
- the more pronounced dispersions of the distribution, indicated by the value of the COV, are higher in the cases of column-related quantities, especially the shear forces on the columns.

It is concluded that careful attention must be paid to the values of the stress and strains in a RC frame with masonry infills, especially if the panels are affected by largely scattered results arising from preliminary experiments on the constituting elements and materials. The examples shown in this work, although carried out on a simple structure and under an equivalent static lateral force procedure, give a preliminary idea of the influence of the masonry infills on a set of response indicators for different modelling assumptions, all related to a macro-modeling approach, and for different distribution assumptions of the relevant equivalent strut widths simulating, in a simplified way, the presence of the stiffening contribution offered by the masonry infills themselves.

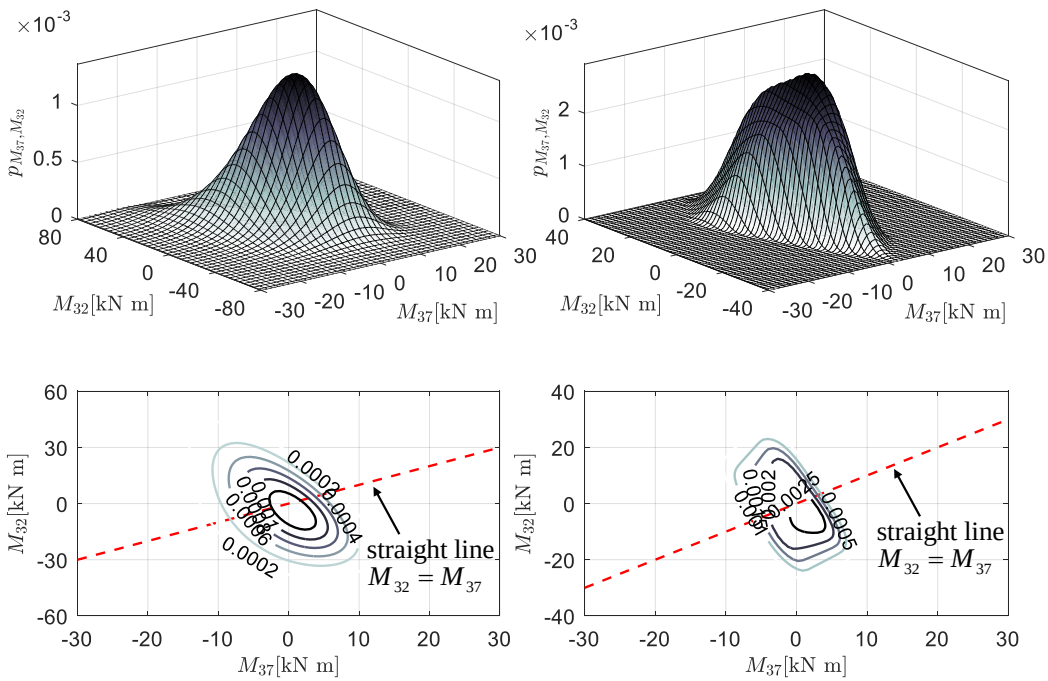

FIGURE 4.35: JPDF between the moment on the column (M_{32}) and on the beam (M_{37}) for normal uncorrelated (left) and uniform (right) distribution assumption of the fluctuations.

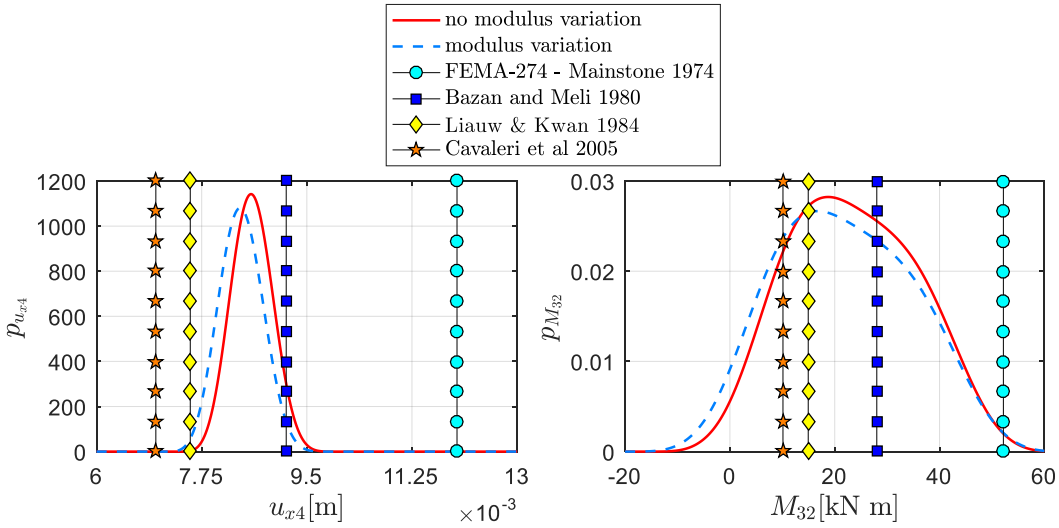

FIGURE 4.36: PDF of the last-floor displacement (u_{x4}) and of the moment on the top of the column (M_{32}) compared to deterministic values predicted by four different deterministic formulations

Finally, in order to provide insight into the reliability of the proposed predicting expressions for the masonry infill stiffening contribution, a final analysis has been conducted. In this final analysis, the influence of the uncertain nature of the Young's modulus has also been investigated. Instead of assuming a deterministic E value, the sensitivity of the results to the variability of the Young's modulus is here studied. The E value has been sampled by assuming a uniform distribution between $E_{wmin} = 4$ GPa and $E_{wmax} = 6$ GPa, and the empirical expressions reported in Table 4.3 have been repeatedly applied in order to have a wider set of statistical data to assess the accuracy of the empirical expressions in comparison with probabilistic results. We here report the PDF of two response indicators: the last-floor displacement u_{x4} and the bending moment on the top of the column M_{32}. Four alternatives of empirical formulae predicting the same response quantities are employed, within a deterministic framework, for comparison purposes. In this way, we can assess the accuracy of four different predicting expressions when compared to a more complete probabilistic analysis. From Fig. 4.36, it is noted that the influence of the Young's modulus on the probabilistic characterization of the response, at least in the range of E_w explored here, is not particularly significant. Indeed, the obtained PDF with modulus variation is very similar to that obtained with the mean value of E_w. Furthermore, the four deterministic values of the two response quantities u_{x4} and M_{32} predicted with the four considered formulations give very large scatter of results. In particular, it is seen that the Mainstone, 1974 expression (Mainstone, 1974), also adopted by FEMA-274 and 306 (Council, 1997; Council and Response, 1999), provides extremely large values of the response, on the conservative side. More reasonable estimates of the response mean value as computed by the probabilistic analysis are provided by the other three formulations considered. However, these three formulations namely, Bazan and Meli 1980 (Bazan and Meli, 1980), Liauw and Kwan 1984 (Te-Chang and Kwok-Hung, 1984), Cavaleri et al. 2005 (Cavaleri, Fossetti, and Papia, 2005)) leads to results that are not particularly close to the mean value of the corresponding PDF, especially for the displacement.
It seems that the formula proposed by Bazan and Meli 1980 (Bazan and Meli, 1980)

is the most accurate one because it is in reasonable agreement with the mean value and it provides conservative estimates of the response.
As a final remark, this comparison definitely highlights the scatter of results that the different formulations may produce, and underlines the importance of probabilistic studies to account for the uncertain nature of the masonry infill mechanical behaviour.

4.3.5 Some remarks

The main contents and findings of this research work are summarized as follows:

- A fully probabilistic approach has been proposed for the analysis of the in-plane response of masonry infilled RC frames. More specifically, this work has been focused on the investigation of the effects of the masonry infills uncertainty on the structural response of RC frames. A macro-modeling approach has been adopted in which the masonry panels are considered via equivalent diagonal pin-jointed struts. The strut widths have been considered as random variables in order to incorporate the stochastic nature of the masonry infills ascribed to their inherent heterogeneous nature and to the large scatter of corresponding experimental results.

- The probabilistic characterization of the complex mechanical behavior of the masonry infills has been based upon an ensemble of empirical expressions proposed in the literature by different authors. For given geometrical and mechanical properties of an assigned masonry infilled RC frame, a procedure for deriving the probabilistic input data of the strut widths has been described, and different modelling assumptions in terms of correlation and shape of the PDF have been explored.

- An effective numerical procedure has been proposed that, unlike Monte-Carlo-based methods, avoids sampling techniques thus implying reduced computational effort, especially for structures with several DOFs. This procedure provides the probabilistic characterization of the system response directly, once the probabilistic characterization of the masonry panels has been established as per the previous bullet point. From the literature on this field, such a direct probability-based procedure has never been considered for the analysis of masonry infilled RC frames, which represents the main novelty of this contribution.

- To demonstrate the kind of results that this procedure can offer, a simple application has been presented, consisting in an equivalent linear analysis of a regular masonry infilled reinforced concrete framed structure. The PDF of a set of response indicators has been determined, and has been compared to the PDF obtained via alternative (more cumbersome) techniques like Monte Carlo method and other strategies earlier proposed in the literature, all requiring sampling operations and providing just an approximation of the PDF as the number of sampling increases.

- The sensitivity of the response to the modeling assumptions, mainly the shape of the PDF and the inherent correlation between the fluctuations of the various strut widths associated with the various masonry panels, has been discussed. For most of the response indicators analyzed, incorporating the correlation of the strut widths in the probabilistic characterization of the input data has led

to more dispersed probabilistic characterization of the system response. Furthermore, it has been observed that a deterministic analysis carried out considering the mean values of the strut widths provides reasonable estimates of the mean response as determined by the probabilistic approach. However, as a matter of fact, deterministic analysis cannot give indications on the probability distribution, which is important for reliability-based design.

- As expected, the influence of the uncertainty of the masonry infills is more pronounced for column-related quantities (e.g., the moment, shear forces, etc.) rather than for beam-related variables. Furthermore, it has also observed that, due to the presence of uncertain masonry infills, the weak-beam-strong-columns principle underlying the strength hierarchy criterion might be jeopardized.
- Based on the last two conclusions, it is recommended that conservative safety factors be applied for designing the columns in masonry infilled RC frames in order to take into account, in a simplified way, the randomness of the response due to the stochastic nature of the masonry panels.
- A more specific analysis on four different formulations proposed in the literature has revealed which are the more reliable formulations that are better able to reproduce the mean value of the response as indicated in the present probabilistic study.

4.4 Conclusion

In this chapter, the structural static response of systems characterized by uncertainties in the model designed due to simplifying assumptions in analytical models and/or simplified methods have been investigated. Two different stochastic approaches of two typical examples in structural engineering are proposed thanks to the PTM. In particular, in section 4.2 a fully probabilistic approach has been presented to describe the structural response of steel beams and frames with uncertain semi-rigid connections. From this study, it was clear that the semirigid connections, by nature characterized by largely scattered results, should be more appropriately dealt with via a probabilistic approach. The static analysis of the in-plane response of masonry infilled RC frames is reported in section 4.3. The main focus of this section is the probabilistic characterization of the complex mechanical behavior of the masonry infills. Through the PTM a direct probability-based procedure has been developed for the analysis of masonry infilled RC frames. From this chapter, it is possible to draw how the PTM is a useful tool also for the stochastic analysis of uncertain structural systems.

Chapter 5

Local and nonlocal randomness in structures and in turbulent velocity fields

5.1 Introduction

In many mechanical problems, the uncertainties in defining geometrical and/or material properties lead to model these latter as random fields (RFs). RFs are characterized, besides of the single-point statistics, such as the mean value and the variance, also by the correlation functions that give the level of stochastic correlation of the RFs evaluated at two, or more, points. Even for equal single-point statistics, the response of any mechanical problem may strongly depend on the kind of correlation functions defining the RFs (Vanmarcke, 2010).
Here, two statistical aspects of random fields, the fractal and Hurst effects, will be introduced. Generally, the fractal dimension, D, is described as a roughness parameter, i.e. a local behavior of the RF; while the Hurst parameter, H, describes the long-range persistence, i.e. a non-local (global) behavior of the RF.
From the literature of the last decades, it is possible to find many papers dealing with the analysis of fractal and Hurst effects in some mechanical problems, such as in fracture surfaces (Turcotte, 1997; Laudani and Ostoja-Starzewski, 2020), turbulence flows (Scotti, Meneveau, and Saddoughi, 1995; Jaw and Chen, 1999; Laudani et al., 2020), random vibrations (Shen, Ostoja-Starzewski, and Porcu, 2015b). In this chapter, a link between the statistical RF theory and the local and non-local randomness in stochastic mechanics will be addressed. In fact, in the literature, it is possible to find some kinds of correlation functions that allow capturing the local behavior of the RF (White Noise, Matérn, and Powered exponential correlation function) or their both local and non-local characteristics (Cauchy and Dagum correlation function). In particular, with Cauchy and Dagum correlation function it is possible to deal separately with the fractal dimension D and the Hurst exponent H, i.e. the local and the non-local (global) behavior of the RF. Typically, i.e. for self-affine RFs (and random processes), the latter two are linked by the relation $H = 2 - D$. The capability of the above two-parameter correlation families allowing a disjoint characterization of fractal and long-dependence properties makes these functions highly appealing, from an engineering point of view, for the study statistical analysis of physical phenomena and mechanical problems.
The use of these classes of correlation functions has made it possible to investigate, from a probabilistic point of view, three apparently different stochastic topics but linked by the same purpose, that means to investigate the incidence of local and nonlocal randomness effects. In particular, in section 5.1, the classical problem of

peeling a beam off a substrate is studied through a re-examination of Griffith's fracture criterion in the presence of multiscale random properties. A paradigm of that theory is offered by the experiment carried out by Obreimoff will be investigate from a stochastic point of view. Although, this topic was treated in that stochastic setting (Ostoja-Starzewski, 2004), albeit without the consideration of the correlation structure of the RF involved. So section 5.1, will investigate the latter aspect. Then, the section 5.2 will try to give an answer to the following question: how a local or nonlocal correlation of the flexibility field affects the level of the randomness response in displacement and/or the internal forces of the redundant beams? Although these kinds of investigations are not new in the literature (Demmie and Ostoja-Starzewski, 2016), here a mathematical similarity between them and the non-local integral constitutive equations (Eringen, 1983) will be shown evidencing analogy between the kernel function considered in the constitutive equations and the correlation function used for representing the statistic dependence level between the deformabilities measured at two different sections of beams. Observations about the properties of the kernel function in the non-local constitutive equations are also not new (Ghavanloo, Rafii-Tabar, and Fazelzadeh, 2019; Challamel, 2018), that is to say, that the spatial non-locality deals with long-range interaction and that the kernel function should converge to the Dirac delta function in order to reduce the non-local elasticity to the classical (local) elasticity. Section 5.3 deals with the statistical description of turbulence flows. The statistical description of turbulence dates back to the seminal works of von Kármán, Robertson, Kolmogorov, Yaglom, and Batchelor (Batchelor, 1953). Various models of the spatial correlation structure and associated spectrum of turbulent velocity fields have been proposed over the last several decades. Classic models, include, among others, the well-known von Kármán, Kaimal, Davenport, Harris, and Lumley-Panofsky. Various formulations for a range of flows using different arguments have also been proprosed. For instance, Mann (Mann, 1994) used Rapid Distorsion Theory to describe the spectral velocity tensor, and Segalini *et al*. (Segalini et al., 2015) proposed a spectral model for the velocity tensor in stratified flows. From the Generalized Cauchy and Dagum models, two novel velocity spectrum will be presented. Close inspection and evaluation of these two models using field data from a sonic anemometer located within the atmospheric surface layer will be done. The content of this chapter is mainly based on two papers under publication (Laudani et al., 2020; Falsone and Laudani, 2020a).

5.2 Fracture of beams with random field properties: fractal and Hurst effects

In this section, the classical problem of peeling a beam off a substrate is studied through a re-examination of Griffith's fracture criterion in the presence of multiscale random properties.

Four types of wide-sense homogeneous Gaussian random fields of the vector Young's modulus E, surface energy density γ, parametrized by the beam axis, are considered: Ornstein–Uhlenbeck, Matérn, Cauchy, and Dagum. The latter two are multiscale and allow decoupling of the fractal dimension and Hurst effects. Also calculated is the variance of the crack driving force G with any given type of random field in terms of the covariances of E and γ, under either fixed-grip or dead-load conditions. This investigation is complemented by a study of the stochastic crack stability which involves a stochastic competition between potential and surface energies.

The linear elastic fracture mechanics involves two material properties: the material stiffness tensor $\mathbf{C}$ and the surface energy γ. A paradigm of that theory is offered by the experiment carried out by Obreimoff on the cleavage of mica off a rigid substrate (Obreimoff, 1930), Fig. 5.1. In this one-dimensional (1d) situation, one deals with the beam bending, so that $\mathbf{C}$ is represented by Young's modulus E, while γ pertains to the beam-substrate interface.

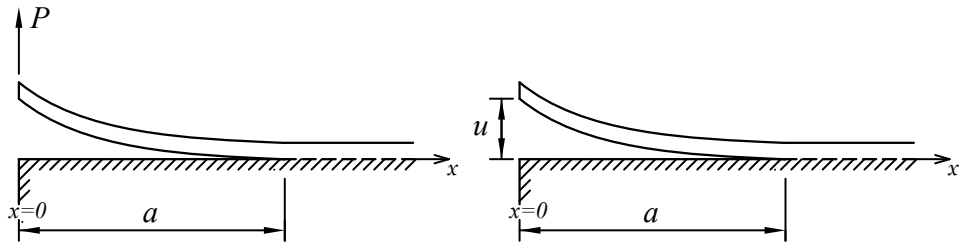

FIGURE 5.1: (A) Dead-load condition with P prescribed at $x = 0$. (B) Fixed-grip condition with u prescribed at $x = 0$.

The theoretical method relies on the Griffith fracture criterion for crack growth (Ostoja-Starzewski, 2004)

$$G = \frac{\partial W}{\partial A} - \frac{\partial U}{\partial A} = 2\gamma, \tag{5.1}$$

where G is the strain energy release rate, W is the work performed by the applied loads, U is the elastic strain energy, A is the crack surface area formed, and γ is the energy required to form a unit of the new material surface. Two special cases – the so-called "dead-load" and "fixed-grips" conditions – are usually encountered in practice. In the dead-load case, with reference to Clapeyron's theorem, the work performed by the constantly applied loads is twice the increase of elastic strain energy $(\partial W/\partial A = 2\partial U/\partial A)$. Thus, Eq. 5.1 takes form

$$G = \frac{\partial U}{\partial A} = 2\gamma. \tag{5.2}$$

In the fixed-grips case, the surface of the continuum on which the loads are applied is assumed to remain stationary during crack growth. If the work of the body forces is ignored, the work performed by the applied loads vanishes and Eq. 5.2 takes the form:

$$G = -\frac{\partial U}{\partial A} = 2\gamma. \tag{5.3}$$

In the above and conventionally (Gdoutos, 1993), both E and γ are taken to be constant, but, given the presence of a randomly multiscale-heterogeneous material structure, E and γ should, more realistically, be taken as random fields (RFs) along the beam's span x. The beam is then described by a vector RF $\{E, \gamma\}$.

One way to classify RFs (equivalently, random processes) is to distinguish between those that do versus those do not possess fractal-and-Hurst properties. Models that do not allow such characteristics are those with white noise, exponential, and Matérn correlations. The need to actually include such characteristics is motivated by the richness of temporal and spatial phenomena in the real world: geophysics, atmosphere, biology, and economy (Mandelbrot, 1982). In particular, fracture mechanics theory provides stepping-stone models to studies of many critical phenomena in

geomechanics (Turcotte, 1997), where long cracks like fault lines in geologically unstable areas are relevant in geotechnical and foundation engineering. In this section, we focus on fracture of beams described by two classes of wide-sense homogeneous RFs with fractal-and-Hurst characteristics: Cauchy (Gneiting and Schlather, 2004b) and Dagum (Porcu et al., 2007). The correlation functions of these two types allow a decoupling (i.e., independent choice) of the fractal dimension D and the Hurst exponent H. Typically, i.e. for self-affine RFs (and random processes), the latter two are linked by the relation $H = 2 - D$.

The objective of the present study is to examine how the strain energy U and the strain energy release rate G are affected by Gaussian RFs E and γ, taken as either Ornstein-Uhlenbeck, Matérn, Cauchy, or Dagum. Moreover, since through the Cauchy and Dagum models it is possible to decouple the fractal-and-Hurst effects, it has been believed that they are particularly useful in order to investigate whether in the mechanics of fracture the response leads more to local or no-local stochastic characteristics.

5.2.1 Background on covariance functions, fractal dimension, and Hurst effect

Here a real-valued Gaussian RF F defined over a probability space (Ω, A, P) is used, where P here denotes a Gaussian measure, and with realizations on $X \subset \mathbb{R}$. F is taken to be zero-mean and wide-sense homogeneous so that it is completely specified by second-order moments, in particular by the associated covariance function $C(\cdot,\cdot) : \mathbb{R} \times \mathbb{R} \to \mathbb{R}$ defines as:

$$C\left(x_1, x_2\right) := Cov\left(F\left(x_1\right), F\left(x_2\right)\right). \tag{5.4}$$

In view of the wide-sense homogeneous assumption, there exists a mapping $C_F : \mathbb{R}_+ : \cup\{0\} \to R$, such that

$$C\left(x_1, x_2\right) := Cov_F\left(|x_1 - x_2|\right). \tag{5.5}$$

This framework allows us to identify two important properties of RFs:

- The fractal dimension D reflects the local properties; it is a roughness measure with a range $[n\ , n+1)$; since the focus is on beams, $n = 1$ is used.
- The long memory in time series (or spatial data) is associated with power-law correlations and often referred to as the Hurst effect, characterized by the H parameter (Mateu, Porcu, and Nicolis, 2007b).

These properties relate to those of the associated correlation function. Next, it is important to assess the local regularity properties of the sample paths of a Gaussian process. To this end, it has been established that, if, in the weakly homogeneous case, for some $\alpha \in (0,1)$, there holds

$$\lim_{r\to 0}\left(1 - C_F(r)\right) r^{-\alpha} = K, \quad 0 < K < \infty; \quad r > 0, \tag{5.6}$$

where $r = x_2 - x_1$. Then, with probability one, the fractal dimension of $F(\cdot)$ satisfies

$$D = dim\left(GrF\right) = min\left(\frac{1}{\alpha/2}, 1 - \alpha/2\right), \tag{5.7}$$

where, as before, C_F= covariance function of F. In Eq. 5.7, $GrF = graph(F) = \{(x, F(x)), x \in [-1,1]\} \subset \mathbb{R}^2$ so that parameter α determines the fractal dimension D.

The scaling laws describe how rather elementary measurements vary with the resolution, a subject that along with the relation between index-α and D is discussed at length in (Hall and Wood, 1993). Besides to the index-α related to the fractal dimension D, for Gaussian RFs, it is also possible to distinguish an index-β related to H [see (Adler, 2010) for an exposition of Gaussian index-β RF, where $\beta = \alpha/2$]. Here, if for some $\beta \in (0,1)$

$$\lim_{r\to\infty} C_F(r) r^{-1+\beta} = 1. \tag{5.8}$$

Then the field is said to have a long memory, with $H = \beta/2$. For $H \in (1/2, 1)$ or $H \in (0, 1/2)$ the correlation is said to be, respectively, persistent or anti-persistent (Beran, 2017). The same properties can be studied through the Fourier transform of the covariance function (i.e., the spectral density) under the conditions stated in Tauberian-type and Abelian-type theorems (Bingham, Goldie, and Teugels, 1989), with the parameters α and β interpreted in the opposite way. Basically, α is associated with the velocity of decay of the spectral density, while β with the local behaviour of the spectral density around near-zero frequencies.

We shall consider these four types of RFs:

1. Ornstein–Uhlenbeck. In this case:

$$C_{OU}(r, \mu) := \frac{\mu}{2} e^{-\mu r}, \quad r \geq 0, \tag{5.9}$$

   where μ is a positive scaling parameter which in the limit $\mu \to \infty$ becomes white noise.

2. Matérn. In this case (Matérn, 1986):

$$C_M(r, \nu) := r^{\nu} K_{\nu}(r), \quad r \geq 0, \tag{5.10}$$

   where ν = a parameter that determines the smoothness at the origin of C_M, and thus the mean square differentiability of F. Here, K_ν= a modified Bessel function of order ν. Note three special cases:

   - $C_M(r, 1/2) = e^{-r}$ which (as is well known) coincides with the covariance function of the Ornstein–Uhlenbeck type;
   - $C_M(r, 3/2) = (1 + r) C_M(r, 1/2)$;
   - $C_M(r, 5/2) = (1 + r + 3r^2/3) C_M(r, 1/2)$;

3. Generalized Cauchy (Gneiting and Schlather, 2004b). In this case:

$$C_C(r, \theta, \eta) := \left(1 + r^{\theta}\right)^{-\eta/\theta}, \quad r \geq 0, \tag{5.11}$$

   which is positive definite for $\eta > 0$ and $0 < \theta < 2$. Special cases of this class will also be of interest. In particular, $C_C(\cdot; 2; \gamma)$ is the characteristic function of the symmetric Bessel distribution, $C_C(\cdot; \alpha; \alpha)$ is the characteristic function of the Linnik distribution, and $C_C(\cdot; 1; \gamma)$ is the symmetric generalized Linnik characteristic function.

4. Dagum (Mateu, Porcu, and Nicolis, 2007b). In this case:

$$C_D(r,\delta,\varepsilon) := 1 - \left(1 + r^{-\delta}\right)^{-\varepsilon/\delta}, \quad r \geq 0, \tag{5.12}$$

which is positive definite for $0 < \varepsilon < \delta$ and $0 < \theta < 2$.

Figure 5.2 shows some sample realizations of the Gaussian Ornstein–Uhlenbeck (which in the limit becomes a white noise), Matérn, Cauchy, and Dagum RFs, for distinct parameter settings, all on 1d (one-dimensional domains, i.e. the beam axis). The plots illustrate the trends in linking the local and global properties of RFs with their associated correlation functions. In particular, in relation to Eqs. 5.6 and 5.8, respectively, the realizations of the RFs have $D = n + 1 - \alpha/2$, with probability 1, while the RF has a long memory with $H = 1 - \beta/2$. Thus, the parameter α is associated with the fractal dimension and the parameter β allows one to evaluate the Hurst effect.

Furthermore, the sub-plots (a)-(d) clearly show that the white noise, Matérn, and Ornstein–Uhlenbeck RFs have no Hurst effects. As is well known, the smoothing parameter ν can be interpreted as the parameter α for the estimation of the fractal dimension (Gneiting, Kleiber, and Schlather, 2010; Gneiting, Ševčíková, and Percival, 2012). In particular, for the Matérn model, the fractal dimension of a sample path in $\mathbb{R}^n$ equals the maximum of n and $n + 1 - \nu$. For a differentiable field with smoothness parameter $\nu > 1$, the fractal dimension of a sample path equals its topological dimension, n. Generally, the larger the ν, the smoother the process. So, with the Matérn model we can take into account the fractal characteristics, albeit with light tails, in fact, in the sub-plots (c)-(d) show a fractal dimension $D = 1$. Moreover, about the Ornstein–Uhlenbeck model, keeping in mind that this model is a special case of the Matérn model when $\nu = 0.5$, for the sub-plot (b), $D = 1.5$. It is worth underlining that, in Eq. (9), μ is only a scalar parameter not linked to the fractal dimension, so for this model the fractal dimension is constant.

In contradistinction to the Ornstein–Uhlenbeck and Matérn models, the Cauchy and Dagum models are capable of generating RFs with independently given fractal dimension and Hurst parameter. One can easily verify that the Cauchy model behaves like Eq. (6) $\alpha = \theta = (0, 2]$ and like Eq. (8), $\beta = \eta = (0, 1)$. If we focus on the sub-plots (e) and (f), the interpretation is twofold: a smoother profile is associated to a low value of D, as in sub-plot (e), ($\theta = 1.6$ corresponding $D = 1.2$), instead of a rougher profile associated with a high D, as in sub-plot (f), ($\theta = 0.2$ corresponding $D = 1.9$). If the long-memory parameter is large, similar values occur in lengthy patches or clusters, and the realization stays at approximately the same level for quite some length without noticeable jumps in value, as in sub-plot (e), ($\eta = 0.2$ corresponding $H = 0.9$), whereas if the long-memory parameter is low, the profile does not persist at any given level and fluctuates rather quickly between two extremes with significant jumps in value, as in sub-plot (f), ($\eta = 1.6$ correspond $H = 0.2$).

Although the Dagum model inverts the relation, as it behaves respectively like (6) and (8) for $\alpha = \varepsilon = (0, 2]$ and $\beta = \delta = (0, 1)$, we observe the same behavior for Dagum RFs as for Cauchy RFs. The sub-plot (g), ($\varepsilon = 0.8$ correspond $D = 1.6$), show quite smoother profiles than the sub-plot (h), ($\varepsilon = 0.2$ correspond $D = 1.9$). Similarly, in the sub-plot (g), ($\delta = 0.2$ corresponds $H = 0.9$), we can see less noticeable jumps than the sub-plot (h), ($\delta = 0.8$ corresponds $H = 0.6$).

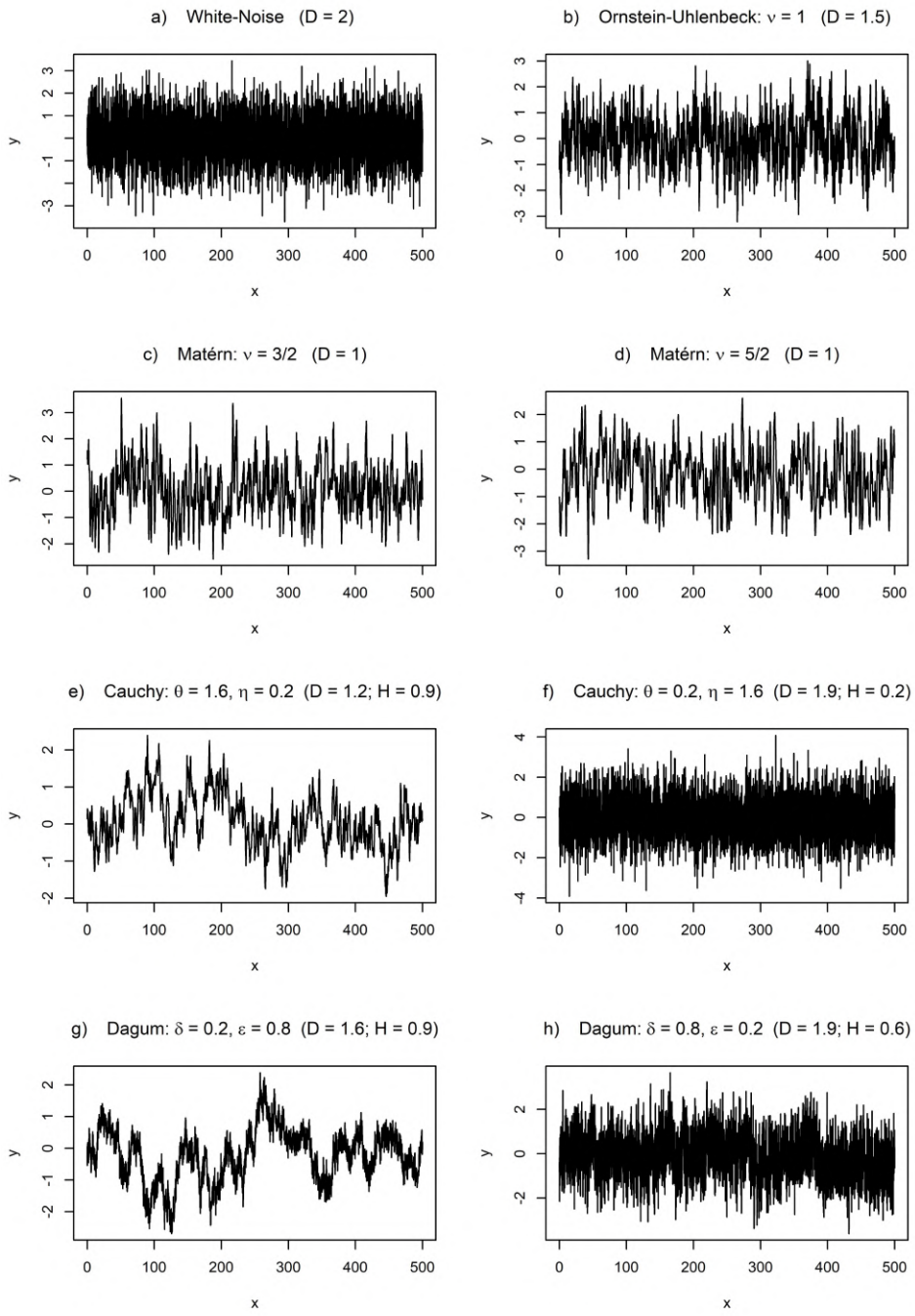

FIGURE 5.2: Samples of random fields in 1d showing models under consideration: (a) white-noise; (b) Ornstein-Uhlenbeck; (c-d) Matérn; (e-f) Cauchy; (g-h) Dagum

5.2.2 Variance of the Strain Energy and the Strain Energy Release Rate

5.2.2.1 Dead-load conditions

The force is deterministic, but the kinematic variable is random (Ostoja-Starzewski, 2004), implying that only the second term in Eq. 5.1 remains, and, assuming a Euler-Bernoulli beam, the strain energy is:

$$U = \int_0^a \frac{M(x)^2}{2IE} dx. \tag{5.13}$$

Here a is the crack length, M is bending moment, I is beam's moment of inertia, and E is elastic modulus. Henceforth, we simply work with $a = A/B$, where B is the constant beam (and crack) width, so that, on account of Clapeyron's theorem, the strain energy release rate is

$$G = \frac{\partial U}{B\partial a}. \tag{5.14}$$

Now, the beam's elastic modulus E is taken as a sum of a constant mean $\langle E \rangle$ and a zero-mean Gaussian WSS random field $E^{'}(\omega, x)$

$$E(\omega, x) = \langle E \rangle + E^{'}(\omega, x), \tag{5.15}$$

where Ω is the sample space of elementary events. The random material is thus defined as an ensemble $B = \{B(\omega); \omega \in \Omega\} = \{E(\omega, x); \omega \in \Omega, x \in [0, a]\}$. Hereinafter, we explicitly show the dependence on Ω , whenever we wish to indicate the random nature of a given quantity prior to ensemble averaging.

It follows from Eq. 5.15 that U is a random integral, such that, for each and every realization $(\omega \in \Omega)$, we should consider

$$U(a, \omega) = \int_0^a \frac{M(x)^2}{2IE(\omega, x)} dx. \tag{5.16}$$

The variance of the strain energy $U(a)$ is determined as follows. First, by applying the expectation operation to Eq. 5.16, we obtain

$$\langle U(a,) \rangle = \left\langle \int_0^a \frac{M(x)^2}{2IE(\omega, x)} dx \right\rangle = \int_0^a \frac{M(x)^2}{2I} \left\langle \frac{1}{E} \right\rangle. \tag{5.17}$$

Next, given two points x_1 and x_2, we have two random variables $E(x_1)$ and $E(x_2)$, so that the variance of U is found as

$$\begin{aligned} Var[U(a)] &:= \langle (U(a, E(x_1)) - \langle U(a) \rangle)(U(a, E(x_2)) - \langle U(a) \rangle) \rangle \\ &= \int_0^a \int_0^a \frac{M(x_1)^2 M(x_2)^2}{4I^2} C_{\mathbf{E}^{-1}}(x_1, x_2)\, dx_1 dx_2, \end{aligned} \tag{5.18}$$

in which we have used the covariance of the reciprocal Young's modulus $E^{-1}(\cdot) := 1/E(\cdot)$:

$$\begin{aligned} C_{\mathbf{E}^{-1}}(x_1, x_2) &= \left\langle \left(\frac{1}{E(x_1)} - \left\langle \frac{1}{E} \right\rangle \right) \left(\frac{1}{E(x_2)} - \left\langle \frac{1}{E} \right\rangle \right) \right\rangle \\ &= \left\langle \left(E^{-1}(x_1) - \left\langle E^{-1} \right\rangle \right) \left(E^{-1}(x_2) - \left\langle E^{-1} \right\rangle \right) \right\rangle. \end{aligned} \tag{5.19}$$

At this point, the PTM is applied to relate the covariance $C_{\mathbf{E}}(x_1, x_2)$ with $C_{\mathbf{E}}^{-1}(x_1, x_2)$. Hence, given the JPDF $p_{\mathbf{E}}(E(x_1), E(x_2))$, it is easy to prove that

$$p_{\mathbf{E}}^{-1}\left(E_1^{-1},E_2^{-1}\right)=\frac{1}{\left(E_1^{-1}\right)^2}\frac{1}{\left(E_2^{-1}\right)^2}p_{\mathbf{E}}\left(E_1^{-1},E_2^{-1}\right), \tag{5.20}$$

where $E_1^{-1}=E^{-1}(x_1)=1/E(x_1)$ and $E_2^{-1}=E^{-1}(x_2)=1/E(x_2)$. Then, the covariance $C_{\mathbf{E}^{-1}}(x_1,x_2)$ is found as

$$\begin{aligned} C_{\mathbf{E}^{-1}}(x_1,x_2) &= \int_{-\infty}^{\infty}\int_{-\infty}^{\infty}E_1^{-1}E_2^{-1}p_{\mathbf{E}}^{-1}\left(E_1^{-1},E_2^{-1}\right)dE_1^{-1}dE_2^{-1} \\ &= \int_{-\infty}^{\infty}\int_{-\infty}^{\infty}\frac{1}{E_1^{-1}}\frac{1}{E_2^{-1}}p_{\mathbf{E}}\left(E_1^{-1},E_2^{-1}\right). \end{aligned} \tag{5.21}$$

On account of Eq. 5.14, the strain energy release rate $G(a)$ becomes

$$G(a,\omega)=\frac{\partial U(a,\omega)}{B\partial a}. \tag{5.22}$$

It follows that a similar procedure to the one used to determine the variance of the strain energy $U(a)$ can be employed in order to obtain the variance of the strain energy relate rate $G(a)$. The mean and the variance function of the strain energy release rate are, respectively,

$$\langle G(a,)\rangle=\left\langle\frac{\partial U(a,\omega)}{B\partial a}\right\rangle=\frac{\langle U(a,\omega)\rangle}{B\partial a}, \tag{5.23}$$

$$\begin{aligned} Var\left[G(a)\right] &:= \langle\left(G\left(a,E(x_1)\right)-\langle G(a)\rangle\right)\left(G\left(a,E(x_2)\right)-\langle G(a)\rangle\right)\rangle \\ &= \frac{\partial^2 Var\left[U(a)\right]}{B^2\partial a^2}. \end{aligned} \tag{5.24}$$

Now, noting the variance $Var\left[U(a)\right]$ of strain energy $U(a)$, it is possible to obtain the variance $Var\left[G(a)\right]$ of the strain energy relate rate $G(a)$. The expressions of these two quantities are not derivable in explicit forms but, using numerical computation of 5.18 and 5.24, have been determined for all the cases of $C_{\mathbf{E}}(x_1,x_2)$ in Figs. 5.3 and 5.4. The results presented aim to investigate the influence of the fractal-and-Hurst effects in the problem under examination. To this aim, several combinations of the parameters that describe these effects are taken into account, Table 5.1. Mainly the parameters have been set so as to have RFs with Hurst parameter (H) between 0.5 to 0.8 and fractal dimension (D) between 1.2 and 1.7.

Overall, we observe that, while the Cauchy and Dagum models represent more realistic scenarios of RFs, the variance on the output is strongest for the Matérn model. Then, for Ornstein-Uhlenbeck and Cauchy models, the variance on output is between those of Matérn and Dagum models; in fact, the latter one is the model with the weakest variance on output. So seems that this problem is more sensitive to the stochastic local variation of $E(\omega,x)$ than to no-local stochastic behavior.

In order to evaluate the dependence on a of the PDF of the strain energy $U(a)$, an approach based on the direct evaluation of the response PDF (Falsone and Laudani, 2018) is applied. The crack axis has been discretized by intervals of constant amplitude da, i.e. a generic crack length $a_i=ida$ is considered. Corresponding to a_i, the

Model	Fractal dimension		Long memory	
Ornstein–Uhlenbeck	$\mu = 10^3$	$D = 1.5$	-	-
$C_{OU}(r,\mu) := \frac{\mu}{2} e^{-\mu r}$; special case of	$\mu = 50$	$D = 1.5$	-	-
$C_M(r, \nu = 1/2)$	$\mu = 1.0$	$D = 1.5$	-	-
Matérn	$\nu = 3/2$	$D = 1.0$	-	-
$C_M(r,\nu) := r^\nu K_\nu(r)$	$\nu = 5/2$	$D = 1.0$	-	-
Generalized Cauchy	$\theta = 1.0$	$D = 1.5$	$\eta = 1.0$	$H = 0.5$
$C_C(r,\theta,\eta) := \left(1 + r^\theta\right)^{-\eta/\theta}$	$\theta = 1.6$	$D = 1.2$	$\eta = 0.8$	$H = 0.6$
	$\theta = 0.6$	$D = 1.7$	$\eta = 0.4$	$H = 0.8$
Dagum	$\delta = 1.0$	$D = 1.5$	$\varepsilon = 0.5$	$H = 0.75$
$C_D(r,\delta,\varepsilon) := 1 - \left(1 + r^{-\delta}\right)^{-\varepsilon/\delta}$	$\delta = 1.6$	$D = 1.2$	$\varepsilon = 0.8$	$H = 0.6$
	$\delta = 0.6$	$D = 1.7$	$\varepsilon = 0.4$	$H = 0.8$

TABLE 5.1: Parameters considered for each model.

strain energy $U(a_i)$ can be defined as a Riemann sum approximating the integral of Eq. 5.16:

$$\begin{aligned} U(a_i,\omega) &= \int_0^{a_i} \frac{M(x_i)^2}{2IE(x_i)} dx_i \\ &\approx \sum_i \frac{M(x_i)^2}{2IE(x_i)} \Delta x_i = \sum_i \frac{M(x_i)^2}{2I} \Delta x_i \frac{1}{E(x_i)} = \sum_i \frac{M(x_i)^2}{2I} \Delta x_i E^{-1}(x_i) \end{aligned} \tag{5.25}$$

where $\Delta x_i = i\Delta xi = ida$. Using the above relationship, $U(a_i)$ can now be written as

$$U(a_i,\omega) = \sum_i G_i E^{-1}(x_i). \tag{5.26}$$

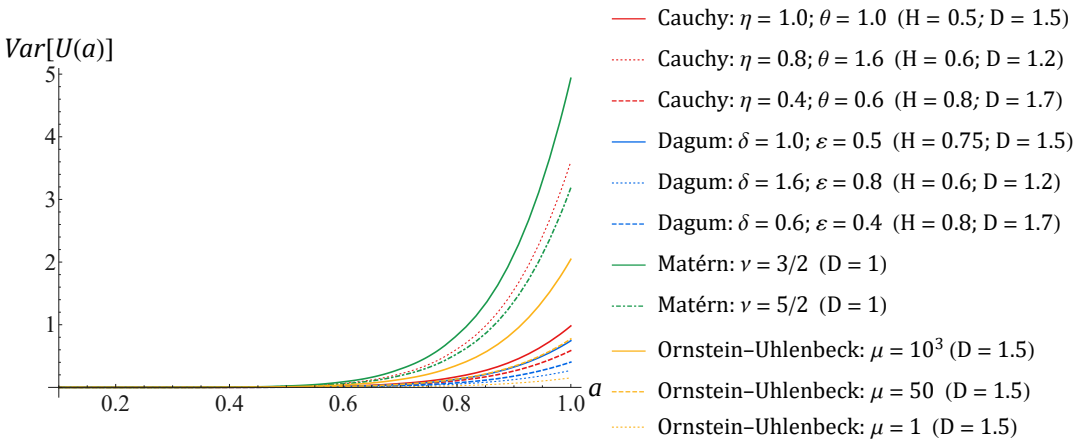

FIGURE 5.3: The variance of strain energy, $Var[U(a)]$, when is: Cauchy ($\eta = 1.0, \theta = 1.0; \eta = 0.8, \theta = 1.6; \eta = 0.4, theta = 0.6$); Dagum ($\delta = 1.0, \varepsilon = 0.5; \delta = 1.6, \varepsilon = 0.8; \delta = 0.6, \varepsilon = 0.4$); Matérn ($\nu = 3/2; \nu = 5/2$) and Ornstein–Uhlenbeck ($\mu = 10^3; \mu = 50; \mu = 1$); $h = B = 1, P = 1$ and $\langle E \rangle = 1$.

This implies that, in the interval of the length crack (a_0, a_i), the value at the generic crack length up to a_i of the strain energy $U(a_i)$ is given by the following

linear algebraic equation system:

$$U\left(a_i,\omega\right)=\sum_i G_i E^{-1}\left(x_i\right)=\mathbf{G}_i\mathbf{E}_i^{-1}, \tag{5.27}$$

where $\mathbf{G}_i$ is the generic row. The Eq. 5.27 establishes a linear algebraic relationship between the strain energy $U\left(a_i\right)$, evaluated at various crack lengths up to a_i, and the stochastic vector $\mathbf{E}_i^{-1}$, evaluated at from crack lengths up to a_i.

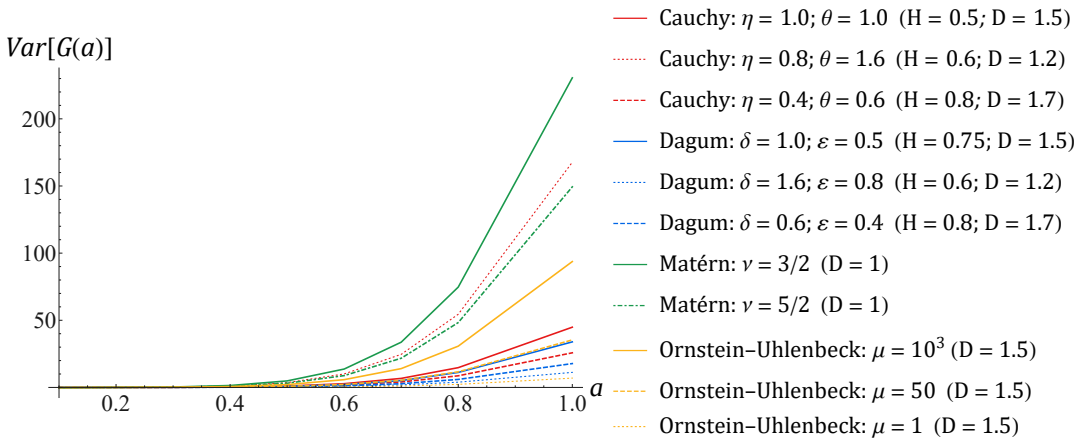

FIGURE 5.4: The variance of strain energy, $Var\left[G(a)\right]$, when is: Cauchy $(\eta=1.0,\theta=1.0;\eta=0.8,\theta=1.6;\eta=0.4,theta=0.6)$; Dagum $(\delta=1.0,\varepsilon=0.5;\delta=1.6,\varepsilon=0.8;\delta=0.6,\varepsilon=0.4)$; Matérn $t(\nu=3/2;\nu=5/2)$ and Ornstein–Uhlenbeck $(\mu=10^3;\mu=50;\mu=1)$; $h=B=1$,$P=1$ and $\langle E\rangle=1$.

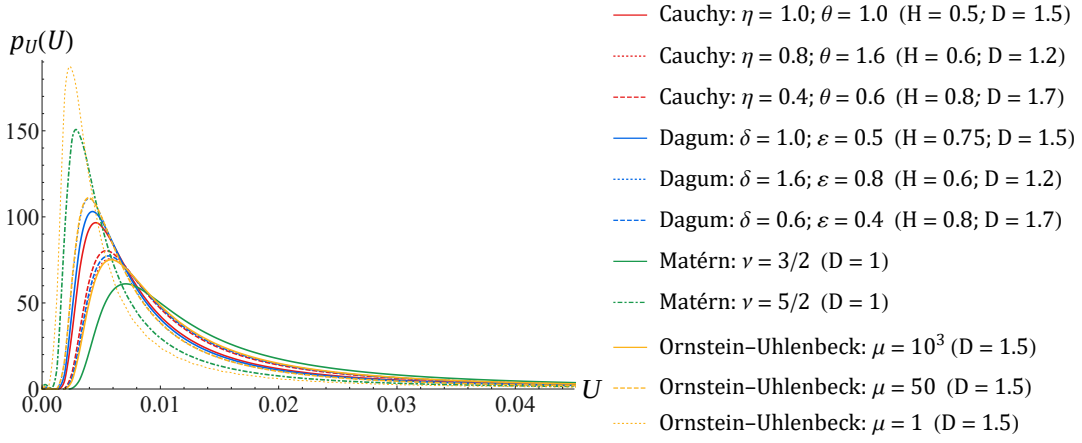

FIGURE 5.5: Probability density function of the strain energy $p_U(U)$, for $a_i=2da$, when is: Cauchy $(\eta=1.0,\theta=1.0;\eta=0.8,\theta=1.6;\eta=0.4,theta=0.6)$; Dagum $(\delta=1.0,\varepsilon=0.5;\delta=1.6,\varepsilon=0.8;\delta=0.6,\varepsilon=0.4)$; Matérn $(\nu=3/2;\nu=5/2)$ and Ornstein–Uhlenbeck $(\mu=10^3;\mu=50;\mu=1)$; $h=B=1$,$P=1$ and $\langle E\rangle=1$.

The PTM is now applied to Eq. 5.27 in order to evaluate $p_U\left(a_i\right)\left(U\left(a_i\right)\right)$. Using numerical computation, we obtain the PDF and plot it in Fig. 5.5, wherein the crack axis is discretized by intervals of constant amplitude $da=0.2$. It is gleaned from Fig. 5.5 that the PDF of the strain energy, evaluated for several cases of D and H, shows a strongly nonlinear character of the relationship between the input and the output.

The fractal-and-Hurst effects appear to be more or less in line with the previous trends observed on the variance of output.

5.2.2.2 Fixed-grip conditions

In this case, the displacement is constant (i.e., non-random), while the load is random. Now, only the first term in 5.1 remains, so that

$$G = -\frac{\partial U}{B\partial a}. \tag{5.28}$$

With the force P at the tip, we have

$$G = -\frac{u}{2B}\frac{\partial P}{\partial a}. \tag{5.29}$$

Taking the cantilever beam of Fig. 5.1 (b), implies $P(a,\omega) = 3uIE(\omega,x)/a^3$, so that

$$G(a,\omega) = -\frac{u}{2B}\frac{\partial P}{\partial a} = \frac{9u^2 IE(\omega,x)}{2Ba^4}. \tag{5.30}$$

Equation 5.30 gives a direct relationship between $G(a,\omega)$ and $E(\omega,x)$ from which we first obtain the mean and variance functions of the strain energy release rate

$$\langle G(a)\rangle = -\frac{u}{2B}\left\langle\frac{\partial P}{\partial a}\right\rangle = \frac{9u^2 I\langle E\rangle}{2Ba^4}, \tag{5.31}$$

$$Var\left[G(a,r)\right] = \left\langle\left(G\left(a,E(x_1)\right) - \langle G(a)\rangle\right)\left(G\left(a,E(x_2)\right) - \langle G(a)\rangle\right)\right\rangle = \left(\frac{9u^2 I}{2Ba^4}\right)^2 C_{\mathbf{E}}(r). \tag{5.32}$$

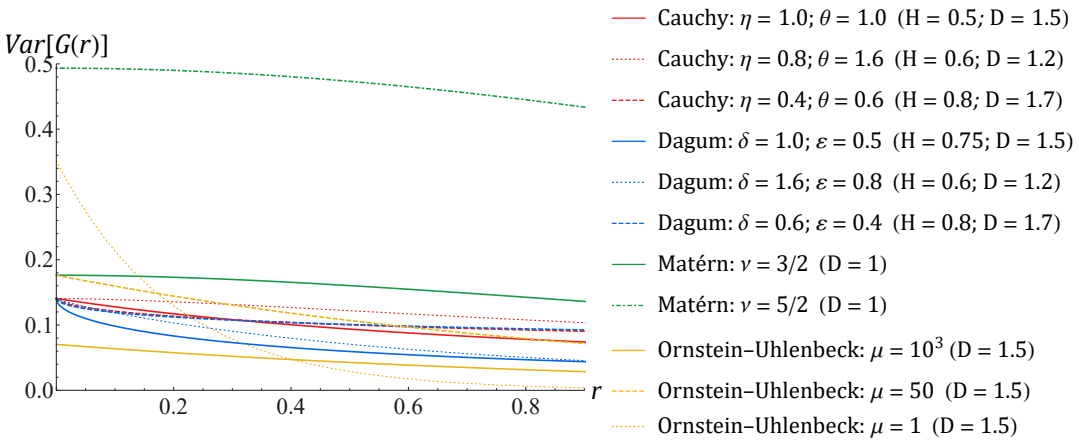

FIGURE 5.6: The variance of the strain energy, $Var\left[G(r)\right]$, when is: Cauchy $(\eta = 1.0, \theta = 1.0; \eta = 0.8, \theta = 1.6; \eta = 0.4, theta = 0.6)$; Dagum $(\delta = 1.0, \varepsilon = 0.5; \delta = 1.6, \varepsilon = 0.8; \delta = 0.6, \varepsilon = 0.4)$; Matérn $t(\nu = 3/2; \nu = 5/2)$ and Ornstein–Uhlenbeck $(\mu = 10^3; \mu = 50; \mu = 1)$; $h = B = 1, P = 1$ and $\langle E\rangle = 1$.

Thus, it is possible to obtain the variance of the strain energy relate rate $G(a,r)$, at a fixed value of r or for a fixed value of a. We employ the same method as before in order to determine the effect of the covariance function $C_{\mathbf{E}}(r)$. Figures 5.6 and

5.7 show the variances $Var\,[G(a,r)]$ for a fixed value of the crack length $(a = 1)$ and a fixed value of $r\,(r = x_2 - x_1 = 0.1)$. Although in this case a linear relationship appears between the input and output, the previous qualitative conclusions for these two cases carry through as supported by several different cases of D and H.

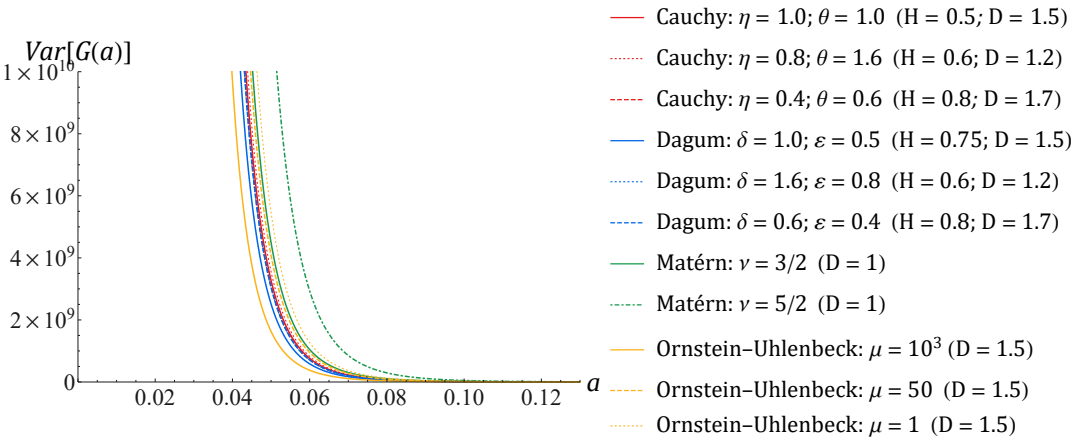

FIGURE 5.7: The variance of the strain energy release ratey, $Var\,[G(a)]$, for $a_i = 2da$, when is: Cauchy $(\eta = 1.0, \theta = 1.0; \eta = 0.8, \theta = 1.6; \eta = 0.4, theta = 0.6)$; Dagum $(\delta = 1.0, \varepsilon = 0.5; \delta = 1.6, \varepsilon = 0.8; \delta = 0.6, \varepsilon = 0.4)$; Matérn $(\nu = 3/2; \nu = 5/2)$ and Ornstein–Uhlenbeck $(\mu = 10^3; \mu = 50; \mu = 1)$; $h = B = 1, P = 1$ and $\langle E \rangle = 1$.

5.2.3 Stochastic crack stability

Crack stability in any particular realization of a random beam, in a general loading situation, is governed by a condition of the same form as that in deterministic fracture mechanics (Ostoja-Starzewski, 2004):

$$\frac{\partial^2 \left(\Pi\left(\omega\right) + \Gamma\left(\omega\right)\right)}{\partial^2} = \begin{cases} < 0: & unstable \quad equilibrium \\ = 0: & neutral \quad equilibrium \\ > 0: & stable \quad equilibrium \end{cases} \tag{5.33}$$

Here both, the total potential energy $\Pi\left(\omega\right)$ and the surface energy $\Gamma\left(\omega\right)$ are random. Two example problems will now be considered with respect to crack stability.

5.2.3.1 First example problem

The first concerns a line crack in an infinite plate subjected to a uniform stress perpendicular to the crack axis. The potential energy of the system is given by

$$\Pi\left(\omega\right) = -U\left(\omega\right) = \frac{-\sigma^2 \pi a^2}{E(\omega)} \tag{5.34}$$

and the surface energy is

$$\Gamma\left(\omega\right) = 4a\gamma(\omega). \tag{5.35}$$

The terms Π, Γ, and $(\Pi + \Gamma)$ are plotted in Fig. 5.8 for E and γ constant. This figure shows that the total potential energy of the system $(\Pi + \Gamma)$ at the critical crack length a_c presents a maximum, which corresponds to an unstable equilibrium.

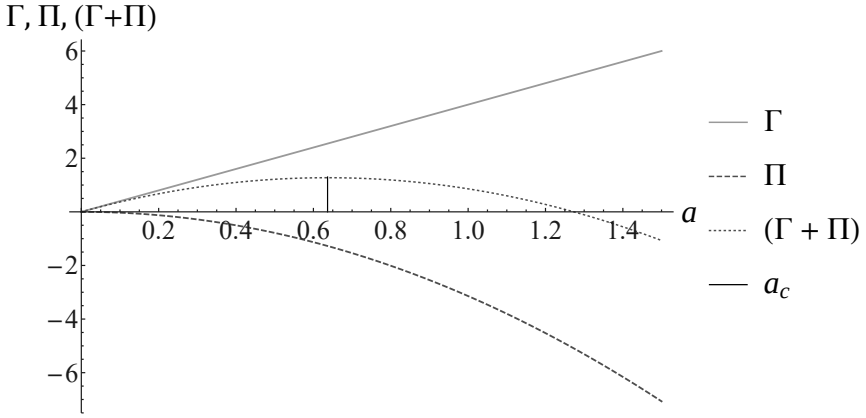

FIGURE 5.8: Potential energy Π, surface energy Γ and the sum of potential and surface energy $(\Pi + \Gamma)$, versus crack length a for a line crack in an infinite medium subjected to a uniform stress perpendicular to crack axis.

Taking into account that beam's material is random, the mean and variance of the potential energy $\Pi(\omega)$ are, respectively,

$$\langle \Pi(\omega) \rangle = \langle -U(\omega) \rangle = -\sigma^2 \pi a^2 \left\langle \frac{1}{E(\omega)} \right\rangle, \tag{5.36}$$

$$Var\left[\Pi(a,r)\right] = \langle (\Pi(a,E(x_1)) - \langle \Pi(a) \rangle)(\Pi(a,E(x_2)) - \langle \Pi(a) \rangle) \rangle = \left(-\sigma^2 \pi a^2\right)^2 C_{\mathbf{E}^{-1}}(r), \tag{5.37}$$

where $C_{\mathbf{E}^{-1}}(r)$ is evaluated by Eq. 5.21.

Next, if we take the surface energy density as an RF made up of a constant mean $\langle \gamma \rangle$ and a zero-mean fluctuation $\gamma'(\omega, x)$

$$\gamma(\omega, x)) = \langle \gamma \rangle + \gamma'(\omega, x). \tag{5.38}$$

The mean and the variance function of the variance of the surface energy $\Gamma(\omega)$ are, respectively

$$\langle \Gamma(\omega) \rangle = 4a \langle \gamma \rangle, \tag{5.39}$$

$$Var\left[\Gamma(a,r)\right] = \langle (\Gamma(a,E(x_1)) - \langle \Gamma(a) \rangle)(\Gamma(a,E(x_2)) - \langle \Gamma(a) \rangle) \rangle = (4a)^2 C_\gamma(r). \tag{5.40}$$

Finally, the variance of the sum $(\Pi(\omega) + \Gamma(\omega))$ is

$$Var\left[\Pi(\omega) + \Gamma(\omega)\right] = Var\left[\Pi(\omega)\right] + Var\left[\Gamma(\omega)\right] + 2Cov\left[\Pi(\omega) + \Gamma(\omega)\right] \tag{5.41}$$

and taking, as in our earlier study, the two-component RFs to be uncorrelated, gives

$$Var\left[\Pi(\omega) + \Gamma(\omega)\right] = Var\left[\Pi(\omega)\right] + Var\left[\Gamma(\omega)\right]. \tag{5.42}$$

Some numerical results are shown in Fig. 5.9 when it was fix $r = x_2 - x_2 = 0.1$. In this case, the beam is described by a vector RF $\{E, \gamma\}$. Nevertheless, by inspection of Fig. 5.9, the qualitative trend is similar to the trends depicted in Subsection

3.5.2, with the scatter of response being weaker than under the Dagum, Cauchy, Ornstein–Uhlenbeck, and Matérn inputs.

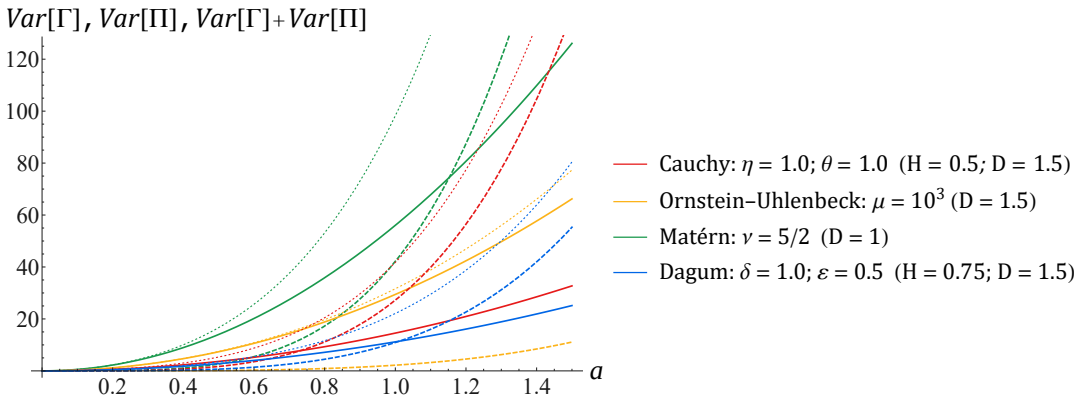

FIGURE 5.9: The variance of the potential energy, $Var\,[\Pi(a)]$ (dashed line), surface energy, $Var\,[\Gamma(a)]$ (continuous line) and the sum of potential and surface energy, $Var\,[\Pi(a)+\Gamma(a)]$ (dotted line); when is: Cauchy $(\eta = 1.0, \theta = 1.0; \eta = 0.8, \theta = 1.6; \eta = 0.4, theta = 0.6)$; Dagum $(\delta = 1.0, \varepsilon = 0.5; \delta = 1.6, \varepsilon = 0.8; \delta = 0.6, \varepsilon = 0.4)$; Matérn $(\nu = 3/2; \nu = 5/2)$ and Ornstein–Uhlenbeck $(\mu = 10^3; \mu = 50; \mu = 1)$; $h = B = 1, P = 1$ and $\langle E \rangle = 1$.

5.2.3.2 Second example problem

The second problem concerns the experiment carried out by Obreimoff on the cleavage of mica (Obreimoff, 1930). A wedge of thickness h is inserted underneath a flake of mica, which is detached from a mica block along a length a, Fig. 5.10.

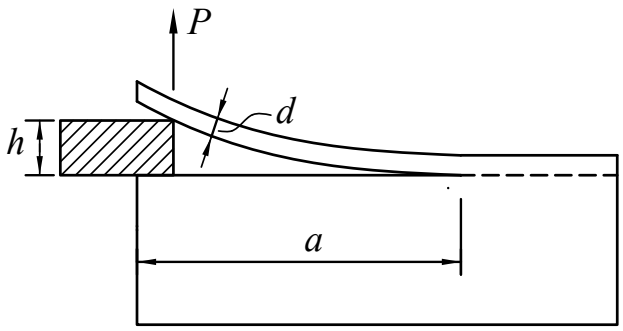

FIGURE 5.10: Wedge insert to peel mica off a substrate, according to Obreimoff's experiment.

The energy of the system is calculated by considering the mica flake as a cantilever beam with height d built-in at distance a from the point of application of the wedge. During crack propagation, the force P does not do any work. According to the elementary theory of beam bending, the stochastic elastic energy stored in the cantilever is:

$$U(\omega) = \frac{E(\omega) d^3 h^2}{8a^3}, \tag{5.43}$$

while the surface energy $\Gamma(\omega)$ is given by

$$\Gamma(\omega) = 2a\gamma(\omega). \tag{5.44}$$

In this second problem, the total energy of the system $(U(\omega) + \Gamma(\omega))$ at the critical crack length a_c is minimum, which corresponds to a stable equilibrium. From the fracture criterion, the equilibrium crack length a_c is obtained as

$$a_c = \left(\frac{3E(\omega)d^3h^2}{16\gamma(\omega)}\right)^{1/4}. \tag{5.45}$$

Figure 5.11 plots $\Gamma = U$, Π and $(U + \Pi)$ when E and γ are constant. This gives the reference deterministic case.

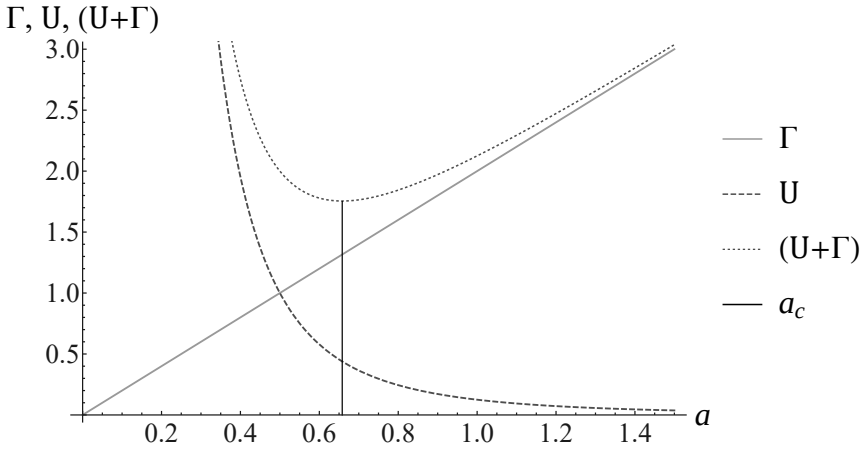

FIGURE 5.11: Potential energy $\Gamma = U$, surface energy Γ, and their sum $(U + \Pi)$ versus the crack length a for Obreimoff's experiment

Now, we take the surface energy density and the beam's stiffness as two RFs: $\gamma(\omega, x)$, $E(\omega, x)$. The mean and variance of the elastic and surface energies are, respectively,

$$\langle U \rangle = \frac{d^3h^2 \langle E \rangle}{8a^3}, \tag{5.46}$$

$$Var\left[U(a,r)\right] = \left(\frac{d^3h^2}{8a^3}\right)^2 C_{\mathbf{E}}(r), \tag{5.47}$$

and

$$\langle \Gamma \rangle = 2a \langle \gamma \rangle, \tag{5.48}$$

$$Var\left[\Gamma(a,r)\right] = (2a)^2 C_\gamma(r). \tag{5.49}$$

Supposing these two RFs to be uncorrelated (i.e., $Cov\left[U(\omega) + \Gamma(\omega)\right] \to 0$), we find

$$Var\left[U(\omega) + \Gamma(\omega)\right] = Var\left[U(\omega)\right] + Var\left[\Gamma(\omega)\right]. \tag{5.50}$$

Numerical results for several parameter cases are shown in Fig. 5.12, where we set $r = x_2 - x_1 = 0.1$. Clearly, for the experiment of Obreimoff similar trends to those already observed in Fig. 5.12 for the first example problem are obtained, and similar conclusions can be drawn.

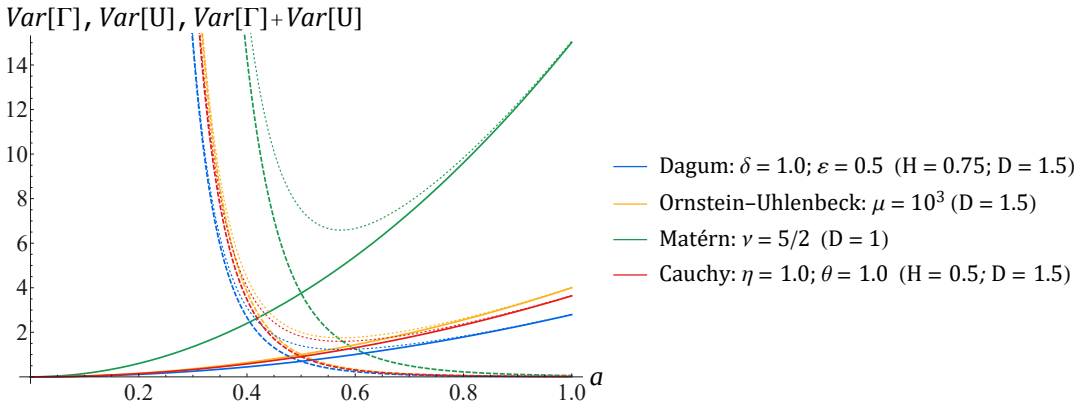

FIGURE 5.12: The variance of the potential energy, $Var\,[U(a)]$ (dashed line), surface energy, $Var\,[\Gamma(a)]$ (continuous line) and the sum of potential and surface energy, $Var\,[U(a)+\Gamma(a)]$ dotted line); when is: Cauchy ($\eta = 1.0, \theta = 1.0$); Dagum ($\delta = 1.0, \varepsilon = 0.5$) ; Matérn ($\nu = 5/2$) and Ornstein–Uhlenbeck ($\mu = 10^3$); $\sigma = 1$ and $\langle E \rangle = \langle \gamma \rangle = 1$; (second example problem).

Considering the critical crack length, a_c, taking into account the relation 5.46, it is possible to obtain the relative PDF by applying the PTM. With the aim to investigate the influence on the response output by the four RFs on input, it seems reasonable to compare the PDF of the critical crack length for the following cases. Since in the stochastic crack stability problem the beam is described by the vector RF $\{E, \gamma\}$, in each sub-plot of Fig. 5.13 γ is fixed as Cauchy (A), Matérn (B), Ornstein–Uhlenbeck (C) or Dagum (D), and then E varies for these four cases of RFs. Hence, the same tendency is observed: the PDF of a_c is the most dispersed for Matérn, then Ornstein–Uhlenbeck, Cauchy, and Dagum models, respectively. Therefore, we observe the same ordering as before.

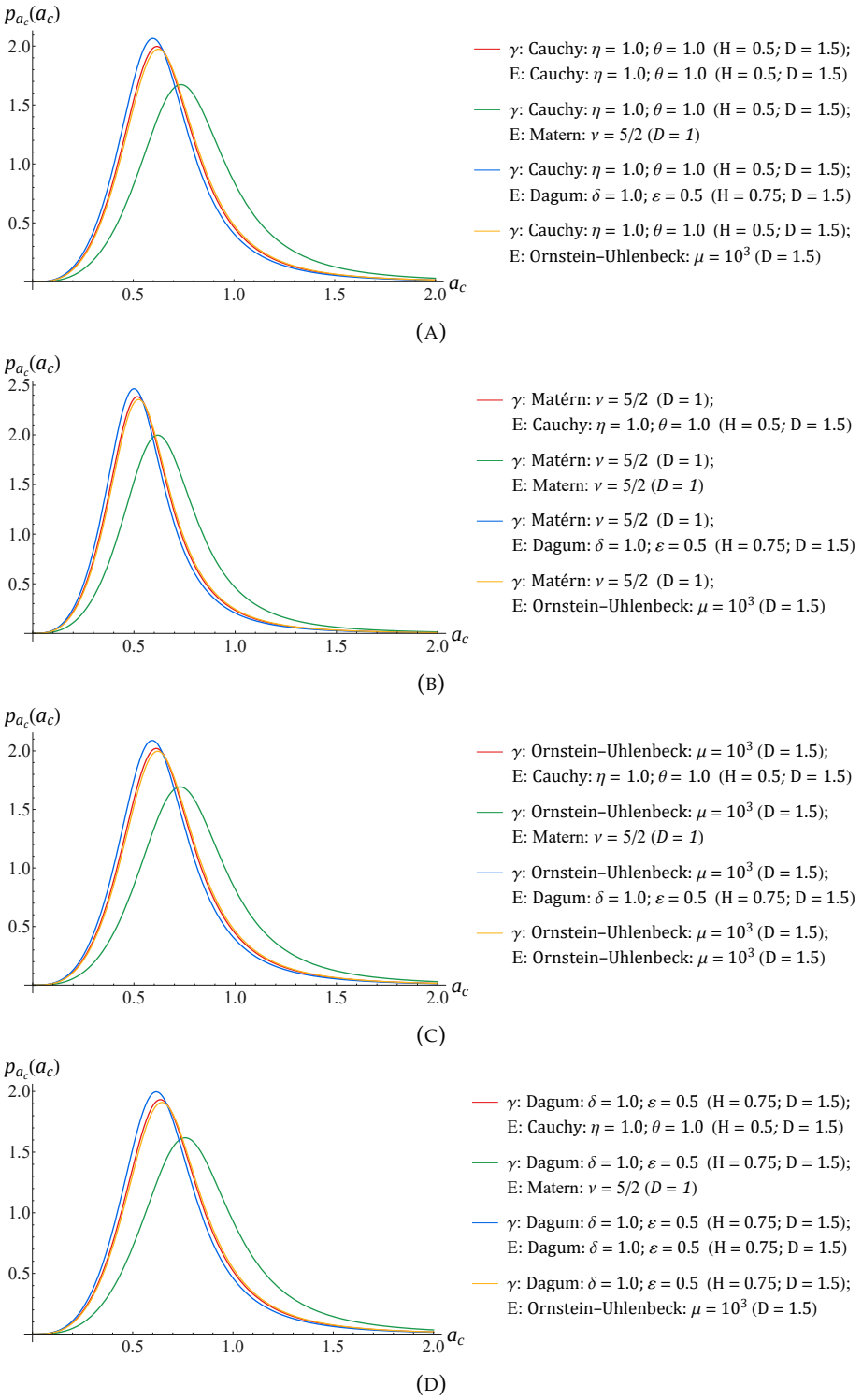

FIGURE 5.13: PDF of the critical crack length for four sub-cases of covariance functions of γ and E. In (A) γ= Cauchy; in (B) γ= Matérn; in (C) γ= Ornstein–Uhlenbeck; (D) γ= Dagum. Then, for each plot, E= Cauchy (red line), Matérn (green line), Dagum (blue line) or Ornstein–Uhlenbeck (yellow line). Cauchy ($\eta = 1.0, \theta = 1.0$); Dagum ($\delta = 1.0, \varepsilon = 0.5$); Matérn ($\nu = 5/2$) and Ornstein–Uhlenbeck ($\mu = 10^3$); $\sigma = 1$ and $\langle E \rangle = \langle \gamma \rangle = 1$; (second example problem).

5.2.4 Some remarks

This section employs the classical Obreimoff's experiment to examine the fractal-and-Hurst effects of the RF material properties on elastic brittle fracture. Two RF models – Cauchy and Dagum – enable such an investigation and, in order to elucidate the fractal-and-Hurst effects, Ornstein–Uhlenbeck (which, in the limiting case, becomes white noise) and Matérn RFs are also considered. All the RFs are assumed to be truncated Gaussian so as to ensure positive values of the elastic modulus and surface energy density along the beam axis. The variance function of the strain energy $U(a)$ and of the strain energy release rate $G(a)$, both for dead-load and fixed-grip conditions, are found in explicit forms. For dead-load condition there is an inverse relationship between $U(a)$ or $G(a)$, with the Young modulus $E(\omega, x)$. In fact, the 2004 study found that, in the case of dead-load conditions, $U(a)$ and/or $G(a)$ computed by straightforward averaging of the spatially random elastic modulus $E(\omega)$ is lower than that obtained by correct ensemble averaging of the stored elastic energy. Thus, in the present study, in order to evaluate the exact covariance function of energy and its release rate, a recently established PTM, has been applied. However, there is a direct relationship between $G(a)$ and $E(\omega, x)$ for fixed-grip condition and, in fact, $G(a)$ is to be computed by a direct ensemble averaging of $E(\omega)$. It was find find that, under these conditions, the variance function depends on a and r. Moreover, an approach based on the direct evaluation of the response PDF by PTM is applied and the PDF of the strain energy $U(a)$ is obtained. In general, it was find that, given the same variance on input, the variance on output is more pronounced for the Matérn RF. These results seem to allow to say that this problem is more sensitive to the stochastic local properties, the fractal dimension, D, and less to the no-local stochastic behavior of memory, H. Moreover, by assuming different values of the fractal dimension and Hurst parameters on the input, we obtain strong differences in the response on the output. Also, the response is stronger for the Cauchy model than for the Dagum model. Furthermore, a study of the stochastic crack stability is conducted: it involves a stochastic competition between potential and surface energies. Then, also in this last case, the fractal and the Hurst effects are taken into consideration through Gaussian Cauchy and Dagum RFs. In particular, it is possible to evaluate the PDF of the critical crack length, $p_{a_c}(a_c)$, from analysis of Obreimoff's experiment. Again, the Matérn model leads to a stronger dispersion of the data than Cauchy and Dagum. Given the fact that fractal-and-Hurst effects are multiscale properties of materials seen primarily in nature, the present study should provide an indication as to the fracture phenomena in geomechanical/geophysical settings.

5.3 The concept of local and non-local randomness for some mechanical problems

Supposing the flexural deformability of the beams to be a Gaussian homogeneous RF, the investigation of the concept of spatial randomness in local and non-local mechanical problems is the aim of this section.
The sensitivity of the stochastic response quantities to the local and non-local randomness dependence of the flexural deformability will be investigated through some examples of statically determinate and redundant stochastic beams, under different conditions of load and constrain. In particular, the response stochastic quantities will

Class	Correlation functions	Parameters
White Noise	$C_{WN}(r) := \delta(r)$	$r \geq 0$
Powered exponential	$C_{EXP}(r) := \exp(\lvert cr\rvert^{\alpha})$	$\alpha \in (0,2]$
Matérn	$C_M(r) := \frac{2^{(\alpha/2)-1}}{\Gamma(\alpha/2)} \lvert cr\rvert^{\alpha/2} K_{\alpha/2}(\lvert cr\rvert)$	$\alpha \in (0,2]$
Cauchy	$C_C(r) := \left(1+\lvert cr\rvert^{\alpha}\right)^{\frac{\beta}{\alpha}}$	$\alpha \in (0,2]; \quad \beta > 0$

TABLE 5.2: Some parametric classes of correlation functions for a Gaussian process

be found thanks to the use of the PTM. It is important to note that, for statically determinated beams, the cinematic response (transversal displacements and rotations) are random. While, for redundant beams, also the internal forces (shear and bending moment) are random responses (Elishakoff, Ren, and Shinozuka, 1995b; Elishakoff, Impollonia, and Ren, 1999).

5.3.1 Local and non-local randomness

With the aim to examine the dependence of the stochastic response on the kind of correlation functions defining the material/geometric RFs, the closed-form solutions of statically and redundantly stochastic bending beams of section 3.4 have been applied. From the section 3.4, an in-depth view of the integral expressions of the variances, for both the statically and redundant stochastics beams, brings up the close similarity of the latter ones with the constitutive equations of the mechanical nonlocal theory of Eringen, 1983. The Eringen non-local integral constitutive equation describes the dependence of the stress at a point on the strain in the rest of the domain through a positive-decaying kernel function (Fernández-Sáez et al., 2016). The analogy with the equations giving the statistics of the response stochastic beam is evident. In particular, the analogy between the effect of the kernel function and that of the correlation function is clear.

The flexural deformability $D(z)$ is constrained in such a way that it is statically determinate and it is characterized by a flexural deformability (that is the inverse of the flexural stiffness) that is supposed to be a Gaussian homogeneous RF given by:

$$D(z) = \frac{1}{EI(z)} = D_0(1+\alpha(z)) \tag{5.51}$$

$D(z)$ appearing in Eq. 5.51 is assumed to be characterized by correlation functions beloging to the classes reported in Table 5.2. It is well known that several properties of a RF can be established through the study of their associated correlation function.

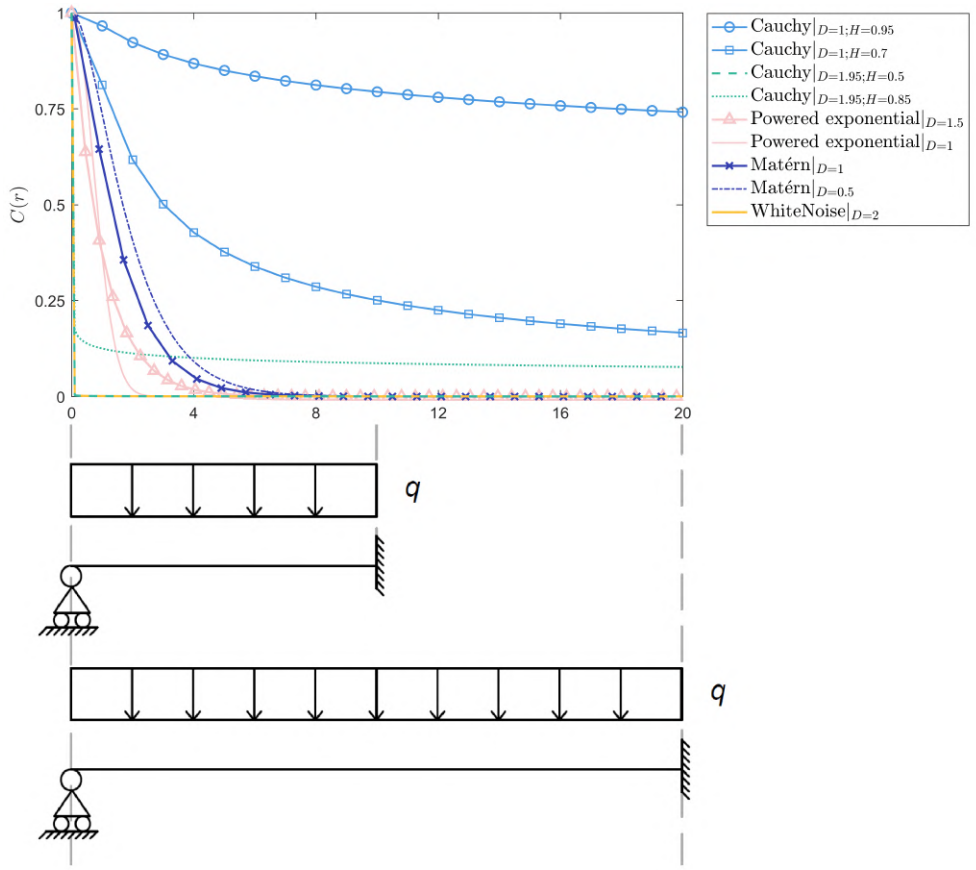

FIGURE 5.14: Some parametric classes of correlation functions for a Gaussian process.

The choice of the above correlation functions is motivated by their particular capability to interpret the local and non-local properties of a RF. Relatively to these two characteristics, the correlation functions are strictly linked to the local and non-local properties of the RF through two important parameters, respectively: 1) the fractal dimension D reflects the local properties; it is a roughness measure with range $[d, d+1)$, where d is the topological dimension. Since the focus of the present work is on mono-axial beams, $d = 1$ is used; 2) the Hurst exponent H reflects a long-length dependence in a RF, or, equivalently, a long memory dependence in time series. In particular, the realization of the RF has $D = d + 1 - \alpha/2$ with probability 1 (Gneiting, Ševčíková, and Percival, 2012), while the RF has a long memory with $H = 1 - \beta/2$ (Gneiting and Schlather, 2004b). Thus, the parameter α is linked to the fractal dimension while the parameter β is connected to the Hurst exponent. Therefore, in the field of stochastic mechanics, it is possible to associate the fractal dimension with the local randomness characteristics and the Hurst exponent with the non-local randomness characteristics. The non-local randomness of the flexural deformability RF means that its probabilistic dependence between two different x-points, even if they are far apart from each other, is persistent, i.e. is non-negligible. In comparison, for the local randomness of the flexural deformability RF, if two x-points are taken sufficiently far to each other, then the corresponding RVs are almost uncorrelated. Fig. 5.14 illustrates the trend of correlation functions reported in Table 5.2, comparing the different correlation lengths of correlation functions with the different beam lengths that will be investigated in the next subsections.

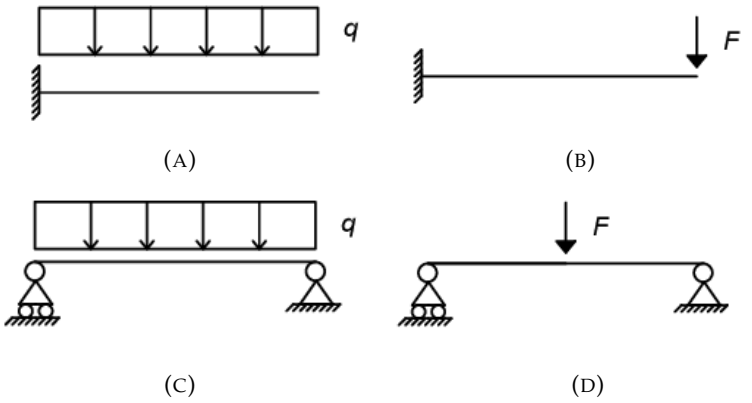

FIGURE 5.15: Statically determinate stochastic beams.

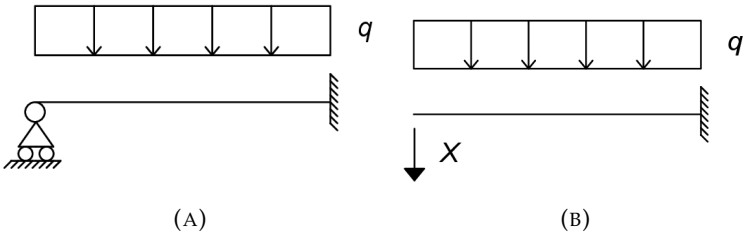

FIGURE 5.16: Example 1: statically redundant stochastic beam.

In particular, the White Noise, the Powered exponential, and the Matérn correlation functions allow capturing only the local randomness of the flexural deformability characteristics in contrast to the Cauchy class (Gneiting and Schlather, 2004b) with which it is possible controlling at the same time the local and non-local randomness dependence of the flexural deformability characteristic.

In order to investigate the sensitivity of the stochastic response quantities to the local and non-local randomness dependence of the flexural deformability characteristic, in the next subsections some examples of statically determinate and redundant stochastic beams, under different conditions of load and constrain, are shown.

5.3.2 Statically determinate stochastic beams

The procedure presented in subsection section 3.4 has been applied to the stochastic analysis of the statically determinate beams reported in Fig. 5.15 for the different

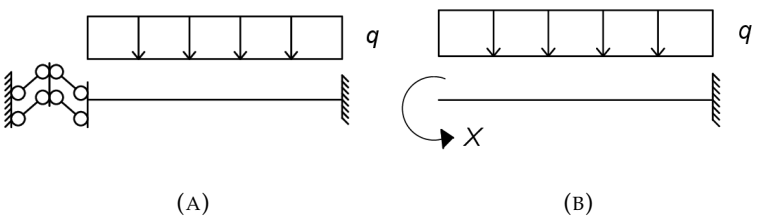

FIGURE 5.17: Example 2: statically redundant stochastic beam.

	COV $= \sigma/\mu$			
Class	(a)	(b)	(c)	(d)
Cauchy$\|_{D=1.95;H=0.5}$	0.008	0.008	0.011	0.011
Cauchy$\|_{D=1.95;H=0.85}$	0.086	0.088	0.096	0.095
Powered exponential$\|_{D=1}$	0.131	0.143	0.198	0.196
Powered exponential$\|_{D=1.95}$	0.132	0.144	0.213	0.209
Matérn$\|_{D=1}$	0.161	0.172	0.224	0.223
Matérn$\|_{D=0.5}$	0.176	0.187	0.234	0.233
Cauchy$\|_{D=1;H=0.7}$	0.205	0.211	0.239	0.238
Cauchy$\|_{D=1;H=0.95}$	0.241	0.242	0.248	0.248

TABLE 5.3: COV values of the stochastic displacement statically determinate stochastic beams.

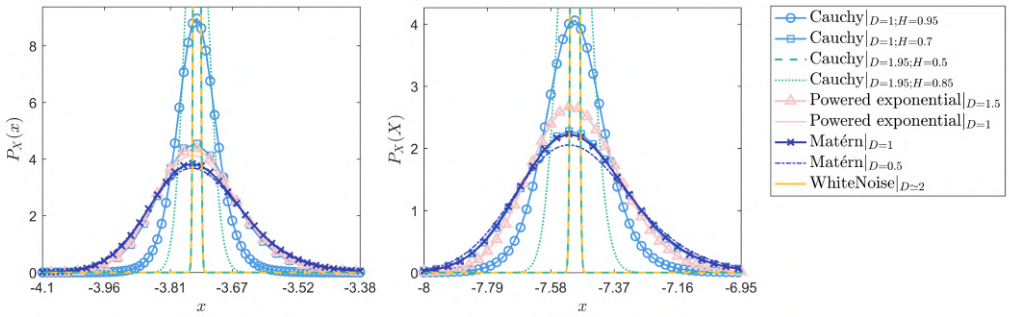

(A) (B)

FIGURE 5.18: Example 1: PDF of the redundant force X: (A) $L = 10$; (B) $L = 20$.

type of laws of $\sigma_\alpha^2(|z_1 - z_2|)$ of Table 5.2. Table 5.3 reports a summary of the results, in particular, the estimation of the COV value of the stochastic displacement is interesting in order to explore, for which class of correlation function, more pronounced dispersions of the displacement distribution are. In subsection 5.3.4 some more comments on these results will be reported.

5.3.3 Statically redundant stochastic beams

The stochastic response quantities, which are the redundant force and the displacement of the two examples reported in Figures 5.16 and 5.17, are examined. To not lose generality in the problem under examination, no-dimensional numerical analyses have been evaluated and the mean value of the random variables involved is taken unitary. In Fig. 5.18 the PDF of the redundant force X, $p_X(x)$, for the different RF is reported. In particular, the PDF of the stochastic variable X has been examined for two different value of length of the beam, i.e. $L = 10$ (Fig.5.18 (A)) and $L = 20$ (Fig. 5.18 (B)); while, Table 5.4 shows the respective COV values of the redundant force. Then, Fig. 5.19 shows the PDF of the transversal displacement $u(\bar{z})$, with $\bar{z} = L/2$, for the all assumptions of Gaussian field $D(z)$. Finally, in order to investigate the influence of the abscissa $\bar{z}$ on the stochastic response displacement, in Figs. 5.20 and 5.21 the $p_U(u)$ for different values of abscissa for $L = 10$ and for $L = 20$, are reported. In Table 5.5 is stored all COV values about the investigation on $u(\bar{z})$.

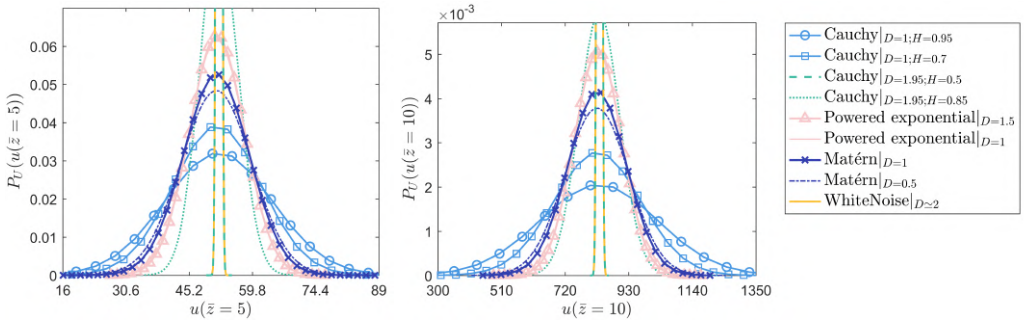

(A) (B)

FIGURE 5.19: Example 1: PDF of the transversal displacement $u(\bar{z}) = L/2$: (A) $L = 10$; (A) $L = 20$.

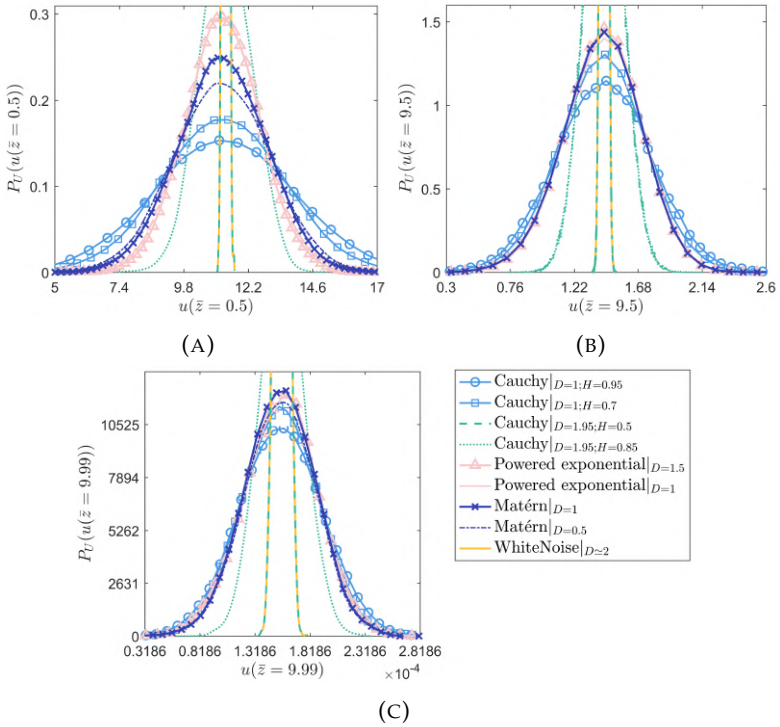

(A) (B)

(C)

FIGURE 5.20: Example 1: PDF of the transversal displacement for $L = 10$: (a) $\bar{z} = 0.5$; (b) $\bar{z} = 9.5$; (c) $\bar{z} = 9.99$.

Class	COV $= \sigma/\mu$	
	$L = 10$	$L = 20$
Cauchy$\|_{D=1.95;H=0.5}$	0.001	0.001
Cauchy$\|_{D=1.95;H=0.85}$	0.007	0.006
Powered exponential$\|_{D=1}$	0.016	0.015
Powered exponential$\|_{D=1.95}$	0.026	0.020
Matérn$\|_{D=1}$	0.028	0.021
Matérn$\|_{D=0.5}$	0.030	0.025
Cauchy$\|_{D=1;H=0.7}$	0.033	0.025
Cauchy$\|_{D=1;H=0.95}$	0.039	0.027

TABLE 5.4: Example 1: COV values of the redundant force X for $L = 10$ and for $L = 20$.

Class	COV $= \sigma/\mu$							
	$L = 10$				$L = 20$			
	$\bar{z} = 0.5$	$\bar{z} = 5$	$\bar{z} = 9.5$	$\bar{z} = 9.99$	$\bar{z} = 0.5$	$\bar{z} = 10$	$\bar{z} = 19.5$	$\bar{z} = 19.99$
Cauchy$\|_{D=1.95;H=0.5}$	0.008	0.013	0.018	0.034	0.009	0.011	0.010	0.098
Cauchy$\|_{D=1.95;H=0.85}$	0.085	0.085	0.098	0.132	0.001	0.081	0.058	0.146
Powered exponential$\|_{D=1}$	0.122	0.124	0.195	0.220	0.113	0.095	0.208	0.224
Powered exponential$\|_{D=1.95}$	0.124	0.126	0.204	0.218	0.116	0.096	0.226	0.250
Matérn$\|_{D=1}$	0.146	0.148	0.210	0.209	0.181	0.117	0.185	0.185
Matérn$\|_{D=0.5}$	0.159	0.161	0.205	0.199	0.169	0.128	0.228	0.192
Cauchy$\|_{D=1;H=0.7}$	0.199	0.197	0.203	0.221	0.145	0.173	0.230	0.220
Cauchy$\|_{D=1;H=0.95}$	0.239	0.234	0.242	0.240	0.236	0.233	0.246	0.266

TABLE 5.5: Example 1: COV values of the redundant force X for $L = 10$ and for $L = 20$.

To finish, about the second example of the redundant beam (Fig. 5.17), the same stochastic response quantities are shown. Fig. 5.22 reports the PDF of X for $L = 10$ (Fig. 5.22 (A)) and for $L = 20$ (Fig. 5.22 (B)) and the Table 5.6 shows the respective COV values. While Fig. 5.23 shows the PDF of the transversal displacement for different values of abscissa $\bar{z}$ when $L = 10$ and $L = 20$, respectively. Finally, the COV values of the latter transversal displacements are all listed in Table 5.7.

Class	COV $= \sigma/\mu$	
	$L = 10$	$L = 20$
Cauchy$\|_{D=1.95;H=0.5}$	0.004	0.003
Cauchy$\|_{D=1.95;H=0.85}$	0.025	0.024
Powered exponential$\|_{D=1}$	0.085	0.065
Powered exponential$\|_{D=1.95}$	0.087	0.064
Matérn$\|_{D=1}$	0.102	0.081
Matérn$\|_{D=0.5}$	0.110	0.090
Cauchy$\|_{D=1;H=0.7}$	0.106	0.091
Cauchy$\|_{D=1;H=0.95}$	0.055	0.057

TABLE 5.6: Example 2: COV values of the redundant force X for $L = 10$ and for $L = 20$.

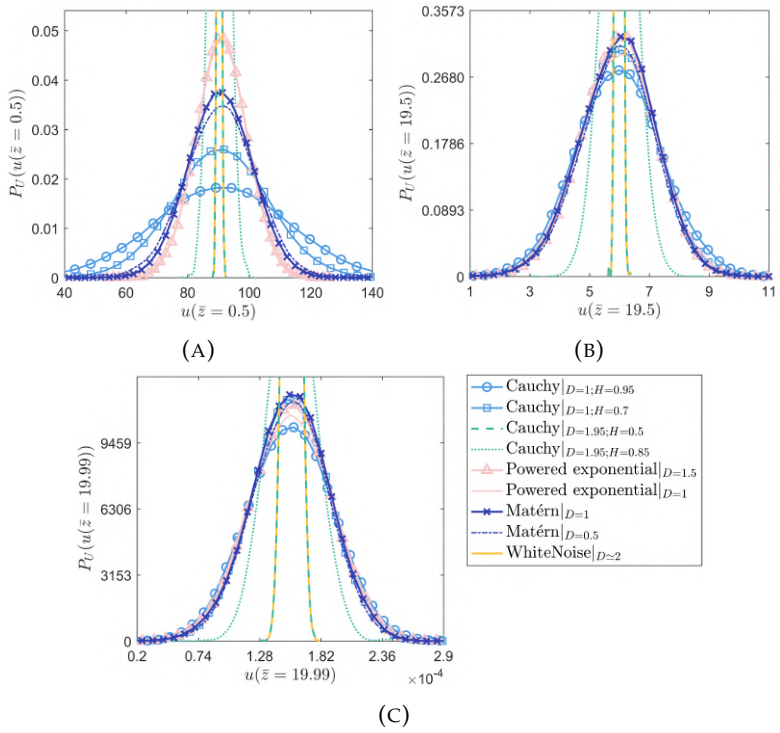

(A) (B) (C)

FIGURE 5.21: Example 1: PDF of the transversal displacement for $L = 20$: (A) $\bar{z} = 0.5$; (B) $\bar{z} = 9.5$; (C) $\bar{z} = 9.99$.

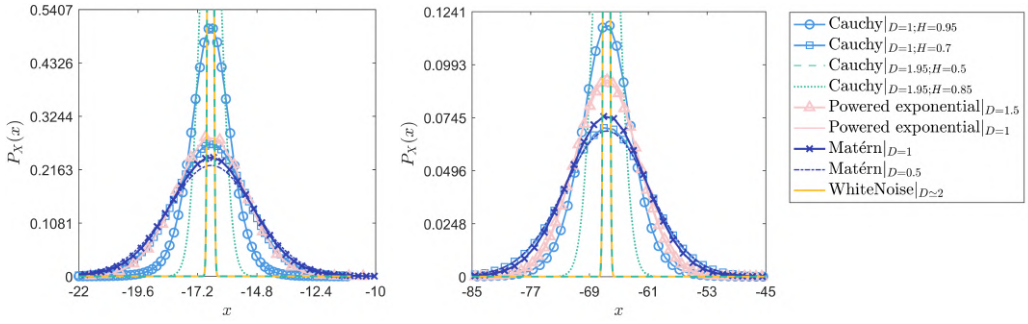

(A) (B)

FIGURE 5.22: Example 2: PDF of the redundant force X: (A) $L = 10$; (B) $L = 20$.

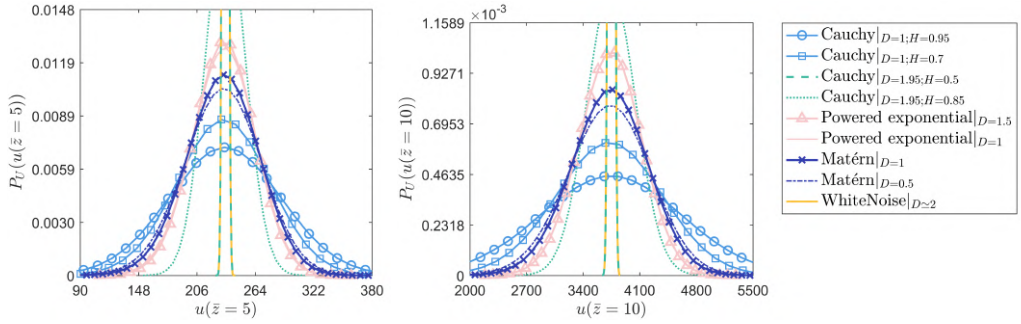

(A) (B)

FIGURE 5.23: Example 2: PDF of the transversal displacement $u(\bar{z}) = L/2$: (a) $L = 10$; (b) $L = 20$.

Class	COV $= \sigma/\mu$	
	$L = 10$	$L = 20$
	$\bar{z} = 5$	$\bar{z} = 10$
Cauchy$\|_{D=1.95;H=0.5}$	0.010	0.013
Cauchy$\|_{D=1.95;H=0.85}$	0.078	0.082
Powered exponential$\|_{D=1}$	0.133	0.105
Powered exponential$\|_{D=1.95}$	0.137	0.106
Matérn$\|_{D=1}$	0.156	0.127
Matérn$\|_{D=0.5}$	0.168	0.140
Cauchy$\|_{D=1;H=0.7}$	0.198	0.177
Cauchy$\|_{D=1;H=0.95}$	0.241	0.235

TABLE 5.7: Example 2: COV values of transversal displacement $u(\bar{z}) = L/2$.

5.3.4 Comments on the results

By the analysis of the results of the previous section, the following conclusions can be drawn:

- About the statically determinate stochastic beams, all the output values of the displacement COV of the beams under examination are bounded in a lower and upper bound limit. We obtain the upper limit, i.e. the maximum value of the displacement COV, when the Gaussian RF $D(z)$ follows the Cauchy class characterized by a low value of local randomness $(D = 1)$ but at the same time with a high value of non-local randomness $(H = 0.95)$. On contrary, a lower bound limit can be appreciated when $D(z)$ is modeled as a RF totally uncorrelated (White Noise correlation function) with fractal dimension $D = 2$. Analogous results are obtained in the case of the Cauchy class with $D = 1.95$ and $H = 0.5$. Another relevant result about the trend of the displacement variances related to the Cauchy class is that, for fixed values of D, the response variance increases when H increases. Finally, about the response variance, for the Powered exponential and Matérn classes of correlation, no significant difference has been revealed, and the concerning results are confined between the above cited lower and upper bound limits.

- Regarding the statically redundant stochastic beams, comparing the results of the transversal displacement at $\bar{z} = L/2$ with the results of the statically determinate examples, it seems that the trend is similar, that is to say, it can be observed an upper bound limit for a high value of non-local randomness of $D(z)$ and a lower bound limit as the local randomness characteristic increases. However, the same conclusion cannot be made if the redundant force is analyzed. Although for the assumption of RF totally uncorrelated a relatively low value of COV can be observed, for other laws of $\sigma_D^2(|z_1 - z_2|)$, the trend of the results seems to invert. More dispersed PDFs are obtained for the RF classes that capture only the fractal dimension, i.e. the local randomness. Furthermore, with a focus on the output for the Cauchy class, the variance value of the redundant force increases as the non-local effect (H) decreases. From this last observation, it seems that, in contrast to the response displacement quantity, which is more sensitive to the non-local randomness of $D(z)$, the stochastic internal force response is more sensitive to the local randomness effect. In order to gain a deeper insight into the effect of the level of randomness

on the type of stochastic response examined, the investigations of the sensitivity of the transversal displacement for different values of abscissa $\bar{z}$ have been evaluated. It can be appreciated how the tendency of sensitivity to the non-local randomness of the transversal displacement decreases when an abscissa value away from the centre of the beam is chosen, so approaching to a major sensitivity to the local randomness, as the redundant force. About this last investigation, the second example of the redundant beam considered shows the same results.

5.3.5 Some remarks

In this work, a study on the sensitivity of some random response quantities of stochastic beams to the local and non-local randomness of their mechanical properties of deformability (or stiffness) has been conducted. In particular, it has been shown the existence of a relationship between the concept of local and non-local constitutive laws in the Eringen mechanical theory integral constitutive and the concept of local and non-local randomness in the RF describing the deformability of the stochastic uncertain beams. In fact, the role of the kernel function, in the Eringen theory, is played by the correlation function of the homogeneous RF considered in the stochastic beams. The level of the response randomness has been related to the shape of the corresponding PDFs and the values of COVs of the transversal displacements, together with the COVs of the shear internal force and of the bending moment, when the statically redundant beams have been examined. From the analysis of the PDFs and the COV values of the response quantities the following conclusions can be underlined: a) for both statically determinate and redundant beams, the stochastic displacements are characterized by COVs which are well ordered, in the sense that the largest COV is related to the RF having the highest values of non-local randomness quantities, while the smallest COV corresponds to the case in which the RF is practically uncorrelated; b) by using the properties of the Cauchy correlation function, referring always the displacement response, when the coefficient H increases, for fixed value of D, the response PDFs are more and more dispersed (that is the corresponding COVs are higher and higher); c) an opposite trend has been observed about the redundant force, that is greater values of COV have been obtained for the RF classes that capture only the fractal dimension. For the Cauchy correlation function, the COV values of the random redundant force increase when the non-local parameter H decreases; d) the level of sensitivity to the non-local randomness of the transversal displacement depends on choice of the position . In particular, the randomness level of the transversal displacement is greater in the midpoint of the beam for RF having non-local randomness, while, away from the midpoint, the randomness level of the transversal displacement decreases and it is more affected by the local RFs. Definitively, it can be affirmed that the randomness level of both cinematic beam response and, for statically redundant beams, static response are strongly affected by the type of correlation function characterizing the RF of the beam deformability. In particular, it is very important to know if this RF has local or non-local properties.

5.4 Empirical velocity spectra with fractal and long-memory effects

The objective of the present study is to develop models of turbulent atmospheric velocity fields with fractal and Hurst properties motivated by (i) the growing literature on the study of natural phenomena characterized by these properties, and (ii) the need to introduce more realistic inputs into dynamic models (Shen, Ostoja-Starzewski, and Porcu, 2015a).

Although, this work doesn't see the application of the PTM, it is believed that its contents enrich the topic of the local and nonlocal randomness addressed in this Chapter.

While the widely-used formulations have been crucial in the understanding and quantitative description of a wide range of environmental and engineering processes across scales, they lack the ability to generate realizations of velocity fields having fractal and long-term spatial (or temporal) memory or Hurst characteristics. As it was described the previous section, D and H effects depend on the second-order properties of a given Gaussian stochastic process.
Taking into account the background concepts on covariance functions reported in section 3.5.1, the two covariance models for random fields (RFs) that decouple the fractal dimension from the Hurst effects are shown below. The Generalized Cauchy covariance function (Matthies et al., 1997b) is defined as

$$C_C(h) = (1 + h^\alpha)^{-\beta/\alpha}, \quad h \geq 0;\ 0 < \alpha \leq 2,\ \beta > 0, \tag{5.52}$$

whereas the Dagum covariance function is defined as

$$C_D(h) = 1 - \left(1 + h^{-\beta}\right)^{-\alpha/\beta}, \quad h \geq 0; \quad 0 < \alpha < 1, \quad 0 < \beta \leq 1.$$

According to Berg *et al* (Berg, Mateu, and Porcu, 2008), D and H of a stationary Gaussian process can be described through the behavior of their correlation function, $C_X(h)$, with the following results for the limiting cases of $h \to 0$ and $h \to \infty$:

Theorem 5.4.1 *If there exists $\alpha \in (0, 2]$, such that, when $h \to 0$,*

$$1 - C_X(h) \sim h^\alpha, \tag{5.53}$$

then a realization of the random field X has a fractal dimension

$$D = d + 1 - \frac{\alpha}{2}, \tag{5.54}$$

with probability 1.

Theorem 5.4.2 *If there exists $\beta \in (0, 1)$, such that, when $h \to \infty$,*

$$C_X(h) \sim h^{-\beta}, \tag{5.55}$$

then the field X is said to have long-memory with a Hurst exponent

$$H = 1 - \frac{\beta}{2}. \tag{5.56}$$

5.4.1 Asymptotic behavior of the covariance function for processes with long-range dependence

5.4.1.1 Basic concepts

Over the past decades, the phenomenon of the long-range dependence in stochastic processes has been defined through the second-order properties. For completeness, some preliminary concepts are report. If C is symmetric, then $C(\tau) = C_X(h)$, for $h = |\tau|$. Clearly, this is a special case of isotropy in $\mathbb{R}^d$ as discussed in the above, when $d = 1$. Through the Fourier transform of the autocovariance function, the spectral density function is defined as:

$$S_X(\omega) = \frac{1}{\pi}\int_0^{+\infty} C_X(h)\, cos(\omega h)\mathrm{d}h, \quad h \geq 0, \quad ! \geq 0, \tag{5.57}$$

where ω is in the frequency domain. In general, a discrete-time stationary stochastic process $X(t)$, with finite variance is said to have a long-memory if its covariance

$$C_X(h) \sim c_\rho h^{-\beta}, \tag{5.58}$$

tends to zero hyperbolically, for $0 < \beta < 1$ and for finite $c_\rho \neq 0$. A consequence of the slow decay of a long-memory process is that the sum of covariance diverges:

$$\sum_{h=0}^{+\infty} |C_X(h)| = \infty. \tag{5.59}$$

The dependence of events that are far apart diminishes very slowly with increasing distance, implying that they are not summable. Because of the Tauberian and Abelian theorems (Stein, 1999), the long/short-range dependence can also be defined in terms of local behavior of the spectral density at the origin. This is equivalent to having an unbounded spectral density at the origin. This implies:

$$S_X(\omega) \sim c_s \omega^{\beta-1}, \quad \omega \to 0 \tag{5.60}$$

where $c_s > 0$ is a positive constant. Thus for $\beta < 1$, $S_X(\omega) \to \infty$ as $\omega \to 0$.
In contrast, a weakly dependent or short-memory process has a summable covariance that often tends to zero exponentially, and a continuous and bounded spectral density (Giraitis, Koul, and Surgailis, 2012). In long-memory processes, the dependence of two observations at different times is persistent, i.e. is non-negligible. In comparison, for weakly dependent processes, observations distant from each other are approximately uncorrelated.

5.4.1.2 On the absence of long-memory in classical probabilistic models of velocity spectrum

Here, it is explored the behavior of the autocorrelation functions of the classic von Kármán and Kaimal models (Giraitis, Koul, and Surgailis, 2012). The von Kármán spectral density of the longitudinal velocity component u is

$$S_u(\omega) = \frac{4L_u\sigma_u^2}{\bar{u}}\left[1 + 70.8\left(\frac{L_u\omega}{\bar{u}}\right)^2\right]^{5/6}. \tag{5.61}$$

Here, L_u is the turbulence length scale of the longitudinal velocity component, $\bar{u}$ is the mean velocity and σ_u is the associated standard deviation. From Eq. 5.61, the spectral density of the longitudinal component follows the simplified form:

$$S_{VK}(\omega) = \left(1 + (c\omega)^2\right)^{-5/6}, \quad c > 0. \tag{5.62}$$

Taking the inverse Fourier transform yields the autocorrelation function

$$C_{VK}(h) = \frac{\sqrt{3}\Gamma\left(\frac{2}{3}\right)\sqrt[3]{h}\mathcal{K}_{-1/3}\left(\frac{h}{c}\right)}{\sqrt[3]{2}\pi\sqrt[3]{c}}, \quad c > 0, \quad h \geq 0, \tag{5.63}$$

where $\mathcal{K}_n(z)$ is the modified Bessel function of the second kind of order n, also called Macdonald function. It can be proved that

$$\lim_{h\to 0}\left(1 - C_{VK}(h)\right)h^{-2/3} = -\frac{\Gamma\left(-\frac{1}{3}\right)}{(2c)^{2/3}\Gamma\left(\frac{1}{3}\right)}. \tag{5.64}$$

Therefore, according to Theorem 5.4.1, the associated process has fractal dimension $D = 2 - \alpha/2 = 5/3$. Also,

$$\lim_{h\to\,\infty}\frac{\log(C_{VK}(h))}{h} = -\frac{1}{c}, \tag{5.65}$$

i.e.,

$$C_{VK}(h) \sim e^{-\frac{h}{c}}, \quad h \to \infty. \tag{5.66}$$

Therefore, the autocorrelation function decays exponentially, which does not fall into the case described by Theorem 5.4.2; *i.e.*, the random process does not have long-memory. Indeed, the von Kármán autocorrelation function in Eq. 5.63 is nothing nothing more than a special case of the Matérn covariance class (Stein, 1999), which describes stochastic processes having only the fractal dimension characteristic.

The Kaimal spectral density of the longitudinal velocity component u is

$$S_u(\omega) = \frac{6.8L_u\sigma_u^2}{\bar{u}}\left[1 + 1.5\times\ 6.8\frac{L_u\omega}{\bar{u}}\right]^{-5/3}. \tag{5.67}$$

Therefore, the spectrum has the form

$$S_K(\omega) = \frac{1}{(c\omega + 1)^{5/3}}, \quad c > 0. \tag{5.68}$$

Taking the inverse Fourier transform, the autocorrelation function is obtained as

$$C_K(h) = {}_1F_2\left(1; \frac{1}{6}, \frac{2}{3}; -\frac{h^2}{4c^2}\right) - 2\pi\, h^{\frac{2}{3}}\left(\sqrt{3}\cos\left(\frac{h}{c}\right) - 3\sin\left(\frac{h}{c}\right)\right),$$

where ${}_pF_q(a_1\cdots, a_p; b_1, \cdots, b_q; z)$ is the generalized Hypergeometric function. Thus,

$$\lim_{h\to\,0}(1 - C_K(h))h^{-2/3} = \frac{2\pi}{3\sqrt{3}c^{2/3}\Gamma(\frac{5}{3})}. \tag{5.69}$$

Again, this implies a fractal dimension of 5/3 according to Theorem 5.4.1. Also,

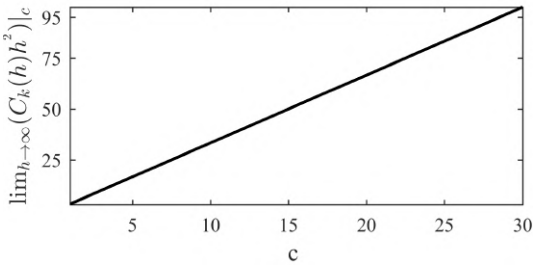

FIGURE 5.24: The asymptotic behavior of the Kaimal covariance for $c = 1, 2, \cdots, 30$.

Figure 5.24 shows the asymptotic behavior of the Kaimal covariance, *i.e.* the limit $\lim_{h\to\infty} C_K(h)h^2\ |_c$ for $c \in [1, 30)$. Therefore, it is plausible that

$$\lim_{h\to\infty} C_K(h)h^2 = const \in (0, \infty). \tag{5.70}$$

Again, this indicates that the covariance decays slower than what is described by Theorem 5.4.2, *i.e.*, the random process does not have long-memory effects.

5.4.2 Generalized Cauchy model and Dagum models

Now, we focus on two models with long-memory effects, and take the variance of the RF $X(x)$ to be $\sigma_X^2 = 1$.

5.4.2.1 Modified Generalized Cauchy

Let us define the class Φ_d of continuous function $f : (0, \infty) \to \mathbb{R}$ such that $f(0) = 1$ and $f(\|\cdot\|)$ is positive definite in $\mathbb{R}^d$. Also, we define $\Phi_\infty := \bigcap_{d\geq 1} \Phi_d$. The Generalized Cauchy (GC) class C_C, defined in (Daley and Porcu, 2014), is a member of the class Φ_∞, provided $\alpha \in (0, 2]$ and $\beta > 0$. The parameter α is crucial for the differentiability at the origin and, as a consequence, for the degree of mean-square differentiability of the associated sample paths. Specifically, they are infinitely differentiable when $\alpha = 2$. The GC family represents a breaking point with respect to earlier literature based on the assumption of self-similarity, since it decouples the fractal dimension and the Hurst effect. The next result follows from Lim and Teo (Lim and Teo, 2009) and describes the spectral density of the GC covariance function.

Let C_C be the Cauchy covariance function defined by Eq. 5.52. Then, for $\beta > 0$ and $\alpha \in (0, 2)$, the Fourier transform in $\mathbb{R}^d$ of C_C is identically equal to

$$S_C(\omega; \boldsymbol{\theta}) = -\frac{\omega^{-d}}{2^{d/2-1}\pi^{d/2+1}} \times \Im\left(\int_0^\infty \frac{\mathcal{K}_\nu(h)}{(1 + e^{i\frac{\pi\alpha}{2}}(h/\omega)^\alpha)^{\beta/\alpha}} h^{d/2} \mathrm{d}h\right), \quad \omega \geq 0,$$

where $\Im$ denotes the imaginary part of a complex argument, $\nu = (d-2)/2$ and $\boldsymbol{\theta} = (\alpha, \beta)$.

Let $C(\cdot; \boldsymbol{\theta})$, the Modified Generalized Cauchy covariance function, defined as:

$$C_{MC}(h; \boldsymbol{\theta}) = (1 + h^\alpha)^{-\beta/\alpha - 1}(1 + (1 - \beta)h^\alpha), \quad h \geq 0, \tag{5.71}$$

with $\boldsymbol{\theta} = (\alpha, \beta) \in (0,2] \times (0,\infty)$. The spectral density of this kind of covariance family can be written according to the following result, that is new.

Theorem 5.4.3 *For $\alpha \in (0,2)$ and $\beta > 0$, we have*

$$S_{MC}(\omega) = \frac{\omega^{-\nu}}{2^{\nu}\pi^{\nu+2}} \Im\left(\int_0^{\infty} \mathcal{K}_{\nu}(\omega h) h^{\nu+1} \frac{1 + (1-\beta)e^{i\pi\alpha/2}h^{\alpha}}{(1 + e^{i\frac{\pi\alpha}{2}}h^{\alpha})^{\beta/\alpha} + 1} \mathrm{d}h \right), \quad \omega > 0,$$

where $\nu = -1/2$.

Proof. Let $\omega = |\varpi|$ with $\varpi \in \mathbb{R}$. We proceed by direct construction:

$$\begin{aligned} S_{MC}(\omega) &= \frac{1}{2\pi} \int_{\mathbb{R}} e^{-i\varpi h} C_{MC}(h) \mathrm{d}h \\ &= \frac{1}{2\pi} \int_{\mathbb{R}} e^{-i\varpi h} (1-\beta) \left(1 + h^{\alpha}\right)^{-\beta/\alpha} \mathrm{d}h + \frac{1}{2\pi} \int_{\mathbb{R}} e^{-i\varpi h} \beta \left(1 + h^{\alpha}\right)^{-\beta/\alpha - 1} \mathrm{d}h \\ &= (1-\beta)\frac{1}{2\pi} \int_{\mathbb{R}} e^{-i\varpi h} \left(1 + h^{\alpha}\right)^{-\beta/\alpha} \mathrm{d}h + \beta \frac{1}{2\pi} \int_{\mathbb{R}} e^{-i\varpi h} \left(1 + h^{\alpha}\right)^{-\beta/\alpha - 1} \mathrm{d}h \\ &= (1-\beta) S_C(\omega; \boldsymbol{\theta}) + \beta S_C(\boldsymbol{\omega}; \boldsymbol{\theta}_1) \end{aligned}$$

where $\boldsymbol{\theta}_1 = (\alpha, \beta + \alpha)$. Applying Theorem 1 of (Bevilacqua and Faouzi, 2019), we have

$$S_{MC}(\omega) = \frac{\omega^{-\nu}}{2^{\nu}\pi^{\nu+2}} \times \Im\left(\int_0^{\infty} \mathcal{K}_{\nu}(\omega h) h^{\nu+1} \frac{1 + (1-\beta)e^{i\pi\alpha/2}h^{\alpha}}{(1 + e^{i\frac{\pi\alpha}{2}}h^{\alpha})^{\beta/\alpha} + 1} \mathrm{d}h \right).$$

Next, have been applied the Proposition 3.3 from Lim and Teo (Lim and Teo, 2009) to study the low frequency limit of the spectral density of $S_{MC}(\omega)$.

Theorem 5.4.4 *For $\alpha \in (0,2)$ and $\beta > 0$, the low frequency limit of the spectral density $S_{MC}(\omega)$ is given by*

1. $S_{MC}(\omega) \sim \frac{(1-\beta)\omega^{\beta-1}\Gamma(\frac{1-\beta}{2})}{2^{\beta}\pi^{1/2}\Gamma(\beta/2)} + \beta\frac{\omega^{\beta+\alpha-1}\Gamma(\frac{1-\beta-\alpha}{2})}{2^{\beta+\alpha}\pi^{1/2}\Gamma(\frac{\beta+\alpha}{2})}$, *if* $\beta + \alpha < 1$;
2. $S_{MC}(\omega) \sim \frac{(1-\beta)}{\pi}\left(\log(\frac{1}{\omega}) - \frac{\beta}{\alpha}(\psi(\beta/\alpha) + \gamma) + \log(2) - \frac{1}{2}(\gamma - \psi(1/2))\right) + \frac{\beta\Gamma(1/\alpha)\Gamma(\frac{\beta+\alpha-1}{\alpha})}{\pi\alpha\Gamma(\frac{\beta+\alpha}{\alpha})}$, *if* $\beta = 1$.
3. $S_{MC}(\omega) \sim \frac{(1-\beta)\omega^{\beta-1}\Gamma(\frac{1-\beta}{2})}{2^{\beta}\pi^{1/2}\Gamma(\beta/2)} + \frac{\beta}{\pi}\left(\log(\frac{1}{\omega}) - \frac{\beta+\alpha}{\alpha}(\psi(\frac{\beta+\alpha}{\alpha}) + \gamma) + \log(2) - \frac{1}{2}(\gamma - \psi(1/2))\right)$, *if* $\beta + \alpha = 1$,
4. $S_{MC}(\omega) \sim \frac{(1-\beta)\Gamma(1/\alpha)\Gamma(\frac{\beta-1}{\alpha})}{\pi\alpha\Gamma(\frac{\beta}{\alpha})} + \frac{\beta\Gamma(1/\alpha)\Gamma(\frac{\beta+\alpha-1}{\alpha})}{\pi\alpha\Gamma(\frac{\beta+\alpha}{\alpha})}$, *if* $\beta > 1$,

where γ is Euler's constant and $\psi(z) = \frac{\Gamma(z)'}{\Gamma(z)}$.

Lim and Teo (Lim and Teo, 2009) provide an expression of the spectral density of the Generalized Cauchy covariance functions.

Theorem 5.4.5 *Let C_C be the Generalized Cauchy covariance function as defined in Eq. 5.71. Let $\alpha = a/b$ and $\beta = e/f > 0$ be rational numbers with the greatest common divisor $gcd(a,b) = gcd(e,f) = 1$. If one of the following conditions hold:*

1. *a is not divisible by f,*
2. *d is an odd integer and e/f is an even integer,*

3. *d is an even integer, a and f are both even integers and a/f is an odd integer,*

then, $S_C(\omega)$ can be represented by:

$$S_C(\omega) = \frac{\omega^{-1}}{\pi^{3/2}} \frac{1}{\Gamma(\beta/\alpha)} \times \sum_{n=0}^{\infty} \frac{(-1)^n}{n!} \frac{\Gamma(\beta/\alpha + n)\Gamma(1/2 - (\beta + n\alpha)/2)}{\Gamma((\beta + n\alpha)/2)} \left(\frac{\omega}{2}\right)^{\beta+n\alpha} + \frac{\omega^{-1}}{\pi^{3/2}} \frac{1}{\Gamma(\beta/\alpha)} \times \sum_{n=0}^{\infty} \frac{(-1)^n}{n!} \frac{\Gamma\left(\frac{2n+1}{\alpha}\right)\Gamma\left(\frac{\beta-2n-1}{\alpha}\right)}{\Gamma(n+1/2)} \left(\frac{\omega}{2}\right)^{2n+1},$$

with $\omega > 0$, where $\alpha \in (0, 2]$ and $\beta > 0$.

Applying Theorem 5.4.5, we obtain another representation of our spectral density S_{MC}.

Theorem 5.4.6 *Let C_{MC} be the Modified Generalized Cauchy covariance function as defined in Eq. 5.71. Let $\alpha = a/b$ and $\beta = e/f > 0$ be rational numbers with the greatest common divisor $gcd(a, b) = gcd(e, f) = gcd(af + be, bf) = 1$. If one of the following conditions hold:*

1. *a is not divisible by f,*
2. *e/f and $(af + be)/(bf)$ are an even integers,*

$$\begin{aligned} S_{MC}(\omega) = {} & \frac{\omega^{-1}}{\pi^{3/2}} \frac{(1-\beta)}{\Gamma(\beta/\alpha)} \times \sum_{n=0}^{\infty} \frac{(-1)^n}{n!} \frac{\Gamma(\beta/\alpha + n)\Gamma(1/2 - (\beta + n\alpha)/2)}{\Gamma((\beta + n\alpha)/2)} \left(\frac{\omega}{2}\right)^{\beta+n\alpha} \\ & + \frac{\omega^{-1}}{\pi^{3/2}} \frac{(1-\beta)}{\Gamma(\beta/\alpha)} \times \sum_{n=0}^{\infty} \frac{(-1)^n}{n!} \frac{\Gamma\left(\frac{2n+1}{\alpha}\right)\Gamma\left(\frac{\beta-2n-1}{\alpha}\right)}{\Gamma(n+1/2)} \left(\frac{\omega}{2}\right)^{2n+1} \\ & + \frac{\omega^{-1}}{\pi^{3/2}} \frac{\beta}{\Gamma(\beta/\alpha + 1)} \times \sum_{n=0}^{\infty} \frac{(-1)^n}{n!} \frac{\Gamma\left(\frac{\beta}{\alpha} + 1 + n\right)\Gamma\left(1/2 - \frac{\beta+(n+1)\alpha}{2}\right)}{2^{\beta+(n+1)\alpha}\Gamma\left(\frac{\beta+(n+1)\alpha}{2}\right)\omega^{-\beta-(n+1)\alpha}} \\ & + \frac{\omega^{-1}}{\pi^{3/2}} \frac{\beta}{\Gamma(\frac{\beta}{\alpha} + 1)} \times \sum_{n=0}^{\infty} \frac{(-1)^n}{n!} \frac{\Gamma\left(\frac{2n+1}{\alpha}\right)\Gamma\left(\frac{\beta+\alpha-2n-1}{\alpha}\right)}{\Gamma(n+1/2)} \left(\frac{\omega}{2}\right)^{2n+1}, \end{aligned}$$

with $\omega > 0$, where $\alpha \in (0, 2]$ and $\beta > 0$.
The proof comes as a corollary of Theorems 5.4.3 and 5.4.5.

5.4.2.2 Dagum

Let C_D be the Dagum covariance function defined by Eq. 5.53. Berg *et al.* (Berg, Mateu, and Porcu, 2008) have shown that $C_D(h) = 1 - (h^\alpha/(1 + h^\alpha))^\beta$ belongs to Φ_∞ if $\beta\alpha \leq 2$ and $\alpha \leq 2$. However, in our case, the Dagum covariance function is defined on the real line.

Theorem 5.4.7 *For $\beta \in \mathbb{N}$, $\beta\alpha \leq 2$ and $\alpha \leq 2$, we have*

$$S_D(\omega) = \sum_{k=0}^{n-1} (-1)^{n-k} C_k^n \frac{\omega^{-\nu}}{2^\nu \pi^{d/2+1}} \Im\left(\int_0^\infty \mathcal{K}_\nu(\omega u) h^{d/2} \frac{1}{(1 + e^{i\pi\alpha/2} h^\alpha)^{n-k}} \mathrm{d}h\right).$$

Proof. Let $\omega = |\varpi|$ with $\varpi \in \mathbb{R}$. Then,

$$S_D(\omega) = \frac{1}{(2\pi)^d}\int_{\mathbb{R}^d} e^{-i\varpi} C_D(h)\mathrm{d}^d h = \frac{1}{(2\pi)^d}\int_{\mathbb{R}^d} e^{-ih\varpi}\left(1-\left(\frac{h^\alpha}{1+h^\alpha}\right)^\beta\right)\mathrm{d}^d h$$
$$= \frac{1}{(2\pi)^d}\sum_{k=0}^{n-1}(-1)^{n-k}C_k^n\int_{\mathbb{R}^d} e^{-i\ h\varpi}\frac{1}{(1+h^\alpha)^{n-k}}\mathrm{d}^d h,$$

where C_k^n is a number of possible combinations of k objects from a set of n objects. From Eq. 5.71, we obtain,

$$S_D(\omega) = \sum_{k=0}^{n-1}(-1)^{n-k}C_k^n\ S_C(\omega;\alpha,n-k).$$

5.4.3 Long-memory effects in time series

Since in a long-memory RF (or random process) the dependence between two instants is persistent, i.e., not independent, it is worth inspecting here the assumption of ergodicity in the estimation of temporal statistics. To that end, this problem, we first show basic concepts of the ergodicity theory; we then use simulated data to examine the ergodic assumption for stochastic processes with short- and long-memory characteristics.

5.4.4 Ergodicity

As is often the case in practice, the determination of probabilistic characteristics (e.g., moments, distributions) of a RF is obtained from the study of a single realization $X(\omega)$ related by sample events ω of the Ω space. An intuitive explanation of such an approach lies in the possibility of treating the realization $X(\omega)$ at hand as a representation of the RF X, which is the ergodic property or ergodicity.

Recall that a process is *mean-ergodic* if any realization $X(\omega)$, $\omega \in \Omega$, is sufficient to get the ensemble average $\langle X(t)\rangle$ at any t from its time average $\overline{X(\omega)}$ for any $\omega \in \Omega$ taken over a sufficiently large interval:

$$\overline{X(\omega)} \equiv \lim_{T\to\infty}\frac{1}{2T}\int_{-T}^{T} X(\omega,t)\,dt = \int_\Omega X(\omega,t)\,dP(\omega) \equiv \langle X(t)\rangle.$$

In practice, the time integration in Eq. 5.72, $\overline{X(\omega)}$ must be replaced by the time average of a finite number N of sampling points (taken over one realization ω) (Ostoja-Starzewski, 2007), *i.e.*,

$$\overline{X(\omega)} \equiv \frac{1}{N}\sum_{n=1}^{N} X(\omega,t_n). \tag{5.72}$$

And $\langle X(t)\rangle$ must be computed from the ensemble average over a finite number M of realizations ω (taken at a chosen sampling time point t), *i.e.*,

$$\langle X(t)\rangle \equiv \frac{1}{M}\sum_{m=1}^{M} X(\omega_m,t). \tag{5.73}$$

The conditions for Eq. 5.72 to hold are provided by the so-called ergodic theorems. Slutsky's theorem (Papoulis and Pillai, 2001). A stationary process $X(t)$ is mean-ergodic if its autocovariance is such that

$$\lim_{T\to\infty}\frac{1}{T}\int_0^T C(h)\,dh \cong \lim_{T\to\infty}\frac{1}{T}\sum_{h=0}^{T} C(h) = 0. \tag{5.74}$$

Sufficient conditions
(i) If

$$\int_0^\infty C(h)\,dh \cong \sum_{h=0}^{\infty}|C(h)| < \infty, \tag{5.75}$$

then, Eq. 5.74 holds; hence the process $X(t)$ is mean-ergodic if the autocovariance function is absolutely summable.
(ii) If

$$\lim_{h\to\infty} C(h) = 0, \tag{5.76}$$

then $X(t)$ is mean-ergodic. In Eqs. 5.74 and 5.75 we show the cases pertaining to continuous and discrete times.
Next, it is possible to extend the properties of ergodicity to the covariance function. A process is *covariance-ergodic* if, independently of the particular sample function,

$$\begin{aligned}\overline{R_X(\omega,t)} &\equiv \lim_{T\to\infty}\frac{1}{2T}\int_{-T}^{T} X(\omega,t_1+t)\,X(\omega,t_1)\,dt_1 r = \int_\Omega X(\omega,t_1+t)\,X(\omega,t_1)\,dP(\omega)\,r \\ &\equiv \langle X(\omega,t_1+t)\,X(\omega,t_1)\rangle,\end{aligned} \tag{5.77}$$

i.e., the temporal covariance function of the process is equal to the ensemble covariance function of any realization. The property of covariance-ergodicity is important because it first allows the derivation of the covariance of the process from a single sample function, and then the determination of the power spectrum of the process. Moreover, Slutsky's theorem implies that the ergodic hypothesis is appropriate if the two random variables $X(t+h)$ and $X(h)$ are almost uncorrelated for large h, or, if taken sufficiently far apart, they are almost independently distributed.

Therefore, the covariance function plays a key role in the ergodic assumption and it is also associated with the definition of long-memory processes, in which a non-negligible persistent correlation may occur. Using simulation data, we investigate in the following whether the ergodic assumption is consistent with the long-memory definition. We present a non-ergodic analysis, i.e. the statistics of the time series are measured across an ensemble of M independent realizations instead of from a single realization.

5.4.5 Simulations

To illustrate the effect of the ergodic assumption on the correct estimation of the empirical covariance, and, consequently, on the empirical spectral density function, we perform a simulation of M-independent Gaussian time series, which are generated using (Schlather, 2015). In particular, $M = 500$ independent observations are generated, each characterized by $N = 2,000$ samples with a sampling frequency of 20 Hz.

We examine two cases characterized by short and long memories, respectively, with Cauchy (Eq. 5.52) and Dagum (Eq. 5.53) covariance functions. Regarding the

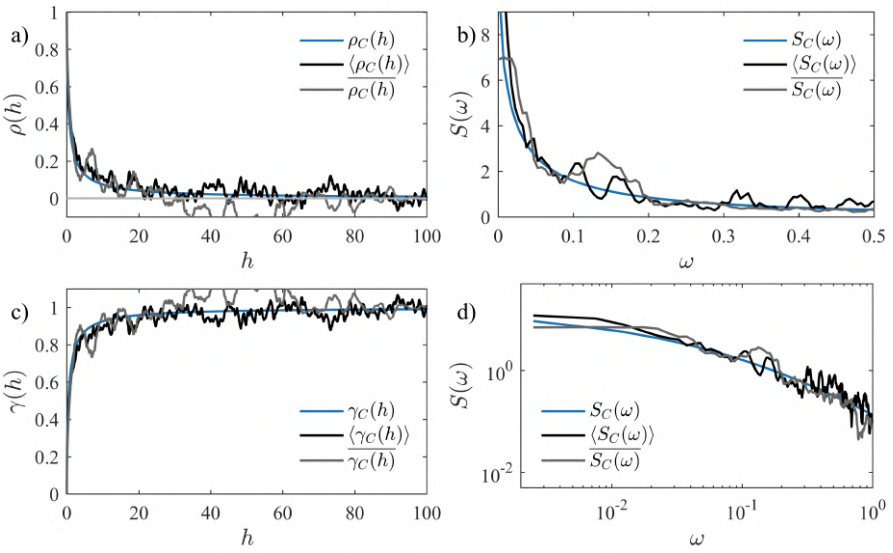

FIGURE 5.25: **a)** Correlogram; **b)** Spectral density; **c)** Variogram; **d)** Spectral density in log scale. Cauchy autocorrelation function: $\alpha = 2/3$ $(D = 5/3)$; $\beta = 1$ $(H = 0.5)$ (blue line), ensemble autocorrelation function (black line) and time autocorrelation function (grey line).

parameters in the Cauchy and Dagum expressions, in the spirit of generalized random processes consistent with the physical characteristics of the turbulence RF, the time series are generated with $\alpha = 2/3$ and different values of long-memory index, $\beta = 1$ $(H = 0.5)$, $\beta = 0.2$ $(H = 0.9)$ and $\beta = 0.32$ $(H = 0.84)$. The fractal index α is consistent with the Kolmogorov $-5/3$ spectrum so that we can interpret the fractal dimension as $D = 5/3$. The particular case of Hurst parameter $H = 0.5$ is chosen in order to investigate the short-memory scenario. The other two cases, $H = 0.9$ and $H = 0.84$, are close to the values of the Hurst parameter measured from the experimental data presented in the next section.

With the generated time series, the theoretical autocorrelation of each model is compared with the sample autocorrelation for one single realization (ergodic process hypothesis):

$$\overline{\rho\left(h\right)} = \frac{\sum_{n=1}^{N-h}\left(x\left(t_n\right)-\bar{x}\right)\left(x\left(t_n+h\right)-\bar{x}\right)}{\sum_{n=1}^{N}\left(x\left(t_n\right)-\bar{x}\right)^2} = \frac{C\left(h\right)}{C\left(0\right)}, \tag{5.78}$$

and then for the estimated autocorrelation over a finite number M of independent realizations (absence of ergodic process hypothesis):

$$\left\langle\rho\left(h\right)\right\rangle = \frac{\sum_{m=1}^{M-h}\left(x_m\left(t_1\right)-\left\langle x_m\left(t_1\right)\right\rangle\right)\left(x_m\left(t_1+h\right)-\left\langle x_m\left(t_1+h\right)\right\rangle\right)}{\sum_{m=1}^{M}\sqrt{\left\langle x_m\left(t_1\right)^2\right\rangle-\left\langle x_m\left(t_1\right)\right\rangle^2}\sqrt{\left\langle x_m\left(t_1+h\right)^2\right\rangle-\left\langle x_m\left(t_1+h\right)\right\rangle^2}} = \frac{\left\langle C\left(h\right)\right\rangle}{\left\langle C\left(0\right)\right\rangle}. \tag{5.79}$$

As additional second-order moment statistics, the variogram and the spectral density can be estimated as well either from one single realization (using the ergodic assumption), or from an ensemble of independent realizations (without the ergodic assumption). Specifically, we have variogram estimates

$$\overline{\gamma(h)} = \overline{C(0)} - \overline{C(h)} \tag{5.80}$$

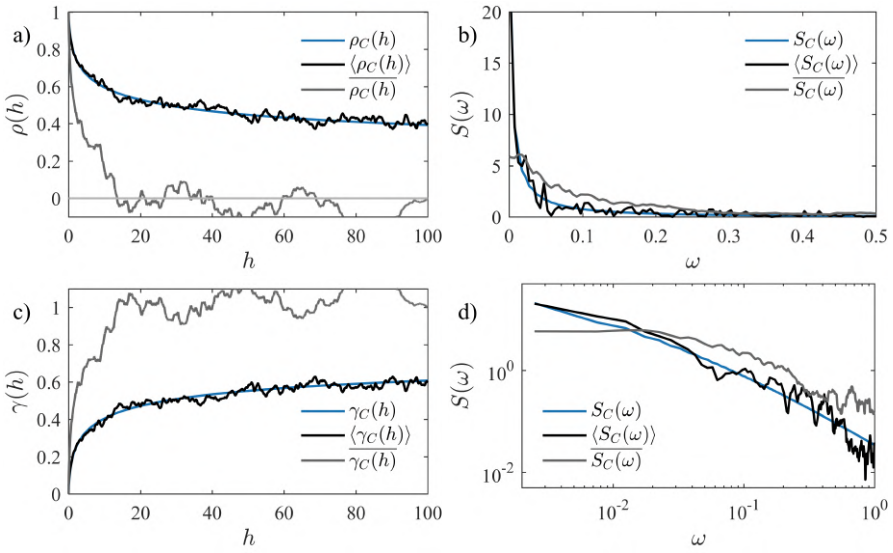

FIGURE 5.26: **a)** Correlogram; **b)** Spectral density; **c)** Variogram; **d)** Spectral density in log frequency domain. Cauchy autocorrelation function: $\alpha = 2/3$ $(D = 5/3)$; $\beta = 0.2$ $(H = 0.9)$ (blue line), ensemble autocorrelation function (black line) and time autocorrelation function (grey line).

and

$$\langle\gamma(h)\rangle = \langle C(0)\rangle - \langle C(h)\rangle. \tag{5.81}$$

Similarly, we can estimate $\overline{S(\omega)}$ and $\langle S(\omega)\rangle$ according to Eq. 5.57, by using $\overline{C(h)}$ and $\langle C(h)\rangle$, respectively.

In the short-memory case, the correlograms, variograms and power spectral densities estimated with and without the ergodic assumption are compared with the corresponding theoretical curves in Fig. 5.25. The autocorrelation function decays to zero quite quickly, while the spectrum has a small peak (the mean effect) at the zero frequency. The most relevant result of this example is that, for the simulated data with the Hurst parameter $H = 0.5$, the sample functions based on the ergodic assumption are in agreement with their theoretical counterparts. However, in the long-memory scenarios as demonstrated in Figs. 5.26 and 5.27 where the simulated data have $H = 0.9$ and $H = 0.8$, respectively, the sample functions evaluated on one single realization significantly deviate from the theoretical curves.

In contrast, the ensemble-based covariance functions provide a close fit of the theoretical autocorrelation functions and, consequently, also for the variogram functions and the power spectral density functions.

The results above clearly suggest that caution needs to be taken in the presence of data with long-memory, in that the ergodic assumption may lead to significant errors. Nevertheless, these results seem not far from the restrictions introduced by Slutsky's theorem on the definition of the ergodic process, indeed it seems to be a direct consequence. With long-memory effects, the correlation between the random variables at two distinct time instants, $X(t+h)$ and $X(h)$, cannot be considered negligible even for large a h. Consequently, in the presence of a strong long-memory, a non-ergodic analysis is more appropriate; a non-ergodic assumption must be evaluated in long-memory phenomena.

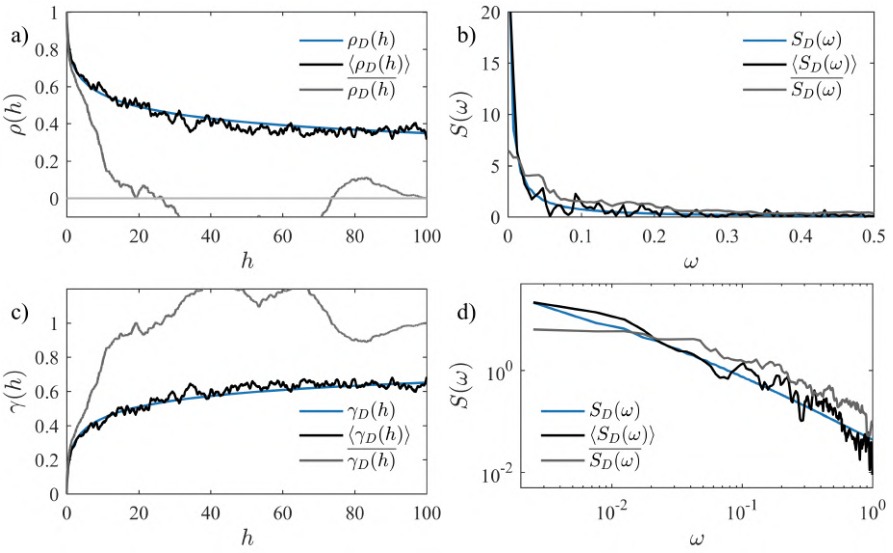

FIGURE 5.27: **a)** Correlogram; **b)** Spectral density; **c)** Variogram; **d)** Spectral density in log frequency domain. Dagum autocorrelation function: $\alpha = 2/3$ $(D = 5/3)$; $\beta = 0.32$ $(H = 0.84)$ (blue line), ensemble autocorrelation function (black line) and time autocorrelation function (grey line).

5.4.6 Field velocity data

We now explore field data from a meteoerological tower at a height of 79.1 m (see details in (Chamorro et al., 2015)). Motivated by the discussion in the previous section, the turbulence data observed in an interval $[X(t_0), X(t_{0+T})]$, obtained at $f = \omega/2\pi = 20$ Hz during 24 hours $(T = 24)$ are treated as a set of separate realizations observed in $M = 96$ intervals $[X(t_0), X(t_1)], [X(t_1), X(t_2)], ..., [X(t_{M-1}), X(t_{0+T})]$, of length $18,000$ s each. In this way we are able to investigate the long-memory properties of the wind data collected.

First, we compare the ensemble averaged autocorrelation function (of the streamwise velocity) with the time averaged autocorrelation functions based on individual intervals. Figure 5.28 shows the sample's autocorrelation and the corresponding spectral density evaluated for three different intervals taken individually, in particular the 30^{th}, 55^{th} and 90^{th} intervals of the 96, in comparison with the autocorrelation function estimated from all the 96 realizations. By inspection, Fig. 5.28(a) shows that each sample function, taken individually, is not representative of the ensemble that constitutes the random process. The spectral density of the experimental velocity data is computed with a discrete Fourier transform.

In order to fit the estimated autocorrelation and power spectrum functions, we utilize the generalized form of the original Cauchy autocorrelation function (Gneiting, 2000),

$$\rho_C(h) = \left(1 + \left|\frac{h}{c}\right|^{\alpha}\right)^{-\beta/\alpha}, \quad c > 0; \quad 0 < \alpha \leq 2, \quad \beta > 0,$$

where c is a scale parameter, α is a shape parameter (known as the fractal index) and β is a long-memory parameter. This class of RFs, referred to as the Cauchy family, allows for simultaneous modelling of the long-range dependence and correlations

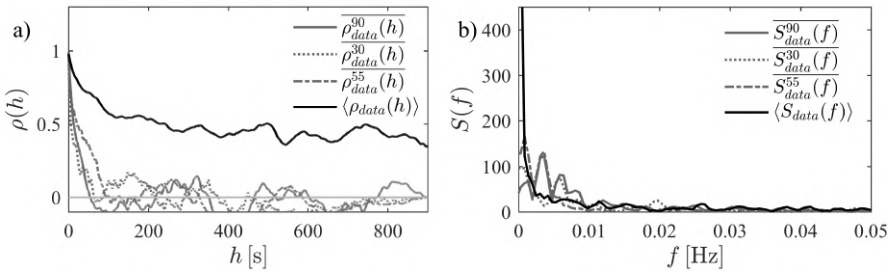

FIGURE 5.28: **a)** Correlogram and **b)** Spectral density of the atmospheric boundary layer data. Ensemble autocorrelation function (continuous black line), time autocorrelation function for the 30^{th} interval (dotted gray line), time autocorrelation function for the 55^{th} interval (dot-dashed gray line) and time autocorrelation function for the 90^{th} interval (continuous gray line).

at short and intermediate lags.

Similarly, the Modified Cauchy autocorrelation function (based on Gneiting and Schlather, 2004a) is generalized to

$$\rho_{MC}(h) = \left(1 + \left|\frac{h}{c}\right|^{\alpha}\right)^{-\beta/\alpha-1} \left(1 + (1-\beta)\left|\frac{h}{c}\right|^{\alpha}\right), \quad c > 0; \quad 0 < \alpha \leq 2, \quad \beta > 0,$$

Finally, the Dagum autocorrelation function in Eq. 5.53 is generalized to

$$\rho_{D}(h) = 1 - \left(1 + \left|\frac{h}{c}\right|^{-\beta}\right)^{-\alpha/\beta}, \quad c > 0; \quad 0 < \alpha < 2, \quad 0 < \beta \leq 1,$$

Within the inertial sub-range, the Kolmogorov $-5/3$ power law implies the fractal index $\alpha = 2/3$.

Once the fractal index (and hence D) is fixed, the key parameter to determine is the Hurst exponent H. The literature regarding the estimation of the Hurst exponent is extensive and various estimators have been proposed. Commonly used estimators are R/S analysis, maximum likelihood method, variogram-based methods, box-counting, detrended fluctuation analysis, spectrum regression, and correlation regression (Beran, 1994). Employing the R/S analysis (Borchers, 2018), we have calculated the Hurst exponent of some extrapolated windows. A summary of the obtained outputs is reported in Table 5.8, showing no significant dependence on the time window size, or the choice of "simple R/S Hurst estimation" versus "corrected R/S Hurst exponent". Hence we obtain the Hurst exponent ~ 0.9.

Now, we examine the generalized autocorrelation function for the von Kármán (Eq. 5.63) and Kaimal (Eq. 5.69) models. The non-linear least squares (NLS) method is used to fit the sample data through the generalized Cauchy and Dagum autocorrelation functions from Eqs. 5.82-5.82, and the von Kármán and Kaimal autocorrelation functions from Eqs. 5.63 and 5.69. The results are summarized in Table 5.9. In particular, we report the confidence bounds of the NLS fits. The values of β indicate the Hurst parameter $\sim$ 0.9 for the Cauchy class and $\sim$ 0.84 for the Dagum class. Note that both are very close to the Hurst parameters estimated directly from the time series with the R/S method, despite the distinct approaches. The validity of these estimations is also supported by the narrow confidence bounds.

Window size	Simple R/S Hurst estimation	Corrected R/S Hurst estimation
10 min	0.87	0.98
30 min	0.88	0.96
1 hour	0.81	0.92
2 hours	0.87	0.93
5 hours	0.86	0.93

TABLE 5.8: Hurst exponent using various temporal windows.

Class	β		c[s]	
	2.5%	**97.5%**	**2.5%**	**97.5%**
Generalized Cauchy	0.21	0.22	11.7	12.8
Mod. General. Cauchy	0.20	0.20	26.1	28.3
Dagum	0.33	0.33	7.6	20.0
von Kármán	-	-	8.9×10^2	9.1×10^2
Kaimal	-	-	1.0×10^3	1.1×10^3

TABLE 5.9: Non-linear least squares fit of the long-memory parameter, β, scale parameter c.

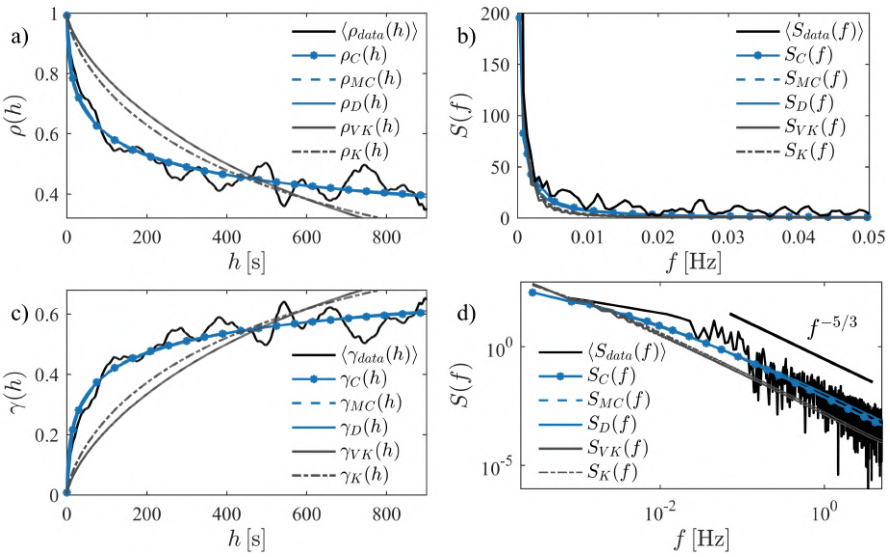

FIGURE 5.29: **a)** Correlogram; **b)** Spectral density; **c)** Variogram; **d)** Log-log scaled spectral density of the atmospheric boundary layer data. Ensemble functions (black line), Cauchy model (dotted blue line), Cauchy Cauchy Modified I model (dashed blue line), Dagum model (continuous blue line), von Kármán model (gray line) and Kaimal model (dashed gray line).

Figure 5.29 shows the result of fitting of each of the models in terms of the autocorrelation, variogram and spectral density. With von Kármán and Kaimal, we can hardly get a good fit, whereas the Cauchy and Dagum models demonstrate excellent agreement with the experimental data. These results support the plausibility of using Cauchy or Dagum models to simulate turbulent velocity data.

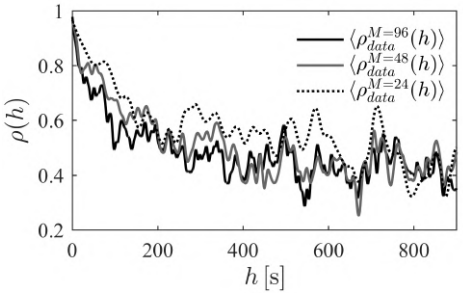

FIGURE 5.30: Correlogram for different interval lengths. Ensemble autocorrelation function for: $M = 96$ (continuous black line), $M = 48$ (continuous gray line) and $M = 24$ (dotted gray line).

Finally, in order to verify that the analysis above is independent of the realizations obtained by segmenting the experimental data into M intervals. The ensemble averaged autocorrelation function is also estimated with $M = 48$ realizations of 30 minutes each, and with $M = 24$ realizations of 1 hour each, respectively. The resulting correlograms are displayed in Fig. 5.30, showing no significant effect of the interval lengths. Moreover, because the other second-order moment statistics are obtained from the autocorrelation function (Wiener Khinchin theorem), the same considerations pertain to the influence of the interval lengths on the estimated variogram and spectral density functions.

5.4.7 Some remarks

The von Kármán and Kaimal models are able to represent the fractal dimension of turbulent velocity field consistently with Kolmogorov $-5/3$ law, however, they fail to capture the long-memory effect. Therefore, two model classes, has motivated this research. To this end, two model classes, the so-called Cauchy (Gneiting and Schlather, 2004a) and Dagum (Mateu, Porcu, and Nicolis, 2007a) belonging to wide-sense-stationary or variogram random fields (Malyarenko and Ostoja-Starzewski, 2019), have been adapted from the modern probability theory. The applicability of these models to turbulent velocity fields have been validated by a relatively large dataset collected within the atmospheric boundary layer. For theoretical completeness, we have also derived explicit forms of the energy spectral densities of Cauchy and Dagum covariances.

5.5 Conclusion

In this Chapter, through a link between the statistical RF theory and the local and non-local randomness in stochastic mechanics, three different mechanical engineering problems have been investigated. Two novel model classes belonging to wide-sense-stationary RF, the so-called Cauchy and Dagum models, for which is possible to deal separately with the local behavior (fractal dimension, D) and the non-local behavior (Hurst effect, H) of the RF have been applied. The first section of this chapter deals with fracture of beams with random filed properties. Thanks to the PTM the Obreimoff experiment, treated first with a stochastic setting in (Ostoja-Starzewski, 2004) was extended taking into consideration the correlation structure of the RF involved. In addition, some considerations about the sensitivity of the response to the local and no-local randomness characteristics have been done. Section 5.2 shows a

study of the effect of the local and non-local characteristics of the flexural deformability on the randomness level of the various stochastic response quantities. Some examples of statically determinate and redundant stochastic beams, under different conditions of load and constrain, showed different sensitivity to these effects if the displacement or the internal forces of the redundant beams are examined. While in Section 5.3, two new velocity spectrum models were presented, which explain and decouple the fractal size and the Hurst effect. The evaluation of these two models using field data from a sonic anemometer located within the atmospheric surface layer showed excellent agreement and much better performance than the conventionally used models of turbulence velocity spectra.

Chapter 6

Random analysis of dynamic systems

6.1 Introduction

An efficient probabilistic characterization of the structural response of a system excited by random process actions often requires a high computational effort, above all when the response is a non-Gaussian process. Actually, even for systems subjected to static actions, the effort can be very high; this is related to the number of random variables involved in the analysis and to the type of probability distribution that characterizes them. A full probabilistic characterization of the structural response of a stochastic dynamic system can be obtained by the knowledge of the evolutionary JPDFs, or, equivalently, by the knowledge of their Fourier transforms, that are the evolutionary C-CFs. The only exception is when the response is represented by a Gaussian process, for which the evolutionary PDF and C-CF depend only on the statistics up to the second order, that are the time variant mean and the two-times dependent correlation function. For all the other cases of response random processes, the knowledge of higher order statistics at multiple times is necessary for a sufficiently accurate probabilistic characterization. Obviously, the necessity of evaluating the response higher order multiple time moments or correlations increases considerably the problem dimensions, without reaching often a satisfying characterization of the probabilistic response (Lin, 1967b; Roberts and Spanos, 2003; Wu and Lin, 1984; Lutes and Sarkani, 2004; Di Paola, Falsone, and Pirrotta, 1992; Di Paola and Falsone, 1994; Falsone, 1994; Di Paola and Falsone, 1997a; Di Paola and Falsone, 1997b; Falsone, 2005; Morikawa and Kameda, 1997; Makarios, 2012; Gioffrè and Gusella, 2002; Mazelsky, 1954; Bucher and Schueller, 1991). Recently, also the perturbation approach has been used in this kind of studies (Kamiński, 2010). Moreover, in some relevant problem, such as the structural reliability evaluation or the stochastic limit analysis, the accurate knowledge of the response PDF is essential, above all at the PDF tails, (Chen and Li, 2007; Alibrandi, 2014). When a single varying time instant is considered in the analysis, the response random process can be characterized through the knowledge of its time varying PDF, or by its time varying CF. But its full probabilistic characterization requires the JPDFs (or the joint C-CFs) at multiple time instants. In the literature, only some papers can be found working directly on the response PDFs, without passing through the knowledge of the response moments or correlations at multiple times, (Conte and Peng, 1996; Adhikari, 2007; Kalogeris and Papadopoulos, 2018; Li, 2016; Calatayud, Cortés, and Jornet, 2018; Calatayud, Cortes, and Jornet, 2018; Liu and Liu, 2018; Hussein and Selim, 2015; Meimaris, Kougioumtzoglou, and Pantelous, 2018; Mamis, Athanassoulis, and Kapelonis, 2019). Indeed, most papers working in this field deal with the response statistics (moments or cumulants) at multiple times, if the dynamical

problem is faced in the time domain (see e.g. Falsone and Settineri (2011b) and Falsone and Settineri (2011a)), or with the spectral moments, if the frequency domain is used (see e.g. Barbato and Conte (2008) and Barbato and Vasta (2010)). A possible alternative to the previous methods is represented by Monte Carlo simulation methods (MCS) (Proppe, Pradlwarter, and Schuëller, 2003; Pradlwarter and Schuëller, 2010), but they exhibit the well-known drawback that the accuracy of the estimates depends on the sampling size of the stochastic processes, besides of the number of samples and this increases the corresponding computational effort.

This Chapter outlines an extension of the PTM to the case of dynamical systems. The main contribution of the chapter is a probabilistic approach able to give the direct relation between the single-time varying PDFs of input and output of a linear structural system subjected to assigned non-Gaussian stochastic process excitations. In particular, Section 6.2 will deal with the extension of the static PTM to the dynamic response analysis. This extension was essentially made by discretizing the classical Duhamel integral. In this way, it will be obtained an efficient approach, able to give the response evolutionary PDF at a single time instant. Moreover, a stochastic procedure for the evaluation of the CF response of structural systems, whose dynamics are characterized by random initial conditions, besides random excitations, will be presented. Then, in Section 6.3 an extension of the above cited approach for the probabilistic characterization of the response at multiple times by the direct evaluation of the corresponding JPDFs will be presented. For each section, some numerical examples are shown with the aim of evidencing the efficiency of the method. Finally, this chapter will end with some notes for the study of dynamic systems having uncertain parameters which lead to handle random differential equations. However, a new formulation of an evolutive PTM for linear uncertain systems is still object of study. So, the contents of Section 6.3 represent the first possible assumptions understudies. Lastly, in Section 6.4, some final overall considerations will be reported. The contributions of this chapter essentially refer to two papers already published (Falsone and Laudani, 2018; Falsone and Laudani, 2020c) and another one under review (Laudani and Falsone, 2020).

6.2 Dynamic stochastic analysis of linear structures

When the dynamic analysis of a linear deterministic structure is performed, the necessity of performing a stochastic analysis may arise: a) if the time-dependent actions are random processes; b) if the system initial conditions are random. Both these possibilities, that could happen contemporaneously, will be treated in the following. The differential motion equations of a n-degree of freedom structure, subject to a time-dependent vector-force $\mathbf{F}(t)$, is written as follows:

$$\mathbf{M}\ddot{\mathbf{U}}(t) + \mathbf{C}\dot{\mathbf{U}}(t) + \mathbf{K}\mathbf{U}(t) = \mathbf{F}(t) \quad \mathbf{U}(0) = \mathbf{U}_0 \tag{6.1a-b}$$

where $\mathbf{M}$, $\mathbf{C}$ and $\mathbf{K}$ are the mass, damping and stiffness matrices, respectively; $\mathbf{U}(t)$ is the n-vector of the response displacements, $\mathbf{U}_0$ defines the initial conditions of the response and $\mathbf{F}(t)$ represents the excitation vector.
If the vector of state variables $\mathbf{X}^T(t) = \left(\mathbf{U}^T(t) \quad \dot{\mathbf{U}}^T(t)\right)$ is introduced, Eqs. 6.1 can be rewritten in the following form:

$$\dot{\mathbf{X}}(t) = \mathbf{D}\mathbf{X}(t) + \mathbf{v}\mathbf{F}(t); \quad \mathbf{X}(0) = \mathbf{X}_0 \tag{6.2a-b}$$

where:

$$\mathbf{D} = \begin{pmatrix} \mathbf{0} & \mathbf{I} \\ -\mathbf{M}^{-1}\mathbf{K} & -\mathbf{M}^{-1}\mathbf{C} \end{pmatrix}; \quad \mathbf{v} = \begin{pmatrix} \mathbf{0} \\ \mathbf{M}^{-1} \end{pmatrix}; \quad \mathbf{X}_0 = \begin{pmatrix} \mathbf{U}(0) \\ \dot{\mathbf{U}}(0) \end{pmatrix}; \tag{6.3a-c}$$

The response vector $\mathbf{X}(t)$ can be calculated by the Duhamel integral, that is:

$$\mathbf{X}(t) = \mathbf{\Theta}(t)\mathbf{X}_0 + \int_0^t \mathbf{\Theta}(t-\tau)\mathbf{v}\mathbf{F}(\tau)d\tau \tag{6.4}$$

$\mathbf{\Theta}(t)$ being the transition (or fundamental) matrix corresponding to the dynamical system; it is expressed as:

$$\mathbf{\Theta}(t) = \exp(\mathbf{D}t) = \sum_{n=0}^{\infty} \frac{1}{n!}\mathbf{D}^n t^n \tag{6.5}$$

The Eq. 6.4 is usually solved numerically and several methods are available in the literature (Di Paola and Falsone, 1994). When the stochastic analysis is performed, the response characterization cannot be obviously reduced to the solution of Eq. 6.4. But the probabilistic description of the response is necessary in this case. Actually, there are a lot of methods in literature that allow obtaining the response PDF. Most parts of them are based on the evaluation of the moments (or cumulants) of the response. These procedures are efficient when the response process is Gaussian. But, if it is not so, it is well known that an accurate probabilistic description of the response, based on the moments (or cumulants) series, is usually a very heavy task.

6.2.1 Random excitations

When the stochastic structural analysis is necessary because of the randomness of the external loads, these last ones are modeled as non-Gaussian random processes, because, as said before, in the case of Gaussian actions, the PTM is unnecessary.
In the following the PTM is applied by making two assumptions: a) the PFFs of input and output are considered at a single time variable t; b) the continuous time axis is discretized by intervals of constant amplitude $\Delta\tau$, so that the generic time instant $t_k = k\Delta\tau$ is considered. The assumption b) implies the transformation of the system of differential equations governing the problem (Eqs. 6.2) into an equivalent discrete algebraic one. Consequently the integral expressed in Eq. 6.4 is transformed into an algebraic equation having the following form:

$$\begin{aligned} \mathbf{X}(t_k) &= \mathbf{\Theta}(t_k)\mathbf{X}_0 + \int_0^{t_k} \mathbf{\Theta}(t_k-\tau)\mathbf{v}\mathbf{F}(\tau)d\tau \approx \mathbf{\Theta}(t_k)\mathbf{X}_0 + \sum_{i=0}^{k-1} \mathbf{\Theta}(t_k-\tau_i)\mathbf{v}\mathbf{F}(\tau_i)\Delta\tau \\ &= \mathbf{\Theta}^k(\Delta\tau)\mathbf{X}_0 + \sum_{i=0}^{k-1} \mathbf{\Theta}^{k-i}(\Delta\tau)\mathbf{v}\mathbf{F}(\tau_i)\Delta\tau \end{aligned} \tag{6.6}$$

where $\tau_i = i\Delta\tau$ and where use has been made of the property of the transition matrix, following the which it is: $\mathbf{\Theta}(t_1+t_2) = \mathbf{\Theta}(t_1)\mathbf{\Theta}(t_2)$. Using the above relationship, the r-th element of $\mathbf{X}(t_k)$, $X^{(r)}(t_k)$, can be written as follows:

$$X^{(r)}(t_k) = \mathbf{1}^T\mathbf{\Theta}^k(\Delta\tau)\mathbf{X}_0 + \sum_{i=0}^{k-1} \mathbf{H}_{ki}^{(r)^T}\mathbf{F}(\tau_i)\Delta\tau \tag{6.7}$$

where $\mathbf{1}^T$ is such a $(2n)$-vector that only its r-th element is equal to the unit and all the other ones are zeros, while the row $\mathbf{H}_{ki}^{(r)^T}$ is given by:

$$\mathbf{H}_{ki}^{(r)^T} = \mathbf{1}_r^T \left[\mathbf{\Theta}^{k-i}(\Delta\tau)\mathbf{v} \right]. \tag{6.8}$$

Without losing the generality of the approach, deterministic zero initial conditions are considered. This implies that, in the time interval $(t_0, t_k]$, the value at the generic time instant up to t_k of the component response $X^{(r)})$ is given by the following linear algebraic equation system:

$$\begin{pmatrix} X^{(r)}(t_1) \\ X^{(r)}(t_2) \\ \vdots \\ X^{(r)}(t_k) \end{pmatrix} = \begin{pmatrix} \mathbf{H}_{10}^{(r)^T} & \mathbf{0}^T & \cdots & \mathbf{0}^T \\ \mathbf{H}_{20}^{(r)^T} & \mathbf{H}_{21}^{(r)^T} & \cdots & \mathbf{0}^T \\ \vdots & \vdots & \ddots & \vdots \\ \mathbf{H}_{k0}^{(r)^T} & \mathbf{H}_{k1}^{(r)^T} & \cdots & \mathbf{H}_{k(k-1)}^{(r)^T} \end{pmatrix} \begin{pmatrix} \mathbf{F}(t_0) \\ \mathbf{F}(t_1) \\ \vdots \\ \mathbf{F}(t_{k-1}) \end{pmatrix} \Delta\tau \tag{6.9}$$

$\mathbf{0}$ being the zero n-vector. The previous relation implies:

$$X^{(r)}(t_k) = \sum_{i=0}^{k-1} \mathbf{H}_{ki}^{(r)^T} \mathbf{F}(t_i)\Delta\tau = \mathbf{H}_k^{(r)^T} \mathbf{F}_k \Delta\tau \tag{6.10}$$

where:

$$\mathbf{F}_k = \begin{pmatrix} \mathbf{F}(t_0) \\ \mathbf{F}(t_1) \\ \vdots \\ \mathbf{F}(t_{k-1}) \end{pmatrix}; \quad \mathbf{H}_{ki}^{(r)} = \begin{pmatrix} \mathbf{H}_{k0}^{(r)} \\ \mathbf{H}_{k1}^{(r)} \\ \vdots \\ \mathbf{H}_{k(k-1)}^{(r)} \end{pmatrix} \tag{6.11}$$

Eq. 6.10 establishes a linear algebraic relationship between the response component evaluated at various time instants up to t_k, and the stochastic load vector evaluated at various time instants up to t_{k-1}. It evidences a very simple way of approximating a dynamic problem in an equivalent discrete problem. The shape of the time-dependent functions appearing as elements of the generic row $\mathbf{H}_{ki}^{(r)^T}$ essentially depends on the powers of the impulse response function of the system. Consequently, these functions decrease to zero more or less rapidly, depending on the system damping and on the power exponent of $\mathbf{\Theta}(\Delta\tau)$. In particular, Eq. 6.8 shows that the exponent of this power is given by $k - i$. This implies that elements of the row $\mathbf{H}_{ki}^{(r)^T}$ become more and more negligible when it is more and more distant from the diagonal blocks. This can be clearly seen in Fig. 6.1, where with reference to an example analyzed in the next section, the first component of the rows $\mathbf{H}_{ki}^{(r)^T}$ with $i = 0, 5, 10, \cdots, k$ is reported. Hence, the blocks that are very distant from the diagonal blocks can be neglected. The number of the negligible blocks obviously depends also on the system damping.

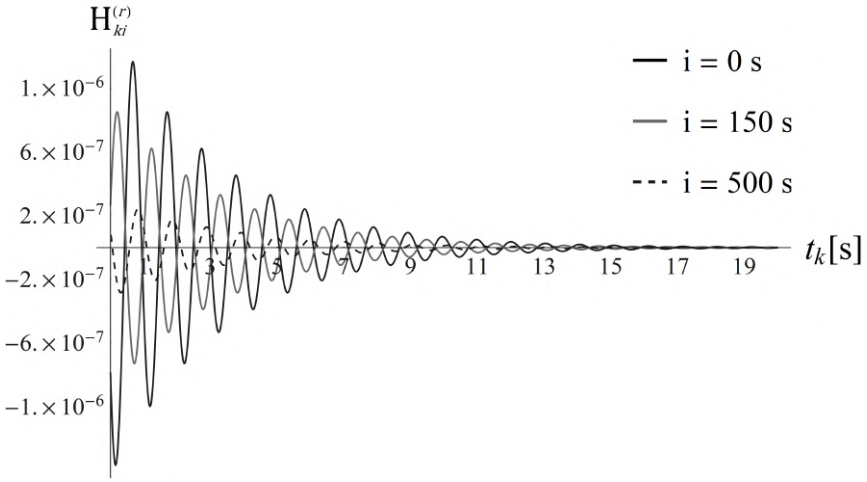

FIGURE 6.1: Typical evolution of the first component of the generic rows $\mathbf{H}_{ki}^{(r)^T}$ for $i = 0, 150, 500$.

From the point of view of the PTM application, Eq. 6.10 defines a linear transformation between the response random variable $X^{(r)}(t_k)$ (output) and the super-vector $\mathbf{F}_k$ (input), built by all the vectors $\mathbf{F}(t_i)$, with $i = 0, 1, \cdots, k-1$.
Due to this form of transformation, it is clear that the more efficient way to apply the PTM is through the evaluation of the response CF, that is:

$$M_{X^{(r)}(t_k)}(\omega_r) = (2\pi)^{nk-1} M_{\mathbf{F}_k}(\boldsymbol{\theta}_k)\big|_{\boldsymbol{\theta}_k=\omega_j \mathbf{H}_k^{(r)}} \tag{6.12}$$

from which the corresponding PDF can be obtained by applying the inverse Fourier transform.
Analogously the JCF of two response components can be obtained by:

$$M_{X^{(r)}(t_k)X^{(p)}(t_k)}(\omega_r, \omega_p) = (2\pi)^{nk-2} M_{\mathbf{F}_k}(\boldsymbol{\theta}_k)\big|_{\boldsymbol{\theta}_k=\omega_r \mathbf{H}_k^{(r)}+\omega_p \mathbf{H}_k^{(p)}} \tag{6.13}$$

The expressions of the results and the way used for obtaining them make clear that this approach can be generalized for the response probabilistic characterization at more than two time instants. It is worth noting that the Eqs. 6.12-6.13 enable a direct relation between the PDFs of the time-dependent input and that one of the time-dependent output. Furthermore, it is important to underline that this approach can be applied for any probabilistic characterization of the stochastic vector-processes $\mathbf{F}(t)$, in both the cases of Gaussian and, above all, non-Gaussian processes.

Another approach, always based on the PTM, could be applied for the stochastic analysis of the structural system governed by Eqs. 6.1 and whose mean square solution is given into Eq. 6.4. By assuming zero initial conditions, Eq. 6.4 is rewritten as:

$$\mathbf{X}(t) = \int_{t_0}^{t} \boldsymbol{\Theta}(t-\tau)\mathbf{v}\mathbf{F}(\tau)d\tau = \int_{t_0}^{t} \mathbf{Z}(\tau)d\tau \tag{6.14}$$

where the vector process $\mathbf{Z}(\tau) = \boldsymbol{\Theta}(t-\tau)\mathbf{v}\mathbf{F}(\tau)$ can be probabilistically defined by the JPDF $p_{\mathbf{Z}}(\mathbf{z}, \tau)$, that is evaluated through the application of the PTM to the linear transformation $\mathbf{F}(\tau) \rightarrow \mathbf{Z}(\tau)$. The last step to do is the characterization of the random vector process $\mathbf{X}$, once that the characterization of the vector process $\mathbf{Z}$ has been found. Due to the time integral relationship between these two processes, an

efficient numerical solution can be used; it is based on the following theorem on the JCFs of **X** and **Z**:

Theorem 6.2.1 *(Soong, 1973) If the m.s. integral* $\mathbf{X}(t)$, $t \in T$, *exists, then:*

$$M_{\mathbf{X}}(\omega, t) = \lim_{\substack{m\to 0 \\ \Delta m \to 0}} M_{\mathbf{Z}}\left(\omega\left(\tau_1 - \tau_0\right), \tau_1'; \cdots; \omega\left(\tau_m - \tau_{m-1}\right), \tau_m'\right); \quad \tau_j' \in \left(\tau_{j-1}, \tau_j\right) \tag{6.15}$$

where $\Delta_m = \max\left(\tau_{j-1} - \tau_j\right)$.

By truncating the value of m to a sufficiently high value, the expression of this theorem becomes an efficient way to evaluate numerically the response CF.
If the characterization of the response random process is required at more instant, Eq. 6.15 must be generalized. This is always possible, even if the corresponding numerical evaluation becomes more and more heavy increasing the number of time instants.

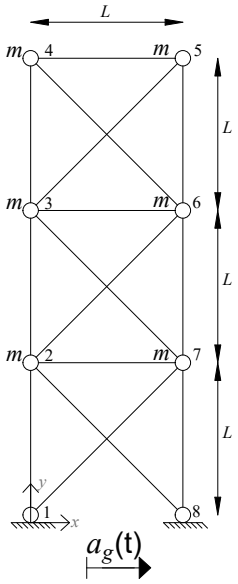

FIGURE 6.2: Truss structure system.

6.2.1.1 Numerical examples

The effectiveness of the proposed method is tested through some numerical examples. The truss structure represented in Fig. 6.2 is first considered. It is characterized by the following geometrical and physical parameters: $L = 10\ m$; the cross-element area is $A = 0.04\ m^2$. The mass is considered as lumped in the nodes 2, 3, 4, 5, 6 and 7, and its value is $m = 10,000\ kg$. The Young's modulus value is $E = 2.1 \times 10^{11}\ N/m^2$, and it is assumed equal for all the bars. The structure is forced by the inertial actions because of a base acceleration $a_g(t)$ that is assumed to be represented as a random process To verify the good level of accuracy for non-Gaussian processes, $a_g(t)$ has been hypothesized to have a PDF given by the weighted mean of two Gaussian PDFs, i.e. as follows:

$$p_{a_g(t)}\left(a_g(t)\right) = \frac{1}{2} p_{a(t)}\left(a(t)\right) + \frac{1}{2} p_{b(t)}\left(b(t)\right) \tag{6.16}$$

where $a(t)$ is the zero-mean Gaussian stationary process corresponding to the Clough–Penzien spectrum, having the following power spectral density:

$$S_a(\omega) = \frac{\omega_r^4 + 4\xi_r^2\omega_r^2\omega^2}{\left(\omega_r^2 - \omega^2\right)^2 + 4\xi_r^2\omega_r^2\omega^2} \frac{\omega^4}{\left(\omega_p^2 - \omega^2\right)^2 + 4\xi_p^2\omega_p^2\omega^2} \frac{0.141\xi_r^2 a_{g0}^2}{\omega_r\sqrt{1+r\xi_r^2}} \tag{6.17}$$

where the following values of the parameters have been chosen: $\omega_p = 2.0$, $\omega_r = 19$, $\xi_p = 0.6$ and $a_{g0} = 0.25g$. Once that the correlation function $R_a(\tau)$ is evaluated by a Fourier transform of the previous spectrum, the covariance function is obtained as:

$$\sigma_a^2(t+\tau, t) = R_a(\tau) \tag{6.18}$$

The Gaussian PDF $p_{b(t)}(b(t))$ has unitary mean and covariance function given by:

$$\sigma_b^2(t+\tau, t) = 0.3\sigma_a^2(t+\tau, t) \tag{6.19}$$

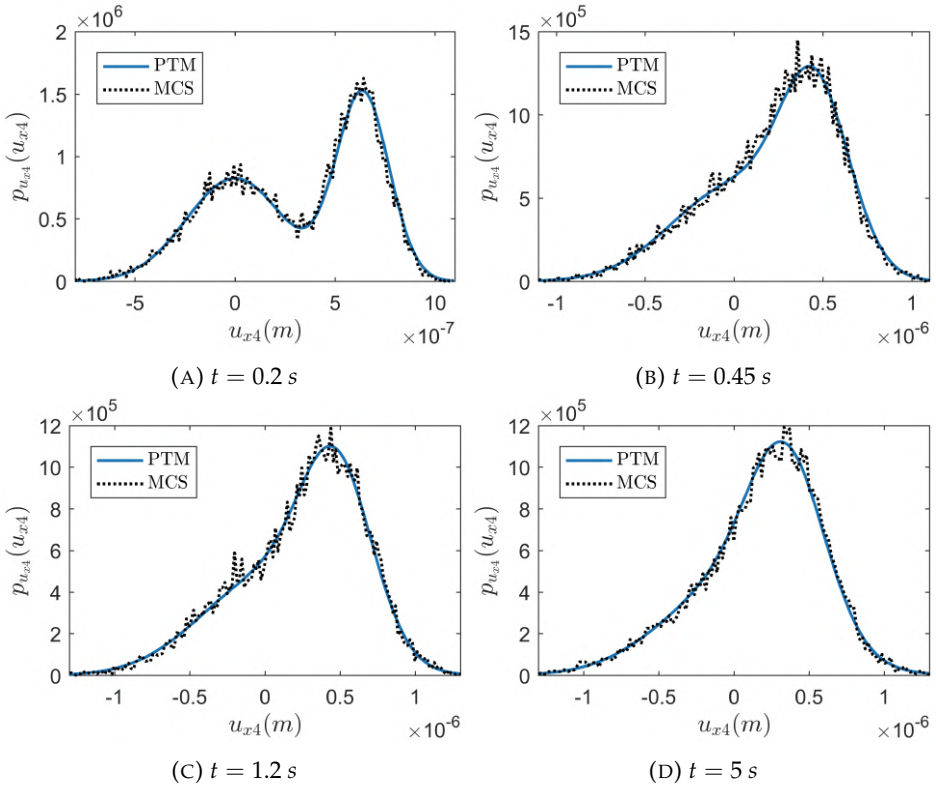

(A) $t = 0.2\ s$ (B) $t = 0.45\ s$

(C) $t = 1.2\ s$ (D) $t = 5\ s$

FIGURE 6.3: Horizontal displacement PDF of Node 4 evaluated for four different instants. PTM (continuous line); MCS (dashed line)

To apply the PTM, it is to note that the load vector $\mathbf{F}(t)$ is given by $-\mathbf{M}\boldsymbol{\tau}a_g(t)$, $\boldsymbol{\tau}$ being the structural incidence vector. The random characterization of the displacements of the r-th DOF at the time instant t_k, $X^{(r)}(t_k)$, has been obtained by the application of Eq. 6.12 or, alternatively, by the application of Eq. 6.15. In Fig. 6.3, the horizontal displacement PDFs of node 4 for four instants are shown in which it is possible to observe that, for the first instants, the random characteristics of the PDF outputs are strongly affected by the random characteristics of the input force, then the responses PDF are gradually filtered. These results are compared with the corresponding quantities obtained by MCS performed with 15,000 samples. From the

analysis of these results, one can appreciate a good level of accuracy of the proposed approach.

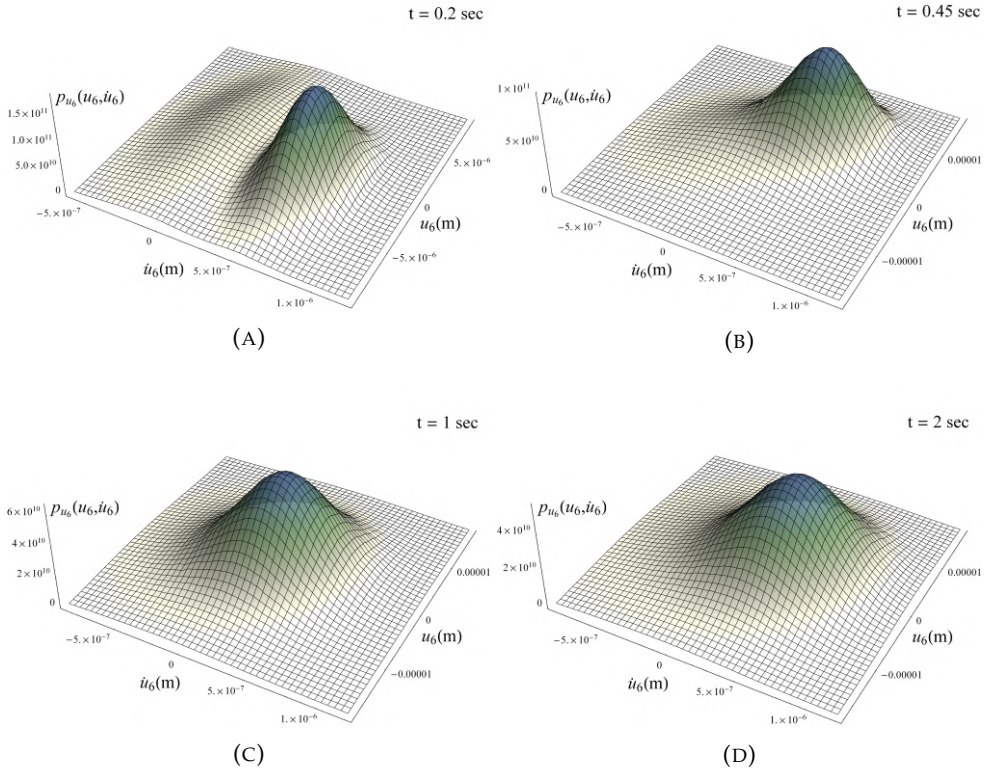

FIGURE 6.4: Example 1: horizontal displacement–velocity JPDF of Node 4 evaluated for four different instants.

Furthermore, it is possible to evaluate the JPDFs displacement–velocity by applying Eq. 6.13. In Fig. 6.4, the JPDFs displacement–velocity for four instants is shown. Finally, in Fig. 6.5, the horizontal displacement PDFs of node 4 are shown in the time instant range $[0.15, 1.00]$.

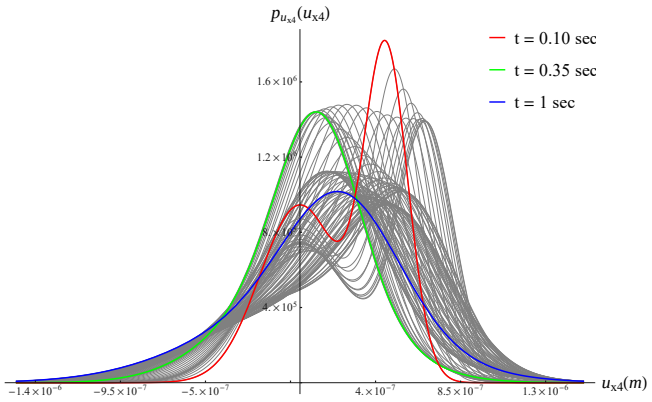

FIGURE 6.5: Example 1: horizontal displacement PDFs of Node 4 evaluated for the time interval $[0.10, 1.00]$

Here, it is want emphasize that the application of the PTM has allowed obtaining

some good results in an efficient way even if the input and, consequently, the output, are defined by strongly non-Gaussian processes. The same quality cannot be appreciated for most of the approaches in literature, such as the moment equation method. Moreover, the present approach has been noticed very effective in the computational effort even with respect to the previous approach (Settineri and Falsone, 2014).

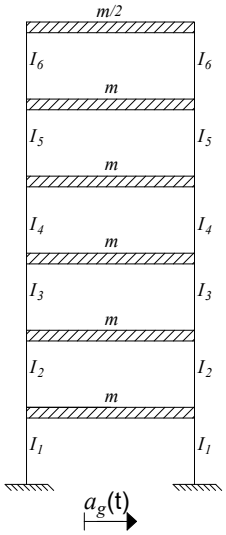

FIGURE 6.6: Shear-type plane system

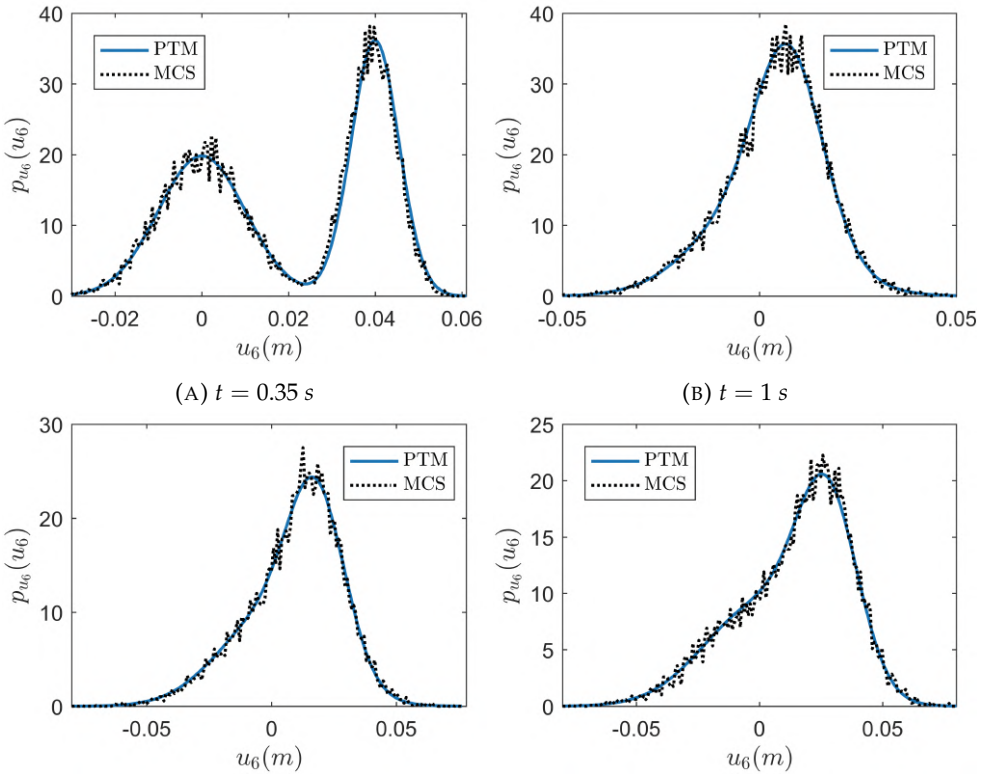

(A) $t = 0.35\ s$ (B) $t = 1\ s$

(C) $t = 3\ s$ (D) $t = 5\ s$

FIGURE 6.7: Example 2: last floor displacement PDF evaluated for four different instants

Then, as a second example, the shear-type plane system shown in Fig. 6.6 is taken into account. The Young's modulus value is $E = 31 \times 10^9\ N/m^2$; all the columns have the same length $h = 3.2\ m$, while the moments of inertia of each column are $I_1 = I_2 = 0.0054\ m_4$, $I_3 = I_4 = 0.0031\ m^4$ and $I_5 = I_6 = 0.016\ m^4$; for the first five floors, a mass $m = 36,000/g\ kg$ is assumed; for the sixth floor, a mass equal to $m/2$ is considered. The structure is forced by the inertial actions because of a base acceleration $a_g(t)$ and is assumed the same non-Gaussian process considered in the previous example.

By application of the equation 6.12, it is possible to obtain the PDF of any degree of freedom. In particular, in Fig. 6.7, the horizontal displacement PDF of the last floor is shown for four instants, and the comparison is made with the analogous results obtained by the MCS performed with 15,000 samples. While, in Figs. 6.8 and 6.9, the jPDFs displacement–velocity for four instants and the displacement PDFs of last floor in the time instant range $[0.15, 2.00]$ are, respectively, shown.

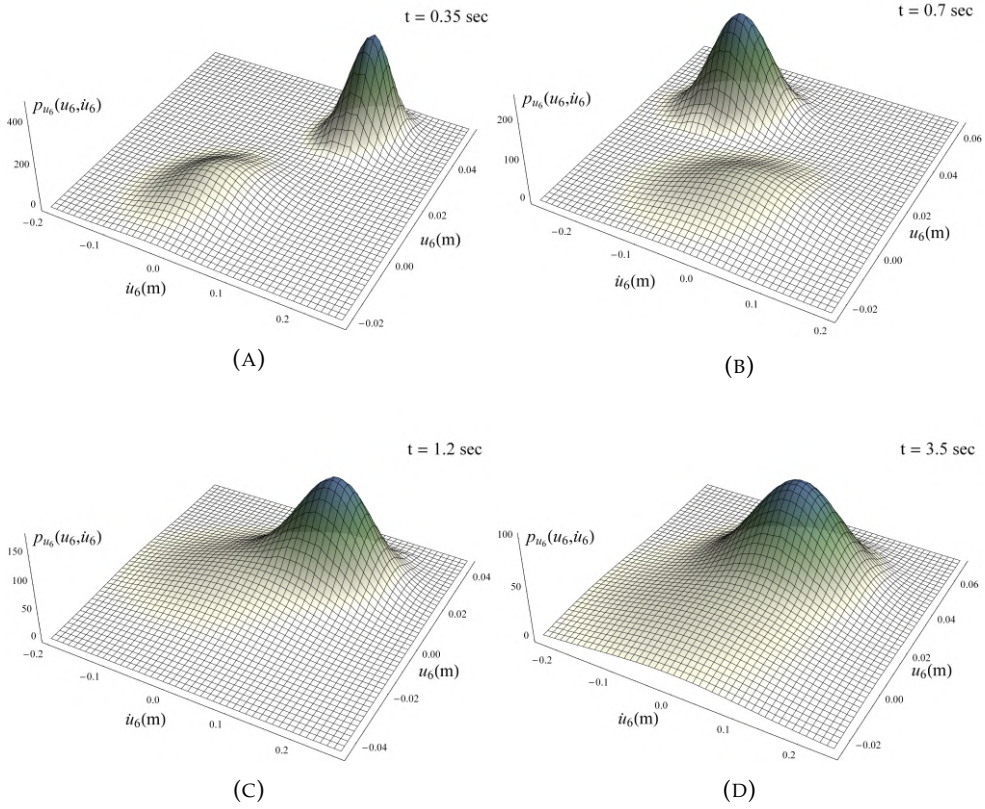

FIGURE 6.8: Example 2: last floor displacement–velocity JPDF evaluated four different instants

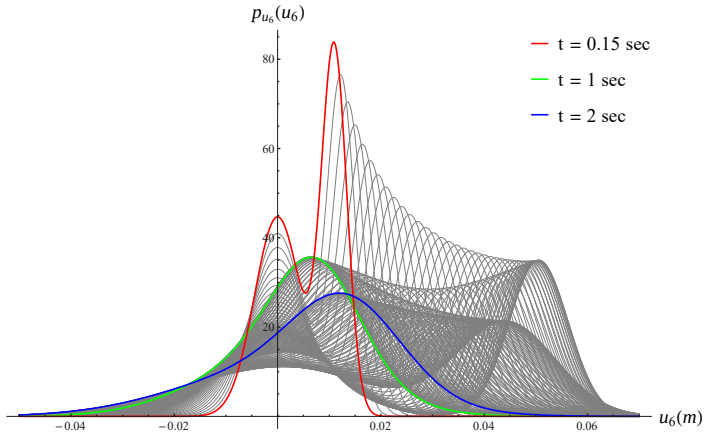

FIGURE 6.9: Example 2: last floor displacement PDF evaluated for the time interval $[0.15, 2.00]$

Finally, the same plane shear-type structure considered in the previous example is now assumed to be forced by actions of wind kind. In this case, the vector load $F(t)$ is written as follows

$$\mathbf{F}(t) = \mathbf{A}V^2(t) \tag{6.20}$$

where $\mathbf{A}$ is a constant vector that in this example has been assumed to have the following expression:

$$\mathbf{A} = \begin{bmatrix} 1.1 & 1.2 & 1.3 & 1.4 & 1.5 & 1.6 \end{bmatrix} \times 31.50 \quad kg/m \tag{6.21}$$

$V(t)$ represents the stochastic wind velocity (in m/s), comprehensive of a fluctuating part. It is here assumed to be a stationary Gaussian process, having a constant mean value $\mu_V = 30\ m/s$, and covariance function $\sigma_V^2\ (t_1, t_2)$that is described by the following correlation function:

$$R_{VV}\ (t_1, t_2) = R_{VV}\ (t_2 - t_1) = 100\exp\left[-0.5\,|t_2 - t_1|\cos\left(t_2 - t_1\right)\right] \tag{6.22}$$

Therefore the system is forced by six stochastic concentrated forces, applied at each floor, depending on the squares of the random process $V(t)$ (Fig. 6.10).

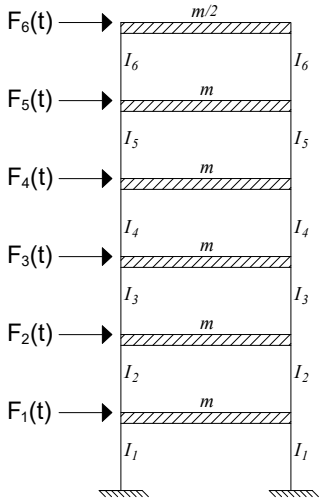

FIGURE 6.10: Shear-type plane system excited by wind-type actions

Gaussian, depending on the square of a Gaussian process. Finally, the PDF of the r-th floor displacement is obtained. In Fig. 6.11, the displacement PDFs of last floor for three increasing instants are shown. The comparisons with the same results obtained by MCS performed with 20,000 samples confirm the efficiency of the proposed approach. Furthermore, the evaluation of the JPDF displacement–velocity of the sixth floor leads to the results depicted in Fig. 6.12. Finally, in Fig. 6.13, the evaluation of the displacement PDFs of last floor in the time instant interval $[0.15, 1.00]$ is shown.

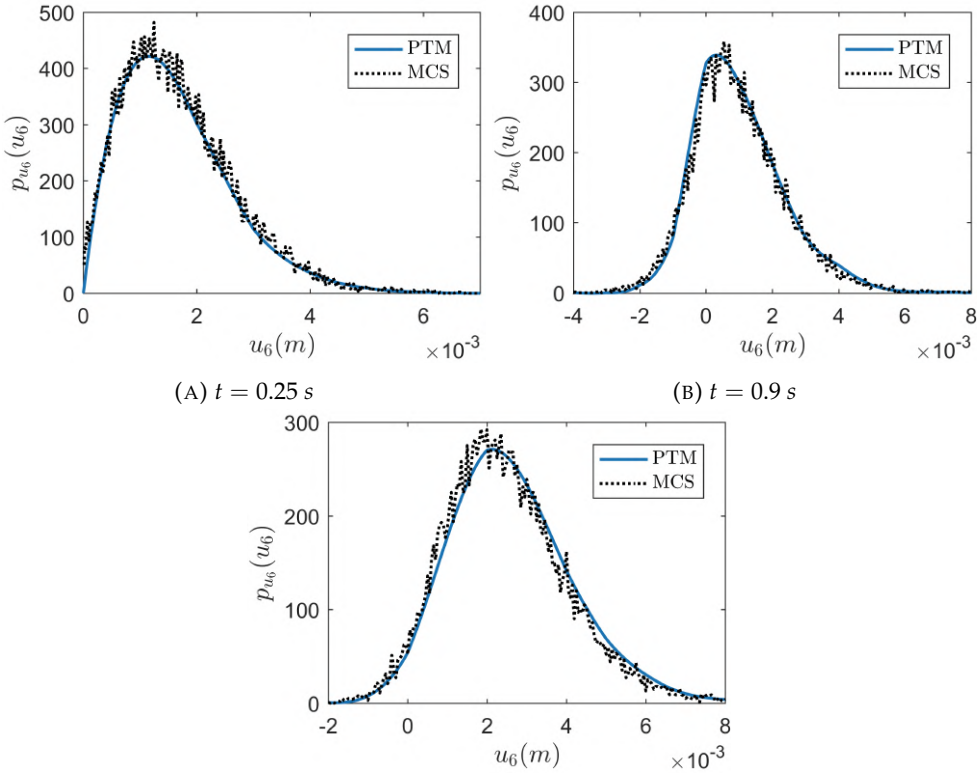

(A) $t = 0.25\ s$ (B) $t = 0.9\ s$

(C) $t = 4\ s$

FIGURE 6.11: Example 3: last floor displacement PDF evaluated for three different instants

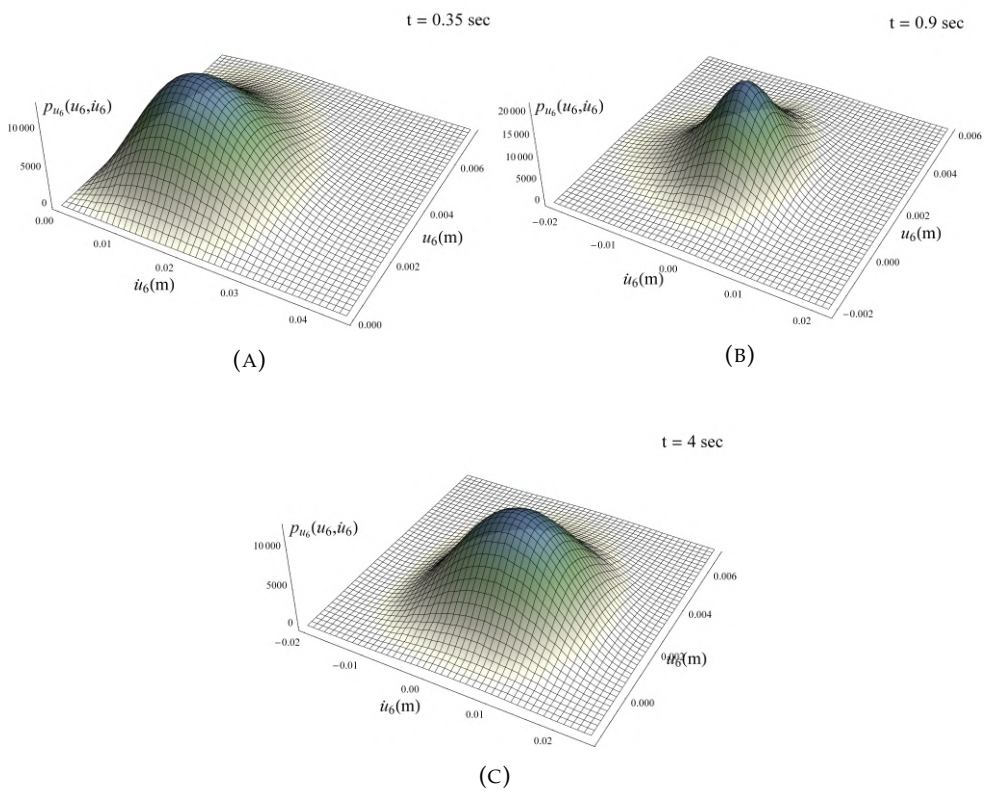

FIGURE 6.12: Example 3: last floor displacement– velocity JPDF evaluated at three different instants

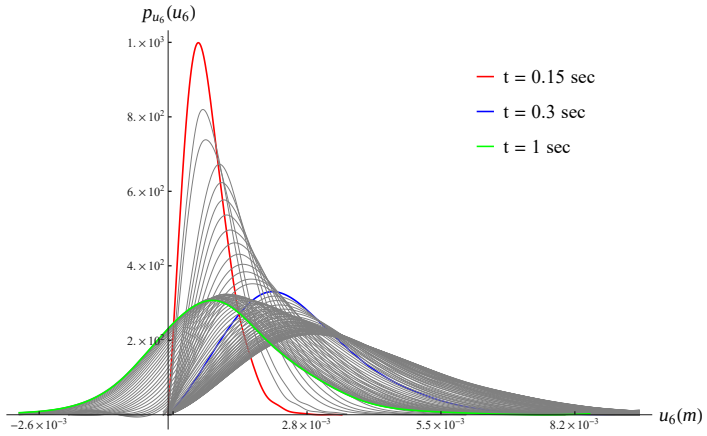

FIGURE 6.13: Example 3: last floor displacement PDF evaluated for the time interval $[0.15, 1.00]$

6.2.2 Random initial conditions

In this subsection, the structural systems, whose dynamics is characterized by random initial conditions, besides of random excitations, are studied. In particular, here, the more plausible assumption of independence between these two kinds of actions is made. This means that, in the expression of the solution $\mathbf{X}(t)$, given in Eq. 6.4, $\mathbf{X}_0$ is a vector of assigned random variables and $\mathbf{F}(\tau)$ is a vector of assigned random process and they are statistically uncorrelated.

The expression of the response vector can be rewritten as follows:

$$\mathbf{X}(t) = \bar{\mathbf{X}}_0(t) + \bar{\mathbf{X}}_F(t) \tag{6.23}$$

$\mathbf{X}_0$ and $\bar{\mathbf{X}}_F(t)$ being two independent random processes given by:

$$\bar{\mathbf{X}}_0(t) = \mathbf{\Theta}(t)\mathbf{X}_0; \quad \bar{\mathbf{X}}_F(t) = \int_0^t \mathbf{\Theta}(t-\tau)\mathbf{v}\mathbf{F}(\tau)d\tau \tag{6.24a-b}$$

Each of these processes can be easily characterized through the evaluation of their CFs. Indeed, $\bar{\mathbf{X}}_0(t)$ is a linear combination of the elements of $\bar{\mathbf{X}}_F(t)$ and, thus, its CF can be evaluated in the form given in Eq. 2.46. The process $\bar{\mathbf{X}}_F(t)$ is the time integral of the process $\mathbf{Z}(\tau) = \mathbf{\Theta}(t-\tau)\mathbf{v}\mathbf{F}(\tau)$. In the previous subsection a procedure giving numerically the CF has be given through Eq. 6.15. Lastly, the response CF $M_{\mathbf{X}(t)}(\omega, t)$ can be obtained by considering an important property of the CF of the sum of two independent random process (Soong, 1973), following the which it is:

$$M_{\mathbf{X}(t)}(\omega, t) = M_{\bar{\mathbf{X}}_0(t)}(\omega, t) M_{\bar{\mathbf{X}}_F(t)}(\omega, t) \tag{6.25}$$

Even in this case, the response PDF is obtained by the Fourier anti-transform of this CF.

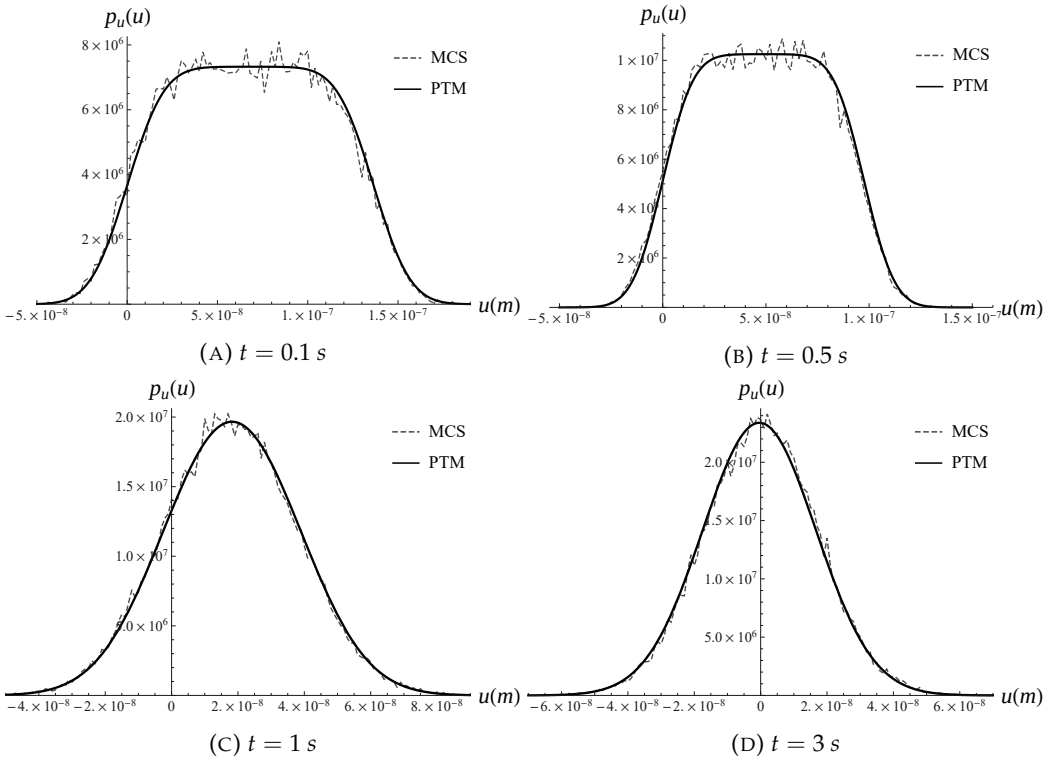

FIGURE 6.14: Displacement PDF evaluated for four different instants. PTM (continuous line); MCS (dashed line)

6.2.2.1 Numeical examples

The following one-degree-of-freedom linear system is now taking into account:

$$\ddot{x}(t) + 2\xi_0\omega_0\dot{x}(t) + \omega_0^2 x(t) = f(t); \quad x(0) = x_0; \quad \dot{x}(0) = \dot{x}_0 \tag{6.26a-b}$$

characterized by damping ratio $\xi_0 = 0.05$ and undamped angular frequency $\omega_0 = 46,13\ rad/s$. The system is forced by a the zero-mean Gaussian stationary ground motion acceleration defined by its one-side power Clough–Penzien spectra density of Eq. 6.17. The initial displacement condition is assumed as random variable with marginal PDF uniformly distributed with $\sigma_{x_0} = 0.15$.
The random characterization of the displacement $x(t)$ has been obtained by the application of Eq. 6.25. In Fig. 6.14, the displacement PDFs for four instants are shown. From the inspection of this last figure, it is possible to appreciate that for the first instants, the PDF outputs are significantly influenced by the random initial conditions, then the responses PDF depends only on the random characteristics of the excitation. Finally, the comparisons with the same results obtained by MCS performed with $50,000$ samples evidence the validity of the proposed approach.

6.3 Multi-time probability density functions of the dynamic non-Gaussian response of structures

In Section 6.2.1, the extension of the static PTM to the dynamic response analysis was essentially made by discretizing the classical Duhamel integral, obtaining an efficient approach able to give the response evolutionary PDF at a single time instant.

Aim of the present section is the extension of the above cited approach for the probabilistic characterization of the response at multiple time by the direct evaluation of the corresponding JPDFs.

6.3.1 Proposed approach

The approach that will be presented in this section mainly is the extension to the multiple time case of a previously introduced dynamic PTM working on a single evolution of the response statistics.
Let take into account Eq. 6.10 which establishes a linear algebraic relationship between the response component, evaluated at various time instants up to t_k, and the stochastic load vector, evaluated at various time instants up to t_{k-1}. If now the time instant $t_j = j\Delta\tau$, with $j < k$, is considered, then it is easy to verify that the following expression holds:

$$X^{(r)}(t_j) \approx \sum_{i=0}^{j-1} \mathbf{H}_{ji}^{(r)^T} \mathbf{F}(t_i)\Delta\tau = \mathbf{H}_{j}^{(r)^T} \mathbf{F}_j \Delta\tau = \hat{\mathbf{H}}_{jk}^{(r)^T} \mathbf{F}_k \Delta\tau \tag{6.27}$$

where $\hat{\mathbf{H}}_{jk}^{(r)^T}$ is the j-th super-row of the matrix defined in the first of Eqs. 6.9, that is:

$$\hat{\mathbf{H}}_{jk}^{(r)^T} = (\mathbf{H}_{j0}^{(r)^T} \quad \mathbf{H}_{j1}^{(r)^T} \quad \dots \quad \mathbf{H}_{j(j-1)}^{(r)^T} \quad \mathbf{0}^T \dots \mathbf{0}^T) \tag{6.28}$$

In Section 6.2.1 have been shown the way for characterizing the response component $X^{(r)}$ at a fixed time instant t_k. In particular, assuming that the load JPDF, $p_{\mathbf{F}_k}(\mathbf{F}_k)$, is known, it is possible to express the response PDF as follows:

$$p_{X^{(j)}(t_k)}(X^{(j)}(t_k)) = \int_{-\infty}^{+\infty} \cdots \int_{-\infty}^{+\infty} p_{\mathbf{F}_k}(\mathbf{y}_k)\delta(X^{(j)}(t_k) - \mathbf{H}_k^{(j)^T}\mathbf{y}_k)dy_1 \cdots dy_{n\cdot k} \tag{6.29}$$

As noted in Section 6.2.1, in the cases of linear relationships between input and output random variables, as this is the case here in examination, a very useful formula

can be obtained if the analysis is made in terms of CFs, instead of PDFs. Indeed, it has been shown that the following expression holds:

$$M_{X^{(r)}(t_k)}(\omega) = (2\pi)^{n\cdot k-1}\, M_{\mathbf{F}_k}(\boldsymbol{\theta}_k)\big|_{\boldsymbol{\theta}_k=\omega\mathbf{H}_k^{(r)}} \tag{6.30}$$

Now, the analysis is extended to the case in which the response probabilistic characterization is required at two different time instants t_j and t_k, with $t_j < t_k$. At this purpose, taking into account Eq. 6.27, it is easy to show that the following relationship holds:

$$\begin{aligned} &p_{X^{(r)}(t_j)X^{(r)}(t_k)}(X^{(r)}(t_j), X^{(r)}(t_k)) = \\ &\int_{-\infty}^{+\infty}\cdots\int_{-\infty}^{+\infty} p_{\mathbf{F}_k}(\mathbf{y}_k)\delta(X^{(r)}(t_j) - \hat{\mathbf{H}}_{jk}^{(r)^T}\mathbf{y}_k)\delta(X^{(r)}(t_k) - \mathbf{H}_k^{(r)^T}\mathbf{y}_k)dy_1\cdots dy_{n\cdot k} \end{aligned} \tag{6.31}$$

Consequently, the response C-CF, can be related to the load CF as follows:

$$M_{X^{(r)}(t_j)X^{(r)}(t_k)}(\omega_1,\omega_2) = (2\pi)^{n\cdot k-2}\, M_{\mathbf{F}_k}(\boldsymbol{\theta}_k)\big|_{\boldsymbol{\theta}_k=\omega_1\hat{\mathbf{H}}_{jk}^{(r)}+\omega_2\mathbf{H}_k^{(r)}} \tag{6.32}$$

It is obvious that this last relationship can be generalized to the case in which $X^{(r)}$ and $X^{(s)}$, with $r \neq s$, are two distinct response components, obtaining:

$$M_{X^{(r)}(t_j)X^{(s)}(t_k)}(\omega_1,\omega_2) = (2\pi)^{n\cdot k-2}\, M_{\mathbf{F}_k}(\boldsymbol{\theta}_k)\big|_{\boldsymbol{\theta}_k=\omega_1\hat{\mathbf{H}}_{jk}^{(r)}+\omega_2\mathbf{H}_k^{(s)}} \tag{6.33}$$

At this point, the generalization of the previous formulation to the case in which the probabilistic characterization of the response components $X^{(r)}, X^{(s)}, \cdots, X^{(t)}$, evaluated at the different temporal instants $t_j, t_k, \cdots, t_l$, is straightforward. For example, it is not difficult to verify that the following expression holds:

$$M_{X^{(r)}(t_j)X^{(s)}(t_k)\cdots X^{(t)}(t_l)}(\omega_1,\omega_2,\cdots\omega_m) = (2\pi)^{n\cdot l-m}\, M_{\mathbf{F}_k}(\boldsymbol{\theta}_k)\big|_{\boldsymbol{\theta}_k=\omega_1\hat{\mathbf{H}}_{jl}^{(r)}+\omega_2\hat{\mathbf{H}}_{kl}^{(s)}+\cdots+\omega_m\mathbf{H}_l^{(t)}} \tag{6.34}$$

Once that the response C-CFs have been obtained, the corresponding JPDFs can be evaluated by the application of the inverse Fourier transform.

6.3.2 Numerical example

6.3.2.1 Example 1

The numerical examples reported in this subsection aim for verifying the feasibility and the accuracy of the proposed approach. In particular, two numerical examples, already studied in Section 6.2.1 in terms of evolutionary single time instant PDFs, have been examined.

At first, the shear-type plane system shown in Fig. 6.7 is taken into account. By using Eq. 6.31, or Eq. 6.32, it is possible to evaluate the JPDF of the response component, $X^{(r)}$, at two different time instants, $t_j < t_k$. The Figs. 6.15-6.18 show the JPDFs of the horizontal displacement of the last floor for $t_j = 0.01$ s and for four different time instants: $t_k = 0.02$ s, $t_k = 0.5$ s, $t_k = 2.5$ s and $t_k = 5$ s.

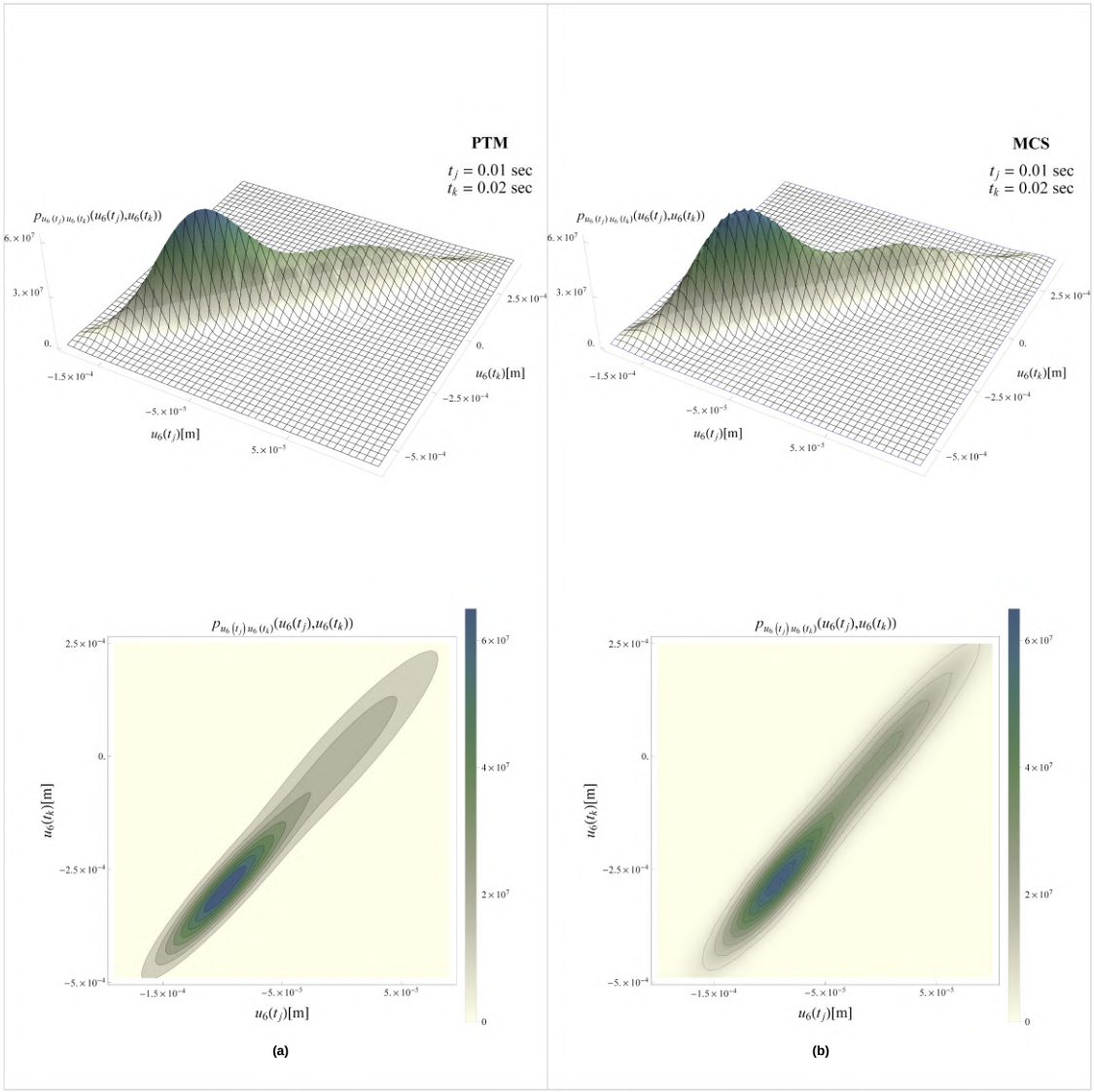

FIGURE 6.15: Example 1: the JPDF of the horizontal displacement of the last floor at two different time instants $t_j = 0.01$ s and $t_j = 0.02$ s. (a) PTM, (b) MCS.

In particular, in Figs. 6.15-6.18 the results are compared with the corresponding quantities obtained by MCS performed with 50.000 samples. From the observation of these figures, it can be observed the high level of correlation between the random variables $X^{(r)}(t_j)$ and $X^{(r)}(t_k)$ when the two time instants are close (Fig. 6.15), while, when the time distance is larger the correlation decreases (Fig. 6.18). Then, another analysis has been performed with $t_j = 0.25$ s and $t_k = 0.5$ s and the corresponding JPDF of the same response components has been reported in Fig. 6.19.

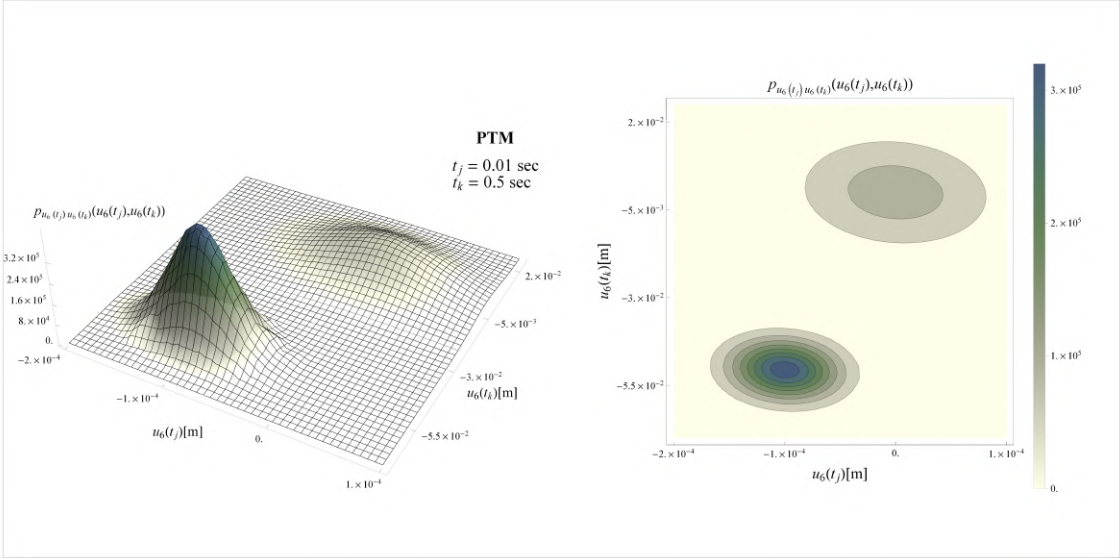

FIGURE 6.16: Example 1: the JPDF of the horizontal displacement of the last floor at two different time instants $t_j = 0.01$ s and $t_j = 0.5$ s.

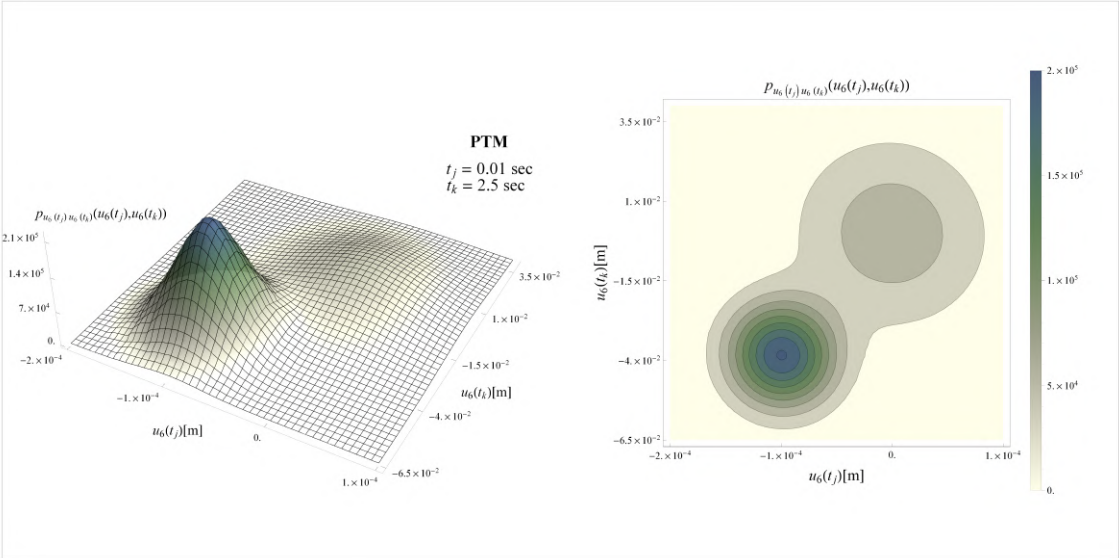

FIGURE 6.17: Example 1: the JPDF of the horizontal displacement of the last floor at two different time instants $t_j = 0.01$ s and $t_j = 2.5$ s.

At last, in order to show better the accuracy of the proposed method, the multi-time moment, $\mathrm{E}[u_6(t_1)\,u_6(t)]$, and the multi-time variance, $\mathrm{Cov}[u_6(t_1), u_6(t)] = \mathrm{E}[u_6(t_1)\,u_6(t)] - \mathrm{E}[u_6(t_1)]\mathrm{E}[u_6(t)]$, have been shown in Fig. 6.20. From the analysis of these results, the good level of accuracy of the proposed approach can be appreciated. The present approach has been noticed to be very effective in the computational effort, too; the use of the approach has allowed a computing time-saving of about 80% respect to the MCS under the same accuracy condition.

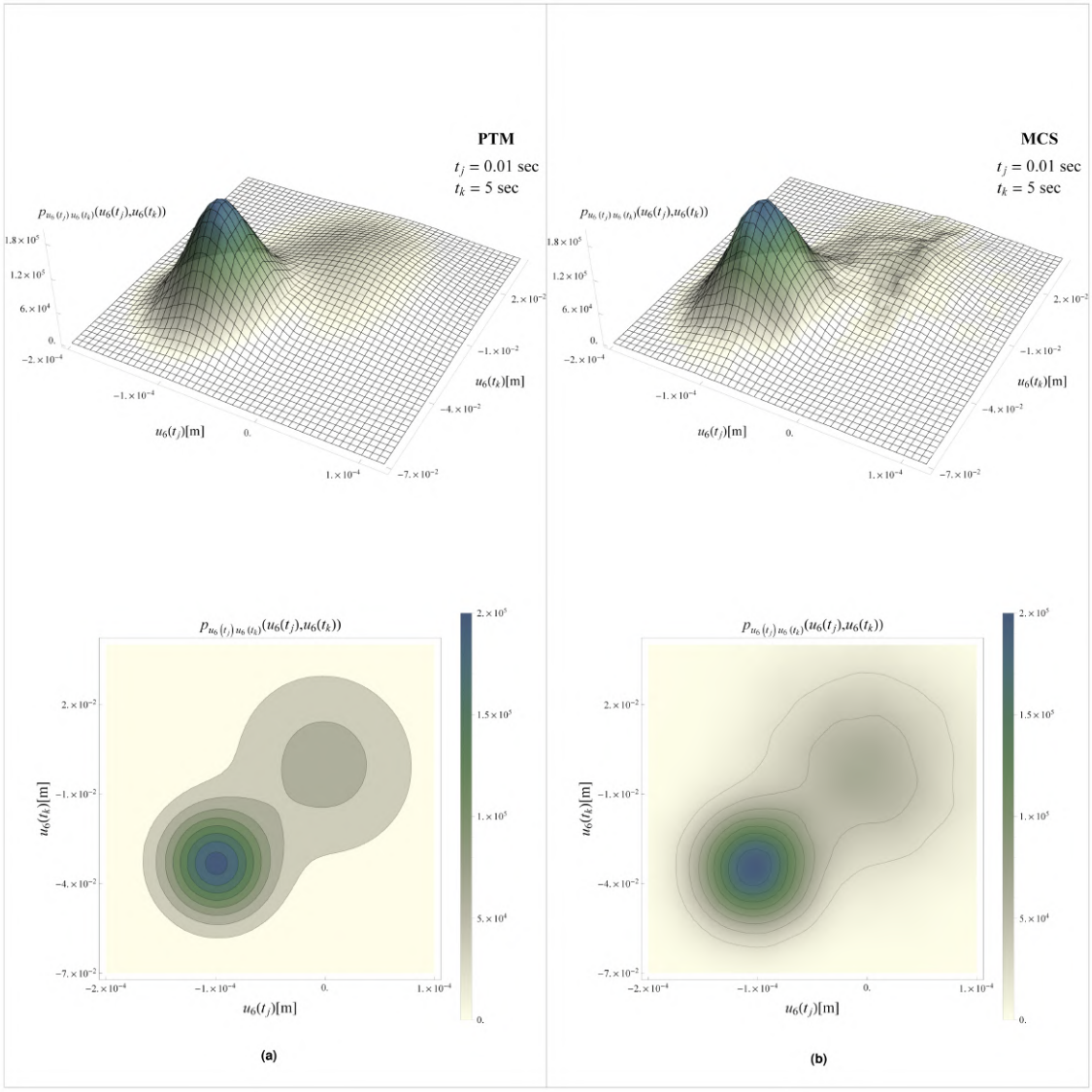

FIGURE 6.18: Example 1: the JPDF of the horizontal displacement of the last floor at two different time instants $t_j = 0.01$ s and $t_j = 5.0$ s. (a) PTM, (b) MCS.

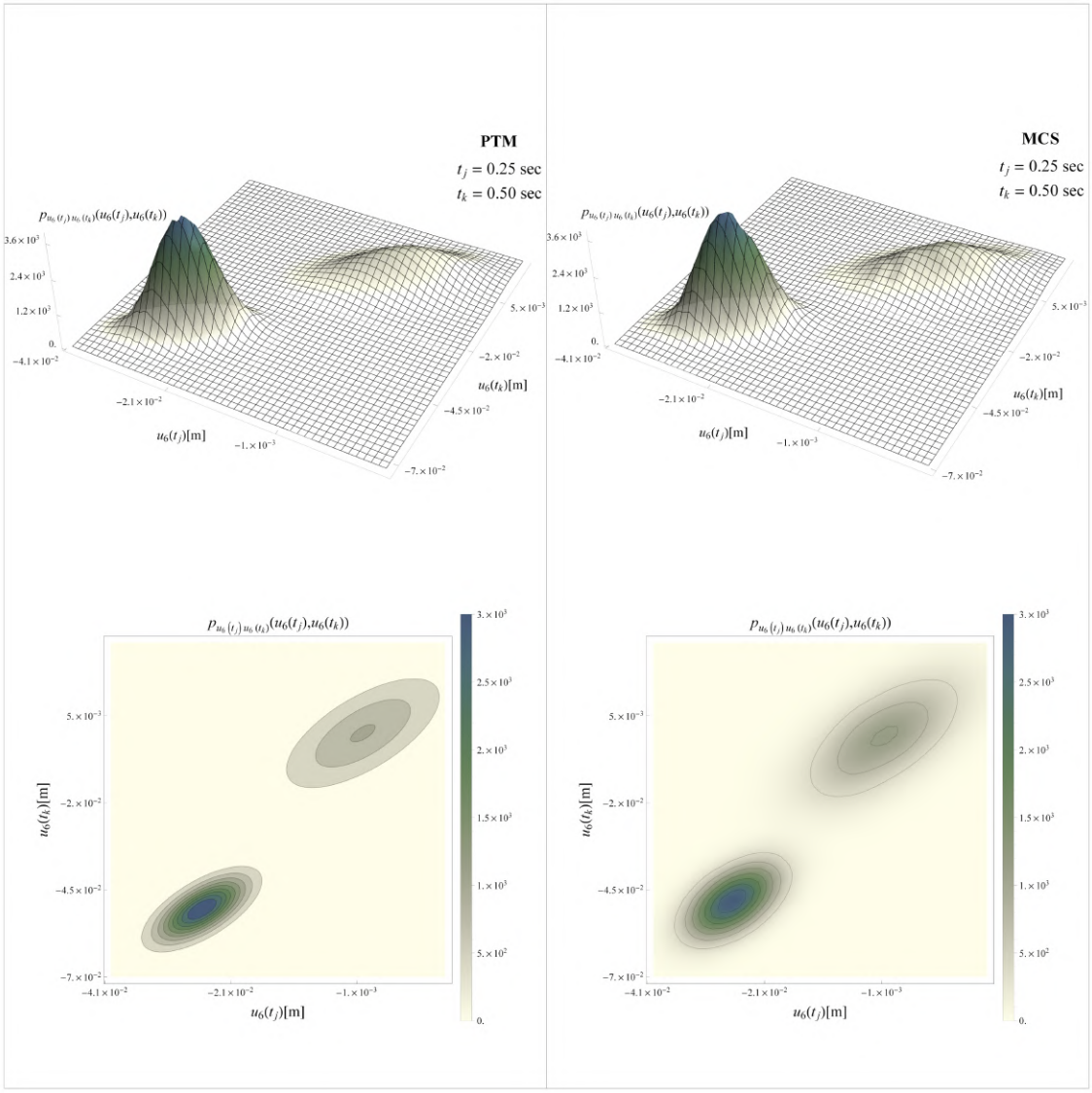

FIGURE 6.19: Example 1: the JPDF of the horizontal displacement of the last floor at two different time instants $t_j = 0.25$ s and $t_j = 0.5$ s. (a) PTM, (b) MCS.

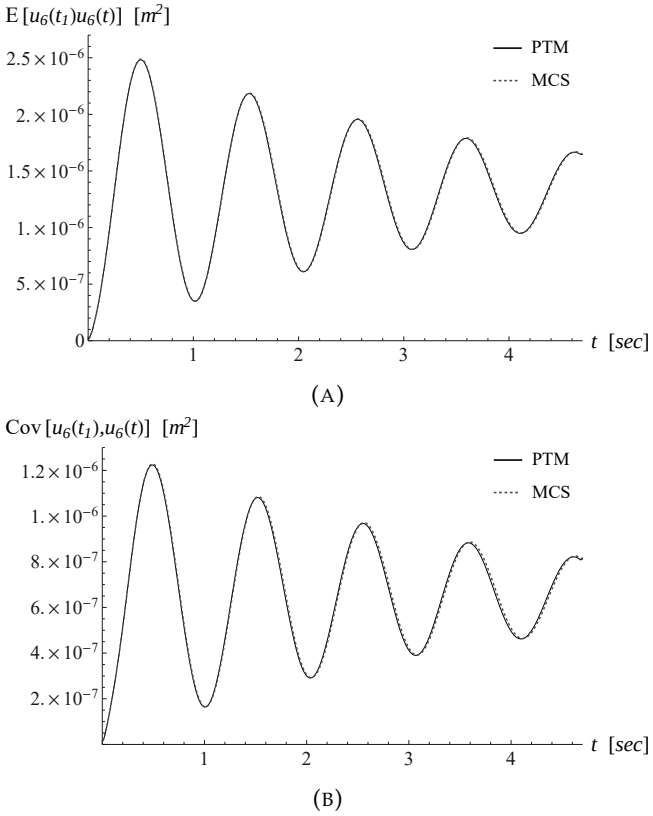

FIGURE 6.20: Example 1: (A) multi-time moment, $\mathrm{E}[u_6(t_1)\, u_6(t)]$; (B) multi-time variance. $\mathrm{Cov}[u_6(t_1), u_6(t)]$.

6.3.2.2 Example 2

The same plane shear-type structure forced by actions of wind kind considered in the previous sections now is assumed (Fig. 6.11) The evaluation of the JPDF of the horizontal displacement of the six-th floor for $t_j = 0.01$ s and for four different time instants: $t_k = 0.02$ s, $t_k = 0.5$ s, $t_k = 2.5$ s and $t_k = 5$ s, has been obtained by the application of Eq. 6.31 or Eq. 6.32, leading to the results depicted in Figs. 6.21-6.24. Finally, another analysis has been performed with $t_j = 0.25$ s and $t_j = 0.5$ s and the corresponding JPDF of the same response components has been reported in Fig. 6.25. These figures show that the level of correlation between the random variables $X^{(r)}(t_j)$ and $X^{(r)}(t_k)$ depends again on the distance between the time instants considered in the analysis. Also for this second example, the comparisons with the same results obtained by MCS performed with 50.000 samples. The multi-time moment $\mathrm{E}[u_6(t_1)\, u_6(t)]$ and the multi-time variance, $\mathrm{Cov}[u_6(t_1), u_6(t)]$ reported in Fig. 6.26 confirm the efficiency of the proposed approach. At last, a computing time-saving of about 80% respect to the MCS has been confirmed, even for this example.

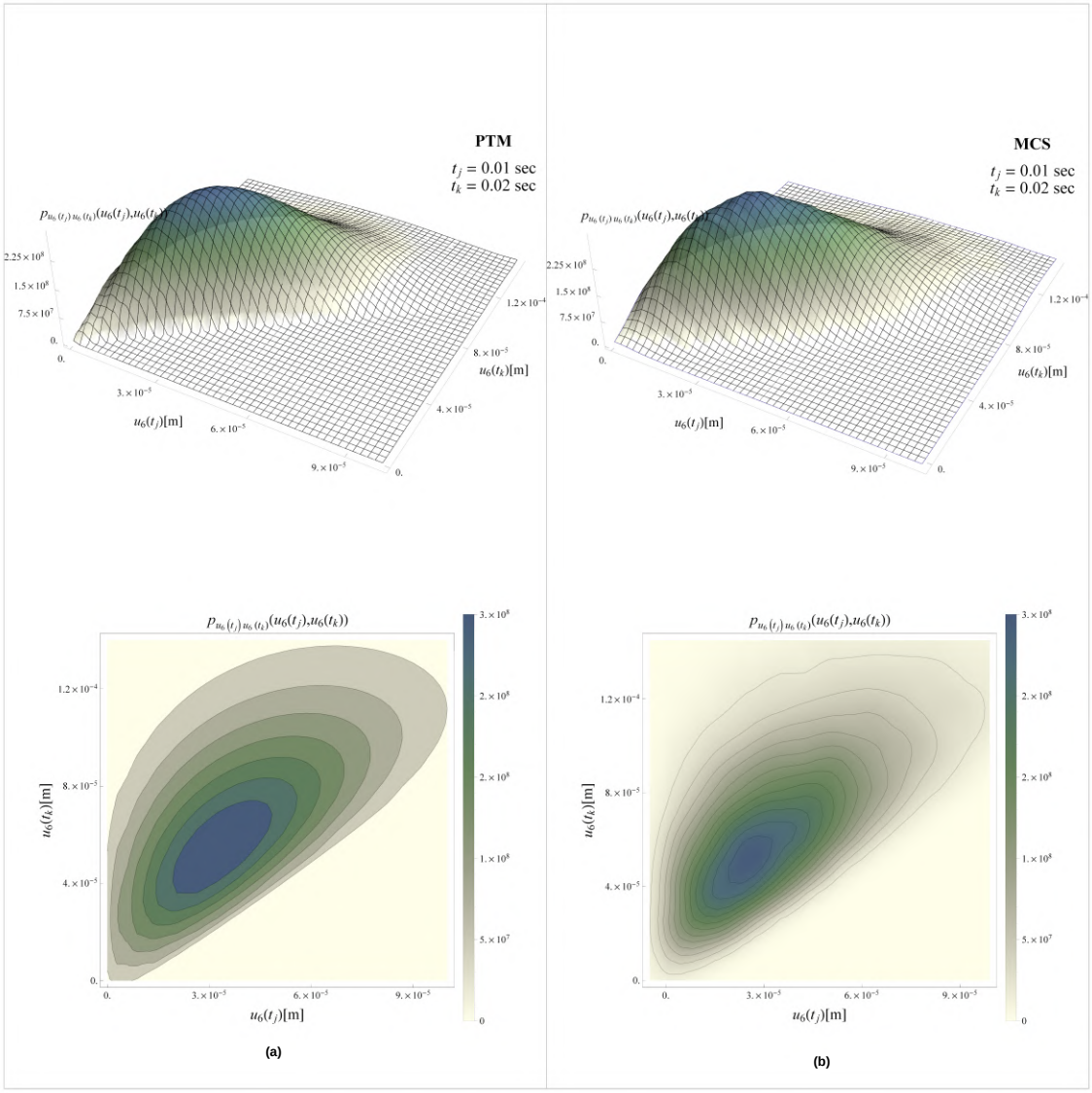

FIGURE 6.21: Example 1: the JPDF of the horizontal displacement of the last floor at two different time instants $t_j = 0.01$ s and $t_j = 0.02$ s. (a) PTM, (b) MCS.

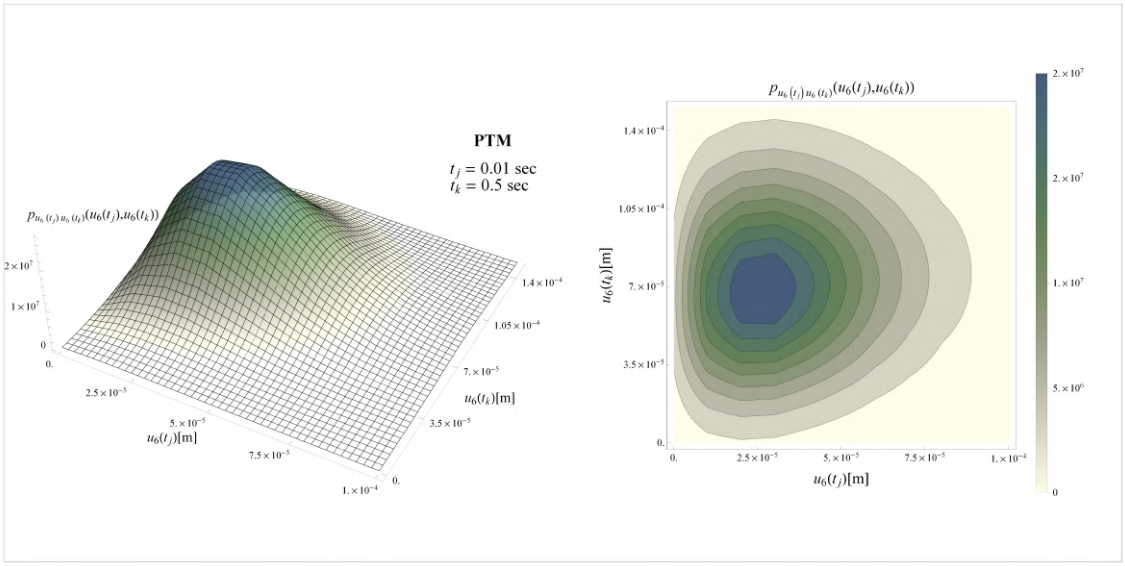

FIGURE 6.22: Example 2: the JPDF of the horizontal displacement of the last floor at two different time instants $t_j = 0.01$ s and $t_j = 0.5$ s. (a) PTM, (b) MCS.

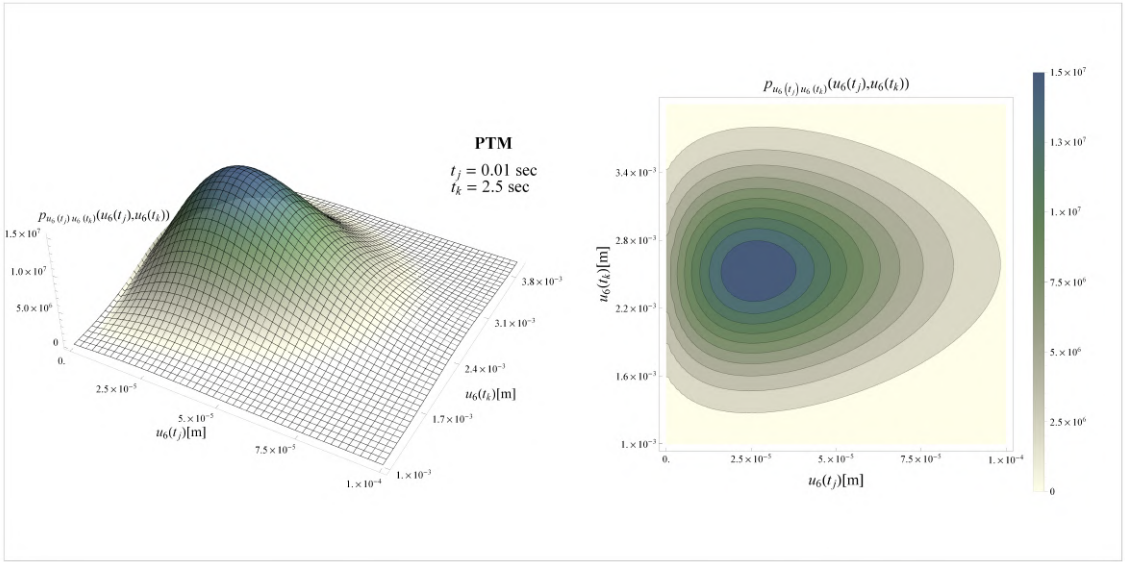

FIGURE 6.23: Example 2: the JPDF of the horizontal displacement of the last floor at two different time instants $t_j = 0.01$ s and $t_j = 2.5$ s.

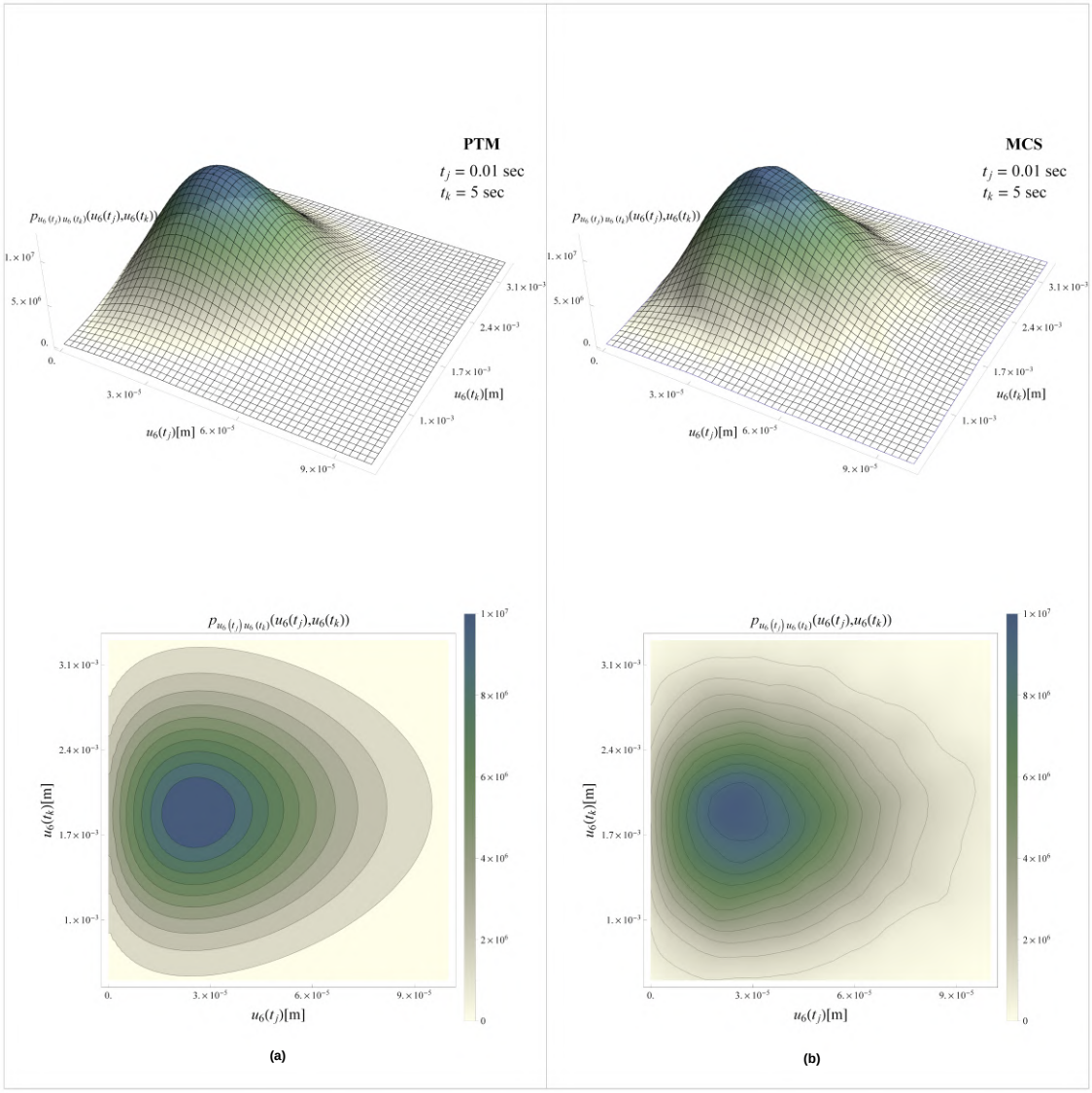

FIGURE 6.24: Example 2: the JPDF of the horizontal displacement of the last floor at two different time instants $t_j = 0.01$ s and $t_j = 5.0$ s.

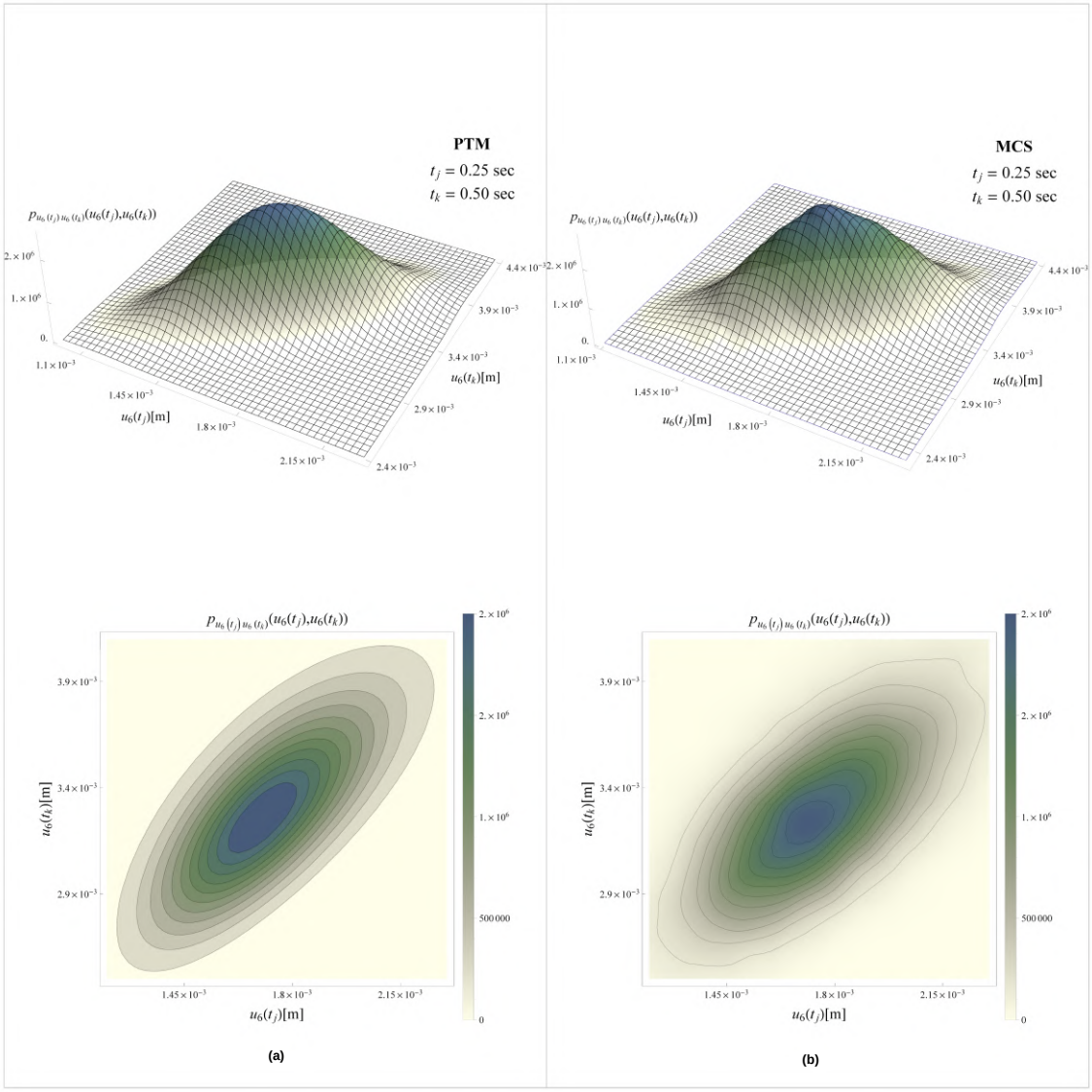

FIGURE 6.25: Example 2: the JPDF of the horizontal displacement of the last floor at two different time instants $t_j = 0.25$ s and $t_j = 0.5$ s. (a) PTM, (b) MCS.

6.3.3 Some remarks

The results of the applications reported in the previous section show the good level of accuracy characterizing the proposed approach, even when the response is clearly non-Gaussian. But it is to be emphasized that the computational effort related to the application of this approach is relatively low, above all if compared with those ones corresponding to the approaches that require the evaluation of the statistical moments at multiple times or of the correlations. The present method can be considered as an extension to the multiple time analysis of the single time approach treated in Section 6.2 that, in turn, is the extension to the dynamic systems of the PTM previously considered for the static case. That this approach can be applied to the study of large scale structures, obviously making some approximation about the number of the degree of freedom on which they are working on. Moreover, they are sure that the approach can be applied to the non-linear systems, too, when the input-output law can be defined.

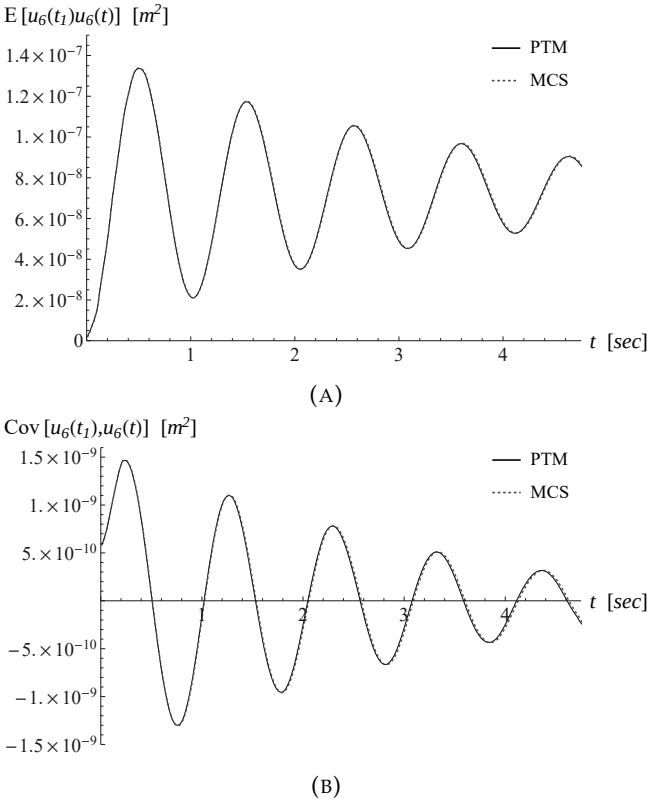

FIGURE 6.26: Example 2: (A) multi-time moment, $\mathrm{E}[u_6(t_1)\, u_6(t)]$; (B) multi-time variance. $\mathrm{Cov}[u_6(t_1), u_6(t)]$.

6.4 Dynamic systems with uncertain parameters

In the dynamic systems of the previous sections, the sources of randomness have been the stochastic excitation and/or the stochastic initial conditions. Taking the multi-degree-of-freedom (MDF) system of Eq. 6.1(a), there may be uncertainty about the appropriate values of the mass (**M**), damping (**C**) and stiffness matrices (**K**). Similarly, in the state-space formulation of the equations of motion (Eq. 6.1(a)), it is possible there is uncertainty about the appropriate values for the **D** matrix and for the **v** vector.

Given the fact that there is almost always uncertainty about the energy dissipation during dynamic motion of a mechanical or structural system, so the components of the **C** matrix may vary significantly from their "design" values (Lutes and Sarkani, 2004). Moreover, there may be significant uncertainty about both mass and stiffness, though, in structural engineering systems, particularly buildings. The mass magnitude and distribution within a building depend on the details of the usage of the building. While a building is in use, the mass distribution can surely be ascertained reasonably well by careful study of the contents, but this can be time-consuming and costly. If one wishes to do a "post mortem" of a building after a disaster, such as an earthquake, there may be much more uncertainty about the mass matrix. Then, probably the greatest uncertainty about the stiffness matrix for a structure has to do with the effect of "nonstructural" components. Testing has shown that partitions within a building do add significant stiffness, at least during small deflections, even though they are not considered load-bearing components (Lutes and Sarkani, 2004).

Therefore, the performance of a dynamical system is a function of the uncertain parameters which constitute the system.
It results from the above that the study of dynamic systems and structures having uncertain parameters leads to handle random differential equations. The term "random differential equations" in general refers to differential equations with random coefficients, having either deterministic or random inhomogeneous parts and initial conditions (Soong, 1973). This section deals with the problem of solving a stochastic differential equation in terms of in time evolutive probability density function. However, it is right to underline that the contents of this section are not new in the literature, but they are the first assumptions underlying the aim of finding a new formulation of an evolutive PTM for linear uncertain systems.

6.4.1 Differential equations with random constant coefficients

Let assume that the system under consideration is random only on its geometrical/mechanical characteristics and let assume that these uncertain properties are defined by the p-vector $\boldsymbol{\theta}$ of random variables. The governing differential equation is written as follows:

$$\dot{\mathbf{X}}(t) = \boldsymbol{A}(\Theta)\mathbf{X}(t) + \mathbf{B}\mathbf{F}(t), \quad \mathbf{X}(t_0) = \mathbf{X}_0 \tag{6.35}$$

where, now, $\mathbf{F}(t)$ is deterministic. The random vector Θ (constant in t) enters the equation through the coefficients, and it is assumed that the joint probability distribution of Θ and the initial condition $\mathbf{X}_0$, is known.
It is easy to show that Eq. 6.35 can be cast in the form of differential equations with only random initial conditions. For this purpose, it is convenient the introduction of the $(n+p)$-th order vector process built as follows:

$$\mathbf{Z}(t) = \begin{pmatrix} \mathbf{X}(t) \\ \Theta \end{pmatrix} \tag{6.36}$$

Consequently, the governing equation (Eq. 6.35) becomes:

$$\dot{\mathbf{Z}}(t) = \mathbf{k}(\mathbf{Z}(t), t); \quad \mathbf{Z}(t_0) = \mathbf{Z}_0 \tag{6.37}$$

where

$$\mathbf{k} = \begin{pmatrix} \boldsymbol{A}(\Theta)\mathbf{X}(t) + \mathbf{B}\mathbf{F}(t) \\ \mathbf{0} \end{pmatrix}; \quad \mathbf{Z}_0 = \begin{pmatrix} \mathbf{X}_0 \\ \Theta \end{pmatrix} \tag{6.38}$$

Here it is important to observe that in terms of $\mathbf{Z}(t)$, Eq. 6.37 describes a vector differential equation where randomness enters only through the initial condition (Soong, 1973). Hence, it is generally possible to determine the statistical properties of the solution process $\mathbf{Z}(t)$, and consequently that of $\mathbf{X}(t)$. An alternate method of solution for Eq. 6.37 is to make use of the fundamental Liouville's theorem in the theory of dynamic systems. This approach, which will be shown in the next subsection, converts the problem to one of solving an initial value problem involving a first-order partial differential equation.

6.4.1.1 Applications of the Liouville equation

For completeness, some preliminary concepts are given below. Let consider the random system described by

$$\dot{\mathbf{X}}(t) = \mathbf{f}(\mathbf{X}(t), t); \quad \mathbf{X}(t_0) = \mathbf{X}_0 \tag{6.39}$$

where the only random element involved is the n-dimensional initial value vector $\mathbf{X}_0$, whose JPDF, $p_{\mathbf{X}_0}(\mathbf{X}_0)$, is known. Assuming that the solution process $\mathbf{X}(t)$ exists, one basic tool for the determination of some of the probability distributions associated with the solution process given the JPDF of $\mathbf{X}_0$, is the Liouville's Theorem.

Theorem 6.4.1 (***Liouville's Theorem***). *Assume that the mean square solution process $\mathbf{X}(t)$ of Eq. 6.39 exists. Then, the joint density function $p_{\mathbf{X}}(\mathbf{x}, t)$ satisfies the Liouville equation*

$$\frac{\partial p_{\mathbf{X}}(\mathbf{x}, t)}{\partial t} + \sum_{j}^{n} \frac{\partial p_{\mathbf{X}}(\mathbf{x}, t)}{\partial x_j} = 0 \tag{6.40}$$

.

Now, taking into account the $(n+p)$-vector process $\mathbf{Z}(t)$ defined by Eq. 6.36, from the Liouville's theorem, the JPDF, $p_{\mathbf{Z}}(\mathbf{z}, t)$ satisfies

$$\frac{\partial p_{\mathbf{Z}}(\mathbf{z}, t)}{\partial t} + \sum_{j}^{n+p} \frac{\partial k_j p_{\mathbf{Z}}(\mathbf{z}, t)}{\partial z_j} = 0 \tag{6.41}$$

The substitution of Eqs. 6.37 into Eq. 6.41 gives

$$\frac{\partial p_{\mathbf{X}\Theta}(\mathbf{x}, \boldsymbol{\theta}, t)}{\partial t} + \sum_{j}^{n} \frac{\partial (\Theta \mathbf{X}(t) + \mathbf{B}\mathbf{F}(t)) p_{\mathbf{X}\Theta}(\mathbf{x}, \boldsymbol{\theta}, t)}{\partial x_j} = 0 \tag{6.42}$$

Eq. 6.42 is satisfied by the joint density function of the solution process $\mathbf{X}(t)$ together with the random coefficient vector Θ. The initial condition associated with Eq. 6.42 is the joint density function of $\mathbf{X}_0$ and Θ, i.e. $p_{\mathbf{X}_0,\Theta}(\mathbf{x}_0, \boldsymbol{\theta})$.
The general solution of Eq. 6.42 is obtained by examining the associated Lagrange system. Following the procedure proposed by Soong, $p_{\mathbf{X}\Theta}(\mathbf{x}, \boldsymbol{\theta}, t)$ is given by

$$p_{\mathbf{X}\Theta}(\mathbf{x}, \boldsymbol{\theta}, t) = p_{\mathbf{X}_0,\Theta}(\mathbf{x}_0, \boldsymbol{\theta}) \exp\left\{ - \int_{t_0}^{t} \nabla p_{\mathbf{X}\Theta}[\mathbf{x} = \mathbf{h}(\mathbf{x}_0, \boldsymbol{\theta}, \tau), \boldsymbol{\theta}, t] d\tau \right\} \Bigg|_{\mathbf{x}_0 = \mathbf{h}^{-1}(\mathbf{x}, \boldsymbol{\theta}, \tau)} \tag{6.43}$$

It is important to say that in general, the procedure presented for the determination of the joint density function of the mean square solution $\mathbf{X}(t)$ presents no conceptual difficulty if the solution of the corresponding deterministic differential equation can be found.

6.5 Conclusion

In this chapter, the suitable applicability of the PTM for the study of the dynamic analyses of structural systems, whose dynamics are characterized by random initial conditions, besides random non-Gaussian actions, has been shown. An approach able to give the single-time varying PDFs of the output for linear structural system subjected to non-Gaussian stochastic process excitations has been developed. Then,

a subsequent approach for the probabilistic characterization of the response at multiple time by the direct evaluation of the corresponding JPDFs has been provided. The applications of the PTM here reported have been confirmed the goodness of the results in terms of evolutive PDF, evidencing, even for the dynamic analyses, good levels of accuracy coupled with a computational effort that is lesser and lesser than that related to MCS. As seen, this chapter does not cover two important classes of dynamic stochastic analyses: a) the nonlinear one for random excitations; b) those related to the uncertain structures. The extension of the PTM on these last two issues is under work and the first assumptions portend possible satisfactory results.

Chapter 7

Conclusions

The research community has become aware that there is a clear need of including uncertainties in the analysis of mechanical and structural systems. In the literature, there are several papers related to the stochastic analysis of structures and, in the last fifty years, many significant results have been obtained in this field.

In this PhD thesis, the use of the probability transformation method (PTM) and of some of its extensions for solving mechanical and structural systems have been addressed. The task of the stochastic analysis of structures is to capture all uncertainties of the system in order to measure how much them influence the out response, which means characterize the structural response from a probabilistic point of view. Unfortunately, a full probabilistic characterization of the response requires a high computational effort, just consider of the evaluation of the response statistical moments or cumulants when the response is a non-Gaussian variable (or process). The PTM introduces a new philosophy in the study of uncertain systems, working directly in terms of input and output PDFs. Operating directly on the response PDF is certainly the easiest and accurate way to do an efficient stochastic analysis.

Several stochastic frameworks have been investigated and a probabilistic approach has been proposed for each framework. Stochastic systems, whose geometric and/or material properties are random, have been analyzed by coupling the PTM with another approach that is the approximated principal deformation mode (APDM) method. An approach able to give the exact probabilistic solution of redundant stochastic beams, when the flexural deformability is random, is proposed. This approach makes the use of the application of the force method for solving the redundancy and of the application of the PTM. The static stochastic analysis of cracked Euler–Bernoulli beams is studied when the cracks are modeled as a rotational internal spring with random amplitude and positions. Then, the PDF of cinematic and static beam stochastic quantities have been found through the application of the PTM. In the context of uncertain structural systems, two practical examples in which the uncertainties in the model designed are due to simplifying assumptions in analytical models and/or simplified methods. In particular, the stochastic analyses carried out through the PTM, allowed to describe the structural response of steel beams and frames with uncertain semi-rigid connections and the effects of the masonry infills uncertainty on the structural response of RC frames. Design considerations have emerged when comparing the presented probability approaches with the deterministic ones based on the average values, the latter could conduct the designer engineer to misguided results. The topic of the local and non-local randomness in stochastic mechanics has been addressed through three research works. Starting from the recent contributions in statistical random filed theory on the fractal dimension and long memory, a link between these two statistical characteristics and the local and non-local randomness in stochastic mechanics is introduced. In particular, the study of the presence of multiscale random properties in Griffith's fracture criterion has

been tackled. Then some examples of statically determinate and redundant stochastic beams, under different conditions of load and constraint when flexural deformability is supposed to be a Gaussian homogeneous RF with correlation functions that capture the fractal and Hurst effects, have been investigated. For both studies, it was possible to make some considerations on the sensitivity of the response quantities to the local and non-local randomness. This thanks to the PTM, which was the tool that has allowed the stochastic analysis, working directly in terms of PDF. At last, models of turbulent atmospheric velocity fields with fractal and Hurst properties have been developed. Although in this last research work the PTM is not applied, however, it has been included in this thesis because it is believed that its contents enrich the topic of the local and non-local randomness, from a physical point of view. An extension of the PTM to the case of dynamical systems has been presented. The main contribution is to provide the definition of an approach that is able to give, instant by instant, a direct relation between the PDFs of input and output of a linear structural system subjected to assigned stochastic process excitations. Then the development of this approach has been presented, which consists of a multi-time probabilistic characterization of the response, necessary if the response probabilistic correlations at various time instants are required. Moreover, this study covers the application of the PTM for the dynamic analyses of structural systems, whose dynamics are characterized by random initial conditions, besides random non-Gaussian actions. Anyway, new formulations of PTM for the cases of nonlinear systems and those related to the uncertain structures are under work.

In conclusion, this PhD thesis collects several research works in which the presented method, the PTM, turned out to be an efficient and easy tool able to perform stochastic analysis in all the studied frameworks.

Bibliography

Abdalla, Khairedin M and Wai-Fah Chen (1995). "Expanded database of semi-rigid steel connections". In: *Computers & Structures* 56.4, pp. 553–564.

Adhikari, Sondipon (2007). "Uncertainty propagation in linear systems: an exact solution using random matrix theory". In: *48th AIAA/ASME/ASCE/AHS/ASC Structures, Structural Dynamics, and Materials Conference*, p. 1957.

Adhikari, Sondipon and CS Manohar (1999). "Dynamic analysis of framed structures with statistical uncertainties". In: *International Journal for Numerical Methods in Engineering* 44.8, pp. 1157–1178.

Adler, Robert J (2010). *The geometry of random fields*. SIAM.

Al-Chaar, Ghassan K (2002). "Evaluating strength and stiffness of unreinforced masonry infill structures". In:

Alibrandi, Umberto (2014). "A response surface method for stochastic dynamic analysis". In: *Reliability Engineering & System Safety* 126, pp. 44–53.

Amanat, Khan Mahmud and Ekramul Hoque (2006). "A rationale for determining the natural period of RC building frames having infill". In: *Engineering structures* 28.4, pp. 495–502.

Amato, G et al. (2008). "Infilled frames: influence of vertical loads on the equivalent diagonal strut model". In: *Proceedings of the 14th World Conference on Earthquake Engineering, Beijing, China*.

Angel, Richard et al. (1994). *Behavior of reinforced concrete frames with masonry infills*. Tech. rep. University of Illinois Engineering Experiment Station. College of ...

Asteris, Panagiotis G (2016). "The FP4026 Research Database on the fundamental period of RC infilled frame structures". In: *Data in brief* 9, pp. 704–709.

Asteris, Panagiotis G et al. (2011). "Mathematical macromodeling of infilled frames: state of the art". In: *Journal of Structural Engineering* 137.12, pp. 1508–1517.

Asteris, Panagiotis G et al. (2013). "Mathematical micromodeling of infilled frames: state of the art". In: *Engineering Structures* 56, pp. 1905–1921.

Asteris, Panagiotis G et al. (2015a). "On the fundamental period of infilled RC frame buildings". In: *Structural Engineering and Mechanics* 54.6, pp. 1175–1200.

Asteris, Panagiotis G et al. (2015b). "Parameters affecting the fundamental period of infilled RC frame structures". In: *Earthquakes and Structures* 9.5, pp. 999–1028.

Asteris, Panagiotis G et al. (2016a). "A macro-modelling approach for the analysis of infilled frame structures considering the effects of openings and vertical loads". In: *Structure and Infrastructure Engineering* 12.5, pp. 551–566.

Asteris, Panagiotis G et al. (2016b). "Prediction of the fundamental period of infilled RC frame structures using artificial neural networks". In: *Computational Intelligence and Neuroscience* 2016.

Asteris, Panagiotis G et al. (2017a). "Fundamental period of infilled RC frame structures with vertical irregularity". In: *Structural Engineering and Mechanics* 61.5, pp. 663–674.

Asteris, PG et al. (2017b). "Numerical modelling of out-of-plane response of infilled frames: State of the art and future challenges for the equivalent strut macromodels". In: *Engineering Structures* 132, pp. 110–122.

Avramidis, Ioannis et al. (2015). *Eurocode-Compliant Seismic Analysis and Design of R/C Buildings*. Springer.

Ayyub, Bilal M (1997). *Uncertainty modeling and analysis in civil engineering*. CRC Press.

Barbato, M and JP Conte (2008). "Spectral characteristics of non-stationary random processes: Theory and applications to linear structural models". In: *Probabilistic engineering mechanics* 23.4, pp. 416–426.

Barbato, Michele and Marcello Vasta (2010). "Closed-form solutions for the time-variant spectral characteristics of non-stationary random processes". In: *Probabilistic engineering mechanics* 25.1, pp. 9–17.

Batchelor, G. K. (1953). *The Theory of Homogeneous Turbulence*. Cambridge University Press.

Bazan, Enrique and Roberto Meli (1980). "Seismic analysis of structures with masonry walls". In: *Memorias, 7th World Conference on Earthquake Engineering, Estambul, Turquía*. Vol. 5, pp. 633–640.

Benjamin, Jack R and Harry A Williams (1957). "The behavior of one-story reinforced concrete shear walls". In: *Journal of the Structural Division* 83.3, pp. 1–49.

— (1958). "Blast and earthquake resistant design data: behavior of one-story reinforced concrete shear walls containing openings". In: *Journal Proceedings*. Vol. 55. 11, pp. 605–618.

Beran, J. (1994). *Statistics for Long-Memory Processes*. Chapman and Hall, New York.

Beran, Jan (2017). *Statistics for Long-Memory Processes (Abingdon*.

Berg, C., J. Mateu, and E. Porcu (2008). "The Dagum family of isotropic correlation functions". In: *Bernoulli* 14.4, pp. 1134–1149.

Bevilacqua, M. and T. Faouzi (2019). "Estimation and prediction of Gaussian processes using generalized Cauchy covariance model under fixed domain asymptotics". In: *Electron J Statist* 13.2, pp. 3025–3048.

Bilello, C (2001). "Theoretical and experimental investigation on damaged beams under moving systems [Ph. D. thesis]". In: *Università degli Studi di Palermo, Palermo, Italy*.

Bingham, Nicholas H, Charles M Goldie, and Jef L Teugels (1989). *Regular variation*. Vol. 27. Cambridge university press.

Bjorhovde, Reidar, Andre Colson, and Jacques Brozzetti (1990). "Classification system for beam-to-column connections". In: *Journal of Structural Engineering* 116.11, pp. 3059–3076.

Borchers, H. W. (2018). *Practical Numerical Math Routines,R Package Version 2.1.8*.

Bucher, CG and GI Schueller (1991). "Non-Gaussian response of linear systems". In: *Structural Dynamics*. Springer, pp. 103–127.

Cacciola, Pierfrancesco and Giuseppe Muscolino (2002). "Dynamic response of a rectangular beam with a known non-propagating crack of certain or uncertain depth". In: *Computers & structures* 80.27-30, pp. 2387–2396.

Caddemi, S and I Calio (2008). "Exact solution of the multi-cracked Euler–Bernoulli column". In: *International Journal of Solids and Structures* 45.5, pp. 1332–1351.

— (2009). "Exact closed-form solution for the vibration modes of the Euler–Bernoulli beam with multiple open cracks". In: *Journal of Sound and Vibration* 327.3-5, pp. 473–489.

Caddemi, S and I Caliò (2013). "The exact explicit dynamic stiffness matrix of multi-cracked Euler–Bernoulli beam and applications to damaged frame structures". In: *Journal of Sound and Vibration* 332.12, pp. 3049–3063.

Calatayud, J, J-C Cortes, and M Jornet (2018). "On the approximation of the probability density function of the randomized heat equation". In: *arXiv preprint arXiv:1802.04190*.

Calatayud, J, J-C Cortés, and M Jornet (2018). "The damped pendulum random differential equation: A comprehensive stochastic analysis via the computation of the probability density function". In: *Physica A: Statistical Mechanics and its Applications* 512, pp. 261–279.

Cavaleri, L, M Fossetti, and M Papia (2005). "Infilled frames: developments in the evaluation of cyclic behaviour under lateral loads". In: *Structural Engineering and Mechanics* 21.4, pp. 469–494.

Çavdar, Özlem et al. (2009). "Stochastic finite element analysis of structural systems with partially restrained connections subjected to seismic loads". In:

CEN, EN (2005). *Eurocode 3: Design of steel structures*.

Challamel, Noël (2018). "Static and dynamic behaviour of nonlocal elastic bar using integral strain-based and peridynamic models". In: *Comptes Rendus Mécanique* 346.4, pp. 320–335.

Chamorro, L. P. et al. (2015). "Turbulence effects on a full-scale 2.5 MW horizontal-axis wind turbine under neutrally stratified conditions". In: *Wind Energy* 18.2, pp. 339–349.

Chandrasekaran, AR and Brijesh Chandra (1970). "Experimental study of infilled frames". In: *Proceedings of the 4th Symposium on Earthquake Engineering, Roorkee UP, India*, pp. 75–80.

Chen, Jian-Bing and Jie Li (2007). "The extreme value distribution and dynamic reliability analysis of nonlinear structures with uncertain parameters". In: *Structural Safety* 29.2, pp. 77–93.

Chen, Wai-Fah (2011). *Semi-rigid connections handbook*. J. Ross Publishing.

Chen, Wai-Fah and Eric M Lui (1987). "Effects of joint flexibility on the behavior of steel frames". In: *Computers & Structures* 26.5, pp. 719–732.

Chiorean, CG (2009). "A computer method for nonlinear inelastic analysis of 3D semi-rigid steel frameworks". In: *Engineering Structures* 31.12, pp. 3016–3033.

Cicirello, Alice and Alessandro Palmeri (2014). "Static analysis of Euler–Bernoulli beams with multiple unilateral cracks under combined axial and transverse loads". In: *International Journal of Solids and Structures* 51.5, pp. 1020–1029.

Conte, Joel P and B-F Peng (1996). "An explicit closed-form solution for linear systems subjected to nonstationary random excitation". In: *Probabilistic Engineering Mechanics* 11.1, pp. 37–50.

Council, Applied Technology and Partnership for Response (1999). *Evaluation of Earthquake Damaged Concrete and Masonry Wall Buildings: Basic Procedures Manual*. The Agency.

Council, Building Seismic Safety (1997). *NEHRP Commentary on the Guidelines for the Seismic Rehabilitation of Buildings (FEMA Publication 274)*.

Crisafulli, Francisco J, Athol J Carr, and Robert Park (2000). "Analytical modelling of infilled frame structures". In: *Bulletin of the New Zealand society for earthquake engineering* 33.1, pp. 30–47.

Crisafulli, Francisco Javier (1997). "Seismic behaviour of reinforced concrete structures with masonry infills". In:

Crowley, H and R Pinho (2004). "Period-height relationship for existing European reinforced concrete buildings". In: *Journal of Earthquake Engineering* 8.spec01, pp. 93–119.

Crowley, Helen and Rui Pinho (2006). "Simplified equations for estimating the period of vibration of existing buildings". In: *First European conference on earthquake engineering and seismology*. Vol. 1122.

Daley, D. and E. Porcu (2014). "Dimension walks and Schoenberg spectral measures". In: *P Am Math Soc* 142.5, pp. 1813–1824.

Dawe, JL, AB Schriver, and C Sofocleous (1989). "Masonry infilled steel frames subjected to dynamic load". In: *Canadian Journal of Civil Engineering* 16.6, pp. 877–885.

De Domenico, D (2015). "RC members strengthened with externally bonded FRP plates: A FE-based limit analysis approach". In: *Composites Part B: Engineering* 71, pp. 159–174.

De Domenico, D, AA Pisano, and P Fuschi (2014). "A FE-based limit analysis approach for concrete elements reinforced with FRP bars". In: *Composite Structures* 107, pp. 594–603.

De Domenico, D et al. (2014). "Strengthening of steel-reinforced concrete structural elements by externally bonded FRP sheets and evaluation of their load carrying capacity". In: *Composite Structures* 118, pp. 377–384.

De Domenico, Dario, Giovanni Falsone, and Rossella Laudani (2018a). "In-plane response of masonry infilled RC framed structures: A probabilistic macromodeling approach". In: *Structural Engineering and Mechanics* 68.4, pp. 423–442.

— (2018b). "Probability-based structural response of steel beams and frames with uncertain semi-rigid connections". In: *Structural Engineering and Mechanics* 67.5, pp. 439–455.

Demmie, PN and M Ostoja-Starzewski (2016). "Local and nonlocal material models, spatial randomness, and impact loading". In: *Archive of Applied Mechanics* 86.1-2, pp. 39–58.

Di Paola, M and G Falsone (1997a). "Higher order statistics of the response of MDOF linear systems excited by linearly parametric white noises and external excitations". In: *Probabilistic engineering mechanics* 12.3, pp. 179–188.

— (1997b). "Higher order statistics of the response of MDOF linear systems under polynomials of filtered normal white noises". In: *Probabilistic engineering mechanics* 12.3, pp. 189–196.

Di Paola, M, G Falsone, and A Pirrotta (1992). "Stochastic response analysis of non-linear systems under Gaussian inputs". In: *Probabilistic engineering mechanics* 7.1, pp. 15–21.

Di Paola, Mario and Giovanni Falsone (1994). "Non-linear oscillators under parametric and external Poisson pulses". In: *Nonlinear Dynamics* 5.3, pp. 337–352.

Dolce, Mauro et al. (2005). "Shaking table tests on reinforced concrete frames without and with passive control systems". In: *Earthquake engineering & structural dynamics* 34.14, pp. 1687–1717.

Doostan, Alireza, Roger G Ghanem, and John Red-Horse (2007). "Stochastic model reduction for chaos representations". In: *Computer methods in applied mechanics and engineering* 196.37-40, pp. 3951–3966.

Doven, Mahmud Sami and Ugur Kafkas (2017). "Micro modelling of masonry walls by plane bar elements for detecting elastic behavior". In: *Struct. Eng. Mech* 62.5, pp. 643–649.

Elishakoff, I, N Impollonia, and YJ Ren (1999). "New exact solutions for randomly loaded beams with stochastic flexibility". In: *International journal of solids and structures* 36.16, pp. 2325–2340.

Elishakoff, I, YJ Ren, and M Shinozuka (1995a). "Improved finite element method for stochastic problems". In: *Chaos, Solitons & Fractals* 5.5, pp. 833–846.

— (1995b). "Some exact solutions for the bending of beams with spatially stochastic stiffness". In: *International Journal of Solids and Structures* 32.16, pp. 2315–2327.

Erdolen, Ayse and Bilge Doran (2012). "Interval finite element analysis of masonry-infilled walls". In: *Structural Engineering and Mechanics* 44.1, pp. 73–84.

Eringen, A Cemal (1983). "On differential equations of nonlocal elasticity and solutions of screw dislocation and surface waves". In: *Journal of applied physics* 54.9, pp. 4703–4710.

Esteva, Luis (1966). "Behavior under alternating loads of masonry diaphragms framed by reinforced concrete members". In: *Proc. International Symposium on the Effects of Repeated Loading of Materials and Structures. RILEM, México City*.

Falsone, G (2002). "The use of generalised functions in the discontinuous beam bending differential equations". In: *International Journal of Engineering Education* 18.3, pp. 337–343.

Falsone, G and N Impollonia (2004). "About the accuracy of a novel response surface method for the analysis of finite element modeled uncertain structures". In: *Probabilistic engineering mechanics* 19.1-2, pp. 53–63.

Falsone, G and R Laudani (2019a). "Matching the principal deformation mode method with the probability transformation method for the analysis of uncertain systems". In: *International Journal for Numerical Methods in Engineering* 118.7, pp. 395–410.

Falsone, G. and R. Laudani (2020a). "The concept of local and non-local randomness for some mechanical problems". In: *Planned Anniversary Volume in honour of Professor Isaac Elishakoff, Manuscript submitted for publication*.

Falsone, G and Rossella Laudani (2019b). "Exact response probability density functions of some uncertain structural systems". In: *Archives of Mechanics* 71.4-5, pp. 315–336.

— (2020b). "Closed-form solutions of redundantly constrained stochastic bending beams". In: *submitted in Probabilistic Engineering Mechanics* 191, pp. 243–253.

Falsone, G and D Settineri (2011a). "A method for the random analysis of linear systems subjected to non-stationary multi-correlated loads". In: *Probabilistic engineering mechanics* 26.3, pp. 447–453.

— (2011b). "New differential equations governing the response cross-correlations of linear systems subjected to coloured loads". In: *Journal of Sound and Vibration* 330.12, pp. 2910–2927.

— (2013a). "Explicit solutions for the response probability density function of linear systems subjected to random static loads". In: *Probabilistic Engineering Mechanics* 33, pp. 86–94.

— (2013b). "Explicit solutions for the response probability density function of nonlinear transformations of static random inputs". In: *Probabilistic Engineering Mechanics* 33, pp. 79–85.

Falsone, Giovanni (1994). "Cumulants and correlations for linear systems under non-stationary delta-correlated processes". In: *Probabilistic engineering mechanics* 9.3, pp. 157–165.

— (2005). "An extension of the Kazakov relationship for non-Gaussian random variables and its use in the non-linear stochastic dynamics". In: *Probabilistic Engineering Mechanics* 20.1, pp. 45–56.

Falsone, Giovanni and Nicola Impollonia (2002). "A new approach for the stochastic analysis of finite element modelled structures with uncertain parameters". In: *Computer Methods in Applied Mechanics and Engineering* 191.44, pp. 5067–5085.

Falsone, Giovanni and Rossella Laudani (2018). "A probability transformation method (PTM) for the dynamic stochastic response of structures with non-Gaussian excitations". In: *Engineering Computations*.

— (2020c). "Multi-time probability density functions of the dynamicnon-Gaussian response of structures". In: *Structural Engineering and Mechanics*.

Felice, Gianmarco De and Renato Giannini (2001). "Out-of-plane seismic resistance of masonry walls". In: *Journal of earthquake engineering* 5.02, pp. 253–271.

Fernández-Sáez, J et al. (2016). "Bending of Euler–Bernoulli beams using Eringen's integral formulation: a paradox resolved". In: *International Journal of Engineering Science* 99, pp. 107–116.

Field Jr, RV and M Grigoriu (2004). "On the accuracy of the polynomial chaos approximation". In: *Probabilistic Engineering Mechanics* 19.1-2, pp. 65–80.

Flanagan, Roger D and Richard M Bennett (1999). "Bidirectional behavior of structural clay tile infilled frames". In: *Journal of structural engineering* 125.3, pp. 236–244.

Gdoutos, EE (1993). "Fracture Mechanics-An Introduction, Kluwer Academic Publishers". In:

Ghanem, Roger G and Robert M Kruger (1996). "Numerical solution of spectral stochastic finite element systems". In: *Computer methods in applied mechanics and engineering* 129.3, pp. 289–303.

Ghanem, Roger G and Pol D Spanos (2003). *Stochastic finite elements: a spectral approach*. Courier Corporation.

Ghavanloo, Esmaeal, Hashem Rafii-Tabar, and Seyed Ahmad Fazelzadeh (2019). "Essential concepts from nonlocal elasticity theory". In: *Computational Continuum Mechanics of Nanoscopic Structures*. Springer, pp. 61–86.

Gioffrè, Massimiliano and Vittorio Gusella (2002). "Numerical analysis of structural systems subjected to non-Gaussian random fields". In: *Meccanica* 37.1-2, pp. 115–128.

Giraitis, L., H. L. Koul, and D. Surgailis (2012). *Large Sample Inference for Long Memory Processes*. Chapman and Hall/CRC.

Gneiting, T. (2000). "Power-law correlations, related models for long-range dependence and their simulation". In: *J Appl Probab* 37.4, pp. 1104–1109.

Gneiting, T. and M. Schlather (2004a). "Stochastic models that separate fractal dimension and the hurst effect". In: *Siam Rev* 46.2, pp. 269–282.

Gneiting, Tilmann, William Kleiber, and Martin Schlather (2010). "Matérn cross-covariance functions for multivariate random fields". In: *Journal of the American Statistical Association* 105.491, pp. 1167–1177.

Gneiting, Tilmann and Martin Schlather (2004b). "Stochastic models that separate fractal dimension and the Hurst effect". In: *SIAM review* 46.2, pp. 269–282.

Gneiting, Tilmann, Hana Ševčíková, and Donald B Percival (2012). "Estimators of fractal dimension: Assessing the roughness of time series and spatial data". In: *Statistical Science*, pp. 247–277.

Graham, Alexander (2018). *Kronecker products and matrix calculus with applications*. Courier Dover Publications.

Hadianfard, MA and R Razani (2003). "Effects of semi-rigid behavior of connections in the reliability of steel frames". In: *Structural Safety* 25.2, pp. 123–138.

Hall, Peter and Andrew Wood (1993). "On the performance of box-counting estimators of fractal dimension". In: *Biometrika* 80.1, pp. 246–251.

Hendry, Arnold W (1981). *Structural brickwork*. Springer.

Hurtado, JE and Alex H Barbat (1998). "Monte Carlo techniques in computational stochastic mechanics". In: *Archives of Computational Methods in Engineering* 5.1, p. 3.

Hussein, Abdallah and Mustafa M Selim (2015). "Solution of the stochastic generalized shallow-water wave equation using RVT technique". In: *The European Physical Journal Plus* 130.12, p. 249.

Jaw, SY and CJ Chen (1999). "Near-wall turbulence modeling using fractal dimensions". In: *Journal of engineering mechanics* 125.7, pp. 804–811.

Jones, Stephen Wynford, PA Kirby, and DA Nethercort (1983). "The analysis of frames with semi-rigid connections—a state-of-the-art report". In: *Journal of Constructional Steel Research* 3.2, pp. 2–13.

Kahn, Herman (1955). "Use of different Monte Carlo sampling techniques". In:

Kalogeris, Ioannis and Vissarion Papadopoulos (2018). "Limit analysis of stochastic structures in the framework of the probability density evolution method". In: *Engineering Structures* 160, pp. 304–313.

Kamiński, Marcin (2007). "Generalized perturbation-based stochastic finite element method in elastostatics". In: *Computers & structures* 85.10, pp. 586–594.

Kamiński, Marcin (2010). "Generalized stochastic perturbation technique in engineering computations". In: *Mathematical and computer modelling* 51.3-4, pp. 272–285.

Kaminski, Marcin (2013). *The stochastic perturbation method for computational mechanics*. John Wiley & Sons.

Kartal, ME et al. (2010). "Effects of semi-rigid connection on structural responses". In: *Electronic journal of structural Engineering* 10.10, pp. 22–35.

Kheirollahi, Mohammad (2013). "Equivalent frame model and shell element for modeling of in-plane behavior of Unreinforced Brick Masonry buildings". In: *Structural Engineering and Mechanics* 46.2, pp. 213–229.

Khoshnoud, Hamid Reza and Kadir Marsono (2016). "Experimental study of masonry infill reinforced concrete frames with and without corner openings". In: *Structural Engineering and Mechanics* 57.4, pp. 641–656.

Kim, Seung-Eock and Se-Hyu Choi (2001). "Practical advanced analysis for semirigid space frames". In: *International journal of solids and structures* 38.50-51, pp. 9111–9131.

Kishi, N and Wai-Fah Chen (1990). "Moment-rotation relations of semirigid connections with angles". In: *Journal of Structural Engineering* 116.7, pp. 1813–1834.

Kleiber, Michał and Tran Duong Hien (1992). *The stochastic finite element method: basic perturbation technique and computer implementation*. Wiley.

Klingner, Richard Evans and V Bertero (1977). "Infilled frames in earthquake-resistant construction". PhD thesis. University of California, Berkeley.

Laudani, Rossella and Giovanni Falsone (2020). "The use of the probability transformation method in some random mechanic problems". In: *Special Issue on Advances on Efficient Numerical Methods for Risk and Reliability Analysis of Large Engineering Structures*.

Laudani, Rossella and Martin Ostoja-Starzewski (2020). "Fracture of beams with random field properties: Fractal and Hurst effects". In: *International Journal of Solids and Structures* 191, pp. 243–253.

Laudani, Rossella et al. (2020). "Empirical velocity spectra with fractal and long-memory effects". In: *Journal of Fluid Mechanics, Manuscript submitted for publication*.

Li, Jie (2016). "Probability density evolution method: background, significance and recent developments". In: *Probabilistic Engineering Mechanics* 44, pp. 111–117.

Li, Jie and Jianbing Chen (2009). *Stochastic dynamics of structures*. John Wiley & Sons.

Lim, S. C. and L. P. Teo (2009). "Generalized Whittle–Matérn random field as a model of correlated fluctuations". In: *J Phys A-Math Theor* 42.10, pp. 105–202.

Lin, YK (1967a). *Probabilistic theory of structural dynamics*. New York: McGraw-Hill.

Lin, Yu-Kweng (1967b). "Probabilistic theory of structural dynamics(Book on probabilistic theory of structural dynamics, analyzing responses of structures to random vibrations)". In: *NEW YORK, MCGRAW-HILL BOOK CO., 1967. 366 P*.

Liu, Wing Kam, A Mani, and Ted Belytschko (1987). "Finite element methods in probabilistic mechanics". In: *Probabilistic Engineering Mechanics* 2.4, pp. 201–213.

Liu, Zhangjun and Zenghui Liu (2018). "Random function representation of stationary stochastic vector processes for probability density evolution analysis of wind-induced structures". In: *Mechanical Systems and Signal Processing* 106, pp. 511–525.

Lutes, Loren D and Shahram Sarkani (2004). *Random vibrations: analysis of structural and mechanical systems*. Butterworth-Heinemann.

Mainstone, Rowland J (1974). *Supplementary note on the stiffnesses and strengths of infilled frames*. Building Research Establishment, Building Research Station.

Makarios, Triantafyllos K (2012). "Evaluating the effective spectral seismic amplification factor on a probabilistic basis". In: *Structural Engineering and Mechanics* 42.1, pp. 121–129.

Malyarenko, A. and M. Ostoja-Starzewski (2019). *Tensor-Valued Random Fields for Continuum Physics*. Cambridge University Press.

Mamis, KI, GA Athanassoulis, and ZG Kapelonis (2019). "A systematic path to non-Markovian dynamics: new response probability density function evolution equations under Gaussian coloured noise excitation". In: *Proceedings of the Royal Society A* 475.2226, p. 20180837.

Mandelbrot, BB (1982). "The fractal geometry of nature WH Freeman and Co". In: *New York*.

Mann, J. (1994). "The spatial strcuture of neutral atmospheric surface-layer turbulence". In: *J Fluid Mech* 273, pp. 141–168.

Matérn, Bertil (1986). *Spatial variation, volume 36 of Lecture Notes in Statistics*.

Mateu, J., E. Porcu, and O. Nicolis (2007a). "A note on decoupling of local and global behaviours for the Dagum random field". In: *Probabilist Eng Mech* 22.4, pp. 320–329.

Mateu, Jorge, E Porcu, and O Nicolis (2007b). "A note on decoupling of local and global behaviours for the Dagum random field". In: *Probabilistic Engineering Mechanics* 22.4, pp. 320–329.

Matthies, Hermann G et al. (1997a). "Uncertainties in probabilistic numerical analysis of structures and solids-stochastic finite elements". In: *Structural safety* 19.3, pp. 283–336.

— (1997b). "Uncertainties in probabilistic numerical analysis of structures and solids-stochastic finite elements". In: *Structural safety* 19.3, pp. 283–336.

Mazelsky, Bernard (1954). "Extension of Power Spectral Methods of Generalized Harmonic Analysis to Determine Non-Gaussian Probabilitv Functions of Random Input Disturbances and Output Responses of Linear Systems". In: *Journal of the Aeronautical Sciences* 21.3, pp. 145–153.

Mehrabi, Armin B et al. (1994). "Performance of masonry-infilled R/C frames under in-plane lateral loads". In: *Structural engineering and structural mechanics research series*.

Meimaris, Antonios T, Ioannis A Kougioumtzoglou, and Athanasios A Pantelous (2018). "A closed form approximation and error quantification for the response transition probability density function of a class of stochastic differential equations". In: *Probabilistic Engineering Mechanics* 54, pp. 87–94.

Metropolis, Nicholas and Stanislaw Ulam (1949). "The monte carlo method". In: *Journal of the American statistical association* 44.247, pp. 335–341.

Milani, Gabriele and Denis Benasciutti (2010). "Homogenized limit analysis of masonry structures with random input properties: polynomial response surface approximation and Monte Carlo simulations". In: *Structural Engineering and Mechanics* 34.4, pp. 417–447.

Morikawa, Hitoshi and Hiroyuki Kameda (1997). "Stochastic interpolation of earthquake ground motions under spectral uncertainties". In: *Structural Engineering and Mechanics* 5.6, pp. 839–851.

Obreimoff, JW (1930). "The splitting strength of mica". In: *Proceedings of the Royal Society of London. Series A, Containing Papers of a Mathematical and Physical Character* 127.805, pp. 290–297.

Ostoja-Starzewski, M (2004). "Fracture of brittle microbeams". In: *J. Appl. Mech.* 71.3, pp. 424–427.

Ostoja-Starzewski, M. (2007). *Microstructural Randomness and Scaling in Mechanics of Materials*. World Scientific Publishing Company.

Palmeri, Alessandro and Alice Cicirello (2011). "Physically-based Dirac's delta functions in the static analysis of multi-cracked Euler–Bernoulli and Timoshenko beams". In: *International Journal of Solids and Structures* 48.14-15, pp. 2184–2195.

Papadrakakis, Manolis and Vissarion Papadopoulos (1996). "Robust and efficient methods for stochastic finite element analysis using Monte Carlo simulation". In: *Computer Methods in Applied Mechanics and Engineering* 134.3-4, pp. 325–340.

Papoulis, A. and S. U. Pillai (2001). *Probability, Random Variables and Stochastic Processes. 4th ed.* McGraw-Hill, Boston.

Papoulis, Athanasios and S Unnikrishna Pillai (2002). *Probability, random variables, and stochastic processes*. Tata McGraw-Hill Education.

Pasca, Monica, Laura Liberatore, and Renato Masiani (2017). "Reliability of analytical models for the prediction of out-of-plane capacity of masonry infills". In: *Structural Engineering and Mechanics* 64.6, pp. 765–781.

Pellissetti, Manuel F and Roger G Ghanem (2000). "Iterative solution of systems of linear equations arising in the context of stochastic finite elements". In: *Advances in Engineering Software* 31.8-9, pp. 607–616.

Pisano, AA, P Fuschi, and D De Domenico (2013a). "A kinematic approach for peak load evaluation of concrete elements". In: *Computers & Structures* 119, pp. 125–139.

— (2013b). "Peak loads and failure modes of steel-reinforced concrete beams: predictions by limit analysis". In: *Engineering Structures* 56, pp. 477–488.

— (2015). "Numerical limit analysis of steel-reinforced concrete walls and slabs". In: *Computers & Structures* 160, pp. 42–55.

Pisano, Aurora Angela, P Fuschi, and D De Domenico (2014). "LIMIT STATE EVALUATION OF STEEL-REINFORCED CONCRETE ELEMENTS BY VON MISES AND MENÉTREY–WILLAM-TYPE YIELD CRITERIA". In: *International Journal of Applied Mechanics* 6.05, p. 1450058.

Polyakov, SV (1960). "On the interaction between masonry filler walls and enclosing frame when loaded in the plane of the wall". In: *Translations in earthquake engineering* 2.3, pp. 36–42.

Porcu, E et al. (2007). "Modelling spatio-temporal data: A new variogram and covariance structure proposal". In: *Statistics & probability letters* 77.1, pp. 83–89.

Pradlwarter, HJ and GI Schuëller (2010). "Local domain monte carlo simulation". In: *Structural Safety* 32.5, pp. 275–280.

Proppe, C, HJ Pradlwarter, and GI Schuëller (2003). "Equivalent linearization and Monte Carlo simulation in stochastic dynamics". In: *Probabilistic Engineering Mechanics* 18.1, pp. 1–15.

Rauscher, Thomas R and Kurt H Gerstle (1992). "Reliability of rotational behavior of framing connections". In: *Eng. J. AISC* 29.1, pp. 12–9.

Roberts, John Brian and Pol D Spanos (2003). *Random vibration and statistical linearization*. Courier Corporation.

Sachdeva, Sachin K, Prasanth B Nair, and Andy J Keane (2006). "Comparative study of projection schemes for stochastic finite element analysis". In: *Computer Methods in Applied Mechanics and Engineering* 195.19-22, pp. 2371–2392.

Sakurai, Shuji, Bruce R Ellingwood, and Shigeru Kushiyama (2001). "Probabilistic study of the behavior of steel frames with partially restrained connections". In: *Engineering structures* 23.11, pp. 1410–1417.

Santoro, Roberta, Giuseppe Failla, and Giuseppe Muscolino (2020). "INTERVAL STATIC ANALYSIS OF MULTI-CRACKED BEAMS WITH UNCERTAIN SIZE AND POSITION OF CRACKS". In: *Applied Mathematical Modelling*.

Santoro, Roberta and Giuseppe Muscolino (2019). "Dynamics of beams with uncertain crack depth: stochastic versus interval analysis". In: *Meccanica* 54.9, pp. 1433–1449.

Schlather, M. (2015). *Random Fields: Simulation and Analysis of Random Fields*. R Package Version 3.1.50.

Schuëller, Gerhart I and HJ Pradlwarter (2009). "Uncertain linear systems in dynamics: Retrospective and recent developments by stochastic approaches". In: *Engineering Structures* 31.11, pp. 2507–2517.

Schuëller, Gerhart I et al. (1989). "On efficient computational schemes to calculate structural failure probabilities". In: *Probabilistic Engineering Mechanics* 4.1, pp. 10–18.

Scotti, Alberto, Charles Meneveau, and Seyed G Saddoughi (1995). "Fractal dimension of velocity signals in high-Reynolds-number hydrodynamic turbulence". In: *Physical Review E* 51.6, p. 5594.

Segalini, A. et al. (2015). "A spectral model of stably stratified surface-layer turbulence". In: *J Phys Conf Ser*. Vol. 625. 1. IOP Publishing, p. 012003.

Sekulovic, Miodrag and Ratko Salatic (2001). "Nonlinear analysis of frames with flexible connections". In: *Computers & Structures* 79.11, pp. 1097–1107.

Settineri, D and G Falsone (2014). "A method for the evaluation of the response probability density function of some linear dynamic systems subjected to non-Gaussian random load". In: *Probabilistic Engineering Mechanics* 38, pp. 165–172.

Shen, L., M. Ostoja-Starzewski, and E. Porcu (2015a). "Harmonic oscillator driven by random processes having fractal and Hurst effects". In: *Acta Mech* 226.11, pp. 3653–3672.

Shen, Lihua, Martin Ostoja-Starzewski, and Emilio Porcu (2015b). "Harmonic oscillator driven by random processes having fractal and Hurst effects". In: *Acta Mechanica* 226.11, pp. 3653–3672.

Simoes, LMC (1996). "Optimization of frames with semi-rigid connections". In: *Computers & structures* 60.4, pp. 531–539.

Soong, TT (1973). *Random Differential Equations in Science and Engineering. 1973*.

Stein, M. (1999). *Interpolation of Spatial Data: Some Theory of Kriging*. Springer, New York.

Tangaramvong, S et al. (2016). "Interval analysis of nonlinear frames with uncertain connection properties". In: *International Journal of Non-Linear Mechanics* 86, pp. 83–95.

Tarasov, Vasily E (2007). "Liouville and Bogoliubov equations with fractional derivatives". In: *Modern physics letters B* 21.05, pp. 237–248.

Tarque, Nicola et al. (2015). "Masonry infilled frame structures: state-of-the-art review of numerical modelling". In: *Earthquakes and structures* 8.3, pp. 733–759.

Te-Chang, Liauw and Kwan Kwok-Hung (1984). "Nonlinear behaviour of non-integral infilled frames". In: *Computers & structures* 18.3, pp. 551–560.

Thai, Huu-Tai et al. (2016). "System reliability evaluation of steel frames with semi-rigid connections". In: *Journal of Constructional Steel Research* 121, pp. 29–39.

Todaro, Vincenzo (2008). "Nuove norme tecniche per le costruzioni". In: *Exeo Edizioni, Piove di Sacco*.

Turcotte, Donald L (1997). *Fractals and chaos in geology and geophysics*. Cambridge university press.

Valiasis, TN and KC Stylianidis (1989). "Masonry infilled R/C frames under horizontal loading—experimental results". In: *European Earthquake Engineering* 3.3, pp. 10–20.

Vanmarcke, Erik (2010). *Random fields: analysis and synthesis*. World scientific.

Wu, WF and YK Lin (1984). "Cumulant-neglect closure for non-linear oscillators under random parametric and external excitations". In: *International Journal of Non-Linear Mechanics* 19.4, pp. 349–362.

Yamazaki, Fumio, Masanobu Shinozuka, and Gautam Dasgupta (1988). "Neumann expansion for stochastic finite element analysis". In: *Journal of engineering mechanics* 114.8, pp. 1335–1354.

Žarnić, Roko and Miha Tomaževič (1985). *Study of the behaviour of masonry infilled reinforced concrete frames subjected to seismic loading*.